USAAVRADCOM-TR-82-D-34

(12)

AD A125642

YAH-63 HELICOPTER CRASHWORTHINESS SIMULATION AND ANALYSIS

V. L. Berry, J. D. Cronkhite, T. J. Haas
BELL HELICOPTER TEXTRON, Inc.
P. O. Box 482
Fort Worth, Tex. 76101

February 1983

Final Report for Period July 1980 - June 1982

Prepared for
APPLIED TECHNOLOGY LABORATORY
U. S. ARMY RESEARCH AND TECHNOLOGY LABORATORIES (AVRADCOM)
Fort Eustis, Va. 23604

APPLIED TECHNOLOGY LABORATORY POSITION STATEMENT

This report further updates the use of computer program KRASH in representing the dynamic behavior of aircraft structures in a crash environment. The KRASH model was applied to the YAH-63 aircraft and results were compared to the US Army's first full-scale crash test (T-41) of an attack helicopter. It is acknowledged that care must be exercised in developing a realistic KRASH model of a specific aircraft. The procedure is classed as a "hybrid" crash analysis method, since input data from other analyses or supporting tests are usually required to achieve a realistic structural response. Results of this contract are being integrated into related crashworthiness R&D ongoing at the Applied Technology Laboratory to establish better guidance in designing more weight and cost-efficient energy absorbing aircraft systems that will minimize personnel and material losses and their associated costs.

Mr. LeRoy T. Burrows, Mr. George T. Singley III, and Mr. Kent F. Smith of the Aeronautical Systems Division served as project engineers for this effort.

Unclassified

SECURITY CLASSIFICATION OF THIS PAGE (When Data Entered)

REPORT DOCUMENTATION PAGE		READ INSTRUCTIONS BEFORE COMPLETING FORM
1. REPORT NUMBER USAAVRADCOM-TR-82-D-34	2. GOVT ACCESSION NO. A125642	3. RECIPIENT'S CATALOG NUMBER
4. TITLE (and Subtitle) YAH-63 HELICOPTER CRASHWORTHINESS SIMULATION AND ANALYSIS		5. TYPE OF REPORT & PERIOD COVERED Final Report July 1980 - June 1982 6. PERFORMING ORG. REPORT NUMBER
7. AUTHOR(s) V. L. Berry, J. D. Cronkhite, T. J. Haas G. S. Perry		8. CONTRACT OR GRANT NUMBER(s) DAAK51-80-C-0027
9. PERFORMING ORGANIZATION NAME AND ADDRESS Bell Helicopter Textron, Inc. P. O. Box 482 Fort Worth, Texas 76101		10. PROGRAM ELEMENT, PROJECT, TASK AREA & WORK UNIT NUMBERS 62209A 1L162209AH76 032 EK
11. CONTROLLING OFFICE NAME AND ADDRESS Applied Technology Laboratory, US Army Research and Technology Laboratories (AVRADCOM) Fort Eustis, Virginia 23604		12. REPORT DATE February 1983 13. NUMBER OF PAGES 257
14. MONITORING AGENCY NAME & ADDRESS(If different from Controlling Office)		15. SECURITY CLASS. (of this report) Unclassified 15a. DECLASSIFICATION/DOWNGRADING SCHEDULE

16. DISTRIBUTION STATEMENT (of this Report)

Approved for public release; distribution unlimited.

17. DISTRIBUTION STATEMENT (of the abstract entered in Block 20, if different from Report)

18. SUPPLEMENTARY NOTES

19. KEY WORDS (Continue on reverse side if necessary and identify by block number)

Helicopter	Crashworthiness	Computer Simulation
Structure	Crash Impact	KRASH
Airframe	Energy Absorption	MIL-STD-1290
Landing Gear	Structure Crash Simulation	
Crashworthy Fuel System	Structure Dynamic Analysis	

20. ABSTRACT (Continue on reverse side if necessary and identify by block number)

Under its ongoing crash research testing program, the Army conducted drop test T-41 using a YAH-63 prototype helicopter as a test article. The YAH-63 was residual hardware from the AAH competition of the mid 70's and incorporated many crashworthy features, including a high energy landing gear, crushable fuselage structure, stroking crew seats, high strength retention of large masses, and a crash-resistant fuel system. The test was conducted in July 1981 at the NASA Langley Impact Dynamics Research Facility. Many onboard experiments were also evaluated in the drop test with participation from NASA, the Navy, and the Army.

DD FORM 1 JAN 73 1473 EDITION OF 1 NOV 65 IS OBSOLETE

Unclassified

SECURITY CLASSIFICATION OF THIS PAGE (When Data Entered)

The planned T-41 drop test impact condition was a 50-ft/sec resultant velocity with a 30-ft/sec forward velocity and a 40-ft/sec vertical velocity and with a 10° nose-up pitch attitude. The 50-ft/sec resultant impact velocity is representative of a 95th percentile accident condition as specified in the Army's crashworthiness requirement MIL-STD-1290. However, the actual impact was a 60-ft/sec resultant impact or about 44% more crash impact energy than planned. The higher impact energy had a significant effect on the stroking and bottoming out of the forward copilot/gunner seat with tension-loaded attenuators. The aft pilot seat with compression-loaded attenuators did not stroke properly due to buckling of the attenuators. The airframe and landing gear performed well and the primary fuselage structure remained intact around the occupants, the large masses were retained, and the landing gear stroked properly, absorbing the equivalent of 30 ft/sec crash energy. In addition, the fuel tanks and breakaway fittings performed well with the exception of some minor leakage in the forward tank due to a bent flange on a tank drain sump cover.

Prior to the T-41 drop test, a main landing gear shock strut drop test was conducted by BHTI to determine the performance of the air/oil shock under a 42-ft/sec vertical impact condition and to help develop a modified load-limiting relief valve for the gear. Modified relief valves were then installed on the YAH-63 test article on the nose and main landing gear.

A KRASH analysis of the planned 50-ft/sec resultant condition was conducted prior to the T-41 drop test and of the actual 60-ft/sec condition following the drop test. The KRASH model used a simplified elastic line representation for the beam-like fuselage, wings, and tailboom. The airframe vibration modes through 20 Hz for the elastic model were correlated with a detailed finite-element model of the airframe using NASTRAN to ensure that proper mass and stiffness distributions were maintained. The crush zones in the lower fuselage were represented by crush springs with load-deflection properties determined by structural analysis. The main rotor transmission, mast, and mounting links were modeled in detail. Each structural member, link, and wheel of the nose and main landing gears was modeled and the shock strut properties were derived from the BHTI shock drop test and landing gear analysis. The stroking seats and occupants were represented as two-element spring-masses for each crew location.

The KRASH results were compared to test and showed generally good agreement for landing gear energy absorption, fuselage crushing, nose structure failure, and copilot/gunner seat stroking and bottoming. The acceleration levels in the fuselage agreed well in the mid fuselage impact, but predicted levels were lower than test levels in the forward fuselage, probably due to the hard armament structure on the test article not represented in the KRASH model. The comparison of results was greatly facilitated by the DATAMAP program that processed both the test and KRASH data and automated the plotting, overplotting, scaling, filtering, and integrating of the data.

PREFACE

The "YAH-63 Helicopter Crashworthiness Simulation and Analysis" study was performed under Contract DAAK51-80-C-0027 from the Applied Technology Laboratory, U.S. Army Research and Technology Laboratories (AVRADCOM), Fort Eustis, Virginia. Mr. Leroy T. Burrows, Mr. Kent F. Smith, and Mr. George T. Singley III of ATL were the Contracting Officer's Technical Representatives and provided technical direction for the program.

The authors wish to thank the personnel at the Impact Dynamics Research Facility, NASA Langley Research Center for their assistance with the post-test data reduction.

BHTI personnel participating in the contract work included J. D. Cronkhite (Project Engineer), V. L. Berry (KRASH Analysis), T. J. Haas (Structural Analysis), and G. S. Perry (Landing Gear Analysis).

TABLE OF CONTENTS

	Page
PREFACE	3
LIST OF ILLUSTRATIONS	7
LIST OF TABLES	11
1. INTRODUCTION	12
2. T-41 DROP TEST PREPARATIONS	17
2.1 Description of the YAH-63 Prototype Test Article	17
2.2 Weights	22
2.3 Instrumentation	22
2.4 Onboard Experiments	25
3. MAIN LANDING GEAR DROP TEST AND ANALYSIS	28
3.1 Drop Test Setup	28
3.2 Drop Test Results and Analysis	31
4. KRASH MODEL OF YAH-63 AND PRE-TEST ANALYSIS	38
4.1 Basic Modeling Approach	38
4.2 KRASH Description	40
4.3 Linear Modeling	41
4.4 Nonlinear Modeling	43
4.4.1 Landing Gear	46
4.4.2 Fuselage	47
4.4.3 Seats	54
4.5 Pre-Test KRASH Analysis (50 ft/sec Resultant Drop Test Condition)	54
5. T-41 CRASH TEST	61
5.1 Summary of Results	61
5.2 Data Analysis	68
6. TEST/ANALYSIS COMPARISON	80
6.1 KRASH Model Modifications	80
6.2 Comparison of Overall Structural Response	82
6.3 Landing Gear Comparisons	88

TABLE OF CONTENTS (Concluded)

	Page
6.4 Fuselage Response Comparisons.....	93
6.4.1 Fuselage Crushing.....	93
6.4.2 Fuselage Accelerations.....	93
6.5 Seat/Occupant Comparisons.....	100
7. CONCLUSIONS.....	104
8. RECOMMENDATIONS.....	108
9. REFERENCES.....	111
APPENDIXES:	
A. STRUCTURE DESCRIPTION.....	113
B. STRUCTURAL ANALYSIS.....	140
C. UNFILTERED TEST DATA TIME HISTORIES.....	168
D. KRASH MATH MODEL LISTING.....	203
E. UNFILTERED AND 20 HZ FILTERED KRASH ANALYSIS TIME HISTORIES.....	227

LIST OF ILLUSTRATIONS

		Page
1	YAH-63 prototype helicopter.....	13
2	YAH-63 energy management system.....	15
3	YAH-63 line drawing data sheet.....	18
4	YAH-63 crashworthiness features.....	21
5	Test article configuration weight items..	22
6	T-41 crash test article weight and cg data.....	23
7	T-41 crash test instrumentation.....	24
8	YAH-63 prototype landing gear.....	29
9	Drop test fixture for YAH-63 main landing gear dynamic tests.....	30
10	Blow-off valve orifice sizing calculations for YAH-63 main landing gear drop test.....	32
11	Shock strut closure velocity from BHTI drop test of YAH-63 main landing gear....	33
12	Test and analysis comparison of YAH-63 main landing gear shock strut load.....	34
13	Effect of blow-off valve orifice diameter on YAH-63 main landing gear shock strut load.....	35
14	Effect of blow-off valve orifice diameter on YAH-63 main landing gear vertical axle load.....	37
15	KRASH math model of YAH-63 test article..	39
16	YAH-63 fuselage structure cross sections.	44
17	Natural frequency comparison between simple KRASH model and detailed NASTRAN model.....	45

LIST OF ILLUSTRATIONS (Continued)

		Page
18	YAH-63 nose landing gear modeling.....	48
19	YAH-63 main landing gear modeling.....	49
20	YAH-63 nose gear shock strut load-deflection data.....	50
21	YAH-63 main gear shock strut load-deflection data.....	51
22	Nonlinear structure inputs to KRASH model of YAH-63.....	52
23	KRASH math model of crew seat and occupant.....	55
24	Pre-test KRASH results for planned T-41 crash test conditions (50 ft/sec resultant).....	57
25	Dynamic Response Index from KRASH analysis of 50 ft/sec planned drop test condition.....	59
26	Effect of friction on YAH-63 main landing gear vertical axle load.....	60
27	NASA pendulum swing test setup.....	62
28	High-speed photographs of T-41 crash test.....	63
29	Comparison of qualitative results from pre-test KRASH analysis and test.....	64
30	Comparison of planned and actual T-41 crash test impact conditions.....	65
31	YAH-63 test article tail and nose structure failures.....	66
32	Post-test structural condition of left and right wings.....	67
33	Copilot/gunner and pilot crashworthy crew seats.....	69

LIST OF ILLUSTRATIONS (Continued)

		Page
34	Pre- and post-test structural condition of YAH-63 forward fuselage showing crew seat stroke.....	70
35	Post-test condition of YAH-63 forward fuel cell drain sump.....	71
36	Post-test condition of YAH-63 main transmission and engine support structure.....	72
37	Pre- and post-test condition of YAH-63 nose landing gear.....	73
38	Data analysis flow diagram for T-41 crash test results.....	74
39	Filtering effects on measured test data..	77
40	Crew seat pan and pelvis vertical acceleration test data.....	78
41	Crew DRI response from test data.....	79
42	Effects of velocity, friction, and pitch on YAH-63 main landing gear load-deflection.....	81
43	Fuselage crushable structure added to KRASH model of YAH-63.....	83
44	Sequence of events comparison between actual test and KRASH analysis.....	85
45	Test/analysis comparison of vertical velocity at the FS 248.50 pilot bulkhead.....	87
46	KRASH energy summaries for simulated 60-ft/sec T-41 crash test.....	89
47	KRASH/test main landing gear drag link load and shock strut rotation comparison.	90
48	Determination of fuselage contact velocity from T-41 crash test data.....	91

LIST OF ILLUSTRATIONS (Concluded)

		Page
49	YAH-63 main landing gear geometry and motions	92
50	Test/analysis comparison of lower fuselage crushing	94
51	Filtering effects on KRASH analysis data.	96
52	Test/analysis comparison of vertical accelerations at the aircraft cg, pilot bulkhead, and copilot/gunner bulkhead	97
53	Test/analysis comparison of peak vertical accelerations on fuselage	98
54	Test/analysis comparison of nose and main transmission cg vertical accelerations	99
55	Test/analysis comparison of crew seat stroke	101
56	Test/analysis comparison of seat pan and pelvis vertical accelerations	102
57	Crew DRI comparison from KRASH analysis and test	103

LIST OF TABLES

		Page
1	Prototype YAH-63 helicopter crashworthiness design criteria.....	20
2	T-41 crash test instrumentation.....	26
3	KRASH input/output features.....	42
4	KRASH math model weight and cg comparison with actual test article.....	43
5	Sequence of events from KRASH analysis of actual test (60-ft/sec resultant).....	84

1. INTRODUCTION

In the early 1960's, the U.S. Army Transportation Research Command (now the Applied Technology Laboratory, U.S. Army Research and Technology Laboratories, USAAVRADCOM) began a long-range program to study aircraft crashworthiness that culminated in the issuance of a Crash Survival Design Guide (References 1 and 2) and the associated MIL-STD-1290 (Reference 3). The first time a comprehensive crashworthiness criterion was applied to a production aircraft was in the early 1970's in the Army UTTAS program and later in the Army AAH program. Although the UTTAS and AAH crashworthiness requirements were not fully compliant with MIL-STD-1290, they were similar. For example, both types of aircraft were required to survive a 42-ft/sec vertical impact (but without the MIL-STD-1290 pitch and roll attitude requirements) while providing injury-free protection for the occupants. An available YAH-63 prototype helicopter (see Figure 1) that was designed to meet Army crashworthiness requirements under the AAH program provided an excellent first opportunity for the Army to evaluate the performance of an aircraft with special crashworthy features under their ongoing crashworthiness research testing program.

---

[1]Turnbow, J. W., et al., CRASH SURVIVAL DESIGN GUIDE, Dynamic Science, the AvSer Facility, USAAMRDL TR 71-22, Eustis Directorate, U.S. Army Air Mobility Research and Development Laboratory, Fort Eustis, Virginia, October 1971, AD 733358.

[2]AIRCRAFT CRASH SURVIVAL DESIGN GUIDE, Simula Inc., USARTL TR 79-22 A-E, Applied Technology Laboratory, U.S. Army Research and Technology Laboratories (AVRADCOM), Fort Eustis, Virginia:

Volume I - DESIGN CRITERIA AND CHECKLISTS, December 1980, AD A093784.
Volume II - AIRCRAFT CRASH ENVIRONMENT AND HUMAN TOLERANCE, January 1980, AD A082512.
Volume III - AIRCRAFT STRUCTURAL CRASHWORTHINESS, August 1980, AD A089104.
Volume IV - AIRCRAFT SEATS, RESTRAINTS, LITTERS, AND PADDING, June 1980, AD A088441.
Volume V - AIRCRAFT POSTCRASH SURVIVAL, January 1980, AD A082513.

[3]Military Standard MIL-STD-1290(AV), LIGHT FIXED- AND ROTARY-WING AIRCRAFT CRASHWORTHINESS, Department of Defense, Washington, D.C., 25 January 1974.

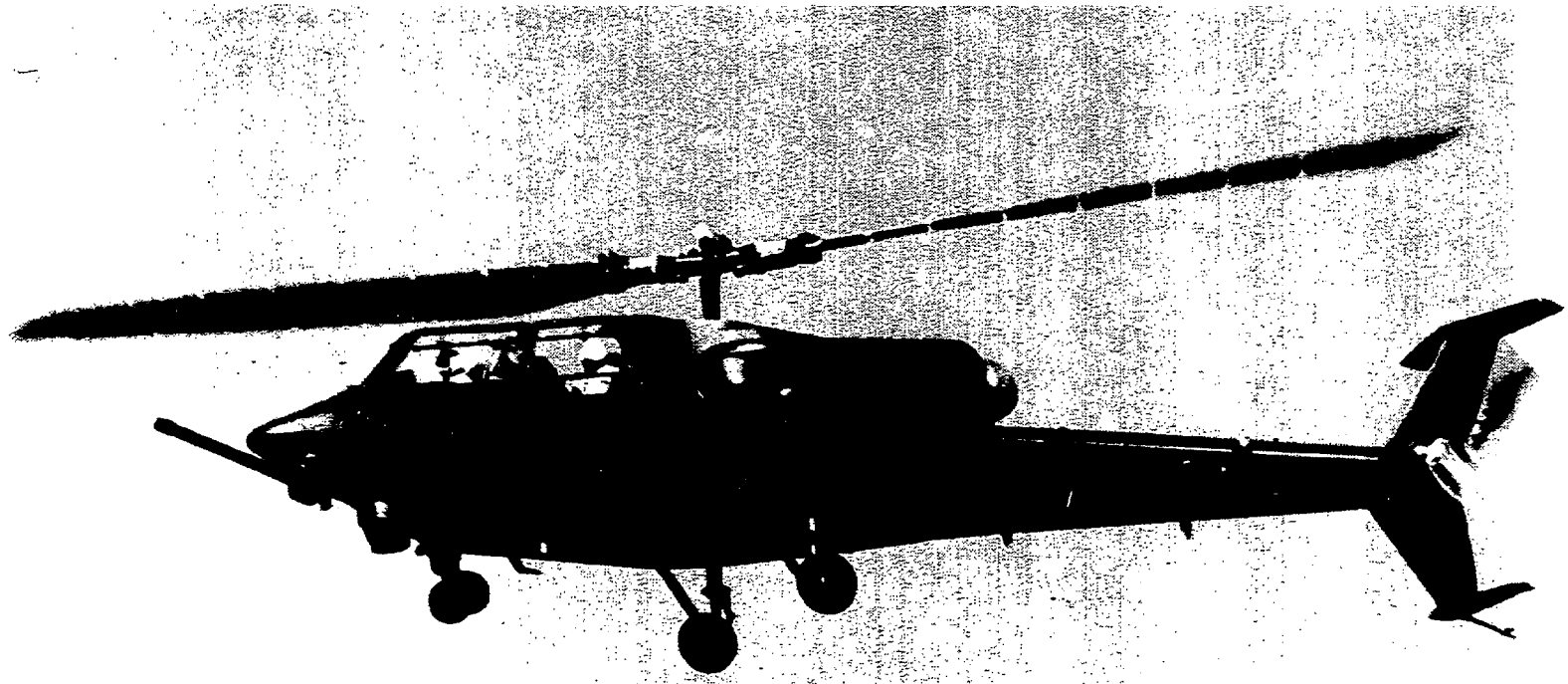

Figure 1. YAH-63 prototype helicopter.

The objective of the Army's YAH-63 drop test program was twofold:

a. Conduct a full-scale drop test of a YAH-63 prototype helicopter and determine its crashworthiness performance under crash impact conditions representative of a U.S. Army 95th percentile potentially survivable accident.

b. Employ the KRASH computer program using available analysis and test procedures to simulate the YAH-63 crash test and compare results with test for evaluation of the analysis as an accurate and reliable crashworthiness design tool.

Crashworthiness is a complex subject involving human tolerance, the crash environment (impact surface, terrain, aircraft velocities/attitudes), seats/restraints, cabin environment, post-crash fire, emergency egress, landing gear, and airframe structure. Of particular interest in the YAH-63 drop test program was the "energy management system," as shown in Figure 2, consisting of the landing gear, fuselage crushable structure, and stroking seats that absorb crash kinetic energy and decelerate the occupants and large masses to rest without causing injuries or allowing large masses or structure to displace into the occupied area and become a hazard to the occupants.

A key to evaluating and optimizing the crashworthiness of helicopters for maximum protection and minimum weight is the implementation of structure crash analysis tools to aid the aircraft designer. Designing a crash-resistant structure requires an understanding of the nonlinear behavior of a complex structure deforming under crash impact loads. An analytical tool that has become widely used is the KRASH structure crash simulation (References 4 and 5). The KRASH analytical models of the structure are rather coarse and are

---

[4]Gamon, M. A., and Wittlin, G., EXPERIMENTAL PROGRAM FOR THE DEVELOPMENT OF IMPROVED HELICOPTER STRUCTURAL CRASHWORTHINESS ANALYTICAL AND DESIGN TECHNIQUES, USAAMRDL Technical Report 72-72, 2 Vols., U.S. Army Air Mobility Research and Development Laboratory, Fort Eustis, Virginia, May 1973.

[5]Wittlin, G., and Gamon, M. A., GENERAL AVIATION AIRPLANE STRUCTURAL CRASHWORTHINESS USER'S MANUAL, DOT Report FAA-RD-77-189, 3 Vols., U.S. Department of Transportation, Federal Aviation Administration, Systems Research and Development Service, Washington, D.C., February 1978.

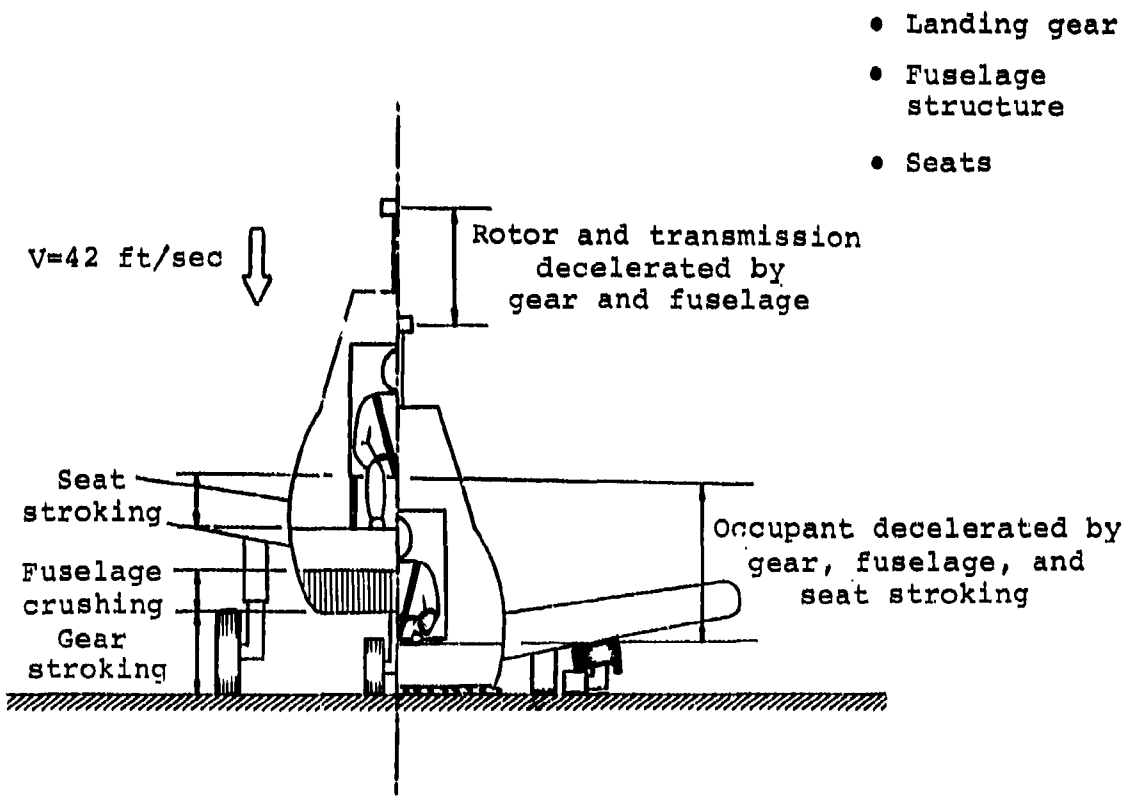

Figure 2. YAH-63 energy management system.

represented by nonlinear beam and spring structural elements with properties derived from test or analysis. However, KRASH is capable of simulating complex three-dimensional crash impacts of aircraft-type structures and determining the responses and energy absorption of the landing gear, fuselage, and seats as well as the crash loads on the occupants and large masses. The accuracy of the results, of course, depends on how well the coarse structure model represents the actual structure response.

This report contains the following:

a. A summary of the drop test setup and instrumentation.

b. A description of the YAH-63 test article.

c. The results of a drop test of a main landing gear shock strut that was conducted by BHTI to size a hydraulic pressure relief valve and determine load-stroke characteristics of the gear.

d. A description of the YAH-63 KRASH model and methods used in developing the linear and nonlinear structural dynamic properties.

e. A summary of the drop test results and a complete set of test data in the form of time histories measured by the Army, NASA, and Navy.

f. The results of the KRASH analysis and comparison with test.

g. Conclusions and recommendations.

Note that the actual drop test conditions (60 ft/sec resultant) were considerably more severe than the 50-ft/sec planned conditions (actual test had about 44% higher energy). KRASH results determined prior to the drop test are presented in Section 4.5 for the 50-ft/sec 95th percentile planned test condition. Following the drop test, the KRASH model was modified to reflect the actual higher impact velocity 60 ft/sec drop test condition and reanalyzed to allow direct comparison with test results. The comparison of results is discussed in Section 6.

2. T-41 DROP TEST PREPARATIONS

This section describes briefly the test preparation for Army drop test T-41, including the YAH-63 test article, the weights added to simulate a typical mission gross weight configuration, the instrumentation, and the special onboard experiments provided by the Army, Navy, and NASA. Prior to the drop test, the Army reassembled the prototype YAH-63 aircraft and restored it to a typical mission weight configuration with technical assistance from BHTI. Further details on the drop test preparations can be found in the Army test report (Reference 6). Modification of the landing gear blow-off valves is discussed in Section 3.

2.1 DESCRIPTION OF THE YAH-63 PROTOTYPE TEST ARTICLE (See also Appendix A)

Three prototype YAH-63 helicopters were built during the U.S. Army's Advanced Attack Helicopter (AAH) competition in the early to mid 1970s. The gunship, shown in Figure 1, had a basic structural design gross weight of 15,984 lb which included eight wing-mounted TOW missiles and 800 rounds of 30mm ammunition in a belly-mounted container. The overall dimensions of the aircraft are provided on the line drawing data sheet in Figure 3. Performance capabilities of the YAH-63 included a 990-ft/min vertical rate of climb, 172-KTAS cruise speed, and 1.9-hour mission endurance. In addition, the airframe and subsystem components were required to meet the U.S. Army's ballistic tolerance criteria for both API and HEI threats. The YAH-63 airframe structure and components (landing gear, seats, main rotor pylon and engine mounting, and fuel system) are described in Appendix A.

The YAH-63 prototype helicopter was designed to meet the Army's crashworthiness requirements that included providing occupant protection from injury for crash impact conditions up to and including the 95th percentile potentially survivable accident (50 ft/sec resultant with 42 ft/sec maximum vertical impact velocity). In meeting these requirements, the YAH-63 incorporated crashworthy structure to control the occupant acceleration environment within human tolerance levels, maintain the livable space around the occupants, and

---

[6] Smith, K. F., FULL-SCALE CRASH TEST (T-41) OF YAH-63 ATTACK HELICOPTER, USAAVRADCOM Technical Report 83-XX, Applied Technology Laboratory, U.S. Army Research and Technology Laboratories, Fort Eustis, Virginia (to be published).

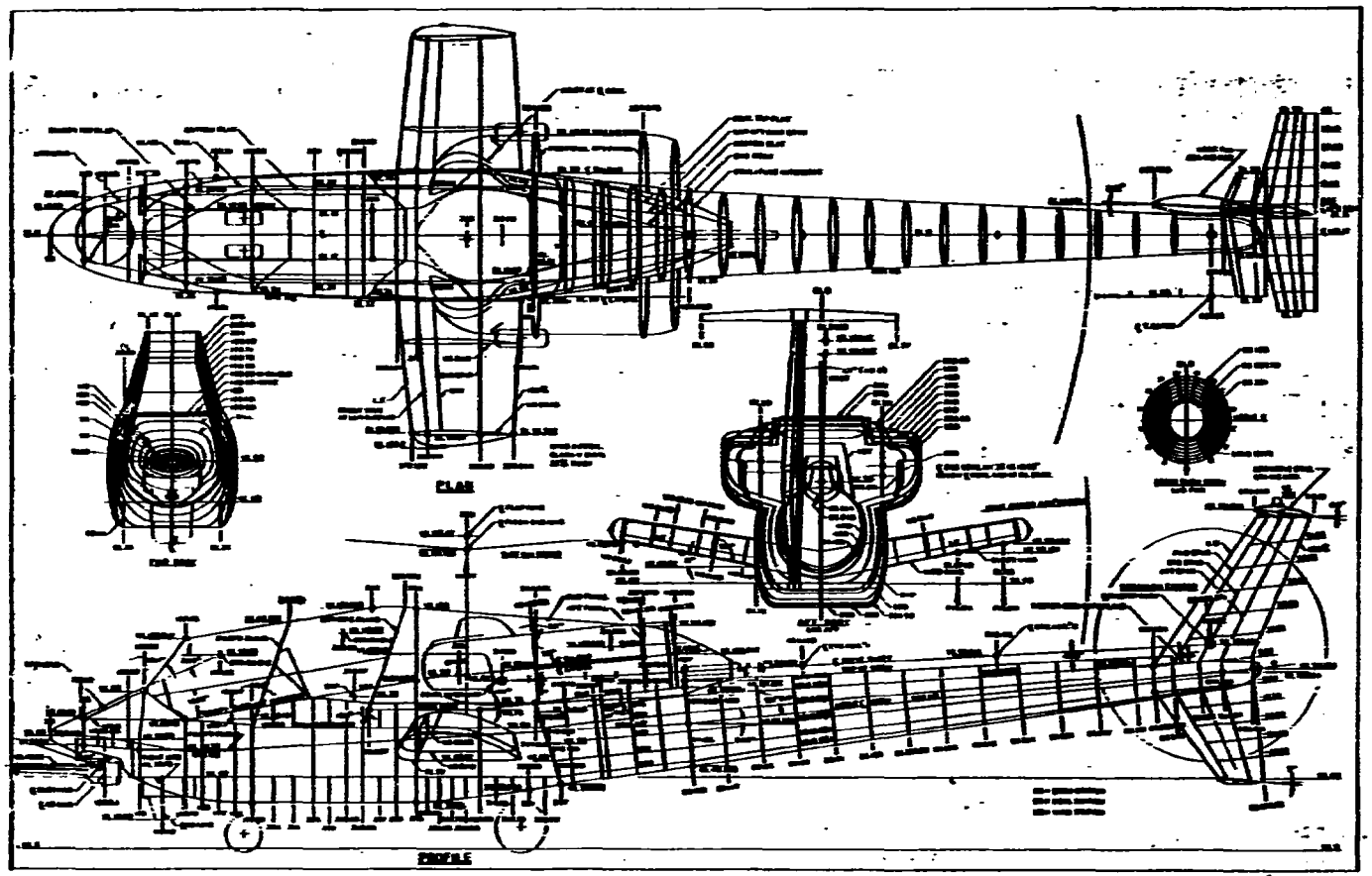

Figure 3. YAH-63 line drawing data sheet.

prevent the penetration of large mass items into the occupied area for 20-ft/sec longitudinal, 30-ft/sec lateral, and 42-ft/sec vertical crash impact conditions as well as for static rollover conditions (see Table 1). The crashworthy structure features are shown in Figure 4, including the high-energy landing gear system, crushable fuselage structure, stroking crew seats, and high-strength retention structure for the large mass items. In addition, the YAH-63 incorporated a crash-resistant, ballistic-tolerant fuel system.

2.2 WEIGHTS

The YAH-63 test article required the addition of useful load items to simulate a typical gross weight configuration as illustrated in Figure 5. Engine mock-ups weighing 487 lb each were fabricated and installed on the existing engine mounts. The weight and mass moments of inertia for the mock-ups were comparable to those of the original General Electric T-700 engines. Nose ballast of 379 lb was added to represent the 30mm gun/turret assembly and lower stabilized sight unit. Tailboom ballast of 278 lb was added to achieve the desired gross weight and cg location for the test article. Following a procedure established in previous CH-47 crash tests, the outer two-thirds of the nonrotating main rotor blades were removed, leaving the inboard one-third blade span (516 lb) and hub (767 lb). (The one-third blade stubs were considered a good representation of the effective blade mass during a crash impact. Also, problems with using full span rotor blades on the test article included interference with the NASA harness system in the pendulum swing test setup and occurrence of unrealistic blade flapping.) Part 572, Hybrid II, 50th percentile testing dummies weighing 175 lb each were placed in the forward AH-64 production crew seat and the aft YAH-63 prototype crew seat. Finally, the fuel cells were filled 64% full by weight with water (1517 lb) to represent the primary mission fuel loading condition.

As shown in Figure 6, the final gross weight and cg location for the test article fell within the design envelope and were comparable to the primary mission configuration without wing stores.

2.3 INSTRUMENTATION

The measurement locations on the aircraft are shown in Figure 7. Accelerometers were placed at pertinent airframe structure locations, including the head, chest, and pelvis of the testing dummies. Strain gages were installed to measure axial loads in the main rotor pylon lift links and

TABLE 1. PROTOTYPE YAH-63 HELICOPTER CRASHWORTHINESS DESIGN CRITERIA

Rigid Surface Impact Conditions

- Energy absorbing landing gear, crushable lower fuselage structure, and stroking seats provide 42 ft/sec vertical impact capability (no roll and pitch requirement)
- Crushable fuselage nose structure provides 20 ft/sec longitudinal impact capability (zero pitch and yaw)
- Crushable fuselage sidewall and wing structure provide 30 ft/sec lateral impact capability

Rollover Protection

- High strength wing helps prevent rollover
- Canopy structure withstands 4g longitudinal, 2g lateral, and 4g vertical static load factors applied separately (1g = BSDGW, 15,984 lb)

Tiedown Strength

- Retention structure for main rotor transmission, engines, and other large masses withstand ±20g longitudinal, ±12g lateral, and +20/-10g vertical static load factors applied separately plus a matrix of combined loading conditions
- Seat retention structure withstands +35/-12g longitudinal, ±20g lateral, and +8/-25g vertical static load factors applied separately plus combined static and dynamic loads per MIL-S-58095 (Reference 7, 1g = 322 lb)

Post-Crash Fire Protection

- Fuel cells withstand 65 ft vertical drop without rupturing
- Breakaway, self-sealing fuel lines prevent fuel spillage
- Outboard engine location provides separation of fuel cells from primary ignition source

[7]Military Specification MIL-S-58095, SEAT SYSTEM, CRASHWORTHY, NONEJECTION, AIRCREW, GENERAL SPECIFICATION FOR, Department of Defense, Washington, D.C., August 1971.

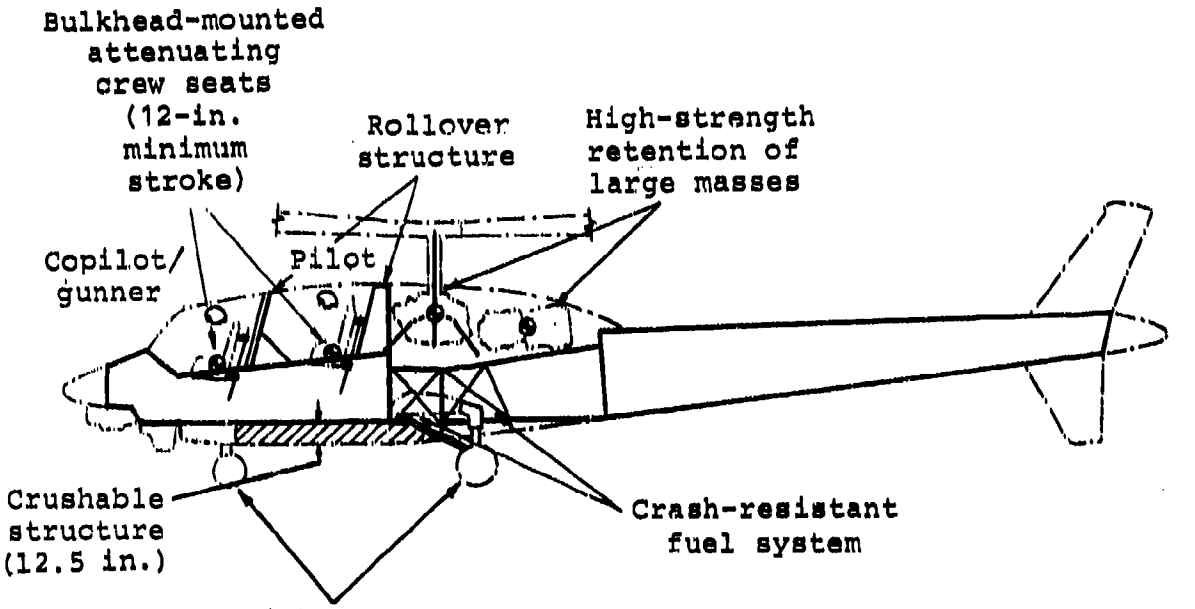

The YAH-63 was designed to meet the 42-ft/sec vertical impact condition through energy absorption in the landing gear, fuselage crushable structure and seats.

Figure 4. YAH-63 crashworthiness features.

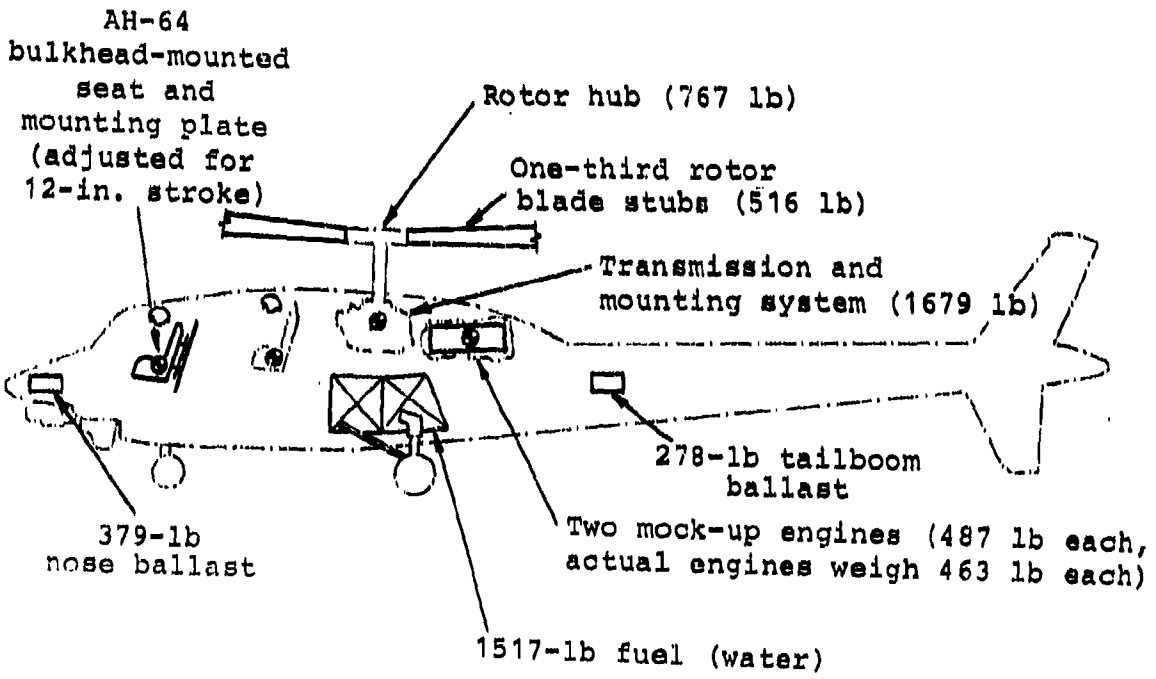

Figure 5. Test article configuration weight items.

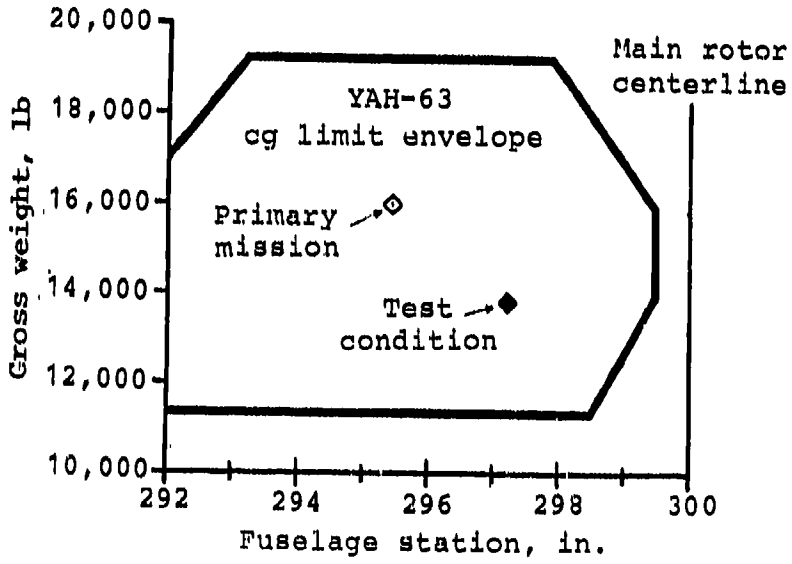

Figure 6. T-41 crash test article weight and cg data.

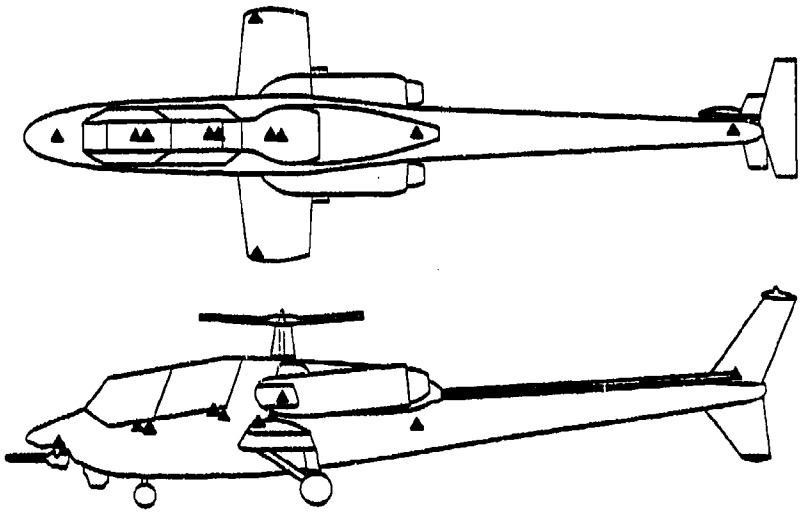

50 accelerometers (▲ symbol)
12 strain gages
7 pressure transducers
6 deflection sensors
5 tensiometers
19 motion picture cameras

Figure 7. T-41 crash test instrumentation.

crash links, the landing gear drag struts, and the crew seat attenuators. Additional instrumentation measured fuel cell pressure, landing gear shock strut pressure, landing gear rotation, seat stroke, and occupant restraint system loads. The complete instrumentation package is listed in Table 2.

NASA provided extensive photographic coverage to document the crash test. High speed motion picture cameras were stationed to film the test from several angles. Still photographs were used to record the aircraft structural condition before and after the test.

2.4 ONBOARD EXPERIMENTS

To obtain maximum benefits from the T-41 test, the Army solicited participation from the Navy and NASA to sponsor pertinent onboard experiments for crash environment evaluation. The experiments included the following:

a. Army/Navy jointly developed Inflatable Body and Head Restraint System, IBAHRS (Reference 8)

b. Army production AH-64 crashworthy crew seat

c. Army Accident Information Retrieval System (AIRS)

d. Navy Flight Incident Recorder and Crash Position Locator (FIR/CPL)

e. Emergency Locator Transmitters (ELTs) provided by NASA

More detailed information on the crash test evaluation of the experiments is found in Reference 6.

---

[8] Schulman, M., and McElhenney, J., INFLATABLE BODY AND HEAD RESTRAINT, NADC-77176-40, Naval Air Development Center, Naval Air Systems Command, Washington, D.C., September 1977.

TABLE 2. T-41 CRASH TEST INSTRUMENTATION

Channel	Remarks	Type	Fuselage Station Location	Record Channel	Sensitivity	Agency
01	Nose Gun Turret	V	120 C	D1A	250	NASA
02	Pilot Bulkhead	V	251 C	D1B	250	NASA
03	Pilot Bulkhead	LA	251 C	D1C	250	NASA
04	Pilot Bulkhead	LO	251 C	D1D	250	NASA
05	Pilot Seat Bot Rev Pol	V	244 C	D1E	250	NASA
06	Copilot Bulkhead	V	193 C	D2A	250	NASA
07	Right Wg Store Outer	V	280 C	D2B	250	NASA
08	Right Wg Store Outer	LO	280 C	D2C	250	NASA
09	Left Wg Store Outer	V	280 L	D2D	250	NASA
10	Left Wg Store Outer	LO	280 C	D2E	250	NASA
11	Aircraft CG	V	290 C	D3A	250	NASA
12	Aircraft CG	LA	290 C	D3B	250	NASA
13	Aircraft CG	LO	290 C	D3C	250	NASA
14	Transmission CG Rev Pol	V	300 C	D3D	250	NASA
15	Transmission CG	LA	300 C	D3E	250	NASA
16	Transmission CG	LO	300 C	D4A	250	NASA
17	Main Rotor Hub	LA	300 C	D4B	250	NASA
18	Main Rotor Hub	LO	300 C	D4C	250	NASA
19	Ctr Fuselage	V	411 C	D4D	250	NASA
20	Pilot Pelvis	V	244 C	D4E	250	NASA
21	Pilot Pelvis	LO	244 C	D5A	250	NASA
22	Pilot Chest	V	244 C	D5B	250	NASA
23	Pilot Chest Rev Pol	LO	244 C	D5C	250	NASA
24	Pilot Head	V	244 C	D5D	250	NASA
25	Pilot Head	LA	244 C	D5E	250	NASA
26	Pilot Head	LO	244 C	D6A	250	NASA
27	Tail Rotor Gearbox	V	665 C	D6B	250	NASA
28	Tail Rotor Gearbox	LA	665 C	D6C	250	NASA
29	Pilot Seat Bot	LO	244 C	D6D	250	NASA
30	Forward Fuel Cell	P	292 L	D6E	250	NASA
31	Rear Fuel Cell	P	322 L	D7A	250	NASA
32	Nose Gear Strut	P	160 C	D7B	7000	NASA
33	Right Gear Strut	P	314 C	D7C	7000	NASA
34	Left Gear Strut	P	314 C	D7D	7000	NASA
35	Pilot Seat Stroke	DP	244 C	D7E	18	NASA
36	Copilot Seat Stroke	DP	183 C	D8A	18	NASA
37	Nose Gear Stroke	DP	185 C	D8B	90	NASA
38	Right Main Gear Stroke	DP	314 R	D8C	90	NASA
39	Left Main Gear Stroke	DP	314 L	D8D	90	NASA
40	Pilot Bulkhead	V	251 C	A9	250	ATL
41	Transmission CG	LO	300 C	A10	250	ATL

TABLE 2. (Concluded)

Channel	Remarks	Type	Fuselage Station Location	Record Channel	Sensitivity	Agency
42	Transmission CG Rev Pol	V	300 C	A11	250	ATL
43	Pilot Seat Bot Rev Pol	V	244 C	B1	250	ATL
44	Lft Pilot Seat Atten Axial	SG	244 C	A1	2700	ATL
45	Rt Pilot Seat Atten Axial	SG	244 C	A2	2700	ATL
46	Rt Fwd Trans Link, Axial	SG	265 R	A3	150K	ATL
47	Rt Rear Trans Link, Axial	SG	330 R	A4	150K	ATL
48	Lft Fwd Trans Link, Axial	SG	265 L	A5	150K	ATL
49	Lft Rear Trans Link, Axial	SG	330 L	A6	150K	ATL
50	Rt Trans Crash Link Axial	SG	300 R	A7	75K	ATL
51	Lft Trans Crash Link Axial	SG	300 L	A8	75K	ATL
52	Copilot Seat Pan	V	183 C	B2	100	NADC
53	Copilot Seat Pan	LA	183 C	B3	100	NADC
54	Copilot Seat Pan	LO	183 C	B4	100	NADC
55	Copilot Pelvis	V	183 C	B5	100	NADC
56	Copilot Pelvis	LA	183 C	B6	100	NADC
57	Copilot Pelvis	LO	183 C	B7	100	NADC
58	Copilot Chest	V	183 C	B8	100	NADC
59	Copilot Chest	LA	183 C	B9	100	NADC
60	Copilot Chest	LO	183 C	B10	100	NADC
61	Copilot Head	V	183 C	B11	100	NADC
62	Copilot Head	LA	183 C	C1	100	NADC
63	Copilot Head	LO	183 C	C2	100	NADC
64	Copilot Bulkhead	V	212 C	C3	250	NADC
65	Copilot Bulkhead	LA	212 C	C4	250	NADC
66	Copilot Bulkhead	LO	212 C	C5	250	NADC
67	Copilot Lap Belt, Right	SG	183 C	C6	4000	NADC
68	Copilot Lap Belt, Left	SG	183 C	C7	4000	NADC
69	Copilot Shoulder	SG	183 C	C8	5000	NADC
70	Copilot Neg G Strap	SG	183 C	C9	4000	NADC
71	IBAHRS Pressure, Right	P	183 C	C10	100	NADC
72	IBAHRS Pressure, Left	P	183 C	C11	100	NADC
73	Airs Crash Sensor	V	212 C	F1	50	Ham Std
74	Airs Crash Sensor	LA	212 C	F2	50	Ham Std
75	Right Main Lg Strut, Axial	SG	308 R	D8-5	75K	NASA
76	Left Main Lg Strut, Axial	SG	308 L	D9-1	75K	NASA
77	Copilot Atten, Right	SG	183 C	E1	2000	NADC
78	Copilot Atten, Left	SG	183 C	E2	2000	NADC
79	Copilot Seat Stroke	DP	183 C	E3	20	NADC
80	Crash Sensor Pulse	SW	183 C	E4	Off On	NADC

3. MAIN LANDING GEAR DROP TEST AND ANALYSIS

The YAH-63 prototype landing gear was a tricycle nose gear configuration with simple blow-off pressure relief valves at the top of the main and nose gear shock struts that attenuate crash loads for up to 42 ft/sec vertical impacts (see Appendix A, paragraph A.2.1 for landing gear description). As shown in Figure 8, the relief valves provided energy absorption by venting hydraulic fluid through a properly sized orifice. Although this type of energy absorbing device is not ideal, since hydraulic fluid (nonflammable type) is sprayed into the open air and the stroking load, which is directly related to energy absorption, decays with the square of the velocity, it was important to obtain the maximum energy absorption possible with the existing gear on the prototype aircraft. (Note that the proposed production YAH-63 landing gear design incorporated mechanical tube-cutting attenuators that exhibit good load control without loading rate sensitivity.) To "tune" the landing gear for maximum energy absorption in a 42-ft/sec vertical impact, a main landing gear shock strut was drop tested by BHTI and correlated with analysis to develop proper orifice sizing of the blow-off valve. The results of the drop testing and orifice sizing analysis are described in this section. The final orifice sizing was used to design the modified blow-off orifices that were installed on the YAH-63 drop test article. Also, the landing gear analysis was used to develop the shock strut load-deflection characteristics for the KRASH model as described later in Section 4.4.1.

3.1 DROP TEST SETUP

A 42-ft/sec drop test of the YAH-63 main landing gear shock strut was conducted at BHTI to determine the load-attenuating characteristics of an air/oil type main landing gear equipped with a hydraulic blow-off relief valve.

The drop test setup, including drop carriage, loading mass, and shock strut, is shown installed in the BHTI drop tower in Figure 9. The carriage was dropped from a height of over 27 ft to cause a 42-ft/sec impact of the carriage on the sand basin at the bottom of the drop tower. The shock strut was loaded by the falling mass on top of the strut. The applied load was obtained by multiplying the mass times the measured mass acceleration. Accelerations were measured on both the carriage and loading mass.

The landing gear shock strut was installed so that it supported only vertical load and was inverted so that the escaping hydraulic fluid was trapped in a reservoir in the

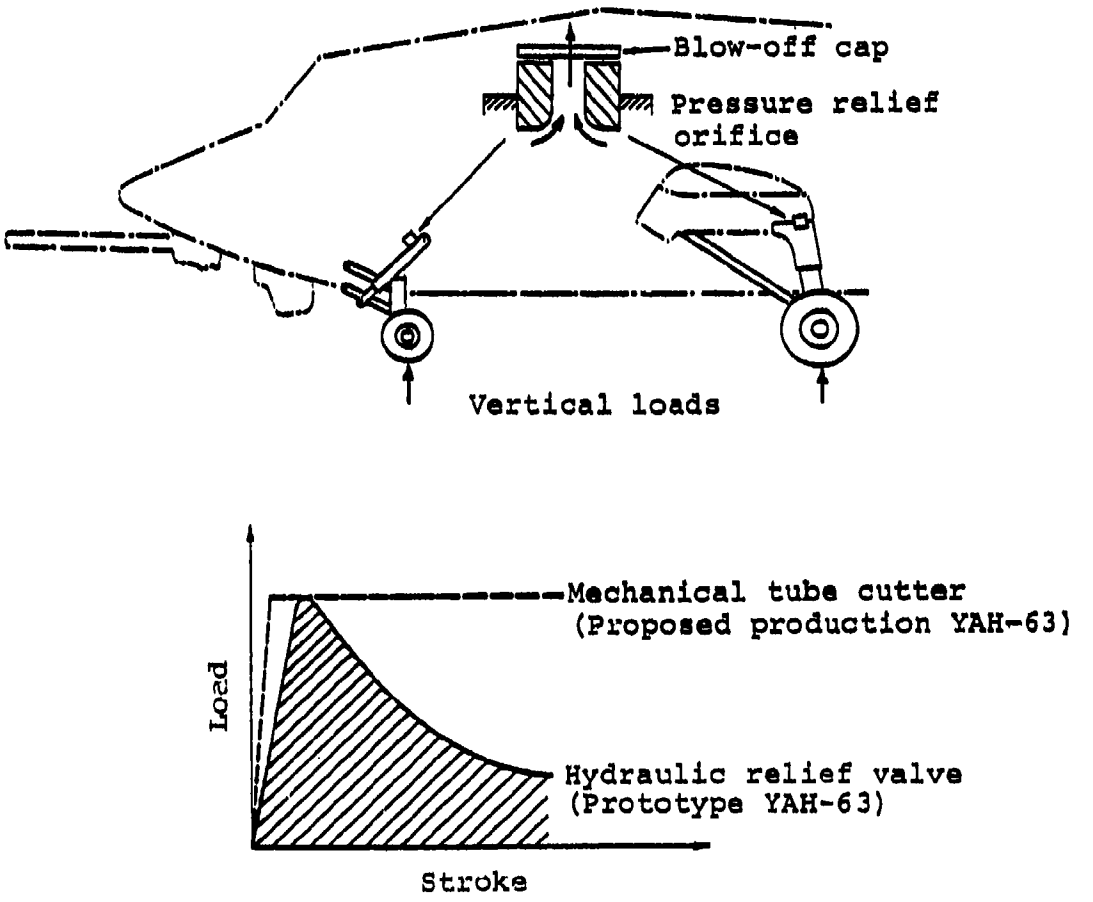

Figure 8. YAH-63 prototype landing gear.

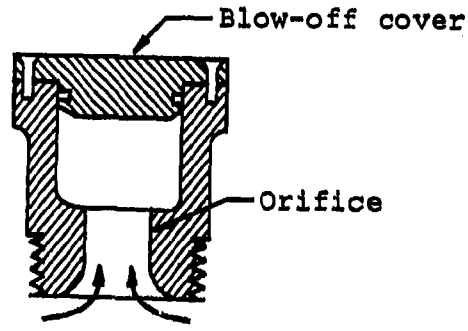

Detail of hydraulic blow-off valve

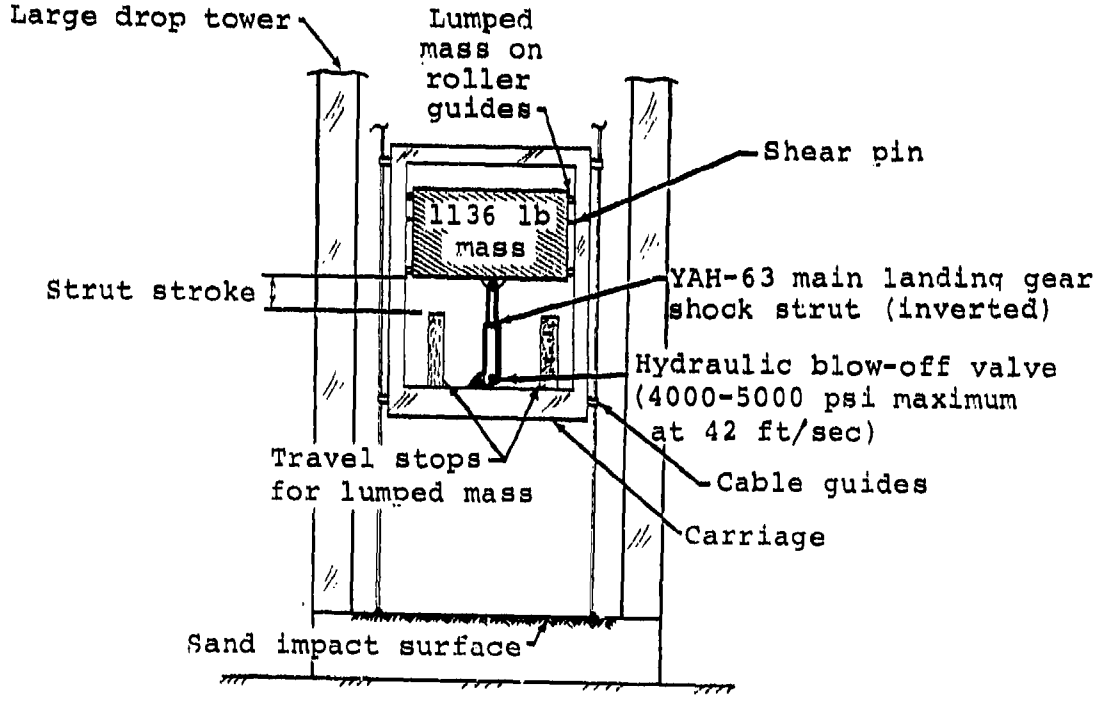

Figure 9. Drop test fixture for YAH-63 main landing gear dynamic tests.

bottom of the carriage. A simple load-limiting blow-off valve orifice was used which was designed to open at about 1200 psig. The shock strut was serviced properly with hydraulic fluid and air prior to the test.

From the test results, load-deflection characteristics of the shock strut were determined. The shock strut axial load time history was obtained from the product of the lumped mass and the mass acceleration time history. The velocity time histories were obtained by integrating the accelerations.

3.2 DROP TEST RESULTS AND ANALYSIS

The orifice diameter for the BHTI drop test of the YAH-63 main gear was selected on the basis of an 8g maximum load applied at the axle. The effective weight of the aircraft over the gear was assumed to be 6093 lb, so the target axle load was 48,744 lb. This axle load resulted in a maximum shock strut load of 62,831 lb due to the gear geometry in the fully extended position. Since the shock strut is vertical at moment of impact, it was assumed that shock strut closure velocity would be 42 ft/sec maximum. This closure velocity, in conjunction with the maximum load of 62,831 lb, was the basis for drop test orifice sizing. The diameter selected was 0.875 inch; a discharge coefficient of 0.80 was assumed. The calculations used to select the orifice diameter are shown on Figure 10.

At the conclusion of the test, it was determined from instrumentation traces that the maximum shock strut load was approximately 32,000 lb, well below the target of 62,831 lb. Subsequent investigation proved that impact of the carriage with the sand produced a softening effect and reduced the closure velocity of the shock strut from 42 ft/sec to approximately 31 ft/sec (Figure 11). In addition, the original calculations did not account for the effect of fluid compression. The analysis was refined to include fluid compression effects as well as velocity decay from sand impact, and a load/stroke curve for the drop test was generated. This curve, Figure 12, provided good correlation with drop test results.

On the basis of the drop test results, the performance of the main landing gear on the YAH-63 aircraft during a 42-ft/sec crash was investigated analytically. An orifice diameter of 0.875 inch and discharge coefficient of 0.80 were used. This analysis proved that the strut closure velocity was less than that assumed by preliminary analysis and that fluid compression further reduced the initial load. The resulting load/stroke curve (Figure 13) provided very

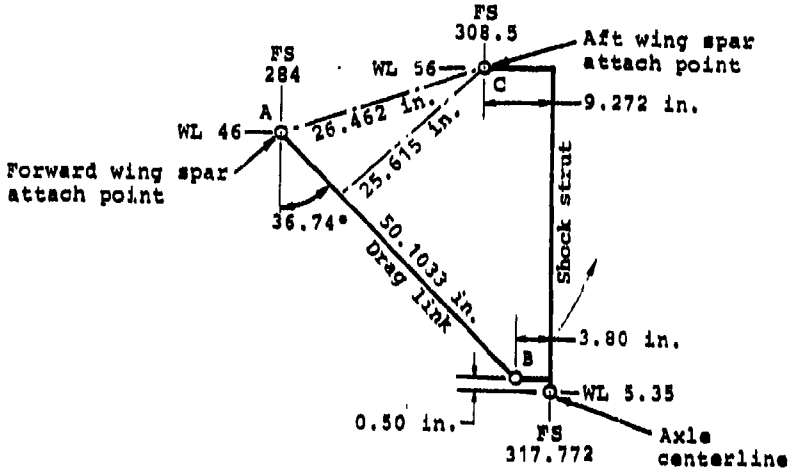

Gravity, $g = 386$ in./sec^2

Shock strut cylinder area, $A_H = 13.318$ in.^{2}

Auxiliary orifice area, $A_{AO} = 0.1665$ in.^{2}

Shock strut closure velocity, $\dot{S} = 42$ ft/sec

Discharge coefficient, $C_D = 0.80$

Weight density of hydraulic fluid, $\gamma = 0.03069$ lb/in.^{3}

Load factor, $L_F = 8$ g

Supported fuselage weight, $W_F = 6093$ lb

- Vertical axle load, $F_A = (L_F)(W_F) = 48,744$ lb
- Drag link load, $F_{DL} = 0.361\ F_A$ (from $\Sigma M_C=0$)
- Oleo load, $F_O = 1.289\ F_A$ (from $\Sigma F_V=0$)
- Fluid flow rate through cylinder, $Q = (A_H)(\dot{S}) = 1743$ gal/min
- Pressure drop through cylinder, $\Delta P = F_O / A_H = 4717.8$ psig
- Total orifice area, $A_O = Q / (C_D\sqrt{(2)(g)(\Delta P)/\gamma}) = 0.7700$ in.^{2}
- Crash valve area, $A_{CV} = A_O - A_{AO} = 0.6035$ in.^{2}
- Crash valve diameter, $D_{CV} = \sqrt{(4)(A_{CV})/\pi} = 0.8766$ in.

Figure 10. Blow-off valve orifice sizing calculations for YAH-63 main landing gear drop test.

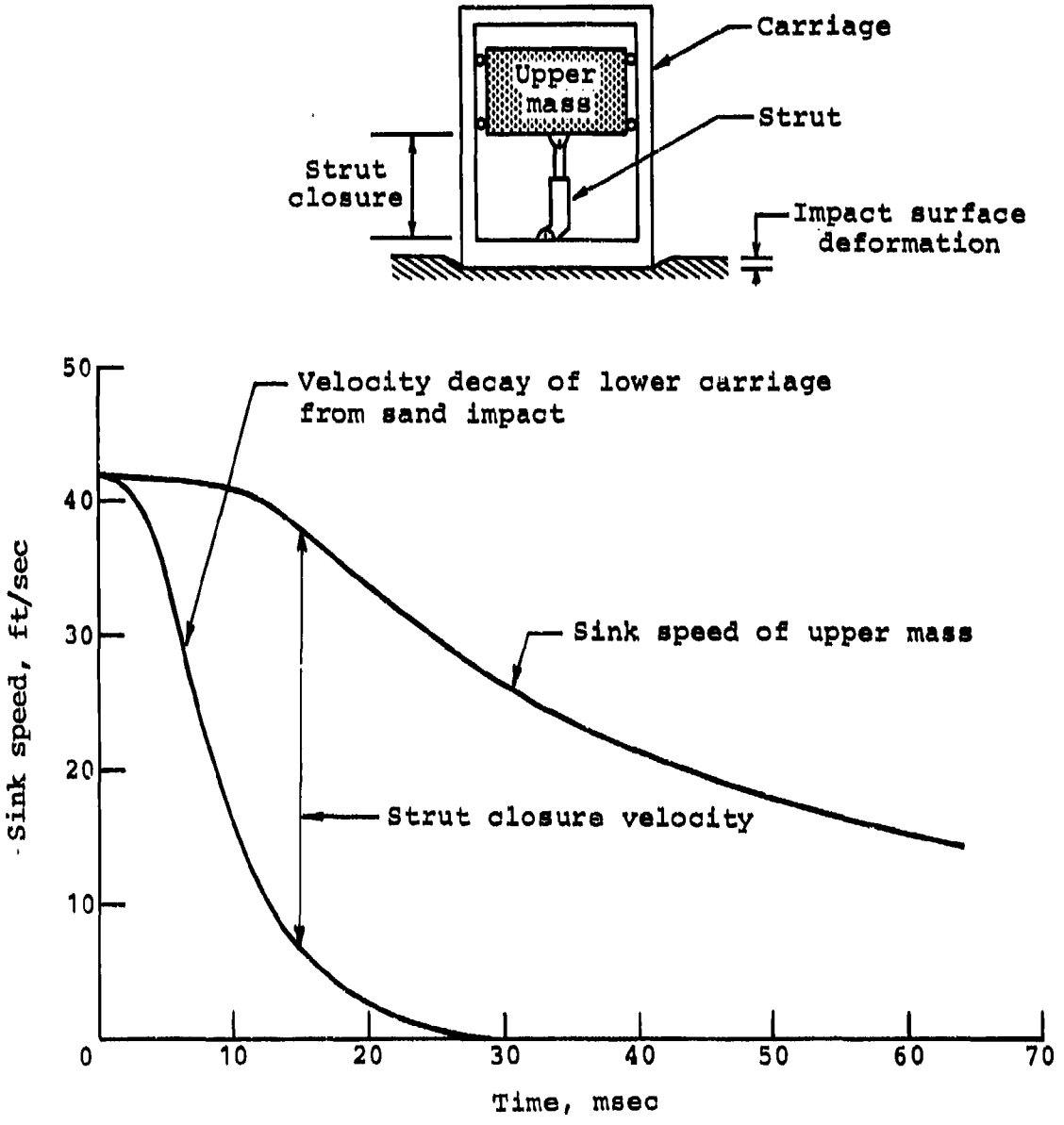

Figure 11. Shock strut closure velocity from BHTI drop test of YAH-63 main landing gear.

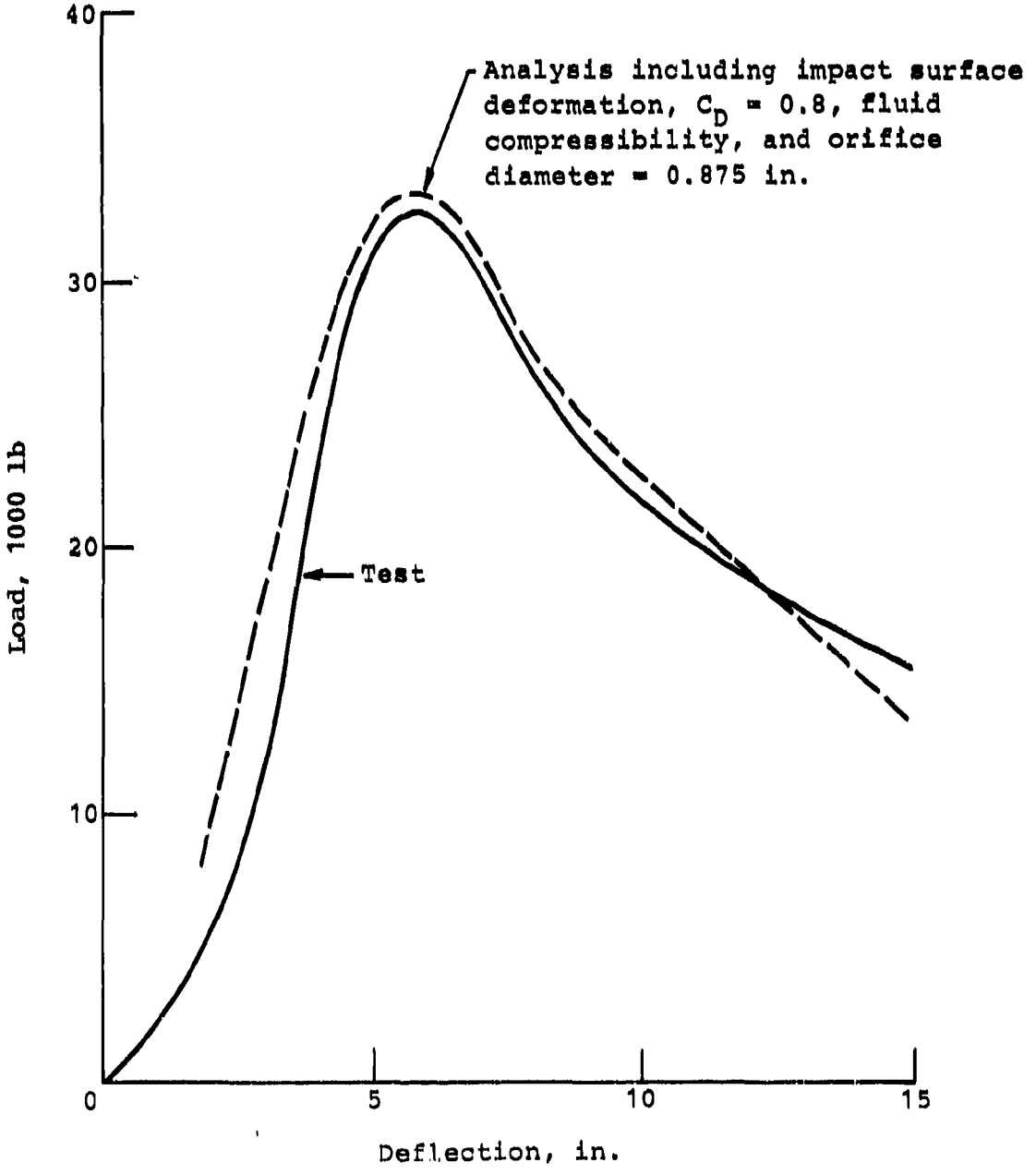

Figure 12. Test and analysis comparison of YAH-63 main landing gear shock strut load.

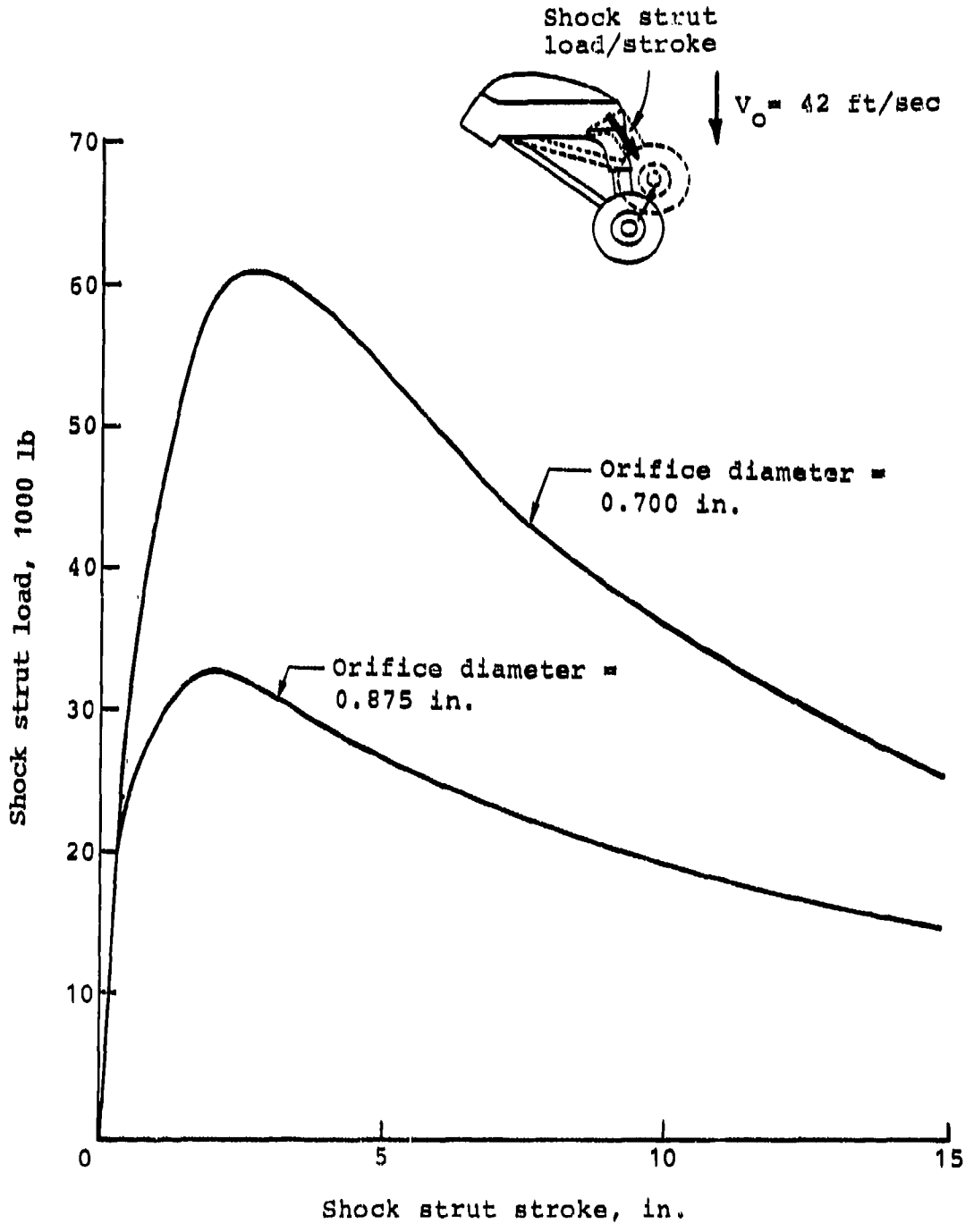

Figure 13. Effect of blow-off valve orifice diameter on YAH-63 main landing gear shock strut load.

poor performance relative to energy attenuation. The resulting loads were well below the structural capability of the gear.

The orifice diameter was reduced to 0.700 inch for the T-41 drop test to improve the crash attenuation of the gear. This increased the peak load to 61,000 lb, consistent with the original target load. The resultant axle load was 42,000 lb. Load/stroke curves for shock strut and axle (ground reaction) are shown in Figures 13 and 14.

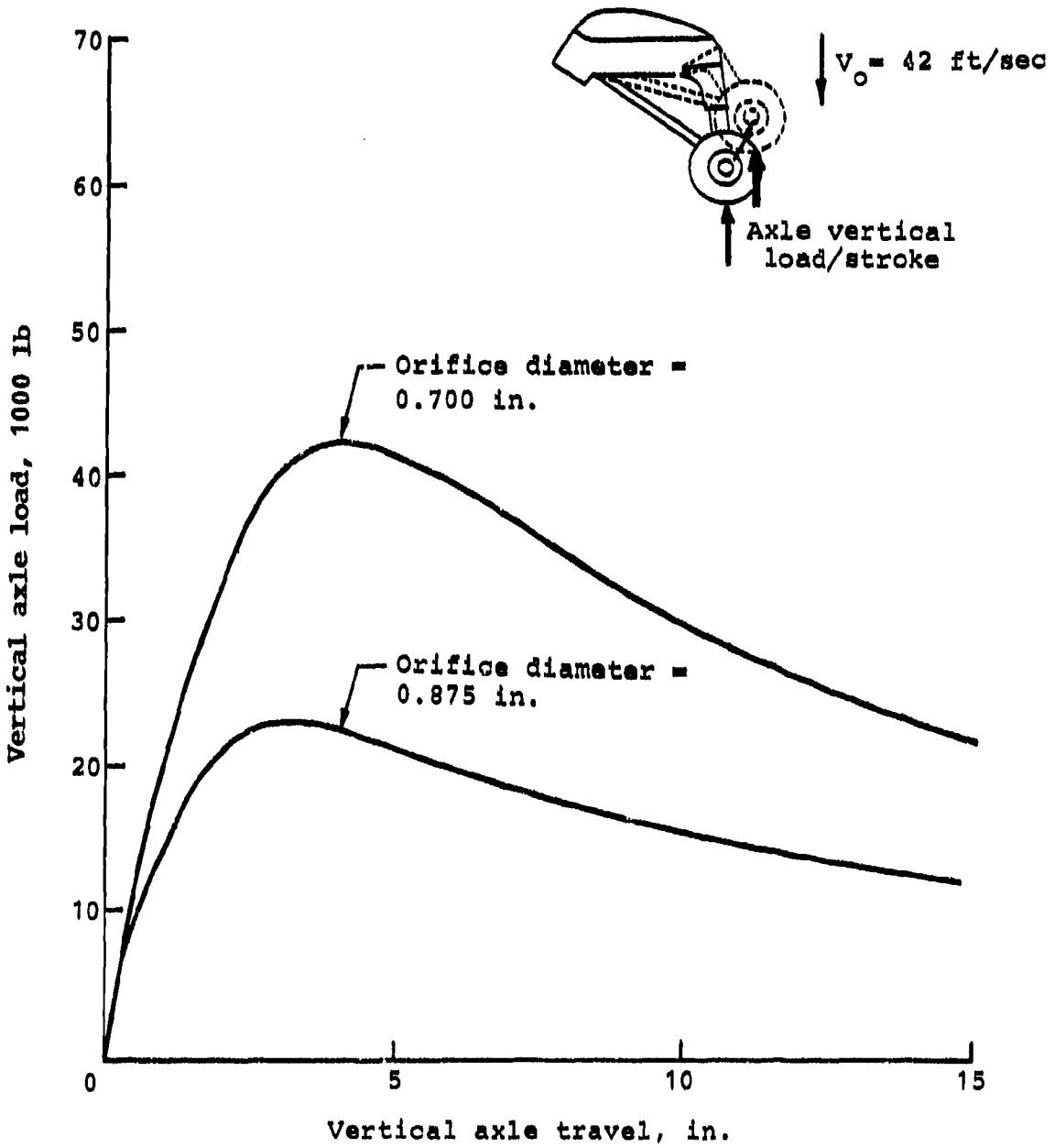

Figure 14. Effect of blow-off valve orifice diameter on YAH-63 main landing gear vertical axle load.

4. KRASH MODEL OF YAH-63 AND PRE-TEST ANALYSIS

This section describes the KRASH modeling of the YAH-63 test article and preliminary KRASH results obtained prior to the drop test. The KRASH model is developed by first representing the basic elastic stiffness and mass distribution of the aircraft and then developing the nonlinear properties for the landing gear, fuselage crushable structure, attenuating (stroking) seats, and structure failures. The landing gear crash impact behavior was determined from the results of drop testing conducted by BHTI (see Section 3) and included development of a hydraulic blow-off valve that was used in the T-41 drop test to control the loads in the nose and main gears. The structure crushing response and failures were determined by structural analysis. Finally, a preliminary KRASH analysis of the planned YAH-63 drop test was conducted which provided guidance in preparing for the test and a prediction of the structural response and damage expected in the actual test. Schematics and an input listing for the KRASH model are included in Appendix D.

4.1 BASIC MODELING APPROACH

The modeling approach used in developing the KRASH model of the YAH-63 (refer to Figure 15) is summarized as follows:

a. The beam-like fuselage, wings, and tailboom structures were modeled as elastic lines with beam elements. The stiffness and mass properties were derived from a detailed NASTRAN finite-element analysis and checked using NASTRAN to assure a good representation of the airframe vibration modes through 20 Hz.

b. Failure loads and bending moments in critical areas, such as the nose structure and tailboom/fuselage junction, were incorporated into the fuselage and tailboom beam elements.

c. The lower fuselage crush zone was represented with crushable nonlinear springs attached to the fuselage beam elements. The crushing load-deflection properties were derived using conventional strength-of-material structural analysis methods following the approach outlined in Army report

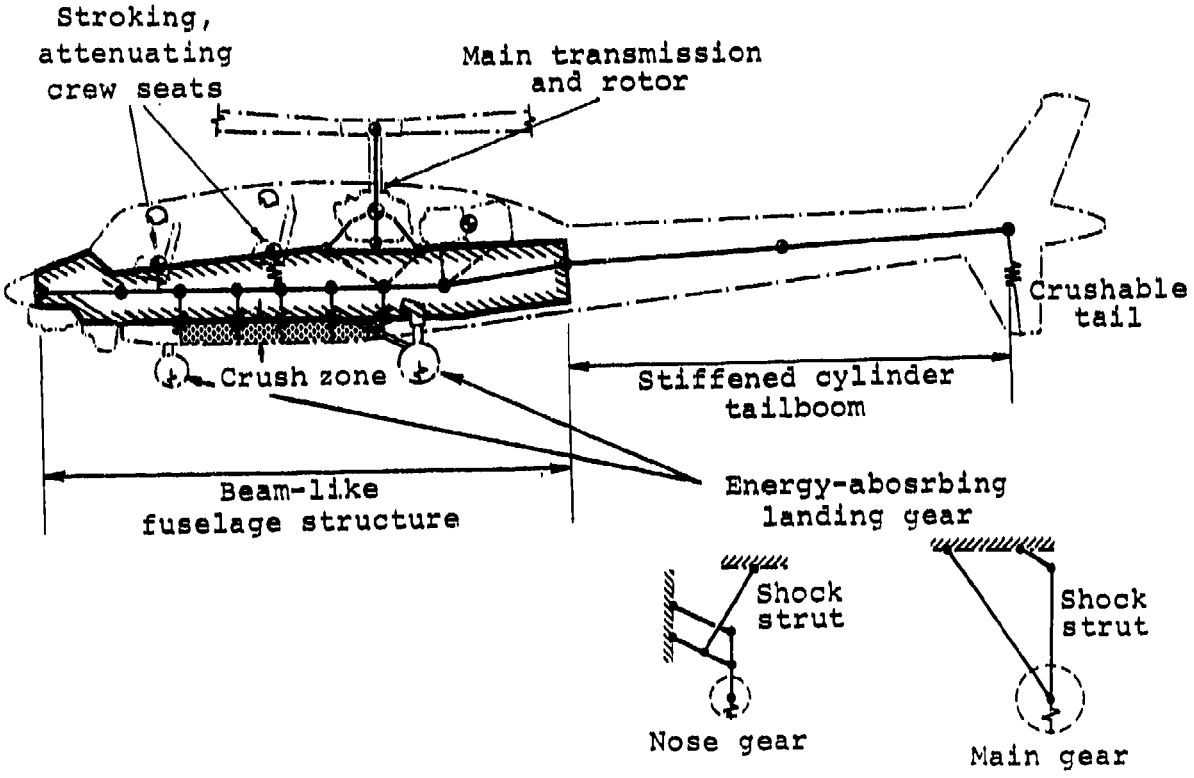

Figure 15. KRASH math model of YAH-63 test article.

TR-74-12 (Reference 9). The vertical fin was modeled with a crushable spring attached to the end of the tailboom. The structural analysis is described in Appendix B.

d. The main rotor pylon was modeled with beams in sufficient detail to represent the nodal beam and lift link assembly, the crash links, and the mast bending flexibility. The main rotor was modeled as a lumped mass. The two engines were modeled as lumped masses properly located and offset from the fuselage beam elements.

e. The main and nose landing gears were modeled with beams that represented all of the linkages and structural members for each gear. The properties of the shock strut were derived from drop test data of a main landing gear shock strut and a landing gear analysis (see Section 3). The tire and wheel load-deflection characteristics were modeled with crush springs.

The linear and nonlinear modeling is discussed further in Sections 4.3 and 4.4 following a brief description of the KRASH program.

4.2 KRASH DESCRIPTION

The KRASH computer program is a widely used analytical tool for the study of aircraft structure crashworthiness. KRASH is a nonlinear dynamic response analysis for simulating the crash impact behavior of any arbitrary three-dimensional structure generally using coarse structure models consisting of beam and spring elements. The analysis includes both geometric and material nonlinear structure behavior capability. In Reference 10, KRASH is described as a "hybrid"

---

[9]Park, K. C., and Wittlin, G., DEVELOPMENT AND EXPERIMENTAL VERIFICATION OF PROCEDURES TO DETERMINE NONLINEAR LOAD-DEFLECTION CHARACTERISTICS OF HELICOPTER SUBSTRUCTURES SUBJECTED TO CRASH FORCES, USAAMRDL TR-74-12, 2 Vols., U.S. Army Air Mobility Research and Development Laboratory, Fort Eustis, Virginia, May 1974.

[10]Cronkhite, J. D., Haas, T. J., Berry, V. L., and Winter, R., INVESTIGATION OF THE CRASH IMPACT CHARACTERISTICS OF ADVANCED AIRFRAME STRUCTURES, USARTL Technical Report 79-11, Applied Technology Laboratory, U.S. Army Research and Technology Laboratories, Fort Eustis, Virginia, September 1979.

crash analysis method because input data derived from other analyses or test usually is required to characterize some of the math model structure parameters.

The KRASH element library consists of mass points and massless nodes for structure geometry definition and weight distribution, beam elements for structure connectivity and stiffness distribution, and external crushing springs for structure/impact surface load introduction. KRASH employs a fixed time step explicit predictor-corrector numerical integration algorithm to solve the Euler differential equations of motion. The program computes the time history structure responses for simulated crash impact conditions. Typical output data includes mass point accelerations, velocities, displacements, kinetic and potential energies; beam element internal loads, stresses, deflections, strain and damping energies; and external spring loads, deflections, crushing and friction energies. Table 3 summarizes available KRASH input and output.

In 1973 Wittlin at the Lockheed-California Company developed the original version of KRASH for the Army (Reference 4) and later, under FAA sponsorship, an updated version of KRASH (Reference 5). The FAA version is the current KRASH analysis available to industry.

4.3 LINEAR MODELING

The first step in the YAH-63A KRASH analysis involved the development of an elastic line math model that accurately represented the beam-like airframe structure mass and stiffness distribution. To define the elastic line geometry, mass points were located along the approximate neutral axis of the airframe at the major bulkhead intersections. Mass points and massless nodes were used to define the geometry of the main rotor pylon, engines, landing gears, and seats. Following distribution of empty weights and mass moments of inertia to the appropriate mass points, the useful loads were added based on the measured test article weights (see Section 2.2). As shown in Table 4, the overall weight and cg location for the KRASH model agreed closely with the test article.

TABLE 3. KRASH INPUT/OUTPUT FEATURES

Input	Output
• Impact conditions, model symmetry, sloped surface	• Input data echo
• Connection points with mass properties (limit = 80)[1], massless nodes (limit = 50)[1]	• Mass point response - displacement, velocity, acceleration
• External springs, friction, soil, plowing (limit = 40)[1]	• Beam strain force, damping force, deflection, rupture, stress
• Internal beams (limit = 150)[1], damping, nonlinear (KR) properties, rupture force or deflection	• Spring load, deflection
• DRI	• DRI response
• Volume change, penetration	• Vehicle cg velocity
• Miscellaneous mass point data-aerodynamic lift, angular momentum, cross products of inertia, acceleration pulse	• Volume change, penetration
• Checkpoint/restart	• Energy distribution - mass (kinetic/potential), beam (strain/damping), spring (crushing/friction)
	• Summary - yield/ruptured beams, energies
	• Print and plot - responses, beam and spring data, DRI

[1]Limits on masses, nodes, springs, and beams pertain to the current released version of KRASH described in Reference 5.

TABLE 4. KRASH MATH MODEL WEIGHT AND CG COMPARISON WITH ACTUAL TEST ARTICLE

Test Article	KRASH Model
GW = 13,768 lb	GW = 13,865 lb
CG: Sta 297.2 BL - WL 79.9	CG: Sta 297.2 BL -0.3 WL 73.9
Inertias (in-lb-sec^2): Roll = N/A Pitch = N/A Yaw = N/A	Inertias (in-lb-sec^2): Roll = 54,700 Pitch = 391,400 Yaw = 362,900

The elastic stiffness distribution for the fuselage, tailboom, and wings was derived from previous NASTRAN math models of the prototype YAH-63. Figure 16 shows the KRASH airframe model and some typical structure cross sections from which the beam element bending properties were computed. Beam element parameters for the main rotor pylon system, engine mounts, and landing gears were taken directly from the actual structure cross sections since a one-to-one correspondence existed with these beam- and linkage-type structures.

As a check on the validity of the coarse KRASH structure representation, the elastic line model natural frequencies were computed using NASTRAN and compared to the corresponding frequencies from a detailed NASTRAN analytical model of the YAH-63. Proper distribution of stiffness and mass in the coarse KRASH model should give a good representation of the important airframe vibration modes up through 20 Hz. The comparison in Figure 17 shows good agreement to verify the accuracy of the simple KRASH math model. Since the T-41 crash test simulated a two-dimensional crash impact in the longitudinal-vertical plane, proper representation of the airframe vertical bending modes was considered most important for predicting structure response. A total of 38 mass points, 28 crush springs, and 60 beam elements were used.

4.4 NONLINEAR MODELING

To achieve the design goal of a crashworthy helicopter, the YAH-63 employed an energy management system comprised of the

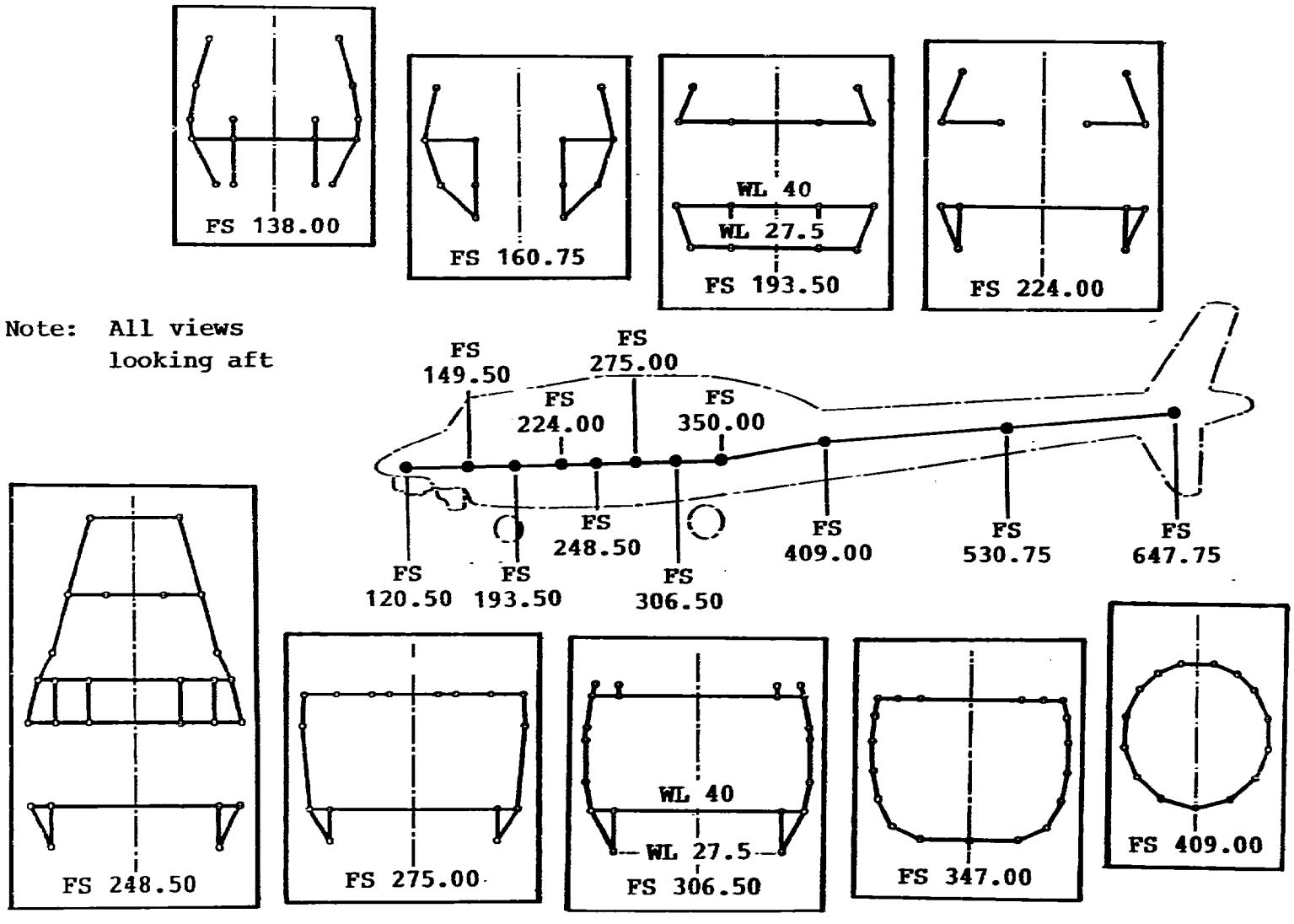

Figure 16. YAH-63 fuselage structure cross sections.

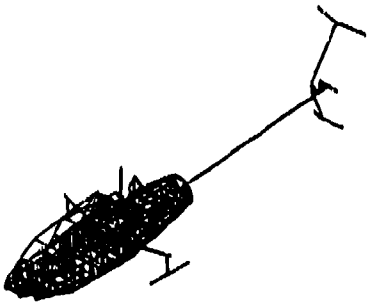

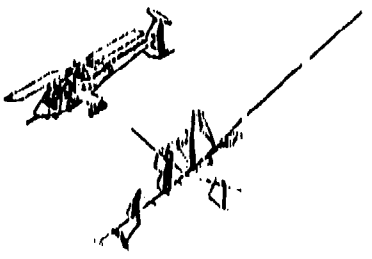

NASTRAN vibration model	Mode	KRASH model
3.60	Pylon roll	4.93
4.64	Pylon pitch	6.87
6.08	First fuselage vertical bending	5.87
6.98	First fuselage lateral bending	6.80
7.61	First nodal beam vertical	7.90
10.15	Nodal beam roll	9.23
11.23	Tailboom torsion	12.93
13.73	Second fuselage vertical bending	13.82
15.64	Main rotor mast lateral bending	16.83
15.84	Main rotor mast longitudinal bending	18.61

Figure 17. Natural frequency comparison between simple KRASH model and detailed NASTRAN model.

landing gear, lower fuselage structure, and seats previously shown in Figure 2. Landing gear stroke and fuselage crush provided energy absorption to limit the vertical crash impact forces transmitted to the large mass items, such as the main rotor transmission and engines. Energy absorption from the stroking crew seats further controlled the vertical crash loads acting on the occupants to prevent spinal injury. The energy management system components characteristically involve nonlinear structural behavior to absorb the helicopter kinetic energy in a crash impact. Test data or other analysis methods are employed to define the math model input parameters that describe the landing gear, lower fuselage structure, and seat nonlinearities, as discussed in the following sections.

4.4.1 Landing Gear

As described in detail in Appendix A, Section A.2.1, the prototype YAH-63 tricycle landing gear system consisted of a forward fuselage-mounted nose gear and two wing-mounted main gears. Each utilized an air/oil shock strut equipped with a constant orifice area pressure relief valve to provide crash impact energy absorption. The load developed in the shock strut is dependent on the closure velocity of the piston in the cylinder during a crash impact. That is, the closure velocity and load decrease nonlinearly as the landing gear strokes to decelerate the aircraft.

A problem was encountered with the KRASH computer program in modeling a shock strut directly, since the special oleo beam element provided in the latest version for this purpose does not function properly. Consequently, an alternative approach was developed that involved modeling the shock strut with a standard nonlinear beam element and using a separate landing gear analysis program to calculate the input load-deflection characteristics. The rigid body fuselage/landing gear analysis described in Section 3.2 was used to simulate a desired crash impact condition and compute the shock strut load-velocity and equivalent load-deflection properties for input to the KRASH math model.

To check out the landing gear analysis program, the YAH-63 main landing gear drop test (see Section 3) was simulated and the results compared with the measured data. Once the math model was correlated, the analysis was run using the planned 50 ft/sec resultant velocity impact conditions prior to the T-41 drop test and the actual 60 ft/sec conditions after the drop test to develop both the nose and main gear shock strut load-deflection data for the KRASH math model.

Figures 18 and 19 illustrate schematics of the YAH-63 nose and main landing gears, respectively. In addition, the pertinent KRASH math model components are shown, including the nonlinear beam elements that represent the geometry and load-deflection characteristics of the air/oil shock struts (see Figures 20 and 21). The pinned-end drag links were modeled with elastic beam elements having stiffness in the axial direction only. The nonlinear load-deflection behavior of the tire and rim was represented with external crushing spring elements.

4.4.2 Fuselage

The YAH-63 KRASH math model represents the structural characteristics of the airframe including the nonlinear behavior associated with lower fuselage crushing, vertical fin crushing, nose failure, and tailboom failure. The YAH-63 airframe structure is described in Appendix A. The calculations and assumptions used to determine the load-deflection and failure load KRASH inputs are described in Appendix B and summarized on Figure 22.

In modeling the YAH-63, a single line representation was used for the beam-like fuselage structure. Crush springs were used for the crushable lower fuselage structure below WL 40 which was assumed to be the significant crushable structure in the fuselage. Note that if the crushing of the bulkheads above WL 40 was to be considered, the fuselage could have been represented as two parallel lines of beams with crushable beam elements between them. For shell-type structures, such as utility or transport helicopters, where crash loads from overhead masses are introduced through the roof and frames to be reacted at the impact surface, modeling of the roof, floor, frames, and sidewalls would have to be considered.

The crushable structure in the YAH-63 lower fuselage (below WL 40.00) extends from FS 193.50 to FS 306.50 and consists of the bulkheads, the side frames, the BL 24.00 longitudinal beams, and the contour skin (refer to Figure 22). In a crash impact, this structure buckles, deforms plastically, and crushes to absorb energy.

The preferred approach for developing reliable structure nonlinear load-deflection data for input to the KRASH math model involves static and/or dynamic testing of typical structure specimens. Since test data was not available, the YAH-63 study employed analytical methods to derive the load-deflection characteristics of the lower fuselage structure.

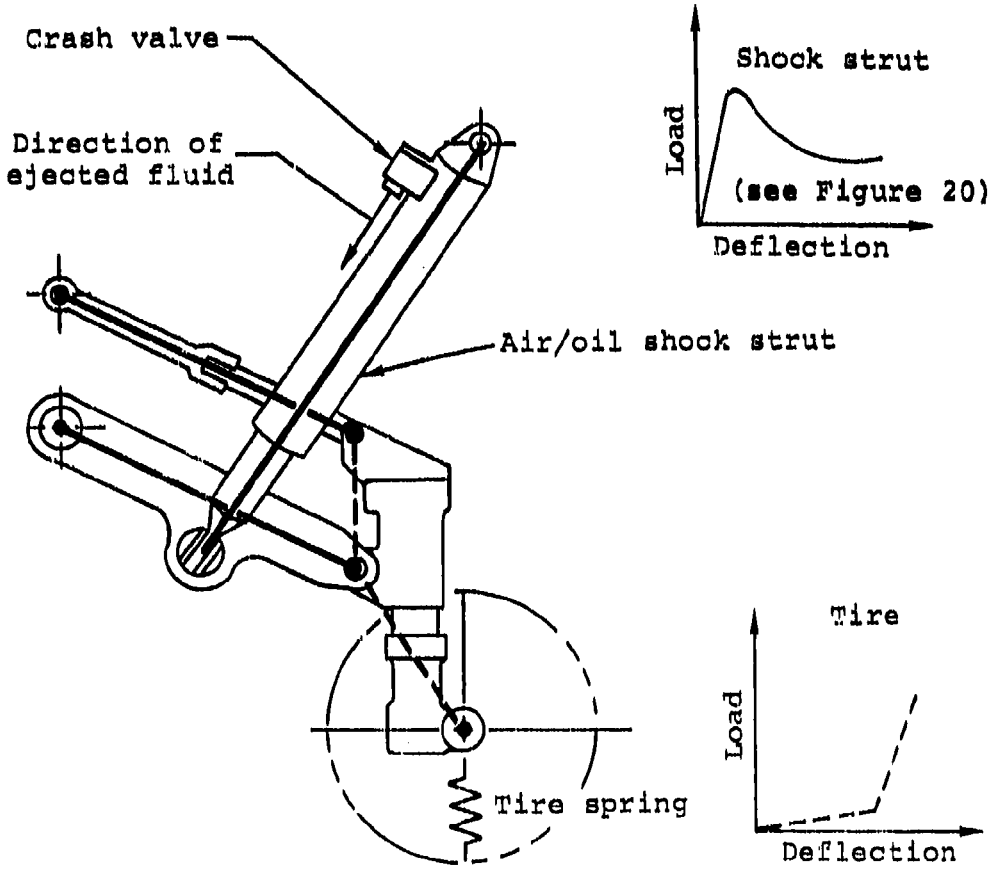

Figure 18. YAH-63 nose landing gear modeling.

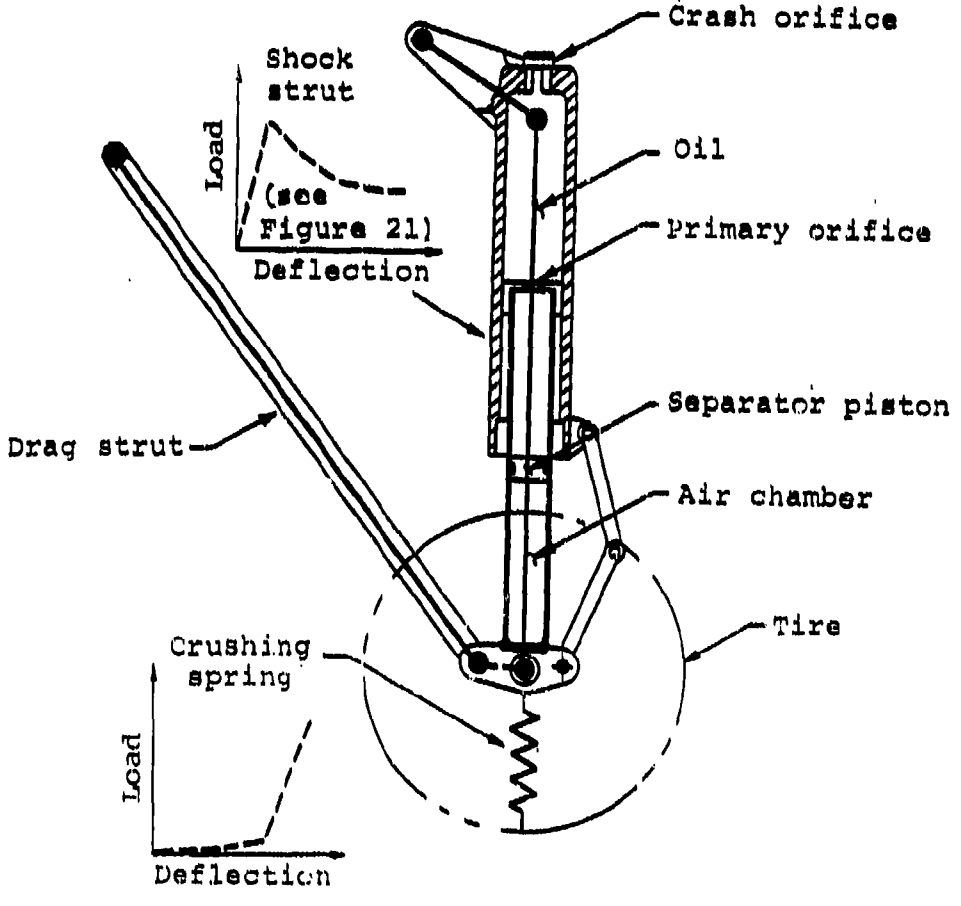

Figure 19. YAH-63 main landing gear modeling.

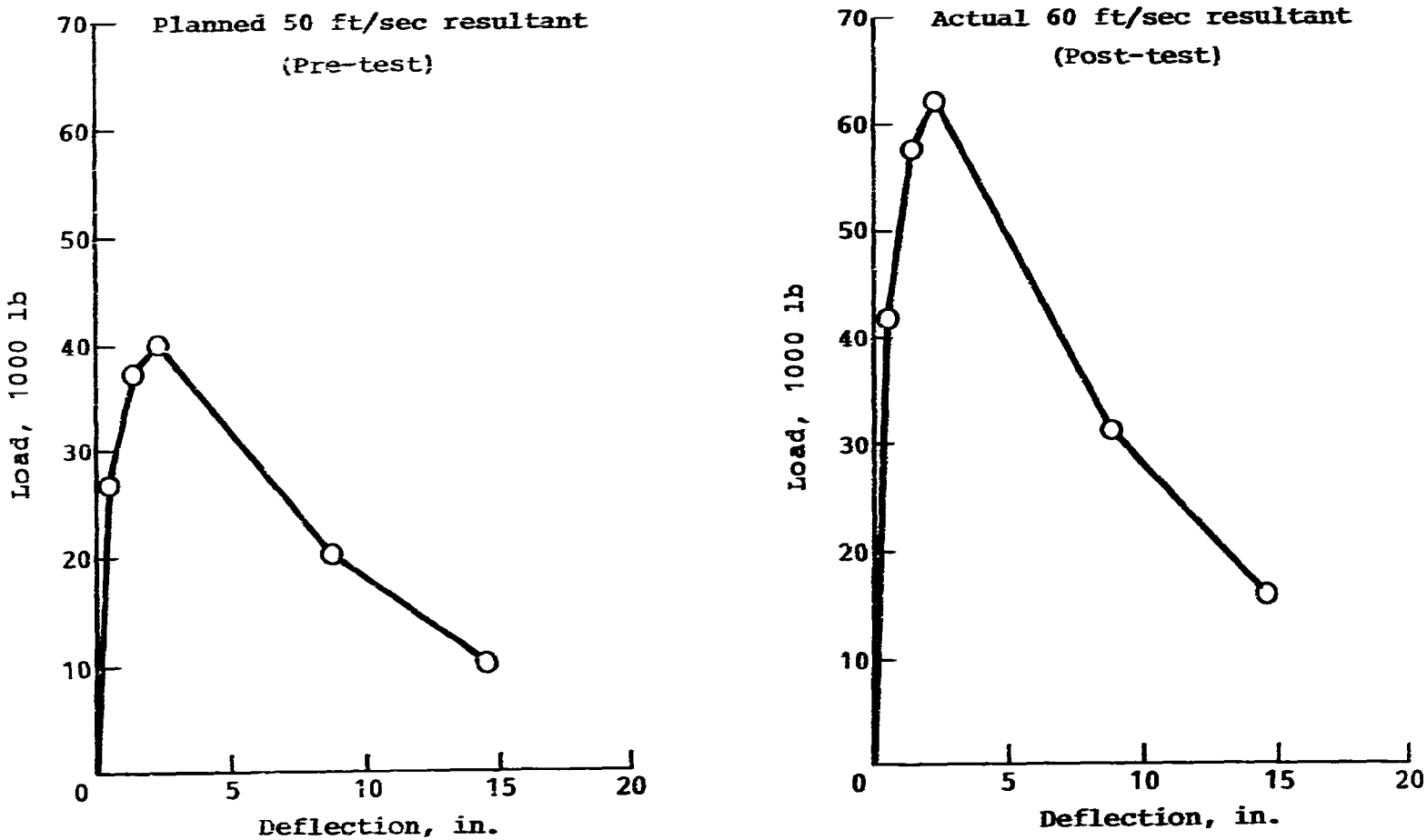

Figure 20. YAH-63 nose gear shock strut load-deflection data.

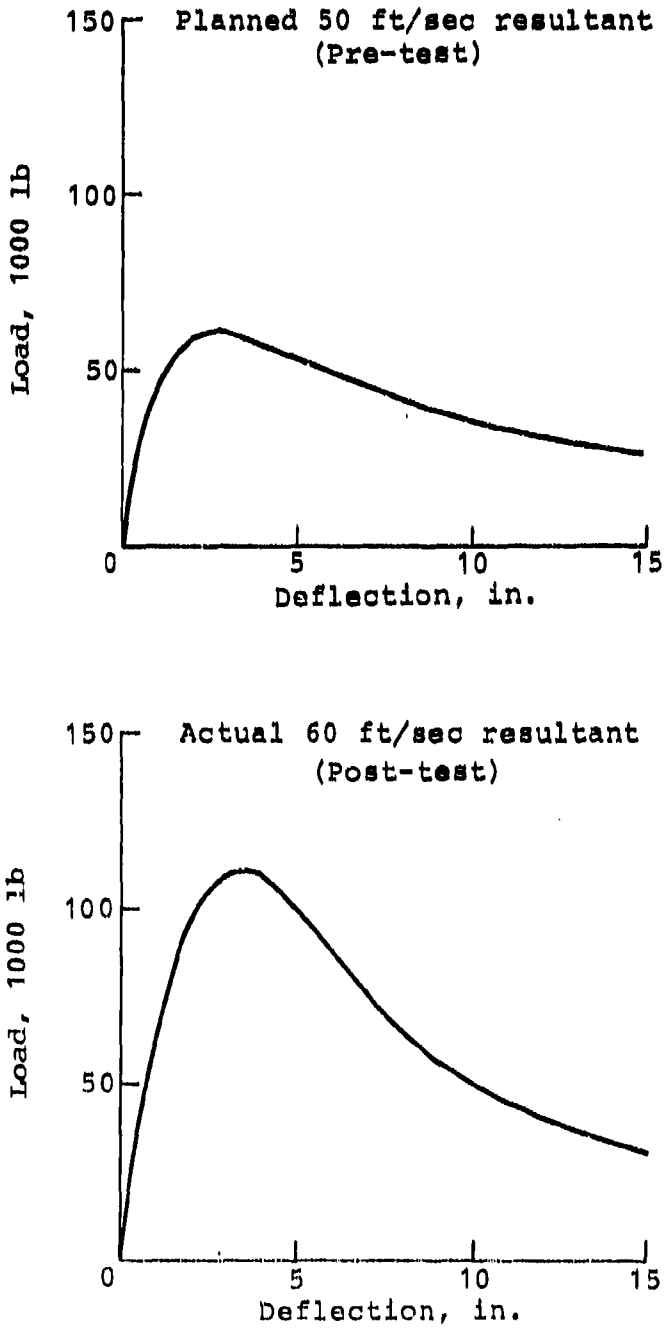

Figure 21. YAH-63 main gear shock strut load-deflection data.

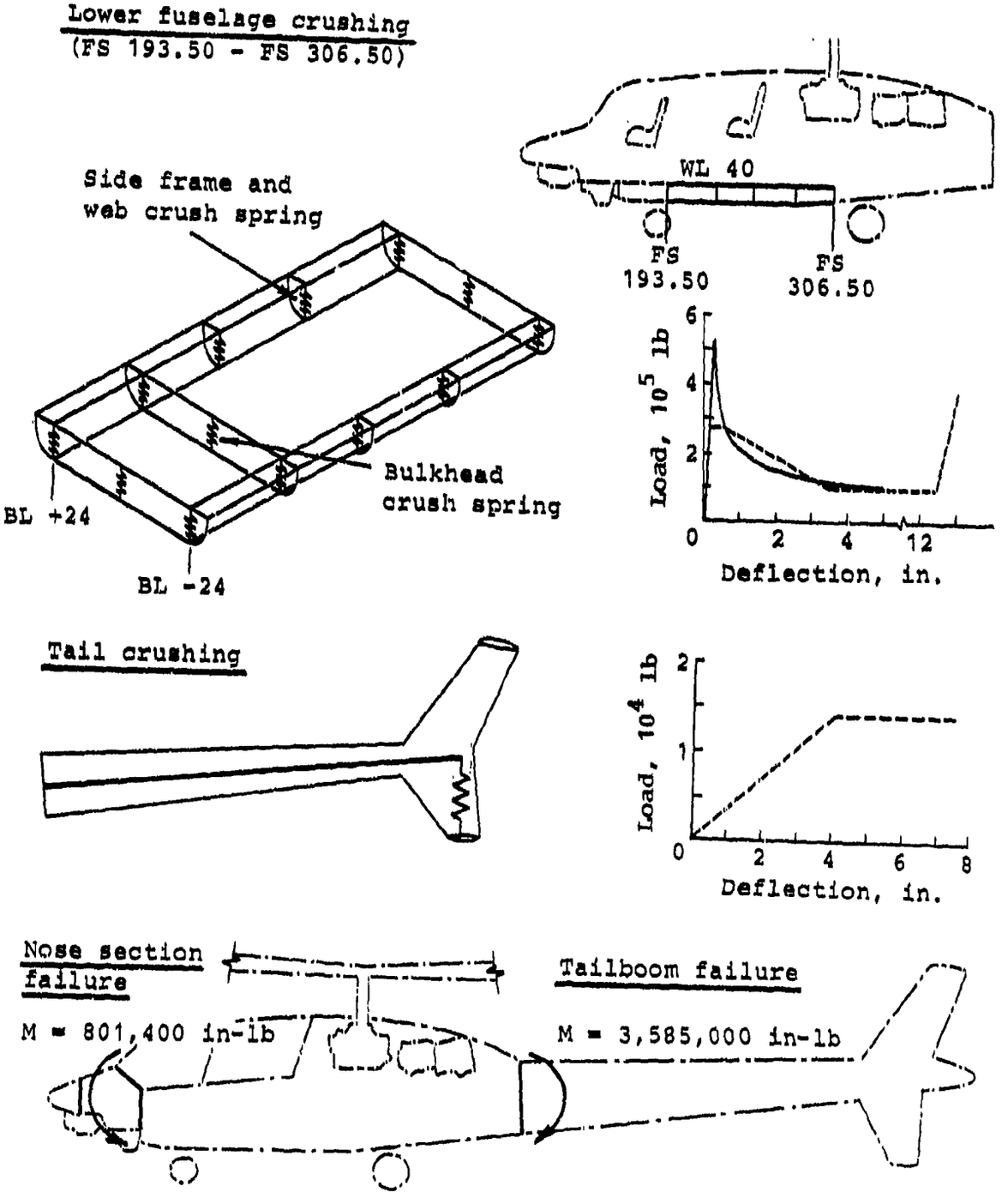

Figure 22. Nonlinear structure inputs to KRASH model of YAH-63.

Using the methods described in Reference 10, the side frame box structure and the bulkheads were analyzed to determine their nonlinear load-deflection characteristics. The side frame box structure consisted of the frames, the BL 24 longitudinal beams, and the contour skin between FS 193.50 and FS 306.50. The linear load-deflection characteristics for the structure were computed at failure using conventional strength of material techniques, while the post-failure nonlinear load-deflection characteristics were calculated using a semi-empirical approach. The structural analysis is presented in Appendix B. Note that there was a jettisonable 30mm ammunition container in the fuselage belly between FS 224 and FS 306.5 that was not considered in the calculations of the lower fuselage crushing characteristics.

In the KRASH math model, external crushing spring elements were used to represent the nonlinear load-deflection behavior of the lower fuselage structure. At each of the major bulkhead station locations (see Figure 22), vertical springs were added: two outboard on the fuselage contour for the side frame box structure and one on the fuselage centerline for the bulkhead below WL 40.

Since the vertical fin was expected to contact the ground during the impact, its crushing characteristics were included in the KRASH math model. This load-deflection data (see Figure 22) was obtained from previous studies which had been conducted during the YAH-63 prototype design program. A vertical spring was attached at the end of the tailboom to represent the lower fin structure in the math model.

Structural failures can occur such as in the tailboom that can significantly affect the structural response of the aircraft in a crash. The KRASH analysis requires representation of these pertinent structural failure modes to be able to predict the overall airframe crash impact response accurately. Considering the T-41 crash test impact conditions, the YAH-63 airframe was examined to identify critical areas where fuselage structural failure might occur. Two areas were found: the nose section from FS 138 to FS 160.75 and the tailboom at BS 100. The calculated failure loads at these locations were input to the appropriate beam elements in the KRASH math model so that a beam element rupture occurs when the internal loads exceed the input failure load. The ruptured beams are flagged and not considered in the KRASH analysis thereafter. The results are summarized in Figure 22.

4.4.3 Seats

The YAH-63 drop test article incorporated two crashworthy bulkhead-mounted crew seats. At the forward crew station (copilot/gunner), a production AH-64 seat manufactured by Norton/Simula was installed that utilized tension-loaded inversion tube energy attenuators. At the aft crew station (pilot), a prototype YAH-63 seat manufactured by Simula, Inc. was installed that utilized compression-loaded tube energy attenuators. Anthropomorphic testing dummies were placed in the crew seats to represent 50th percentile military aviators. Together with the landing gear and crushable fuselage, the crashworthy seats acted to absorb the crash impact kinetic energy and control the occupant deceleration forces within human tolerance levels.

In the KRASH math model, the crashworthy crew seats and 50th percentile occupants were represented by beam elements and lumped masses as shown in Figure 23. In addition, the model included a DRI (Dynamic Response Index) beam element and lumped mass for occupant spinal injury criteria. The seat model mass (219.5 lb) was the sum of the effective stroking weight of the seat plus the occupant lower torso weight not supported by the floor. The occupant and DRI lumped masses (74.5 lb each) represented the occupant upper body weight. The seat beam element represented the nonlinear behavior of the energy attenuators with the load-deflection properties derived by assuming that a constant 14.5g vertical stroking load was acting on the combined weight of the seat and 80% of the occupant (294 lb). The occupant body and DRI beam elements represented the upper body dynamics and spinal injury criteria, respectively, with the stiffness parameters of each standardized in the KRASH code.

In a crash impact simulation, the KRASH analysis computes the time history acceleration and DRI responses of the occupants. The potential for occupant injury can be assessed by comparing the results of the Eiband curves and DRI criteria. Based on the comparison, the energy management system, in particular the stroking seats, can be evaluated for effectiveness in decelerating the occupants to rest without injury.

4.5 PRE-TEST KRASH ANALYSIS (50 FT/SEC RESULTANT DROP TEST CONDITION)

The preliminary KRASH analysis was performed using the 50-ft/sec resultant velocity impact condition with 10° nose-up pitch attitude planned for the T-41 crash test. The

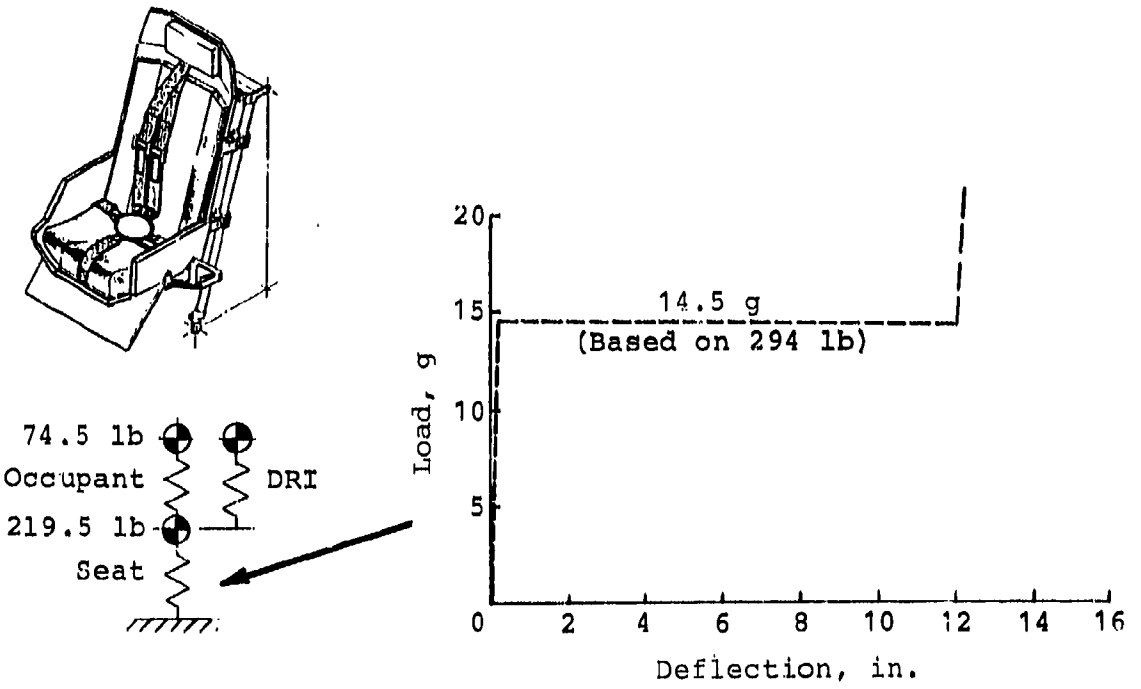

Figure 23. KRASH math model of crew seat and occupant.

sequence of important events obtained from the KRASH analytical simulation is summarized below:

a. The lower vertical fin contacts ground initially because of the aircraft structure geometry and 10° nose-up pitch impact attitude.

b. The main landing gear tires contact ground and the shock struts begin to stroke, absorbing kinetic energy.

c. The nose structure fails at FS 160.75.

d. The nose landing gear tires contact ground and the shock strut begins to stroke, absorbing kinetic energy.

e. The main landing gear structure fails after the shock struts have stroked completely.

f. The lower fuselage structure contacts ground and begins to crush from FS 306.50 forward.

g. The crashworthy crew seats begin to stroke, decelerating the occupants.

h. The nose landing gear structure fails after the shock strut has stroked completely.

i. The fuselage and larger masses come to rest.

j. The seats and crew come to rest, the forward seat fully stroking and the aft seat using about 80% of its stroke.

Some important responses from the KRASH simulation for the 50-ft/sec condition (40 ft/sec vertical, 30 ft/sec forward) are summarized below and are shown on Figure 24:

a. The fuselage vertical contact velocity was 30 ft/sec, indicating that the landing gear equivalent energy absorption capability was 26.5 ft/sec.

b. Lower fuselage structure crushing varied from a maximum of 6.2 inches at FS 275.0 to 4.6 inches at FS 193.50.

c. Vertical accelerations computed on the airframe structure included 20 g's at the aircraft cg (FS 300), 35 g's at the main transmission cg, and 28 g's at the engine cg.

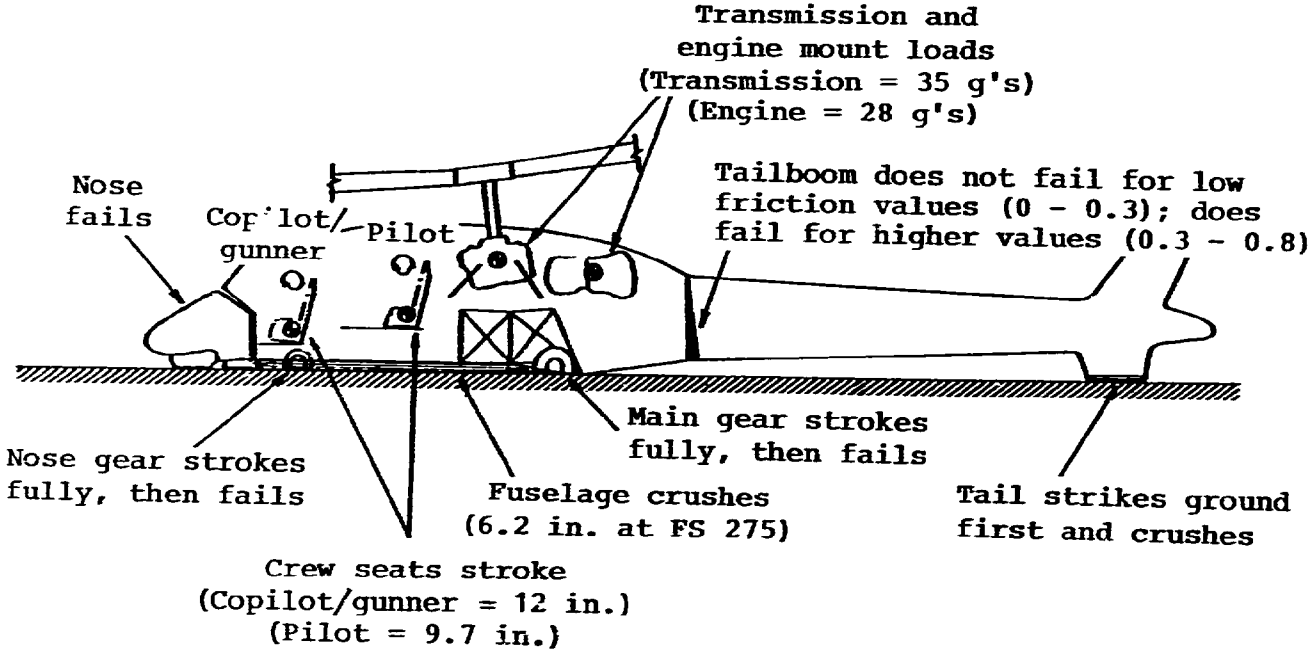

Figure 24. Pre-test KRASH results for planned T-41 crash test conditions (50 ft/sec resultant).

d. The copilot/gunner seat (forward crew station) stroked a full 12 inches (maximum capability) and bottomed out, while the pilot seat (aft crew station) stroked only 9.7 inches. The forward seat probably required more stroke because of the higher impact velocity in the nose area due to greater initial free fall drop height plus fuselage pitching and "slap-down" resulting from the initial nose-up impact attitude. Note that the free fall drop height of the nose gear above the ground when the tail contacts at 40 ft/sec is about 4 ft and can result in an additional 3.1 ft/sec nose contact velocity. Thus, due to increased free fall drop height, the nose impact velocity can be 43 ft/sec or more whereas the tail contact velocity was only 40 ft/sec. As shown in Figure 25, the DRI output indicated less than 5% probability of spinal injury for the pilot but more than 50% probability for the copilot/gunner since the seat bottomed out.

e. The 50-ft/sec impact KRASH simulation was conducted for various coefficients of friction ranging from zero to 0.80. For coefficients of friction between zero and 0.3, no tailboom failure occurred in the KRASH simulation. However, for coefficients of friction greater than 0.3, tailboom failure did occur with more fuselage pitching, which also increased the bottoming out load of the copilot/gunner seat.

The KRASH analysis predicted a phenomenon associated with the main landing gear that later was demonstrated in the T-41 crash test. For impact conditions with a forward velocity component, the friction force usually is assumed to be acting rearward on the tire at all times, putting the drag strut in tension. However, the analytical results indicated drag strut compression occurring initially before the development of a tension load. This is because of the landing gear kinematics that require that as the shock strut strokes, the wheel moves both up and aft. The resulting aftward velocity component of the gear was greater than the aircraft forward velocity, causing the friction force to act forward. Hence, the drag strut was loaded in compression initially, resulting in a considerably higher axle load until the aft velocity of the gear decreased to less than the aircraft forward velocity and then was loaded in tension. As shown in Figure 26, rearward-acting friction reduces the vertical axle load, whereas forward-acting friction increases the vertical axle load. In the discussion of the KRASH analysis correlation in Section 6.3, typical time histories are presented to demonstrate the drag strut compression-tension load reversal.

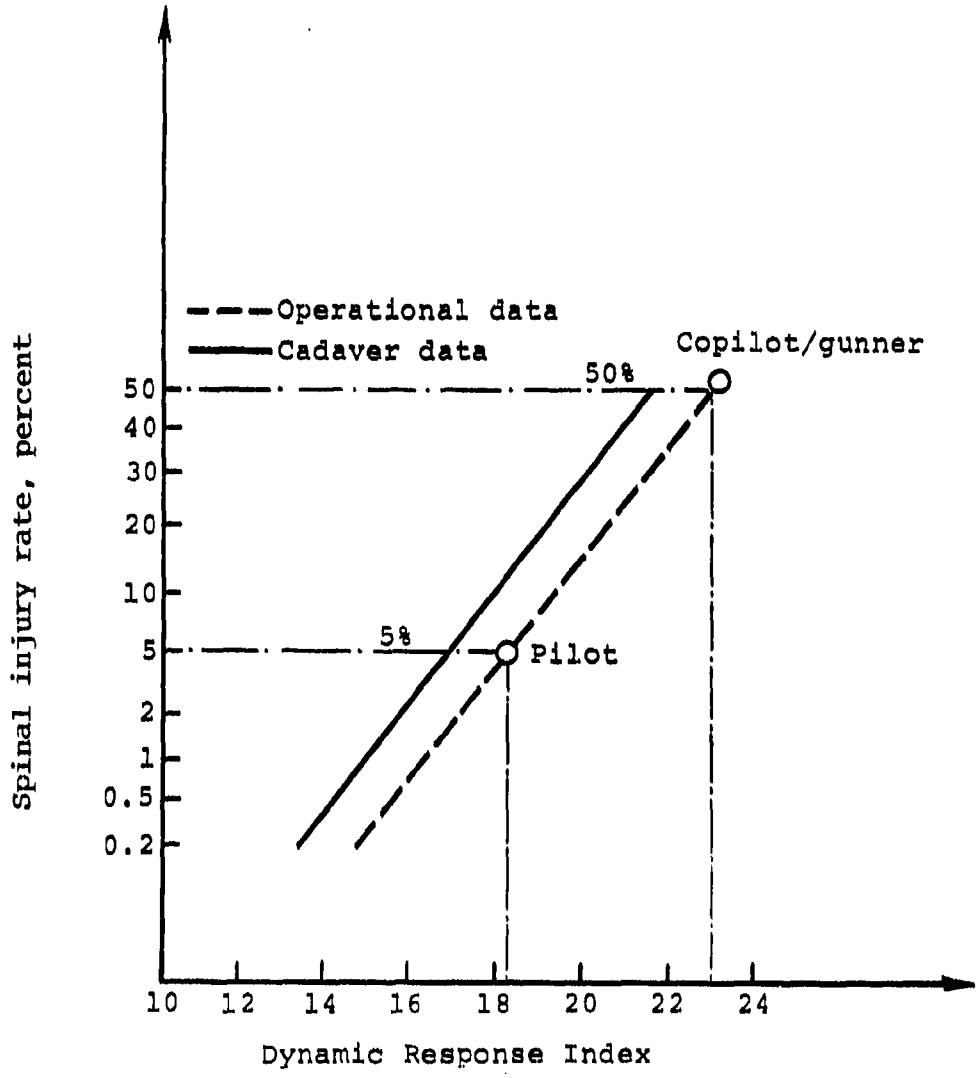

(Taken from Reference 2,
Volume II, page 66)

Figure 25. Dynamic Response Index from KRASH analysis of 50 ft/sec planned drop test condition.

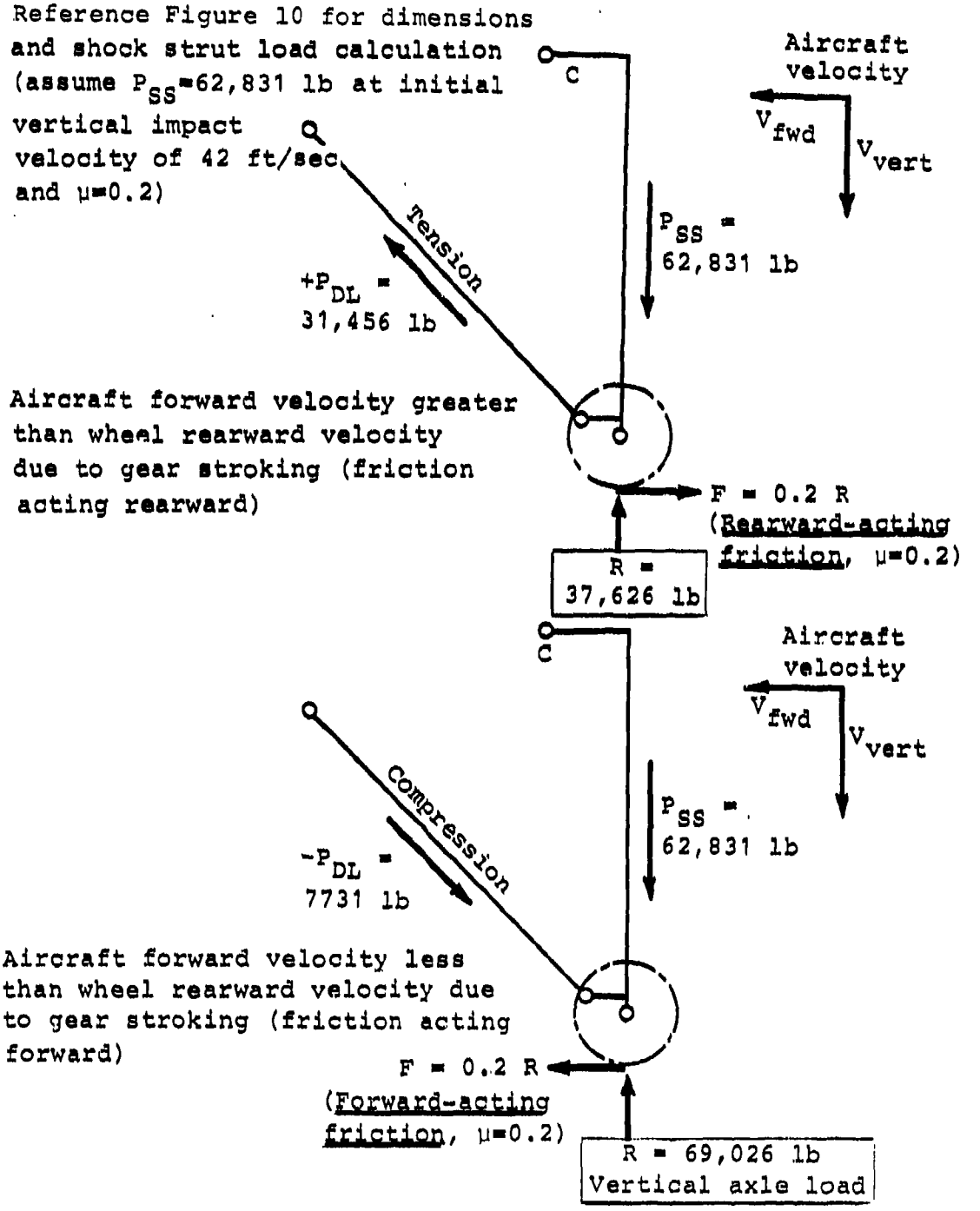

Figure 26. Effect of friction on YAH-63 main landing gear vertical axle load.

5. T-41 CRASH TEST

5.1 SUMMARY OF RESULTS

The YAH-63 crash test occurred on July 8, 1981, at the Impact Dynamics Research Facility, NASA Langley Research Center. The test setup is shown in Figure 27. In Figure 28, high-speed still photographs of the test are presented that show the sequence of events. The top row photos from left to right illustrate the major events which include tail contact, main gear contact and shock strut stroke releasing hydraulic fluid upward through the relief valve, nose gear contact and stroke, main gear failure, fuselage contact and crush, and nose failure. With regard to overall structural behavior, the predicted KRASH analytical results qualitatively agreed well with the test results, as shown in Figure 29.

A post-test analysis of the high-speed motion pictures by NASA and the Army indicated the T-41 impact conditions were much more severe than anticipated. As shown in Figure 30, the increase of resultant velocity from the targeted 50 ft/sec to the actual 60.1 ft/sec resulted in about 44% more helicopter kinetic energy at impact. Considering that the YAH-63 was designed for a maximum vertical impact velocity of 42 ft/sec, the aircraft performed well by retaining the large masses and maintaining a protective shell to demonstrate its crashworthiness capability.

The overall condition of the YAH-63 fuselage structure is shown in Figure 29. For the most part, the fuselage withstood intact the 60-ft/sec resultant impact condition, without major structural failures that might be hazardous to the occupants. The I-tail and tail rotor assembly failed the tailboom in torsion at the aft end and separated from the aircraft, as shown in Figure 31(a). The nose failed in vertical bending at the FS 160.75 bulkhead, as shown in Figure 31(b). The failure was in part caused by the 379-lb additional ballast located in the nose for the test article. The canopy structure at the forward end experienced large structural deformations striking the copilot helmet. The canopy frame deformation was caused by the absence of the flat glass in the canopy which was removed for the test. The tailboom did not fail at BS 100 due in part to the load attenuation from the separation of the I-tail and indicating a low coefficient of friction based on the KRASH analysis. As shown in Figure 32, the left wing failed at the WS 21.19 location near the landing gear upper support attachment which failed after the gear completed stroking; however, the right wing stayed on the aircraft.

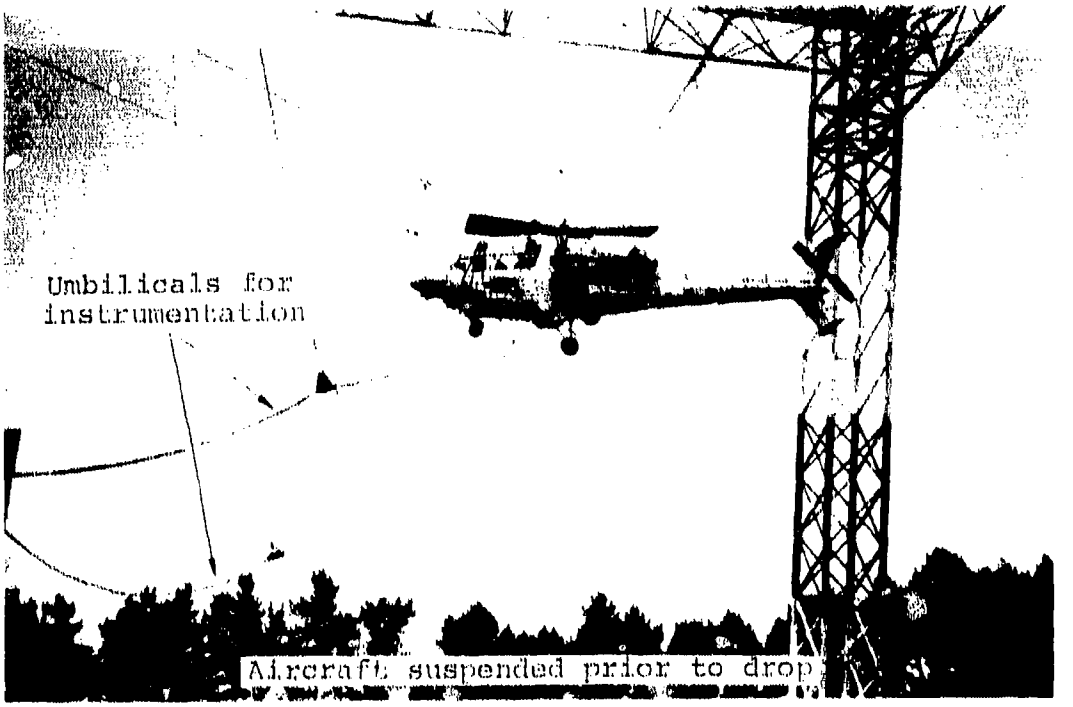

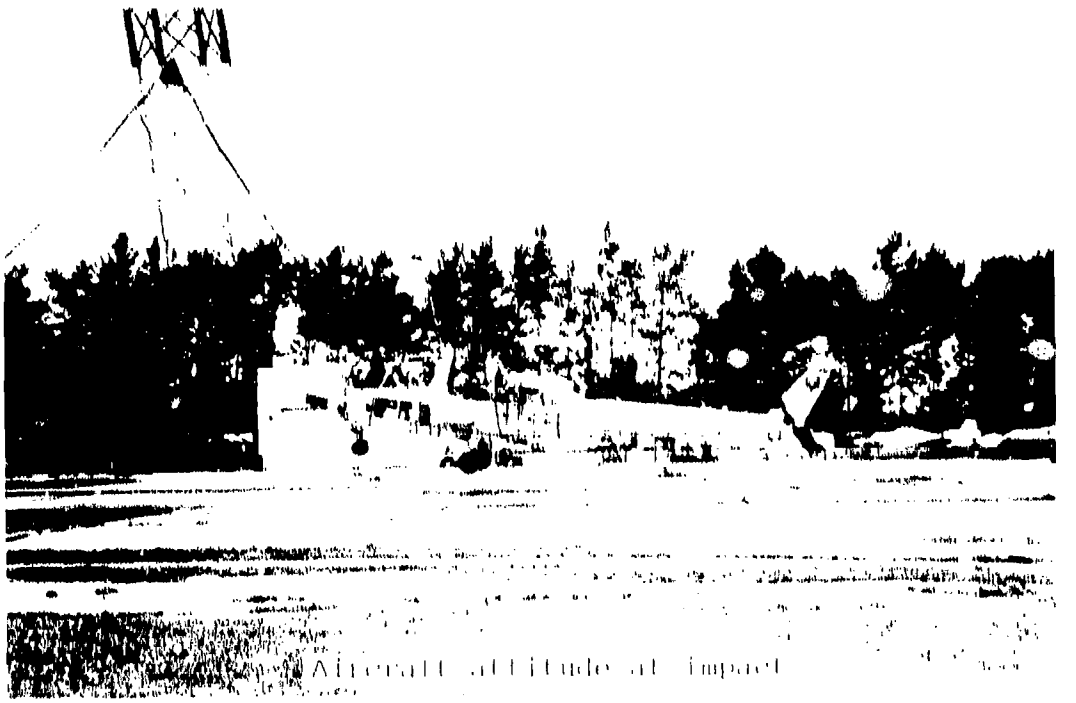

Figure 27. Water pendulum swing test setup

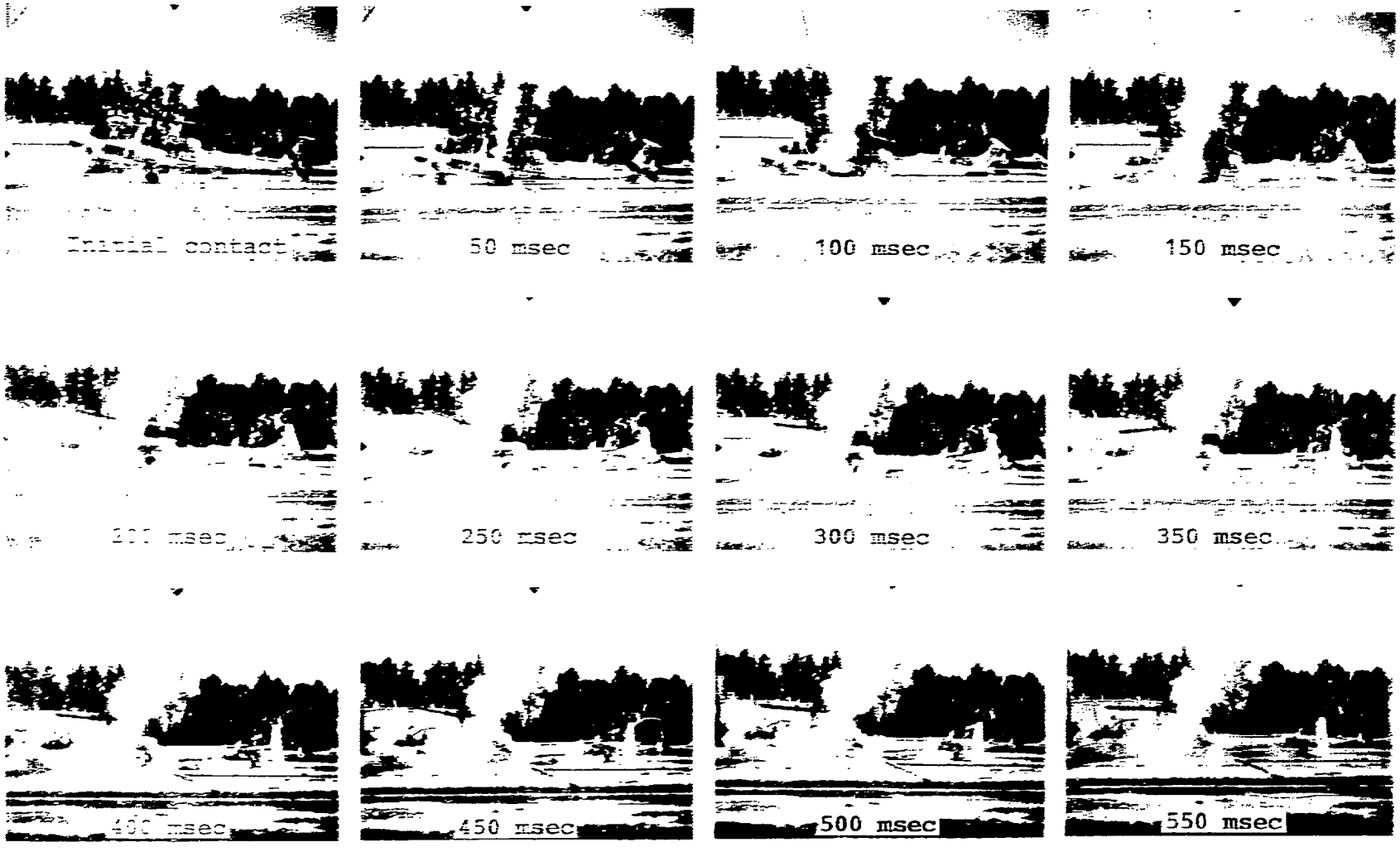

Figure 28. High-speed photographs of T-41 crash test.

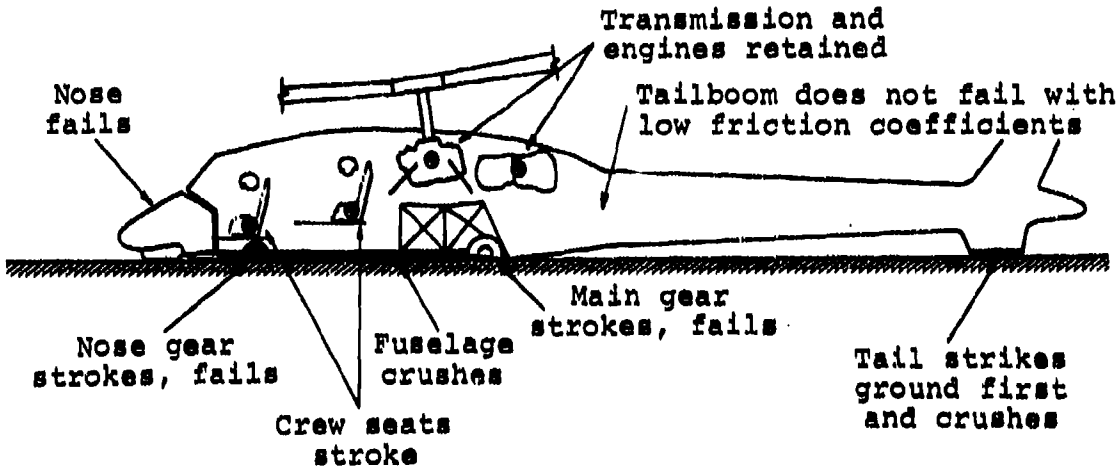

Pre-test KRASH results

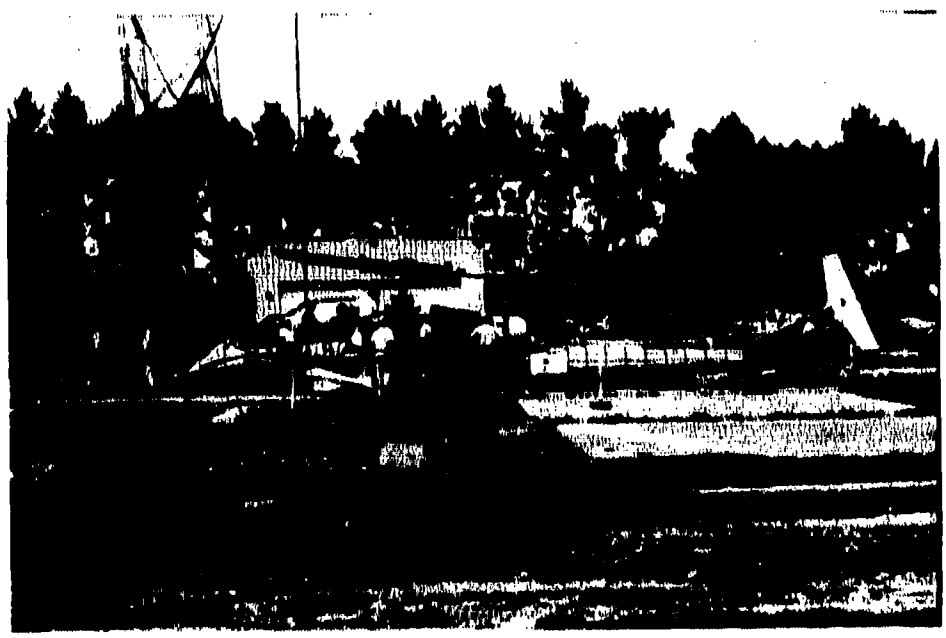

Test results

Figure 29. Comparison of qualitative results from pre-test KRASH analysis and test.

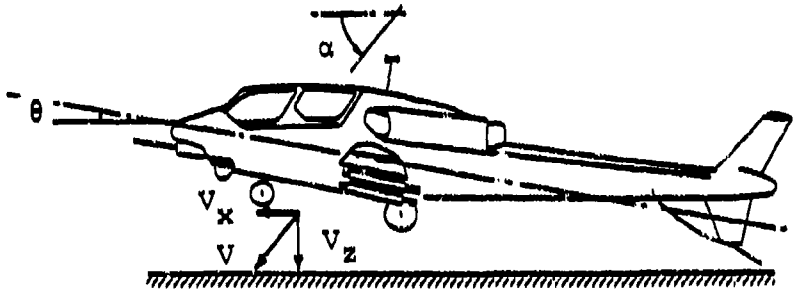

Impact condition	Planned	Actual
• Flight path angle (deg)	-53.0	-53.0
• Pitch angle, nose up (deg)	10.0	9.25
• Roll angle, left (deg)	0.0	0.5
• Resultant velocity (ft/sec)	50.0	60.1
– Forward velocity (ft/sec)	30.0	36.2
– Vertical velocity (ft/sec)	40.0	48.0

Figure 30. Comparison of planned and actual T-41 crash test impact conditions.

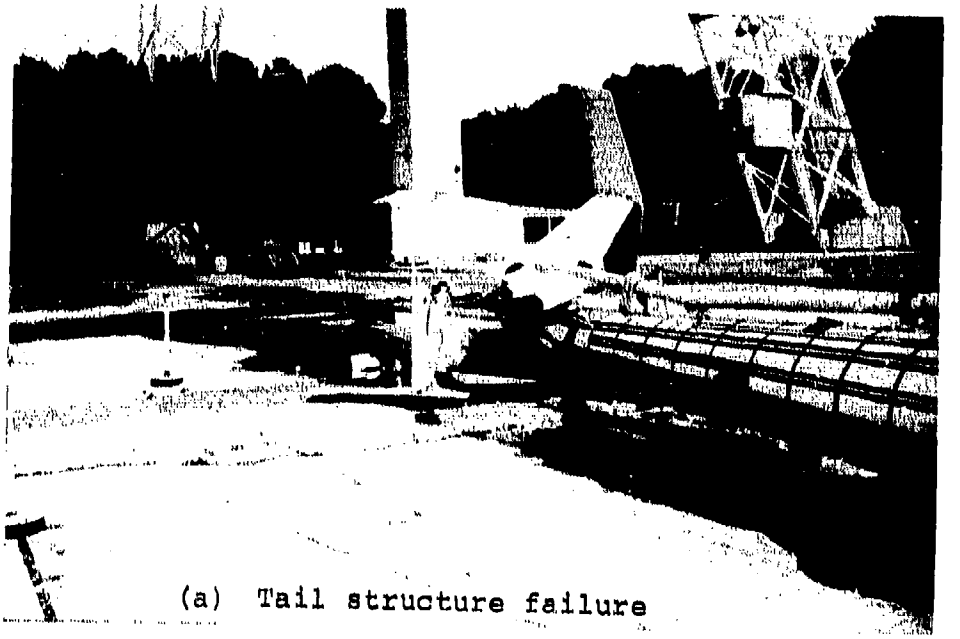

(a) Tail structure failure

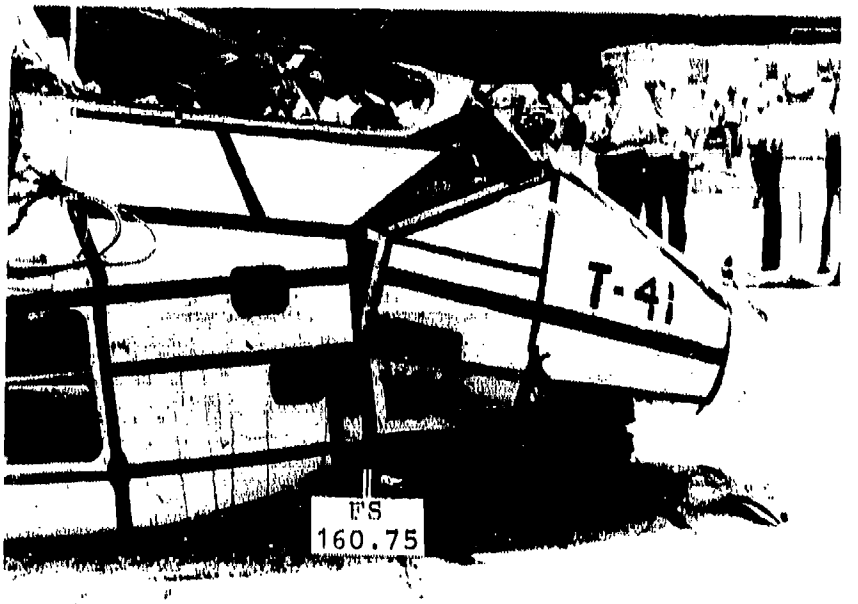

(b) Nose section structure failure

Figure 41. YAH 63 test article tail and nose structure failures.

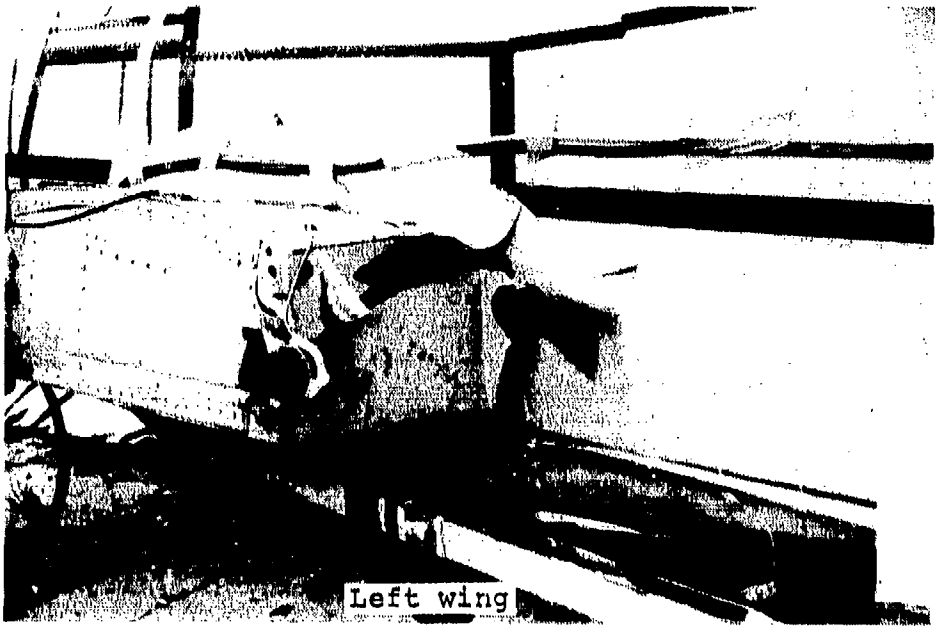

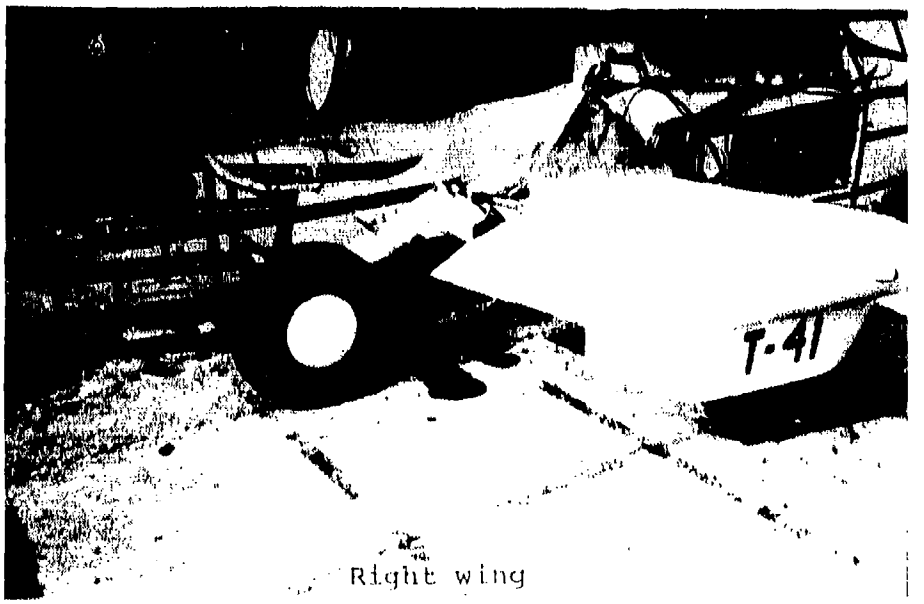

Figure 32. Post-test structural condition of left and right wings.

Other T-41 crash test results included:

a. The forward production AH-64 crew seat shown in Figure 33(a) stroked properly a full 12 inches before bottoming out, whereas the aft prototype YAH-63 crew seat shown in Figure 33(b) stroked only 2.5 inches before the compression-loaded attenuators buckled. The relative positions of the seated occupants in the aircraft before and after the test are shown in Figure 34 to further illustrate the difference in seat stroke.

b. Some fuel spillage was evident after the test. Later examination of the crashworthy fuel cells and self-sealing breakaway fittings showed no failure in these critical components. The leak was found at the forward fuel cell drain sump. As shown in Figure 35, the flange around the drain sump insert was damaged by the impingement of a piece of angle from the mock-up prototype 30mm ammunition container.

c. The main rotor pylon lift links, crash links, and support structure, as well as the engine mounts, had no visible damage, thereby retaining the large mass items in place on the aircraft as shown in Figure 36. In addition, the crashworthy crew seat attachments had no visible damage where they were mounted at the bulkhead.

d. The failure modes of the two main landing gear were similar to each other. As shown in Figure 32, the left gear failed both the shock strut upper lug attachment to the wing and the drag link lower lug attachment to the shock strut and actually separated from the aircraft. The right gear also failed the drag link lower lug attachment and the wing attachment of the shock strut was fractured, but the shock strut remained attached to the aircraft. The nose gear shown in Figure 37 failed at the forward lug attachment of the upper link to the fuselage and folded up into the well in the fuselage without interfering with the copilot/ gunner seat stroke.

5.2 DATA ANALYSIS

After the test, the recorded analog data tapes of the YAH-63 instrumentation were digitized for playback and processing

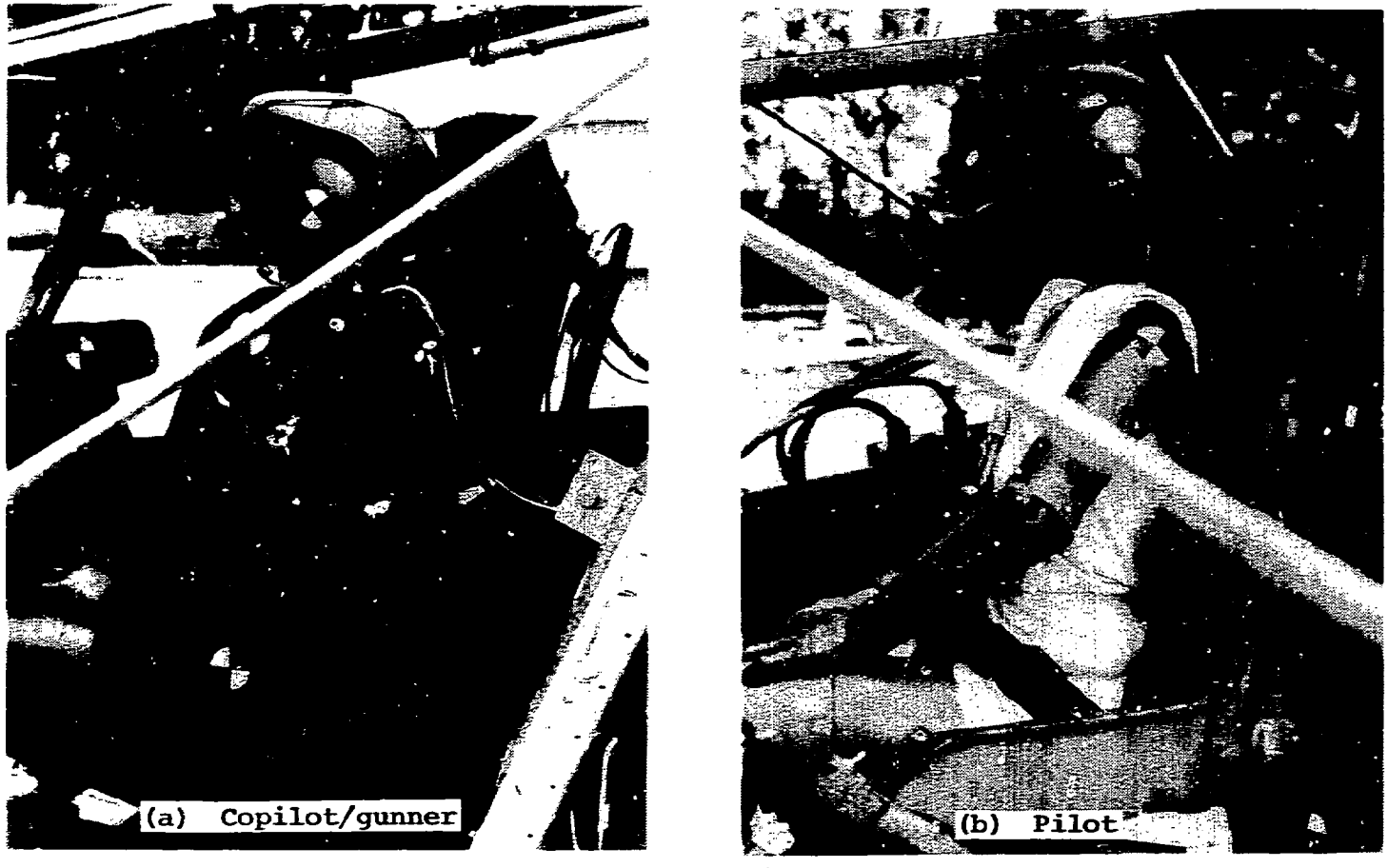

(Pre-test)

Figure 33. Copilot/gunner and pilot crashworthy crew seats.

Figure 34. Pre- and post-test structural condition of YAH-63 forward fuselage showing crew seat stroke.

Figure 35. Post-test condition of YAH-63 forward fuel cell drain sump.

Figure 36. Post-test condition of YAH-63 main transmission and engine support structure.

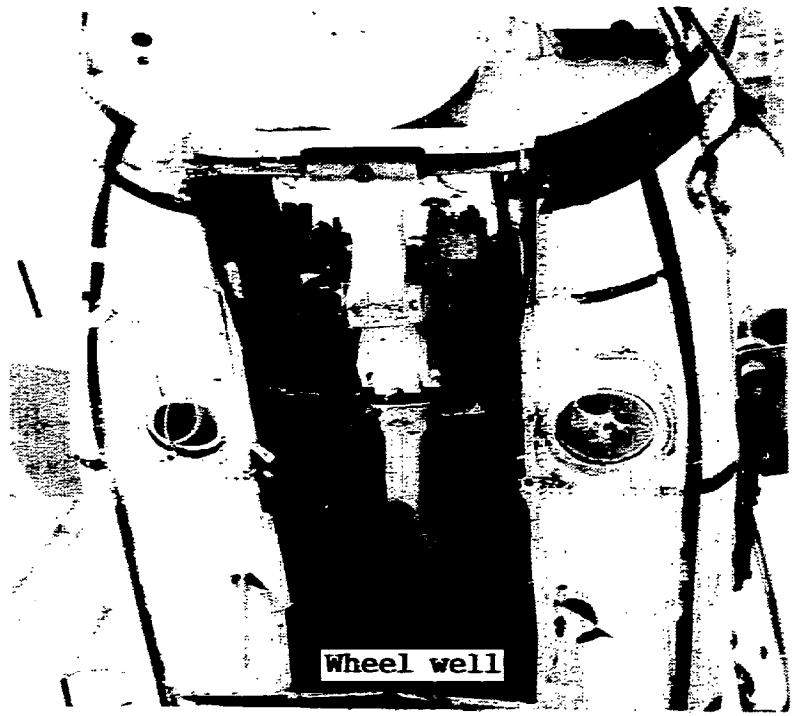

Post-test condition

Figure 37. Pre- and post-test condition of YAH-63 nose landing gear.

as shown in Figure 38. The data playback and analysis included the following steps:

a. Playback - Data tapes were played back using a Honeywell Model 9600 playback tape recorder. Depending on the number of channels to be digitized per pass, the data tape could be played back at a rate slower than 15 ips in order to expand the time scale.

b. Presample Filtering - Due to the transient nature of the test data, extreme caution was used in the application of filters. The unfiltered data had a nominal bandwidth of 0 to 5000 Hz although the transducers often limited data content to 1000 Hz or less, depending on accelerometer range. This unfiltered data was carefully examined for overloads prior to filtering.

   Next, a 2000-Hz, eight-pole Butterworth filter was used for anti-aliasing purposes and the data was digitized at 4096 samples/sec using an 11-bit analog-to-digital converter on the XEROX 530 computer. The relatively broad frequency band was sufficient to pass significant data without distortion. In addition, the broad frequency band resulted in acceptable levels of filter oscillations in the presence of step inputs.

c. Digital Filtering - Both test data and KRASH analysis data were digitized and processed through the DATAMAP program (Reference 11) for digital filtering. The filter type primarily used was a two-pole Butterworth type. For the comparison of test and analysis, low pass filtering with a 60-Hz cutoff frequency was used.

d. Double Integration - In general, double integration of test data is a difficult problem and is avoided wherever possible. Low-frequency electronic and other noise can magnify and possibly dominate the entire signal. However, when integration was used, the 180-Hz filtered acceleration data was integrated repeatedly via the DATAMAP program using Simpson's rule.

---

[11] Philbrick, R. B., THE DATA FROM AEROMECHANICS TEST AND ANALYTICS - MANAGEMENT AND ANALYSIS PACKAGE (DATAMAP), USAAVRADCOM Technical Report 80-D-30, 2 Vols., Applied Technology Laboratory, U.S. Army Research and Technology Laboratories, Fort Eustis, Virginia, December 1980.

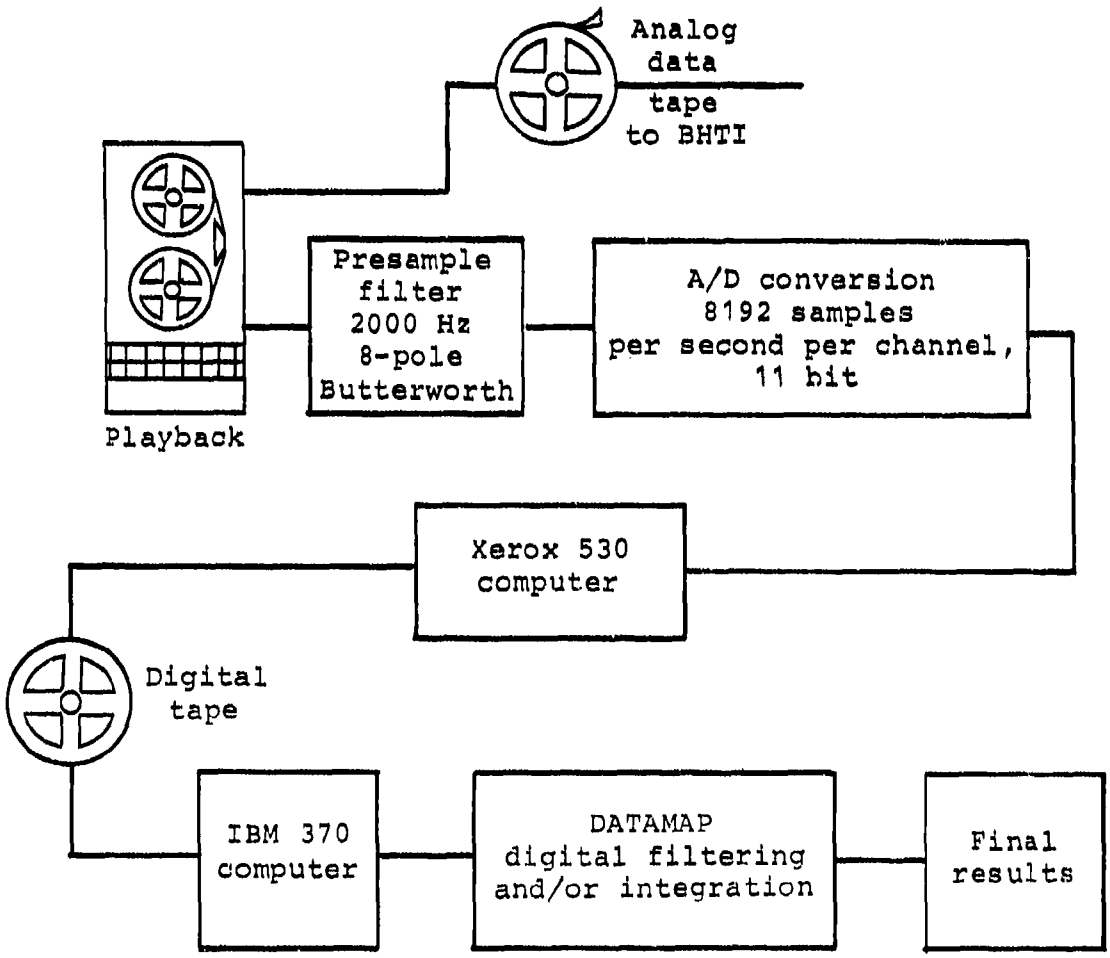

Figure 38. Data analysis flow diagram for T-41 crash test results.

For comparison with the KRASH analysis, the measured accelerometer data was filtered at 60 Hz since high frequency unimportant responses are eliminated and the major crash pulses involving significant displacement and deformation of the structure are retained. (Note that a complete set of unfiltered test data is presented in Appendix C.) Figure 39 presents typical test results for the aircraft cg vertical acceleration and shows the effects of filtering. Noise from the excitation of local modes is eliminated as more filtering is applied to the data. Because double integration of accelerometer data is unreliable for obtaining displacements, filtered accelerations are used judiciously in order to weigh more heavily the lower frequency responses indicative of significant structural deformation. For example, comparison of equal 20 Hz and 200 Hz acceleration amplitude data shows that the displacement of the 200 Hz data is only 1% that of the 20-Hz data (relative displacement is inversely proportional to the square of the frequency ratio).

The strain gage instrumentation channels were not filtered. The basic unfiltered axial load data (about 2000 Hz, low pass) was required to evaluate structural strength requirements. Filtering tends to attenuate the load (strain) time histories and is not desirable.

The complete set of unfiltered time history data measured on the T-41 crash test is contained in Appendix C. The recorded data channels known to have accuracy problems are labeled on the corresponding time history plots.

The crash impact sequence of events is evident in some of the acceleration time histories. For example, in Figure 39 the helicopter cg acceleration time history clearly shows the occurrences of initial impact, landing gear stroke, and fuselage crush. Relating actual events with the time histories is useful for understanding the test data.

The most important aspect in the design of a crashworthy helicopter is to prevent occupant injury in a crash impact. To better evaluate the YAH-63 crashworthiness capability, the occupant acceleration environment in the T-41 crash test was examined. Figure 40 shows the vertical acceleration response time histories for the crew seat bottom and pelvis. To determine the probability of occupant spinal injury, the DATAMAP computer program calculated the Dynamic Response Index (DRI) using the pilot seat bottom and copilot/gunner pelvis acceleration response. The results shown in Figure 41 indicate that the copilot/gunner would have greater than 5% but less than 50% probability of injury while the pilot would have greater than 50% probability of injury. Instrumentation problems with the copilot/gunner seat bottom and pilot pelvis acceleration channels precluded their use for the DRI calculations.

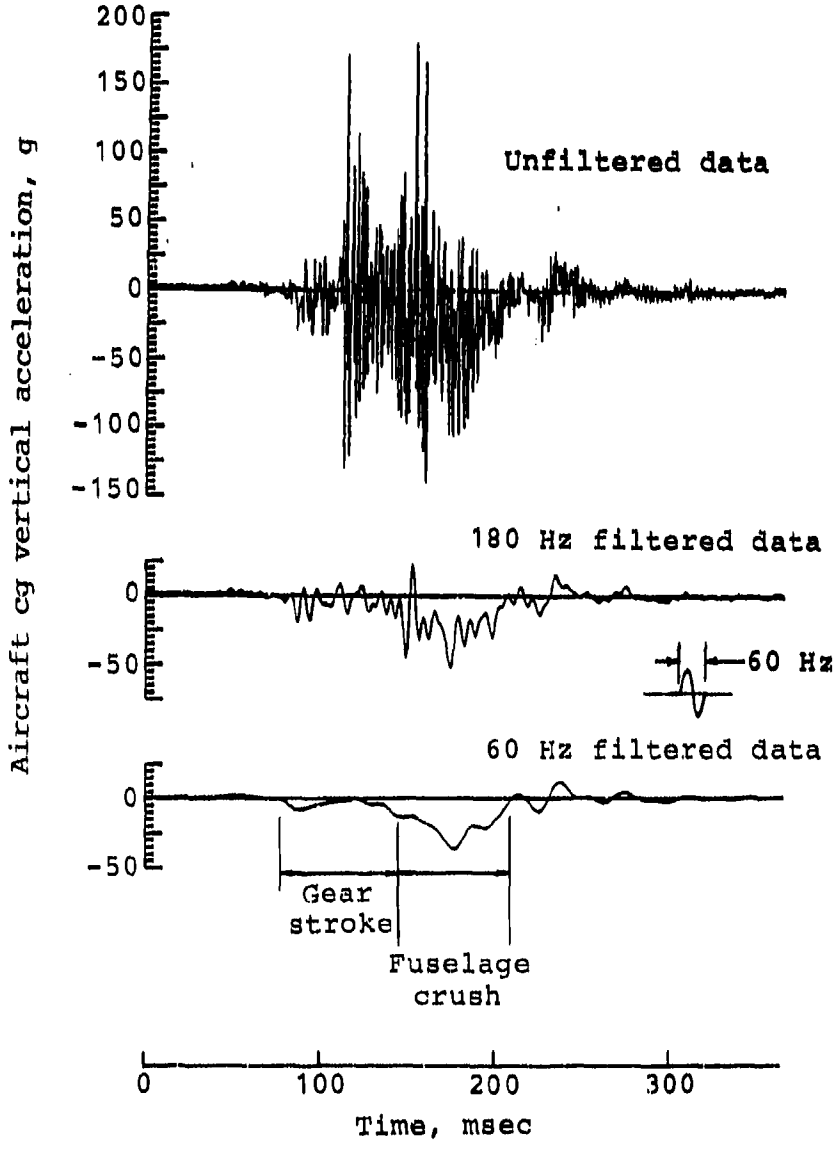

Figure 39. Filtering effects on measured test data.

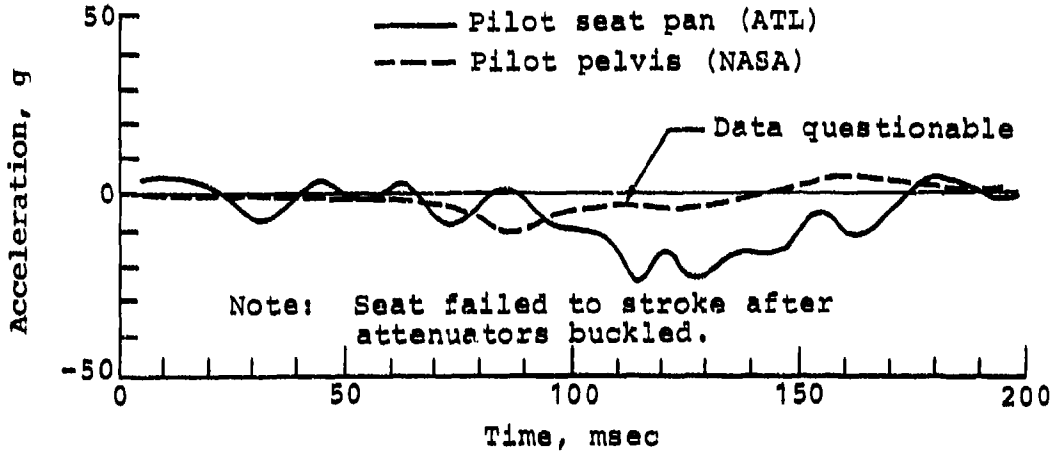

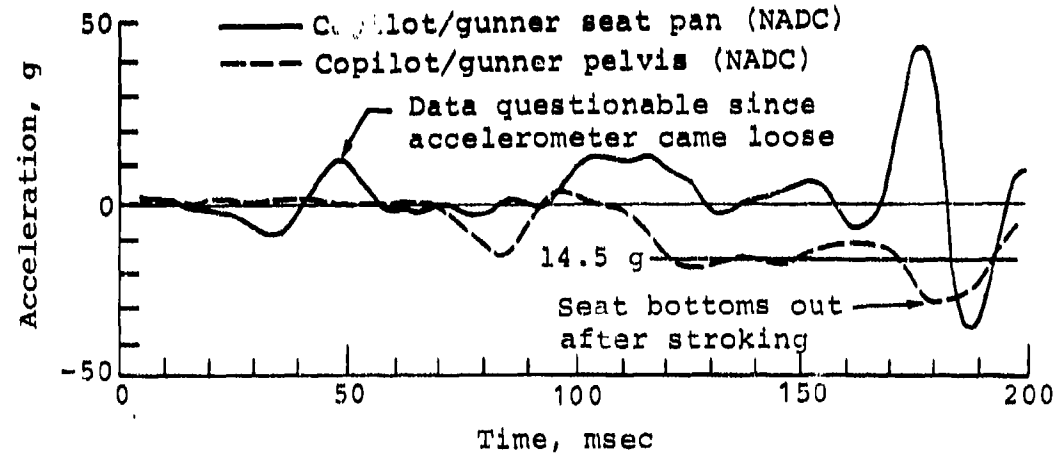

Figure 40. Crew seat pan and pelvis vertical acceleration test data.

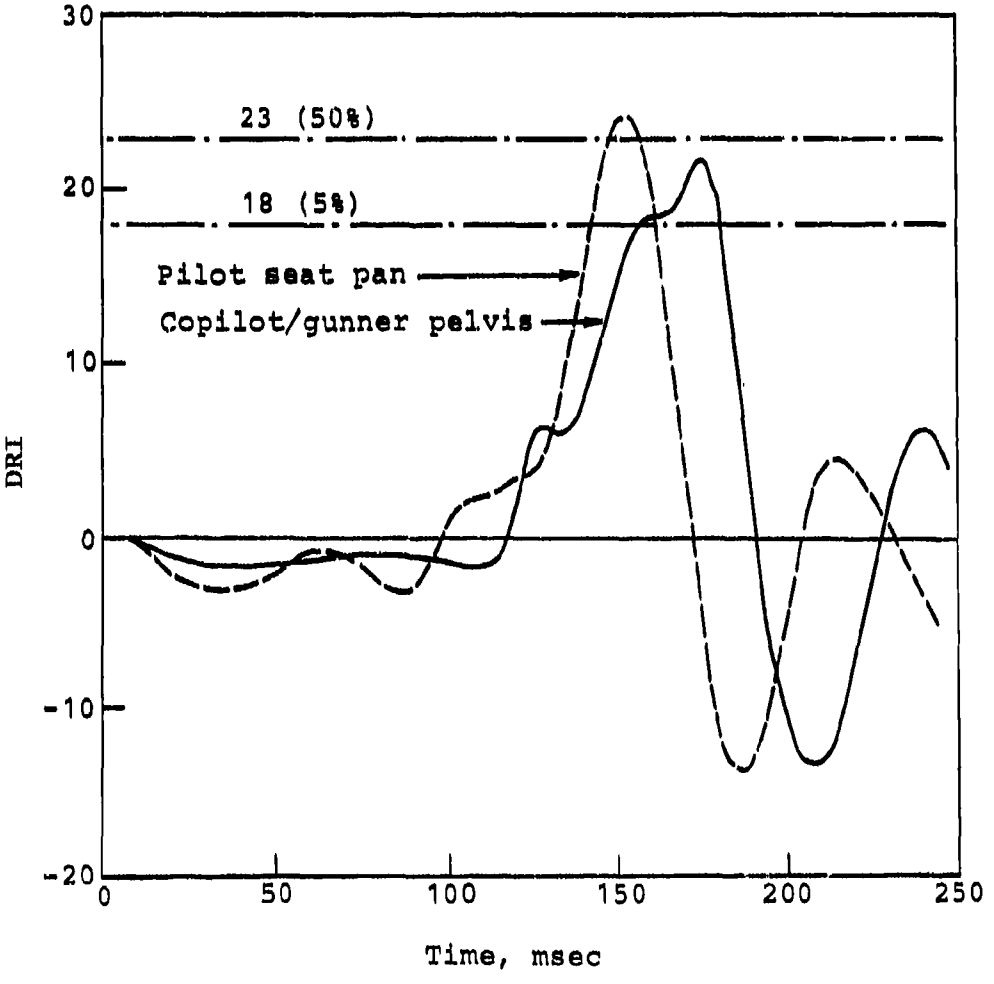

Figure 41. Crew DRI response from test data.

6. TEST/ANALYSIS COMPARISON

Because the T-41 drop test impact velocities were higher than planned (60 ft/sec compared to the planned 50 ft/sec), math model modifications were necessary to reflect the actual drop test conditions so that a direct comparison could be made between analysis and test.

DATAMAP (Reference 11) was used to facilitate the plotting and filtering of the KRASH output data for comparison with test. DATAMAP features a versatile plotting capability in addition to test data analysis methods such as digital filtering and integration. In the following sections after describing the KRASH model modifications, calculated and measured acceleration, velocity, load, and deflection time histories are compared at various points on the airframe. First, the overall structural responses are compared followed by the individual components of the energy management system (landing gear, fuselage, and seats). Note that a complete set of unfiltered test data can be found in Appendix C and filtered/unfiltered KRASH results used in the test comparison are presented in Appendix E.

6.1 KRASH MODEL MODIFICATIONS

The math model of the YAH-63 test article required modifications from the pre-test configuration to account for the higher velocity impact conditions present on the T-41 crash test. First, the 48-ft/sec vertical velocity component affected the load-deflection characteristics of the landing gear shock struts. As previously discussed, the behavior of the hydraulic energy absorber is rate-sensitive to the closure velocity of the piston in the cylinder. The pre-test KRASH analysis used load-deflection parameters corresponding to a 42-ft/sec vertical velocity impact condition with no friction or pitch angle effects considered. For the actual T-41 drop test KRASH model, the shock strut characteristics were modified for the higher closure velocity, 10° pitch angle, and friction effects based on the landing gear analysis discussed earlier in Section 3. As shown in Figure 42(a), the load-deflection data was significantly different for 48 ft/sec, having much more energy absorption capability than the 42-ft/sec condition. In addition, Figure 42(a) illustrates that friction does not alter the shock strut load-deflection significantly, whereas the pitch angle does because of its effect on the strut closure velocity. Friction, however, does increase the vertical ground

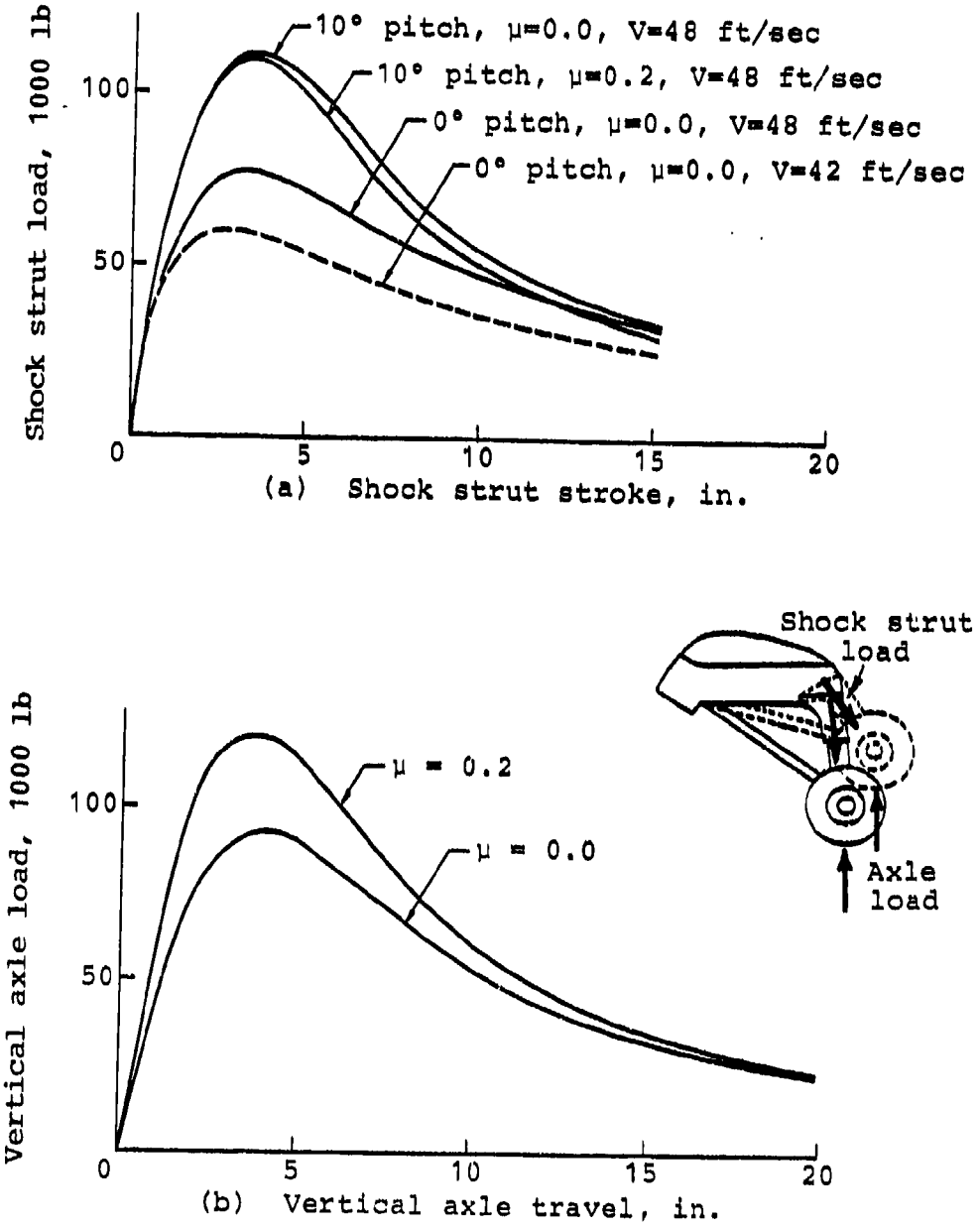

Figure 42. Effects of velocity, friction, and pitch on YAH-63 main landing gear load-deflection.

load reaction, as shown in Figure 42(b) (see also Figure 26, Section 4.5). Both the main and nose gear shock struts were updated similarly in the KRASH math model. Note that only the shock strut load-deflection data is input to KRASH. The vertical ground reaction load is calculated by the KRASH analysis, which includes the effects of gear geometry and friction.

The next modification involved extending the lower fuselage crushable structure aft. The high-speed photographs from the T-41 drop test showed that the structure aft of FS 306.50 was contacting the ground and crushing. Figure 43 shows the actual deformed structure of the test article at 100 msec from tail contact and a schematic of the original crush zone with the approximate crush line from test drawn. Substantial crushing occurred between the fuel cell bulkhead at FS 306.50 and the tailboom junction bulkhead at FS 409. As a result, the load-deflection characteristics of the additional lower fuselage structure were determined for input to the KRASH math model. The properties were based on the calculations for the original crushable structure and extrapolated for the additional structure. Essentially, the calculations assumed that the shell structure aft of FS 347 would crush similarly to the forward structure. Nonlinear crush beams in series with linear ground contact springs were placed at the FS 347 contour and centerline and at the FS 409 centerline.

The KRASH analysis was run using the modified math model and T-41 drop test impact conditions. The analysis simulated 250 msec of the drop test with a fixed integration time step of 5 μs. . Using an AMDAHL C470-V7 computer, the simulation required 122 CPU minutes to complete.

6.2 COMPARISON OF OVERALL STRUCTURAL RESPONSE

The KRASH analysis simulation of the T-41 drop test having a 30 ft/sec resultant impact velocity predicted the sequence of events listed in Table 5. Figure 44 compares actual photographs of the drop test with computer-generated deformed structure plots of the KRASH simulation. Beginning with the first photograph taken at approximate tail contact, the airframe structure condition is compared at 50 msec intervals as discussed below:

a. From initial contact to 50 msec, the main landing gear tires contact ground and the main gear shock struts begin to stroke, ejecting hydraulic fluid through the pressure relief valve at the top.

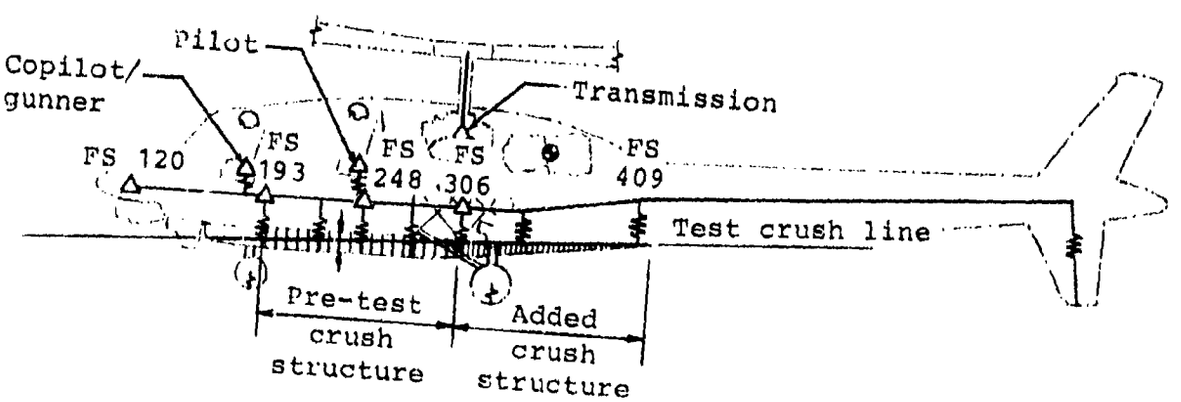

Figure 43. Fuselage crushable structure added to KRASH model of YAH-63.

TABLE 5. SEQUENCE OF EVENTS FROM KRASH ANALYSIS OF ACTUAL TEST (60 FT/SEC RESULTANT)

Event	Time (sec)
Tail contact	0.000
Left main gear tire contact	0.011
Right main gear tire contact	0.012
Left main gear stroke begins	0.024
Right main gear stroke begins	0.026
Nose failure	0.034
Nose gear tire contact	0.052
Nose gear stroke begins	0.062
Left main gear failure	0.083
Right main gear failure	0.084
FS 306.5 lower fuselage crushing begins	0.096
Pilot seat stroke begins	0.027
Copilot/gunner seat stroke begins	0.031
FS 350 lower fuselage crushing begins	0.098
FS 275 lower fuselage crushing begins	0.101
FS 409 lower fuselage crushing begins	0.105
FS 248.5 lower fuselage crushing begins	0.113
Nose gear failure	0.120
FS 224 lower fuselage crushing begins	0.122
FS 193.5 lower fuselage crushing begins	0.129
Vehicle cg zero vertical velocity	0.147
Pilot seat bottoms out	0.158
Copilot/gunner seat bottoms out	0.175

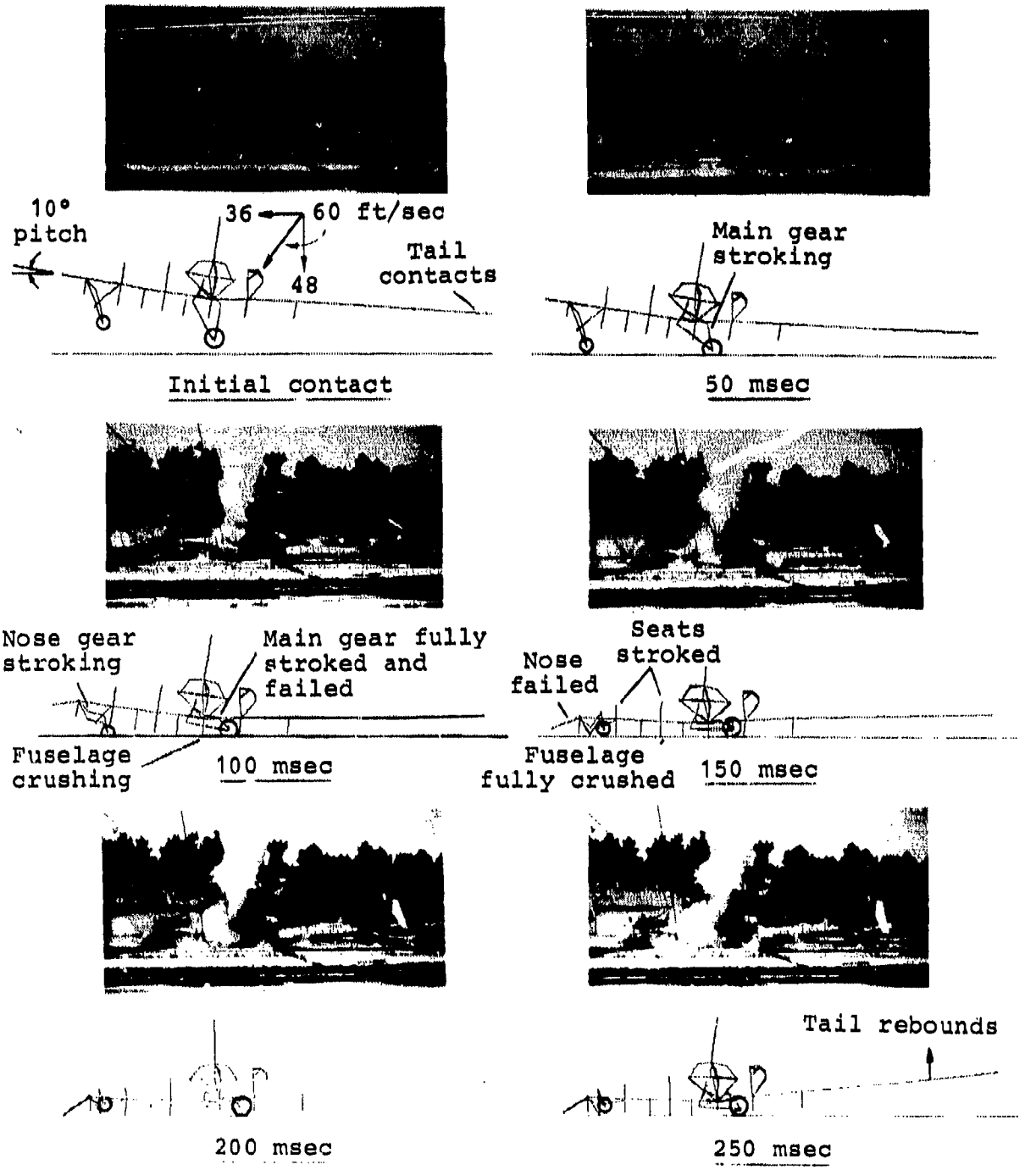

Figure 44. Sequence of events comparison between actual test and KRASH analysis.

b. In the next 50 msec interval, the nose gear tires contact ground and the nose gear shock strut begins to stroke similar to the main gear shock struts which by now have stroked fully and failed. The lower fuselage structure from FS 306.50 aft has contacted ground and begun to crush. The KRASH analysis predicts nose structure failure during this interval, although significant deformation is not yet evident in the actual photograph.

c. From 100 msec to 150 msec, the nose gear shock strut has compressed fully and failed. Crushing of the lower fuselage structure has extended forward of FS 306.50 and reached a maximum. The crew seats have begun to stroke.

d. Nose structure deformation due to failure is clearly evident. In the next interval to 200 msec, the fuselage is rebounding off the ground with nose-down pitch. The crew seats have fully stroked.

e. The final 50 msec interval shows more fuselage and tail rebound and nose-down pitch attitude with no new events occurring.

The post-test structural condition of the YAH-63 test article showed in general good agreement with the KRASH analysis. The landing gears stroked to absorb energy before failing. The lower fuselage structure crushed to absorb energy and further decelerated the aircraft to rest and attenuated the crash impact loads to the large mass items. The retention strengths of the main rotor pylon, engine, and crew seat support structure were adequate to prevent potentially hazardous displacement of the large mass items into the occupied area. The copilot/gunner seat stroked a full 12 inches and bottomed out while the pilot seat stroked only 2.5 inches before the compression-loaded energy attenuators buckled.

To correlate the events between test and analysis more precisely, the acceleration and integrated velocity time histories at the FS 248.50 pilot's bulkhead are presented in Figure 45 with the important structural events labeled. The time history comparisons show favorable agreement between test and analysis. The occurrence of main landing gear failure and fuselage contact indicates that the landing gear decelerated the aircraft from 48 ft/sec vertical velocity to about 38 ft/sec. An energy summary from the KRASH analysis

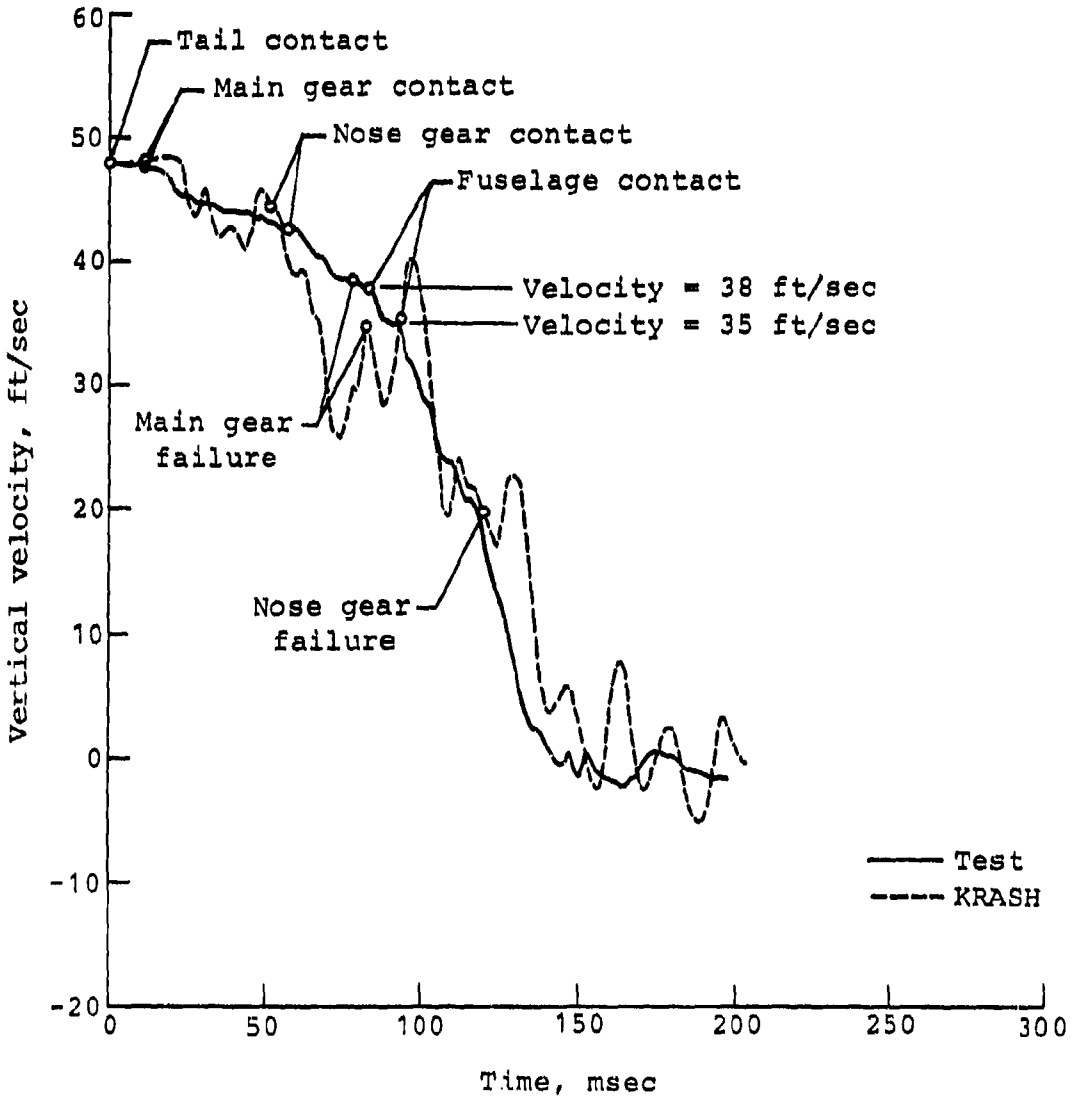

Figure 45. Test/analysis comparison of vertical velocity at the FS 248.50 pilot bulkhead.

is shown in Figure 46 and clearly indicates that most of the kinetic energy of the aircraft is reduced as the amount of strain energy is increased due to landing gear stroking and fuselage crushing. The landing gear, fuselage, and seat energy absorption capabilities are discussed in more detail in the following section.

6.3 LANDING GEAR COMPARISONS

One of the more important items of interest from the KRASH analysis was the behavior of the landing gear system and its correlation with the actual test results. In Figure 47, drag link load and shock strut rotation time histories are compared for analysis and test. In Figure 47(a), the drag link axial load shows good agreement including the initial friction-induced compression load and the final time of structural failure. The initial compression load develops because the stroking of the shock strut at a 48-ft/sec closure velocity requires the gear to move aft with a longitudinal velocity greater than the 36-ft/sec forward velocity of the aircraft at impact. Consequently, the friction force is acting forward, putting the drag link in compression. Friction increases the vertical ground reaction load and acts to stiffen the landing gear. A coefficient of friction of about 0.2 gives good agreement for drag link loads using landing gear analysis methods described in Section 3. In Figure 47(b), the shock strut rotation from KRASH analysis and test shows good agreement up to the time of structural failure (thereafter, the rotation is not important, since the gear is failed and unloaded). In Figure 45, the FS 248.50 pilot's bulkhead integrated vertical velocity was compared. The velocities agreed relatively well. Test shows the velocity reduced from 48 to 38 ft/sec prior to fuselage contact. KRASH indicates some additional landing gear energy absorption, slowing the aircraft from 48 to 35 ft/sec.

To determine the time and vertical velocity at which the actual test article contacts ground, the drag link load and shock strut rotation time histories in Figure 48 are correlated with known gear geometry shown in Figure 49. From the drag link load trace, tire contact occurs at 77 msec when the compression load first builds up. Structural failure occurs at 138 msec. Based on gear geometry, shown in Figure 49, the shock strut is compressed fully when the gear has rotated 31°. The shock strut rotation time history from test shows that 31° corresponds to a time of about 132 msec. From the landing gear and fuselage geometry, the ground line is 10 inches from fuselage contact when the gear is compressed fully at 31°. Also, at 132 msec the aircraft velocity is about 42 ft/sec. Since at least 20 msec is required

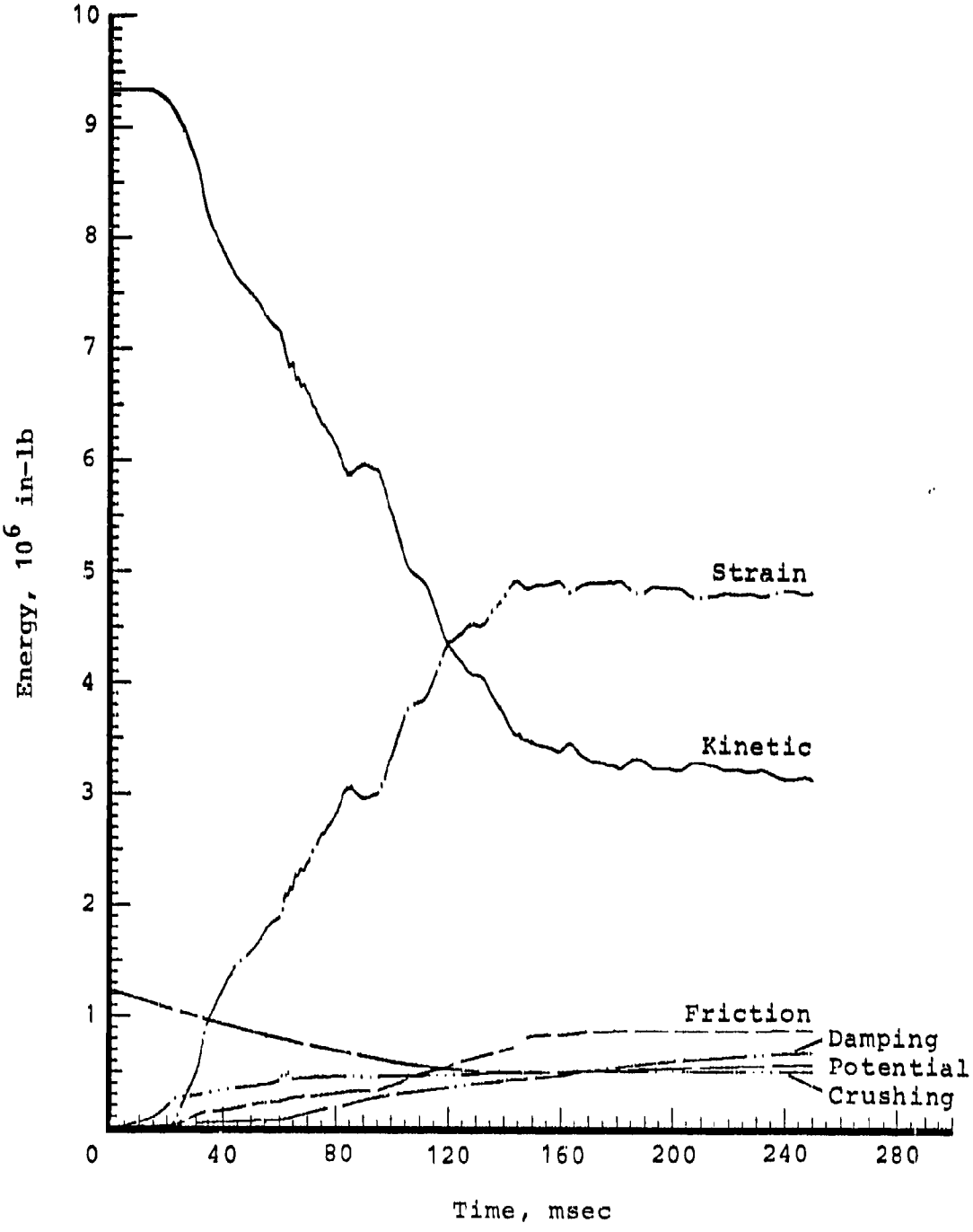

Figure 46. KRASH energy summaries for simulated 60-ft/sec T-41 crash test.

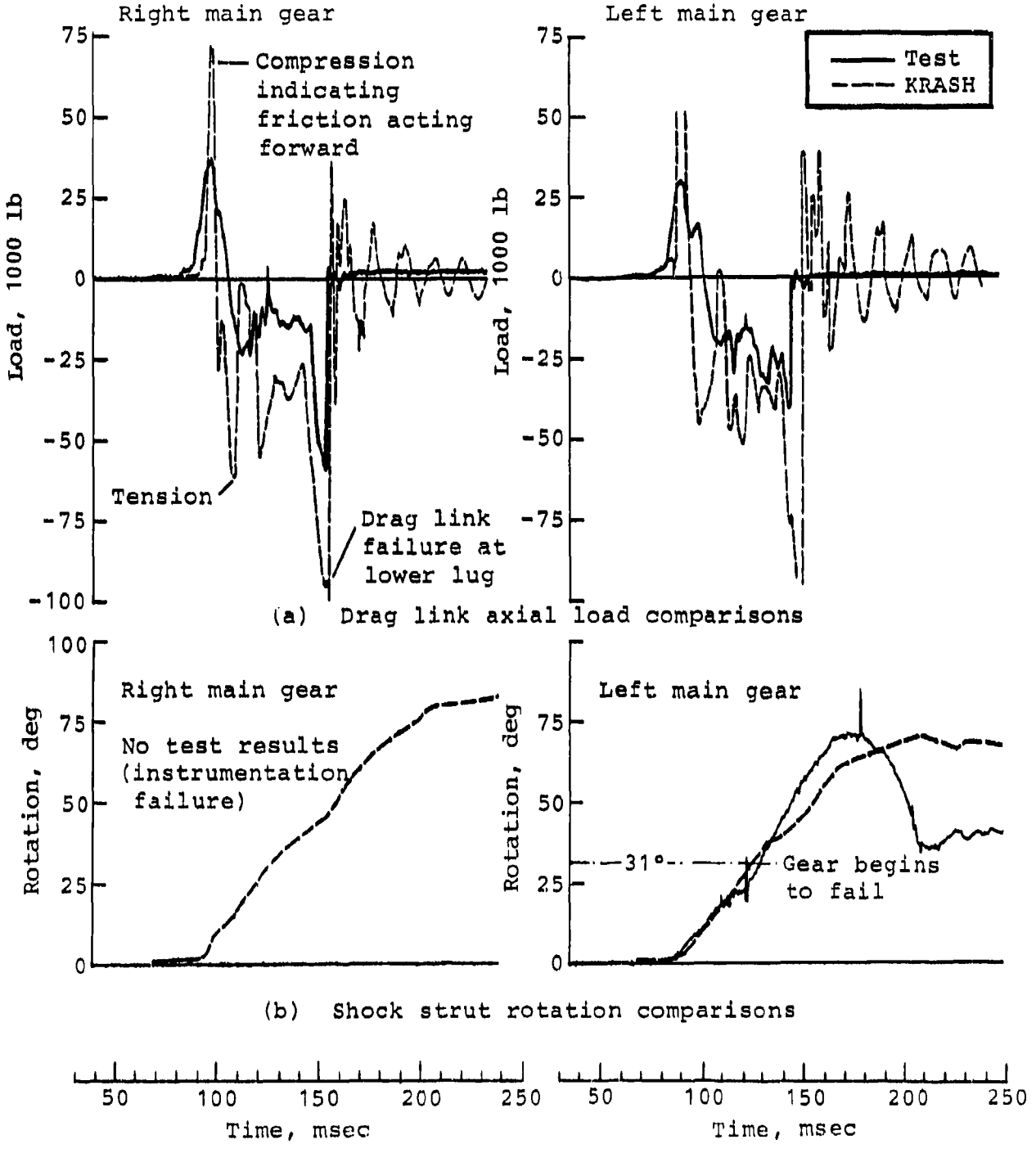

Figure 47. KRASH/test main landing gear drag link load and shock strut rotation comparison.

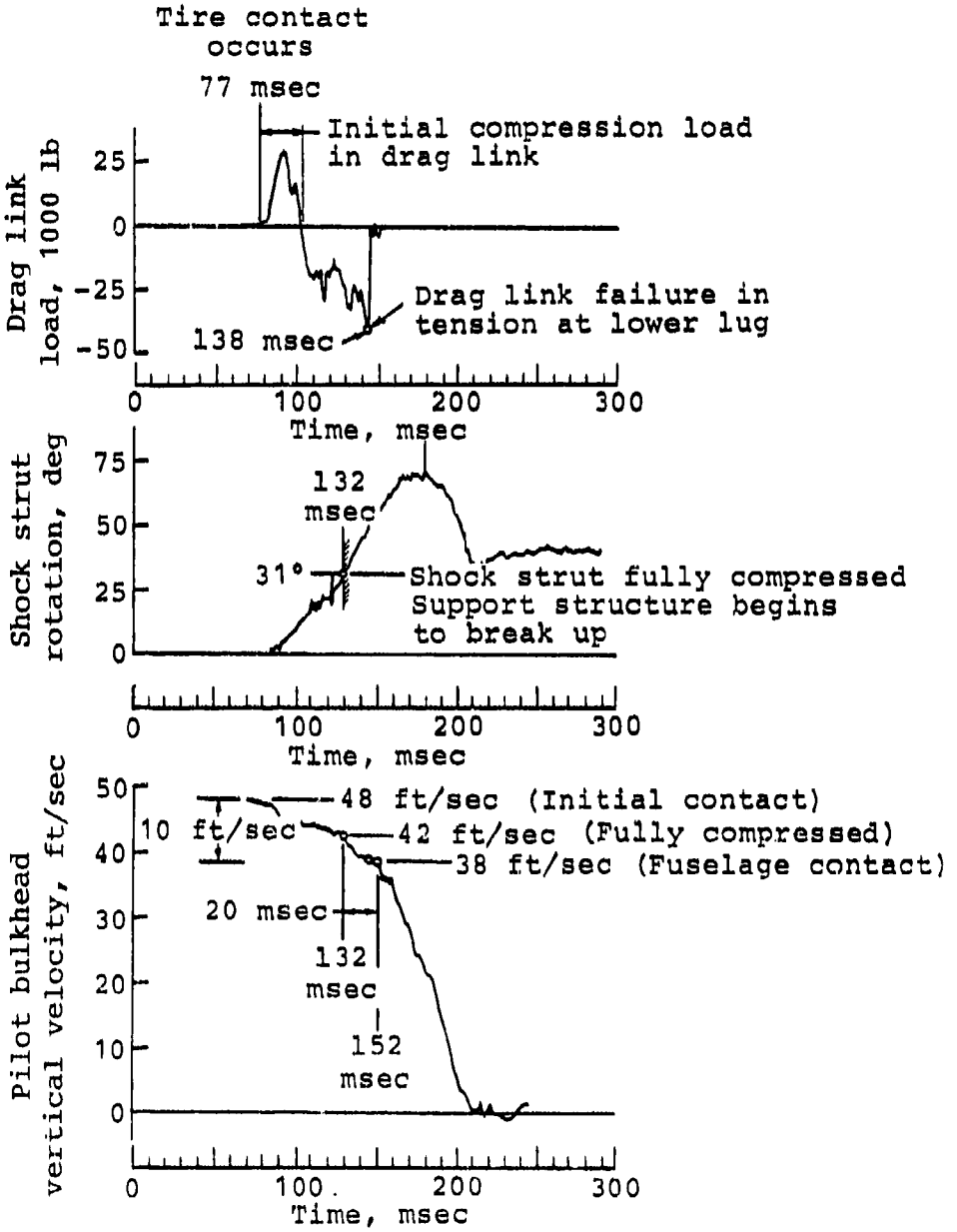

Figure 48. Determination of fuselage contact velocity from T-41 crash test data.

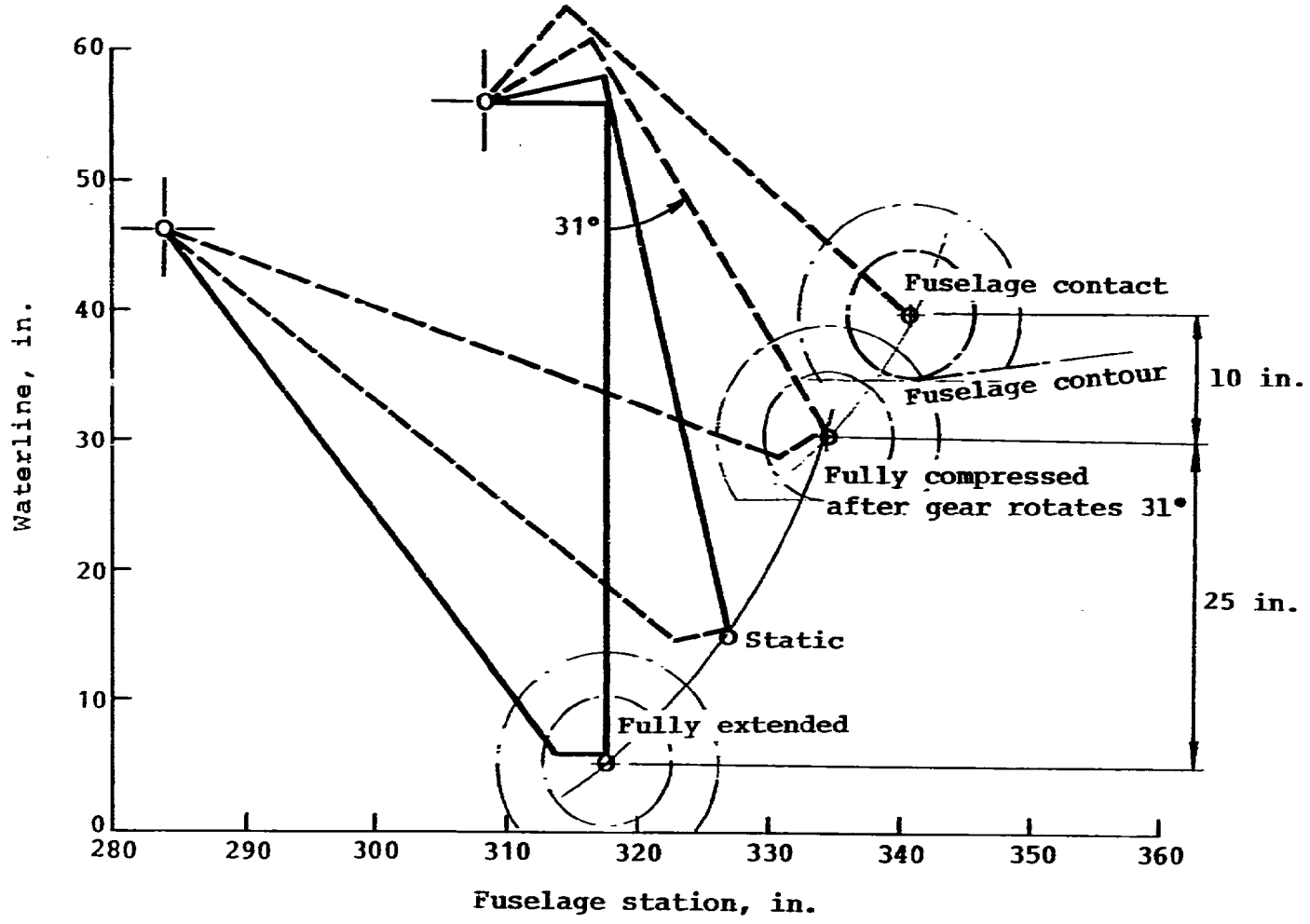

Figure 49. YAH-63 main landing gear geometry and motions.

for the aircraft to displace 10 inches at 42 ft/sec, the fuselage contact occurs at 152 msec or greater. (Even after the main landing gear is fully compressed, the aircraft continues to decelerate since there is still additional energy absorption in the landing gear due to main gear deformation prior to failure and in the nose gear.) Therefore, from the pilot's bulkhead velocity time history (Figure 48), the vertical velocity at fuselage contact (152 msec) is 38 ft/sec, which results in a landing gear energy absorption capability of approximately 29 to 30 ft/sec ($\sqrt{48^2-38^2}$ = 29.3 ft/sec).

KRASH predicts a little more aircraft velocity reduction from the energy absorbing landing gear than test (aircraft slows to 35 ft/sec in KRASH versus 38 ft/sec in test). The resulting landing gear equivalent energy absorption capability is 32-ft/sec with KRASH compared to 29 to 30 ft/sec for test.

6.4 FUSELAGE RESPONSE COMPARISONS

6.4.1 Fuselage Crushing

After the T-41 drop test, measurements were taken along the lower fuselage structure to determine the amount of crushing. Similar data was obtained from the KRASH simulation for comparison. Figure 50 compares the fuselage crushing from test and analysis at several fuselage station locations. KRASH and test agree well except in the forward fuselage area, where test shows lower crushing displacement. The difference is most likely due to the hard armament structures such as the turret and sight mount (see Figure 31b) that were not included in the load-deflection characteristics of the nonlinear crush beams in the KRASH model.

6.4.2 Fuselage Accelerations

The KRASH and test acceleration time histories were correlated using filtered data. The test data was filtered at 60 Hz while the KRASH data was filtered at 20 Hz. As discussed earlier in Section 5.2 and shown in Figure 39, filtering the test data at 60 Hz yielded an acceleration time history that preserves the major pulses from the crash impact. However, the KRASH time histories when filtered at 60 Hz had what was considered excessive response of high frequency vibration

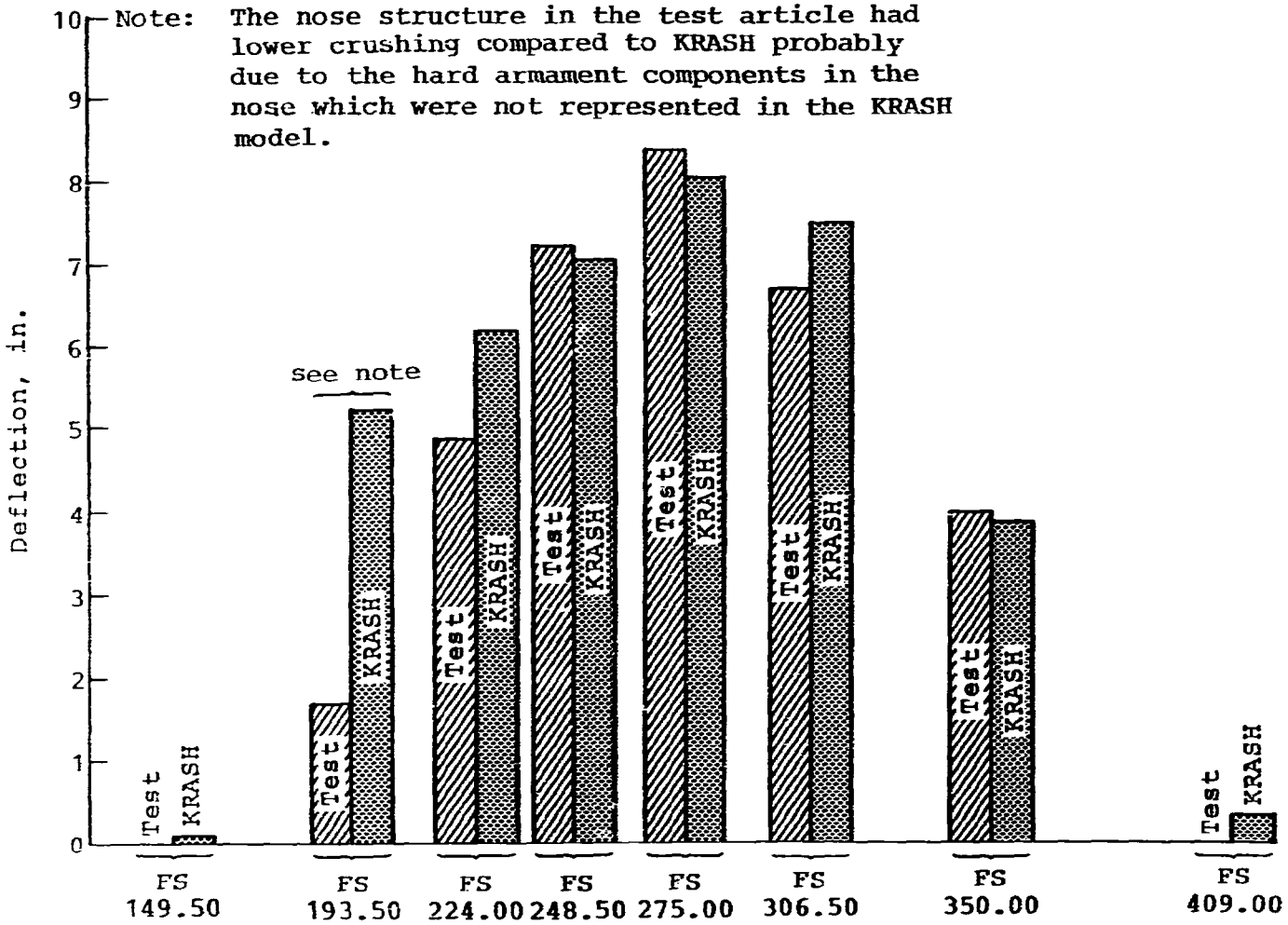

Figure 50. Test/analysis comparison of lower fuselage crushing.

modes associated with the idealized beam element representation of the test article as shown in the pilot bulkhead response in Figure 51. As discussed in Section 4, the KRASH elastic line airframe modeling was intended to represent the important vibration characteristics through 20 Hz. The vibrations in the 60-Hz frequency range were considered artificial and masked the important structural responses. The local modes of the beams were excited by the crash impact which was evident from the high oscillatory response. To eliminate the undesirable response, the KRASH data was filtered at 20 Hz to clarify the major structural acceleration pulse. (Note that increasing the structural damping may have produced similar results.)

Figure 52 compares the test and KRASH analysis acceleration response time histories along the fuselage at the FS 193.50 copilot/gunner bulkhead, the FS 248.50 pilot bulkhead, and the FS 306.50 aircraft cg. Generally, the KRASH accelerations are uniform over the fuselage with peak amplitudes ranging from 20 g's to 25 g's, whereas the test accelerations definitely increased from the mid fuselage (35 g's) forward to the nose (55 g's). The fuselage peak acceleration environment is summarized in Figure 53 and shows the test accelerations are about 10% to 30% higher than analysis in the mid-fuselage area. Good agreement is shown for the fuselage response at nose gear ground contact prior to fuselage contact. The high forward fuselage acceleration response in test is attributed to the hard armament structure in the nose. As discussed earlier, the load-deflection data for the KRASH model was calculated based on the crushable lower fuselage structure alone and did not consider the hard armament structure located in the forward fuselage. Consequently, the load-deflection data input to the KRASH math model represented uniform crushing. Note that design support testing of lower fuselage structure components is desirable to provide better load-deflection data, including the effects of secondary structure and hard points.

Other pertinent structural response time histories from test and analysis were compared and showed good agreement. In Figure 54, the FS 120 nose acceleration response shows good agreement between test and analysis for the time at which the nose strikes the ground after failure occurred. The figure also compares the vertical acceleration of the main transmission cg from test and analysis and indicates good agreement in duration and amplitude of the major pulse.

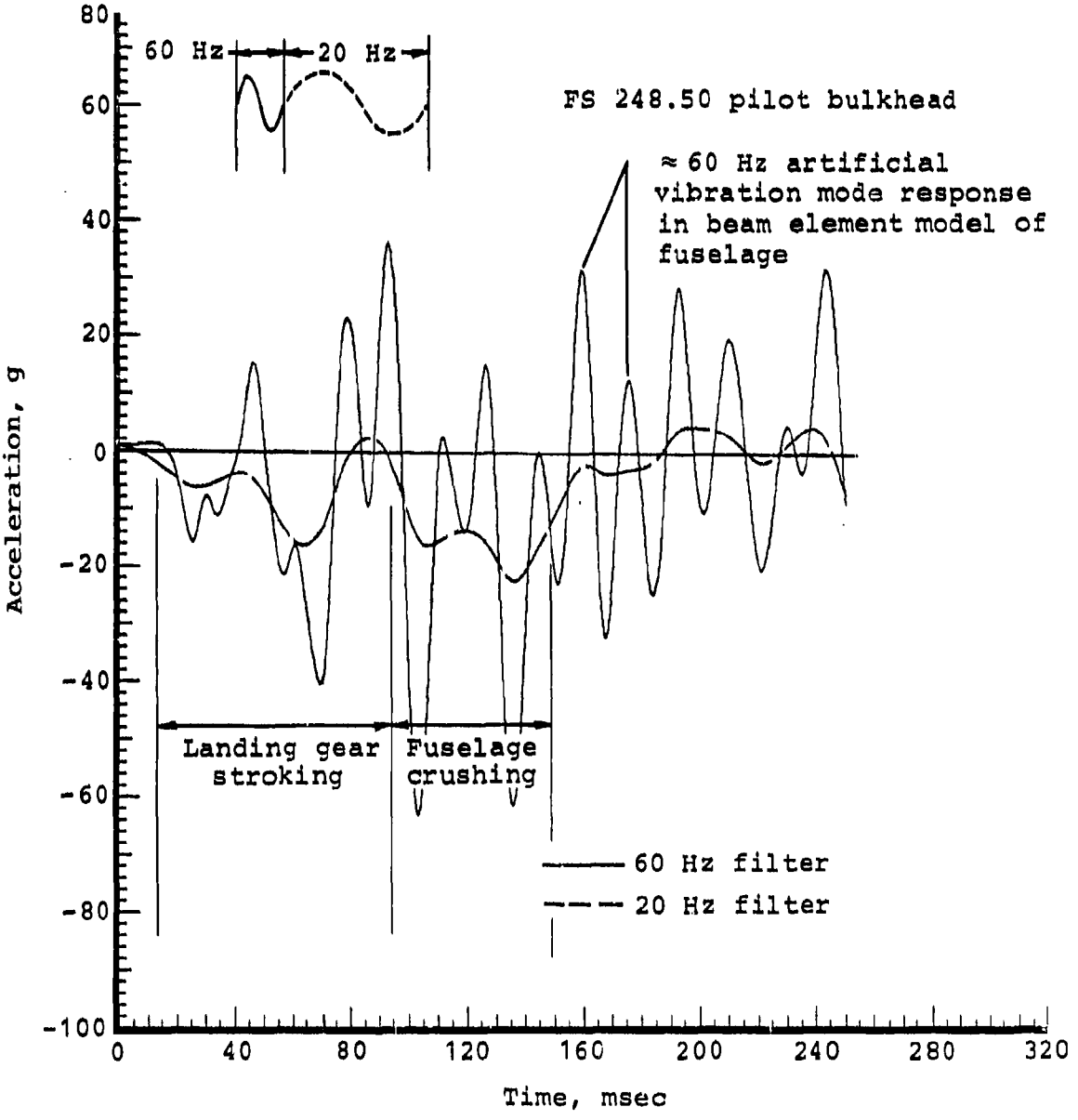

Figure 51. Filtering effects on KRASH analysis data.

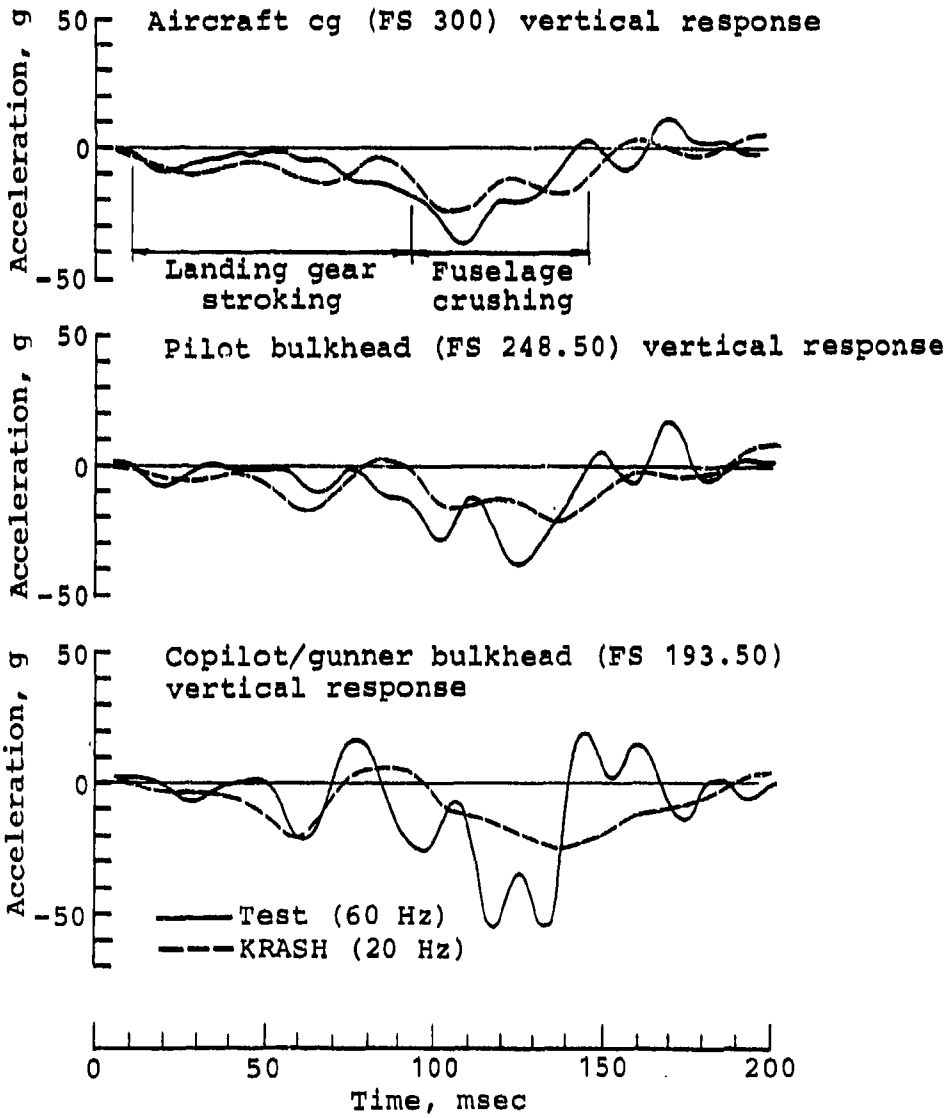

Figure 52. Test/analysis comparison of vertical accelerations at the aircraft cg, pilot bulkhead, and copilot/ gunner bulkhead.

Note: The higher g's in the nose of the test article compared to KRASH are probably caused by the hard armament structure located in the nose.

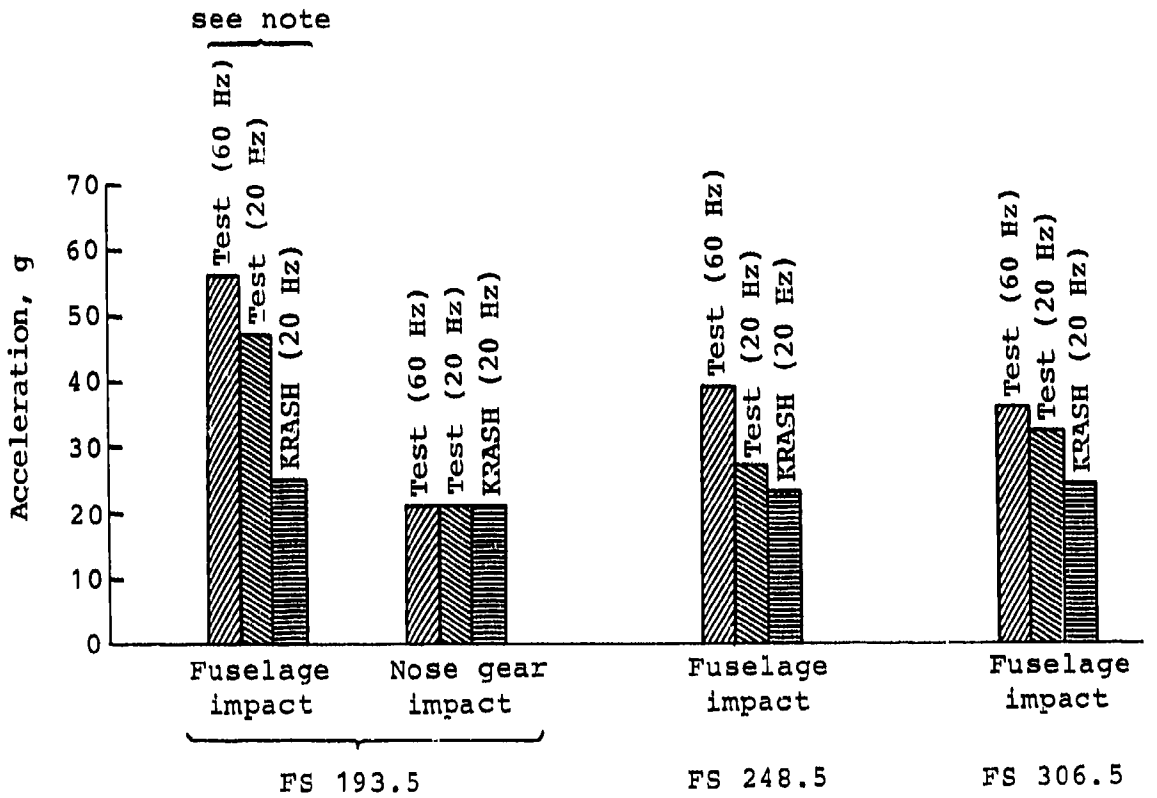

Figure 53. Test/analysis comparison of peak vertical accelerations on fuselage.

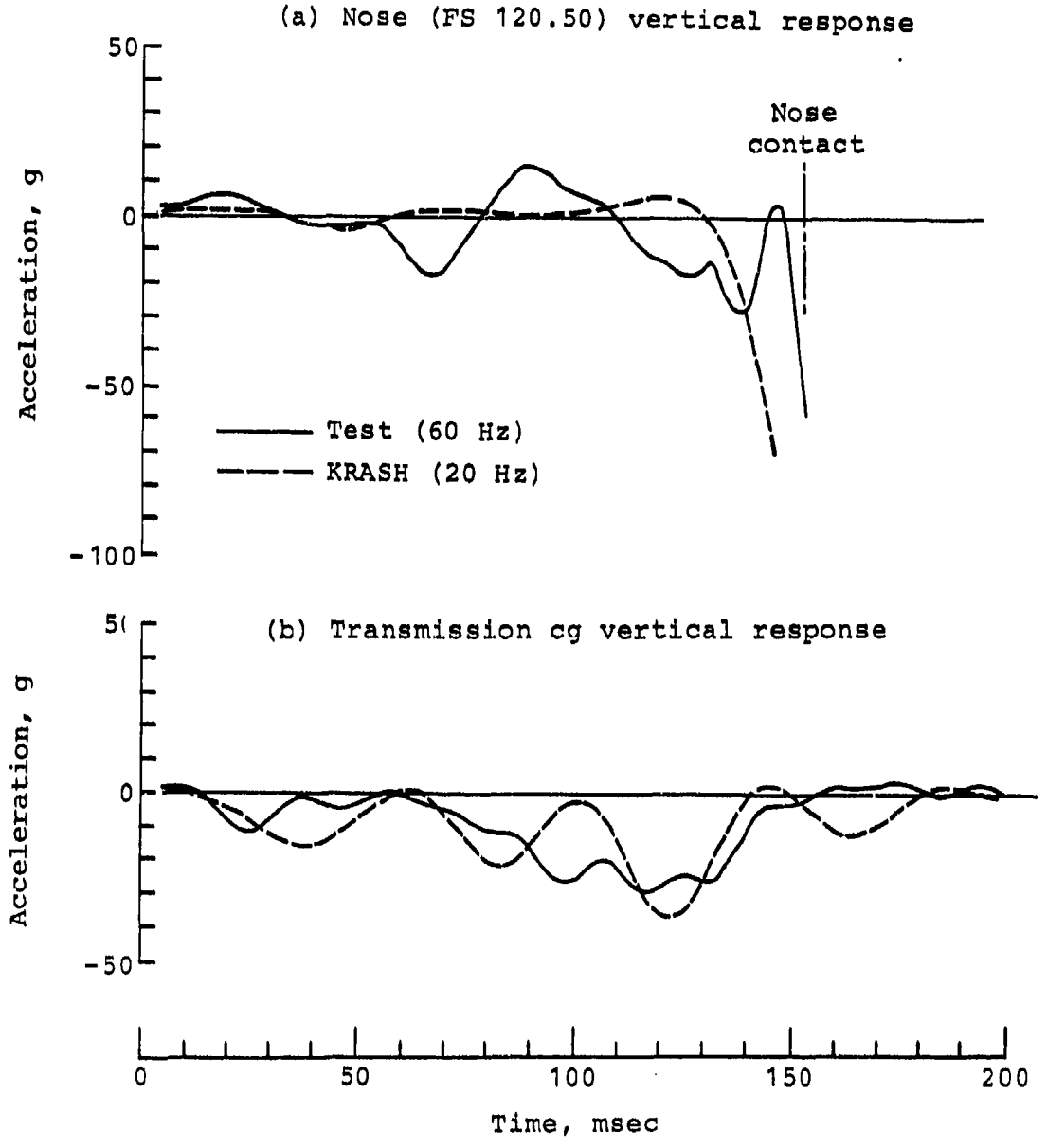

Figure 54. Test/analysis comparison of nose and main transmission cg vertical accelerations.

6.5 SEAT/OCCUPANT COMPARISONS

For the T-41 drop test, 50th percentile male anthropomorphic testing dummies were installed in the energy-absorbing crew seats. The KRASH math model idealized both the seats and dummies with spring-masses, as discussed in Section 4.4.3. As shown in Figure 55, the copilot/gunner seat stroke comparison between test and analysis agrees well, especially in the time at which maximum seat stroke is reached. In the T-41 drop test, the pilot seat attenuators buckled and stopped the seat from further stroking after 2.5 inches. Although this failure was not represented in the KRASH math model, the analysis indicated that the pilot seat would have stroked 12 inches and bottomed out.

The vertical acceleration response of the crew pelvis and seat pan from test is presented in Figure 56 with the seat response from KRASH. The time histories show the occurrence of seat stroke and subsequent bottoming out. Considering that the body dynamics can significantly affect seat response, the agreement between test and analysis is considered adequate with the spring-mass model used in KRASH.

The crew Dynamic Response Index (DRI) comparisons are shown in Figure 57. The copilot/gunner was predicted to have a potentially injurious acceleration environment and exceeded the 50% probability of injury level as did the actual test but with a higher peak (probably due to the representation of bottoming characteristics used in KRASH). The analysis also indicated that the pilot exceeded the 50% probability of injury level and again showed the peak DRI higher than test. The pilot seat that did not stroke properly in the test had a higher DRI response and was above the 50% probability of injury level, while the copilot/gunner DRI was above the 5% level but below 50%.

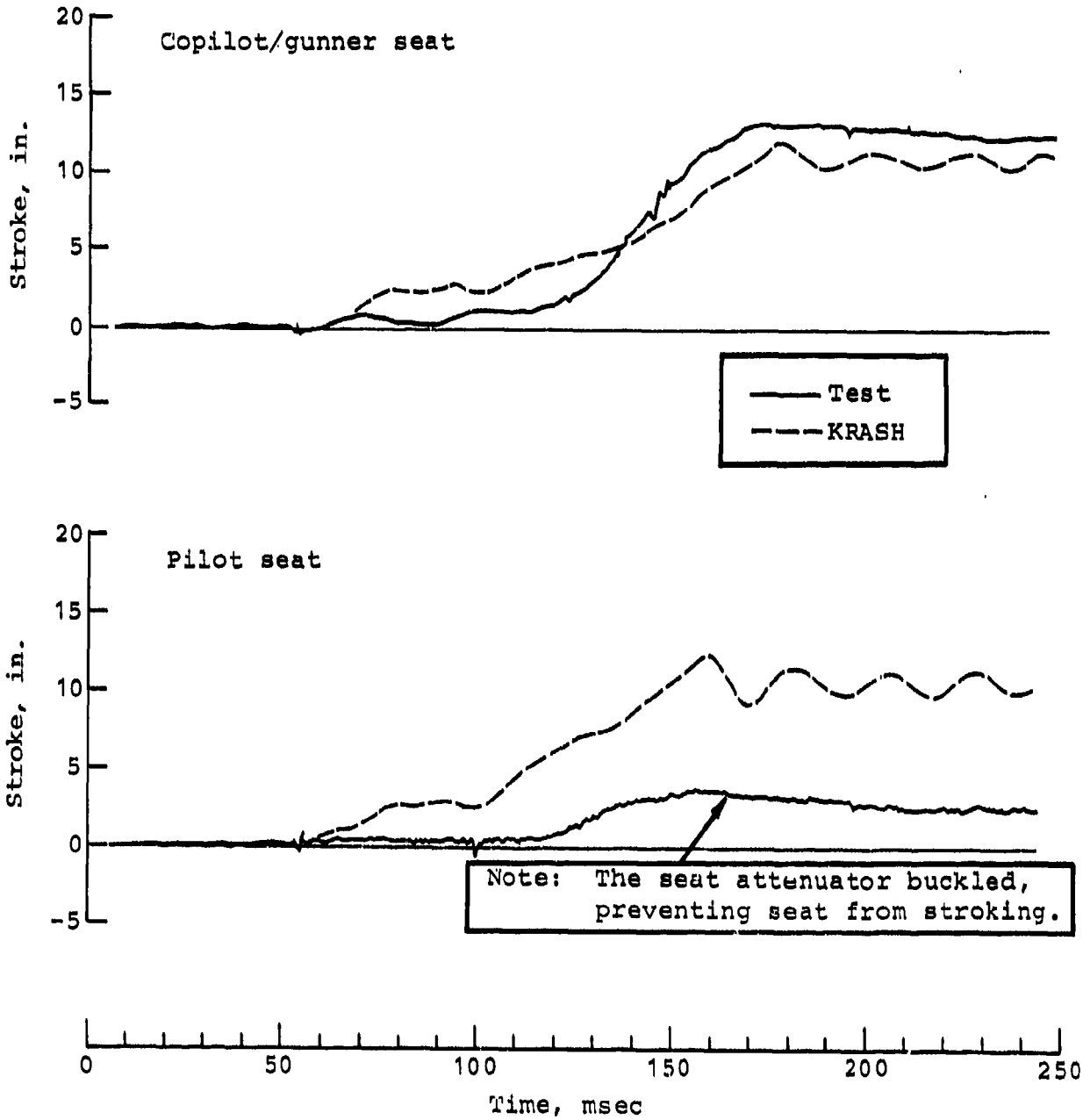

Figure 55. Test/analysis comparison of crew seat stroke.

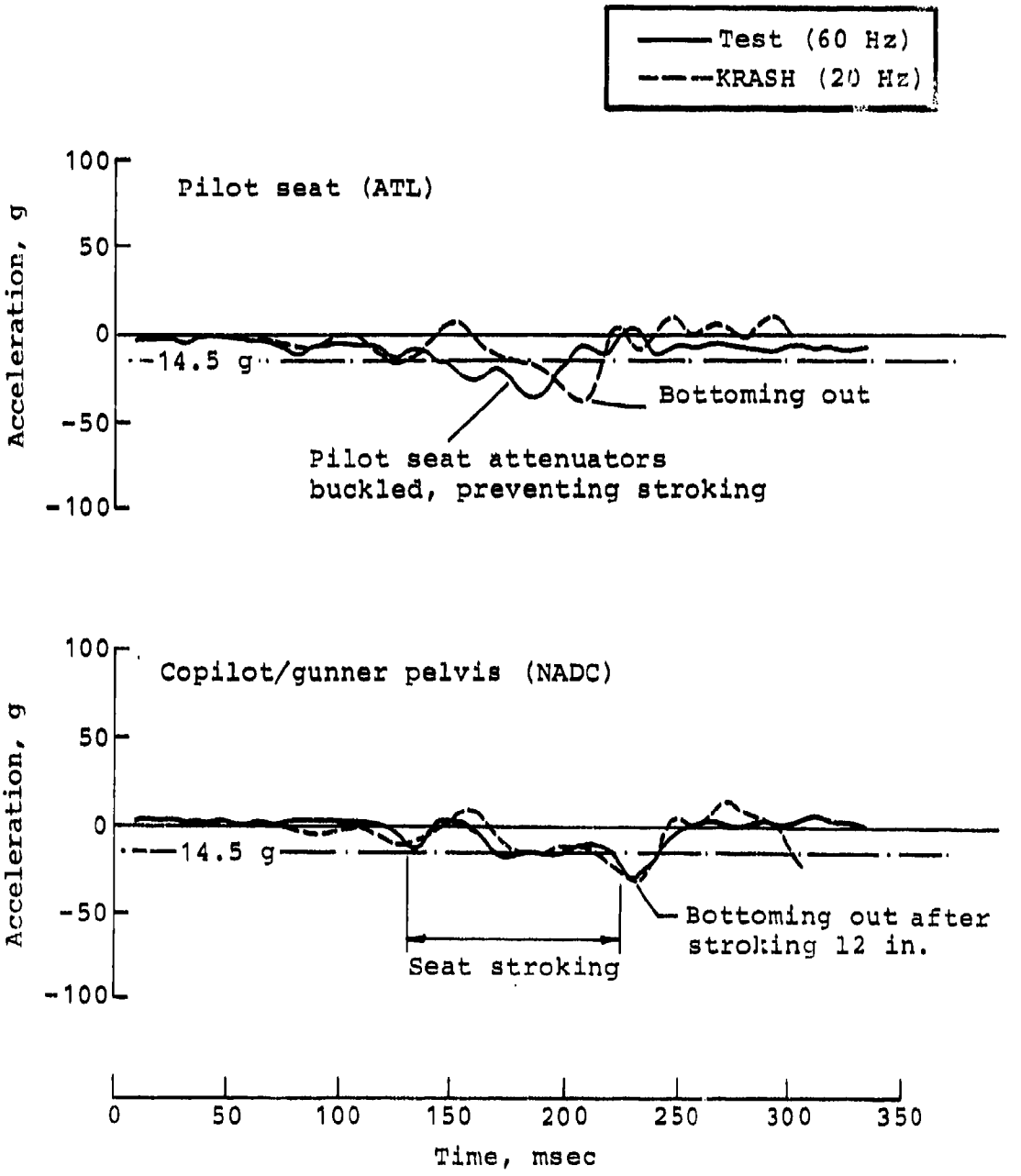

Figure 56. Test/analysis comparison of seat pan and pelvis vertical accelerations.

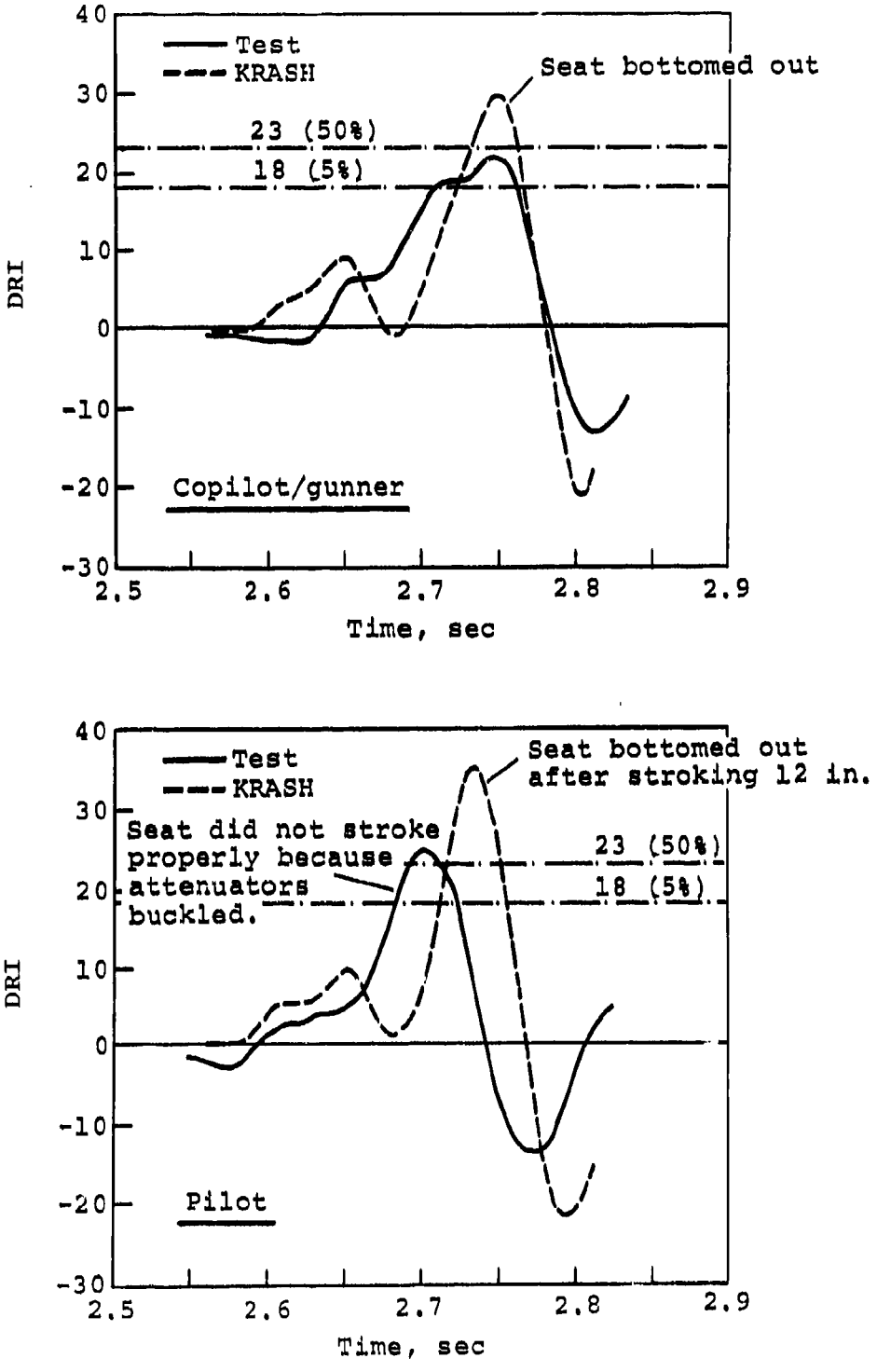

Figure 57. Crew DRI comparison from KRASH analysis and test.

7. CONCLUSIONS

The following conclusions summarize the results of the T-41 YAH-63 prototype drop test and the math simulation of the test using program KRASH.

- From the review of the test results, the following comments can be made about the crashworthiness of the YAH-63:
  - The actual drop test had approximately a 60-ft/sec resultant velocity that was 44% higher energy than the planned 50-ft/sec impact condition. In the vertical direction, the impact velocity component was 48 ft/sec, or about 30% more than the maximum 42 ft/sec vertical impact design condition with level attitude (no roll and pitch) used for the YAH-63. The 10° nose-up impact attitude introduced increased nose-down pitching and made the nose impact somewhat more severe than the level attitude design condition.
  - The airframe structure performed well even though the impact conditions were more severe than the conditions for which the YAH-63 was designed. The fuselage structure remained intact around the occupied area and retained the seats and large masses. In fact, no detectable damage was found in the main transmission and engine support structure areas. The crushing took place in the lower fuselage structure crush zone except in the forward fuselage where crushing appears to have been prevented by the hard armament structure located in the nose. Also, crushing of the vertical tail occurred as well as failure of the nose forward of the copilot/gunner station.
  - The prototype YAH-63 landing gear equipped with blow-off valves to attenuate the loads in a high energy crash worked properly. The blow-off valves were modified and sized via design support tests and landing gear analysis conducted by BHTI. Analysis of the T-41 drop test data indicated that the landing gear vertical energy absorption capability was equivalent to approximately 30 ft/sec, slowing the aircraft vertical velocity from 48 ft/sec to 38 ft/sec prior to fuselage contact. Note that the prototype YAH-63 landing gears with pressure relief valves were not highly efficient as energy absorbers. Other types of energy absorbing devices should be considered such as

mechanical load-limiters that have better energy absorption efficiency without loading rate sensitivity; for example, the tube cutting device that was proposed for the production YAH-63.

- The test article was equipped with bulkhead-mounted stroking seats with invert-tube attenuators. The forward copilot/gunner seat was a current AH-64 seat with tension-loaded attenuators and stroked properly using all of the available 12 inches of stroke, although it did bottom out due to the excessive crash impact energy. The pilot seat in the rear was an obsolete seat design having compression-loaded attenuators that buckled and prevented stroking. The DRI exceeded 50% probability of injury levels for the pilot seat. The copilot/gunner seat DRI was lower but exceeded the 5% level which was due to bottoming out after stroking.

- The fuel tanks and breakaway self-sealing fittings functioned properly and did not leak with the exception of the forward fuel tank, which had a minor leak due to a bent metal flange on the sump drain panel. The flange was bent due to an angle member from a mockup prototype ammo container located beneath the tank being driven up into the tank. However, the tank material itself remained intact.

- From the results of the KRASH analysis of the YAH-63 and comparison to the T-41 test data, the following conclusions are made:

  - By comparing high speed photos of the test with the KRASH model structure plots at the same times, the overall sequence of events and structural responses agreed well. Also, vertical velocity time history comparisons agreed well.

  - Landing gear modeling and comparison with test. The landing gear modeling in KRASH required representation of the air/oil shock strut equipped with relief valve as a load-stroke curve developed from independent landing gear analyses rather than letting the KRASH model develop the shock strut load depending on the instantaneous closure velocity. (The oleo element in KRASH that would have allowed this does not function properly.) The landing gear shock strut drop test conducted by BHTI was used to correlate the landing gear analyses and develop the load-stroke KRASH input for the shock struts.

Both the planned 50-ft/sec resultant impact condition and the actual 60-ft/sec T-41 impact condition were analyzed with KRASH. For the 50-ft/sec condition, the landing gear energy absorption was equivalent to 26.3 ft/sec and the actual 60-ft/sec condition was equivalent to 33 ft/sec (compared to approximately 30 ft/sec from test).

The drag link loads in the main landing gear agreed well between KRASH and test. Both showed load reversals indicating ground friction reversal depending on gear stroking velocity relative to aircraft forward velocity.

- Fuselage Modeling and Comparison with Test. The fuselage was represented by an elastic axis line of beam elements with vertical crushable elements attached to the line model that represent the crushable lower fuselage structure below WL 40. The load-deflection properties of the crushable structure were determined by structural analysis using methods similar to those described in Reference 9. Although the crush deflections agreed reasonably well with test, design support testing of key structure crush elements is preferred because of simplifying assumptions that must be made in order to analyze the complex structure crushing behavior.

  Checking the KRASH model vibration modes with NASTRAN was found useful. In representing the elastic stiffness and lumped mass distributions, vibration modes and frequencies were compared between the KRASH model and a detailed finite element model of the airframe structure using NASTRAN to ensure that important vibration modes through 20 Hz were preserved in the coarse KRASH model.

  Comparing KRASH and test, the fuselage crushing and acceleration agreed fairly well with test in the aft and mid fuselage but test showed less crush and much higher g's in the forward fuselage due to the location of the hard armament structure in the nose which was not represented in the KRASH model. KRASH results show 20 to 25 g's throughout the fuselage, while test results are about 30 g's in the mid and aft fuselage and about 50 g's in the forward nose area.

The nose failure predicted by the KRASH analysis agreed well with test.

Artificial vibration modes around 50 to 60 Hz were encountered in the fuselage and transmission responses due to the beam element modeling in KRASH. These were effectively removed by filtering at 20 Hz to preserve the important structural response while eliminating unwanted vibration modes prior to comparison with test. (Note that normally it is desirable to retain responses through 60 Hz when comparing structural responses.)

- Seats. The forward copilot/gunner seat stroke and acceleration time histories from KRASH agreed well with test. The KRASH results showed proper stroking and bottoming out, as was found in test for the 60-ft/sec condition. Note that the 50-ft/sec KRASH results also showed some bottoming out of the forward copilot/gunner seat. This was probably caused by the nose-up impact attitude producing nose-down pitching moments resulting in nose slap-down. More efficient nose gear energy absorption would have helped reduce the nose impact velocity and thus the copilot/gunner seat stroking.

  The pilot seat in the KRASH analysis stroked a full 12 inches and then bottomed out, whereas the pilot seat in test did not stroke properly due to the attenuators buckling and, therefore, did not agree well with analysis. The KRASH analysis of the 50-ft/sec planned test condition showed that the pilot seat stroked but did not bottom out and the pilot would have survived with no injurious loads.

- The DATAMAP data analysis program proved to be a valuable tool for analyzing and comparing test and KRASH data.

8. RECOMMENDATIONS

Based on the results of this investigation, recommendations for modeling and crash analysis procedures to use in design are as follows:

- An elastic line idealization of the beam-like fuselage and modeling of key energy-absorbing components such as the landing gear, fuselage crush structure, and seats was considered an adequate representation for the KRASH analysis of the YAH-63 aircraft. For shell-type structures found in utility or transport aircraft and having roof-mounted transmissions, the roof, floor, bulkheads, and frames need to be represented.

- Airframe stiffness and mass distribution for the coarse KRASH math model should be checked against a more detailed finite-element model by comparing the important vibration modes as was done with NASTRAN to ensure that the dynamics have been preserved in the coarse model.

- Key structural elements that are important in absorbing energy and controlling loads to the fuselage should be tested statically and dynamically to determine load-deflection characteristics both for understanding the failure modes and structural behavior in a crash and for input to the KRASH model. Although the structural analysis that was done for the YAH-63 was found to be reasonable for determining the fuselage response, many simplifying assumptions were made that ignored the effects of structural interaction and combined loading.

- As with the fuselage, the landing gear key load-attenuating, energy-absorbing structural elements should be tested to determine crash impact behavior.

- Both crew and troop seats, normally developed and tested separately, have comprehensive criteria to assure proper functioning in a crash. Spring-mass modeling was considered adequate for determining contributions of the seats to the energy management system and control of occupant loads in the vertical direction. However, analysis of the seat structure,

restraint, and occupant modeling using fuselage accelerations for excitation is needed to determine seat and restraint loads, loads to structure, and strike envelopes. KRASH can be used with a "stick figure" occupant model tied to a seat with tension-only beams for the restraint system. However, other computer codes such as SOM-LA (Reference 12) have been developed specifically for this purpose and should be considered.

- Other computer programs with more detailed modeling capability such as DYCAST (Reference 13) should continue to be investigated. However, the cost of running this highly nonlinear type of analysis can be excessive if the number of degrees-of-freedom is not kept to a minimum. Using the coarse KRASH type of modeling for overall vehicle response and then using a finite-element model for a local area of the structure requiring more detailed modeling may be a practical approach.

Recommended improvements to the KRASH computer program include the following:

- A numerical integration method having improved stability for highly nonlinear structural responses typical in a crash analysis is needed.

- The oleo landing gear element in KRASH does not function properly and should be corrected. Variable diameter metering pin capability should be added also.

- Tire crush springs should rotate as the landing gear strokes such that they remain normal to the ground.

---

[12]Laananen, D. H., Coltman, J. W., and Bolukbasi, A. O., COMPUTER SIMULATION OF AN AIRCRAFT SEAT AND OCCUPANT IN A CRASH ENVIRONMENT, FAA TR 81415, 2 Vols., Federal Aviation Administration Technical Center, Atlantic City, New Jersey, October 1981.

[13]Pifko, A. B., Winter, R., and Ogilvie, P., DYCAST NONLINEAR STRUCTURAL DYNAMIC FINITE ELEMENT COMPUTER CODE - USER'S MANUAL, Research and Development Center, Grumman Aerospace Corporation, Bethpage, New York.

- The external crushing springs should be improved by expanding the input data parameters to include more detailed definition of the load-deflection loading and unloading characteristics.

- The allowable number of massless nodes (50) and beam elements (150) should be increased to 100 and 250, respectively to allow more detailed modeling of structures.

- The mass points and massless nodes should be user-numbered to facilitate the preparation of input data, in particular, modifications involving the addition or deletion of mass points and nodes. Currently, mass points and nodes are numbered internally.

- The KRASH computer program should be interfaced with a data analysis procedure such as DATAMAP to analyze and plot the KRASH time history output.

- A KRASH-to-NASTRAN and NASTRAN-to-KRASH pre-processor program should be developed for initial checkout of coarse KRASH model input data.

- Plotting capability should be added to generate plots of the structure crash impact deformations for any user-selected viewing angle.

- A shear panel element should be included in the KRASH analysis element library for modeling shell-type structures and shear webs in beams.

- Interactive beam failure modes for combined loading should be added.

9. REFERENCES

1. Turnbow, J. W., et al., CRASH SURVIVAL DESIGN GUIDE, Dynamic Science, the AvSer Facility, USAAMRDL TR 71-22, Eustis Directorate, U.S. Army Air Mobility Research and Development Laboratory, Fort Eustis, Virginia, October 1971, AD 733358.

2. AIRCRAFT CRASH SURVIVAL DESIGN GUIDE, Simula Inc., USARTL TR 79-22 A-E, Applied Technology Laboratory, U.S. Army Research and Technology Laboratories (AVRADCOM), Fort Eustis, Virginia:

   Volume I - DESIGN CRITERIA AND CHECKLISTS, December 1980, AD A093784.
   Volume II - AIRCRAFT CRASH ENVIRONMENT AND HUMAN TOLERANCE, January 1980, AD A082512.
   Volume III - AIRCRAFT STRUCTURAL CRASHWORTHINESS, August 1980, AD A089104.
   Volume IV - AIRCRAFT SEATS, RESTRAINTS, LITTERS, AND PADDING, June 1980, AD A088441.
   Volume V - AIRCRAFT POSTCRASH SURVIVAL, January 1980, AD A082513.

3. Military Standard MIL-STD-1290(AV), LIGHT FIXED- AND ROTARY-WING AIRCRAFT CRASHWORTHINESS, Department of Defense, Washington, D.C., 25 January 1974.

4. Gamon, M. A., and Wittlin, G., EXPERIMENTAL PROGRAM FOR THE DEVELOPMENT OF IMPROVED HELICOPTER STRUCTURAL CRASHWORTHINESS ANALYTICAL AND DESIGN TECHNIQUES, USAAMRDL Technical Report 72-72, 2 Vols., U.S. Army Air Mobility Research and Development Laboratory, Fort Eustis, Virginia, May 1973, AD 764985 and AD 764986.

5. Wittlin, G., and Gamon, M. A., GENERAL AVIATION AIRPLANE STRUCTURAL CRASHWORTHINESS USER'S MANUAL, DOT Report FAA-RD-77-189, 3 Vols., U.S. Department of Transportation, Federal Aviation Administration, Systems Research and Development Service, Washington, D. C., February 1978.

6. Smith, K. F., FULL-SCALE CRASH TEST (T-41) OF YAH-63 ATTACK HELICOPTER, USAAVRADCOM Technical Report 83-XX, Applied Technology Laboratory, U.S. Army Research and Technology Laboratories, Fort Eustis, Virginia (to be published).

7. Military Specification MIL-S-58095, SEAT SYSTEM, CRASHWORTHY, NONEJECTION, AIRCREW, GENERAL SPECIFICATION FOR, Department of Defense, Washington, D.C., August 1971.

8. Schulman, M., and McElhenney, J., INFLATABLE BODY AND HEAD RESTRAINT, NADC-77176-40, Naval Air Development Center, Naval Air Systems Command, Washington, D.C., September 1977.

9. Park, K. C., and Wittlin, G., DEVELOPMENT AND EXPERIMENTAL VERIFICATION OF PROCEDURES TO DETERMINE NONLINEAR LOAD-DEFLECTION CHARACTERISTICS OF HELICOPTER SUBSTRUCTURES SUBJECTED TO CRASH FORCES, USAAMRDL TR-74-12, 2 Vols., U.S. Army Air Mobility Research and Development Laboratory, Fort Eustis, Virginia, May 1974, AD 784191 and AD 784192.

10. Cronkhite, J. D., Haas, T. J., Berry, V. L., and Winter, R., INVESTIGATION OF THE CRASH IMPACT CHARACTERISTICS OF ADVANCED AIRFRAME STRUCTURES, USARTL Technical Report 79-11, Applied Technology Laboratory, U.S. Army Research and Technology Laboratories, Fort Eustis, Virginia, September 1979, AD A075163.

11. Philbrick, R. B., THE DATA FROM AEROMECHANICS TEST AND ANALYTICS - MANAGEMENT AND ANALYSIS PACKAGE (DATAMAP), USAAVRADCOM Technical Report 80-D-30, 2 Vols., Applied Technology Laboratory, U.S. Army Research and Technology Laboratories, Fort Eustis, Virginia, December 1980, AD A095188 and AD A094674.

12. Laananen, D. H., Coltman, J. W., and Bolukbasi, A. O., COMPUTER SIMULATION OF AN AIRCRAFT SEAT AND OCCUPANT IN A CRASH ENVIRONMENT, FAA TR 81415, 2 Vols., Federal Aviation Administration Technical Center, Atlantic City, New Jersey, October 1981.

13. Pifko, A. B., Winter, R., and Ogilvie, P., DYCAST NONLINEAR STRUCTURAL DYNAMIC FINITE ELEMENT COMPUTER CODE - USER'S MANUAL, Research and Development Center, Grumman Aerospace Corporation, Bethpage, New York.

APPENDIX A

STRUCTURE DESCRIPTION

This appendix briefly describes the YAH-63 prototype aircraft used as the test article in the Army's T-41 drop test. The aircraft description is presented in two parts; first, the primary airframe structure including fuselage, wings, and tailboom, and second, the subsystem components including landing gear, seats, main rotor pylon, engine, and fuel system.

A.1 PRIMARY AIRFRAME STRUCTURE

As shown in Figure A-1, the primary airframe structure consisted of three major sections or subassemblies: forward fuselage, mid fuselage and inboard wing, and tailboom.

A.1.1 Forward Fuselage

The fuselage forward section shown in Figures A-2 and A-3 extended from FS 93 to FS 275 and was semi-monocoque construction. A system of eight longerons (four on each side) fabricated from both sheet and extruded aluminum comprised the load path for bending. The side skins, crew floors, and electronics bay floors reacted vertical and side shears and provided closed cells for torque reaction. The skins were 7075-T6 aluminum with 7075-T6 aluminum stiffeners; however, the skins forward of FS 160.75 were 2024-T42 aluminum with honeycomb reinforcement. The sandwich construction floors were aluminum honeycomb core with chem-etched aluminum face sheets.

The bulkheads were of built-up sheet metal construction using aluminum webs with extruded or bent aluminum caps and stiffeners. The FS 110 and FS 132.5 bulkheads provided the forward and aft support structure for the 30mm gun mount platform at WL 58.5 while the FS 138 and FS 160.75 bulkheads supported the gun sight ring. The bulkheads at FS 160.75 and FS 165, together with the BL 12.5 longitudinal beams, supported the fittings for the nose landing gear drag link trunnions. The FS 193.5 bulkhead provided vertical reaction for the nose landing gear shock strut loads. In addition, the bulkhead closed the forward electronics bay and supported the forward crew seat. Above WL 64 the bulkhead contained both transparent and opaque armor material. The opaque armor was considered as an effective bulkhead shear web. The FS 224 bulkhead supported the aft crew floor, consoles, and electronics bay floors. Finally, the FS 248.5

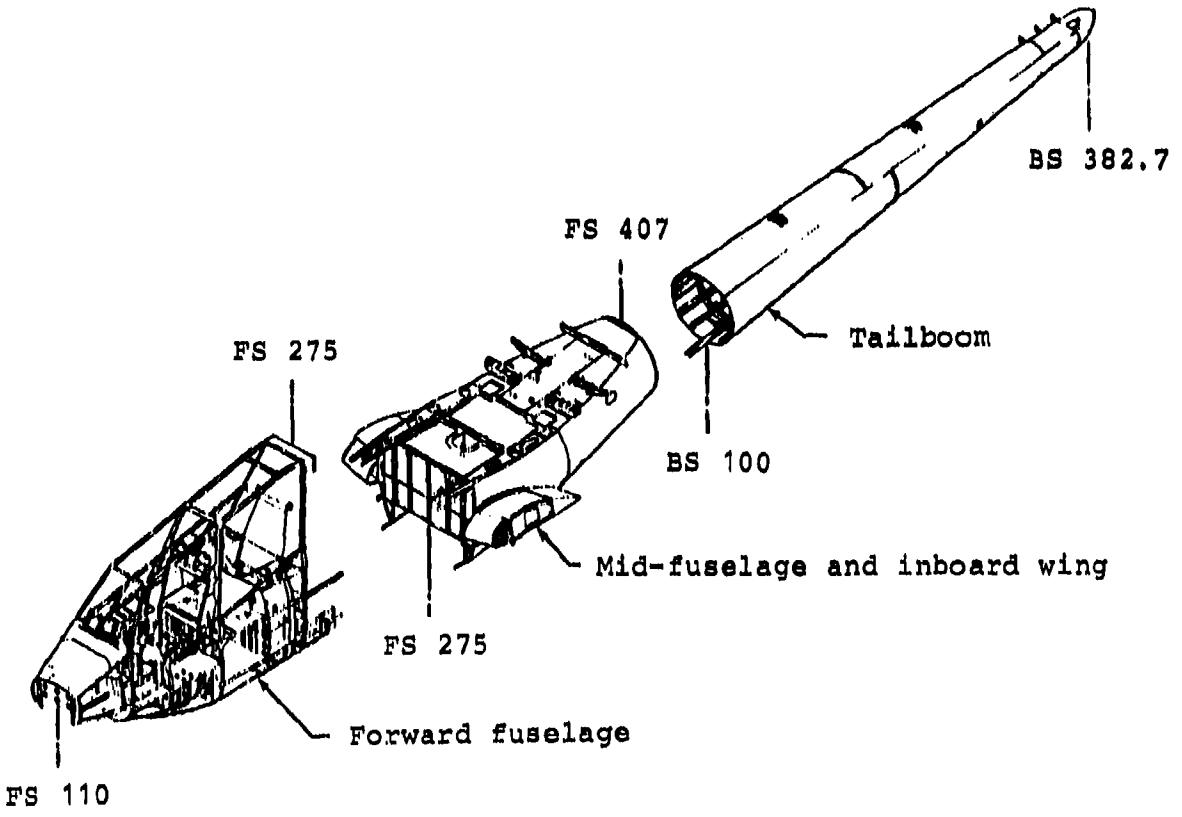

Figure A-1. YAH-63 airframe structure.

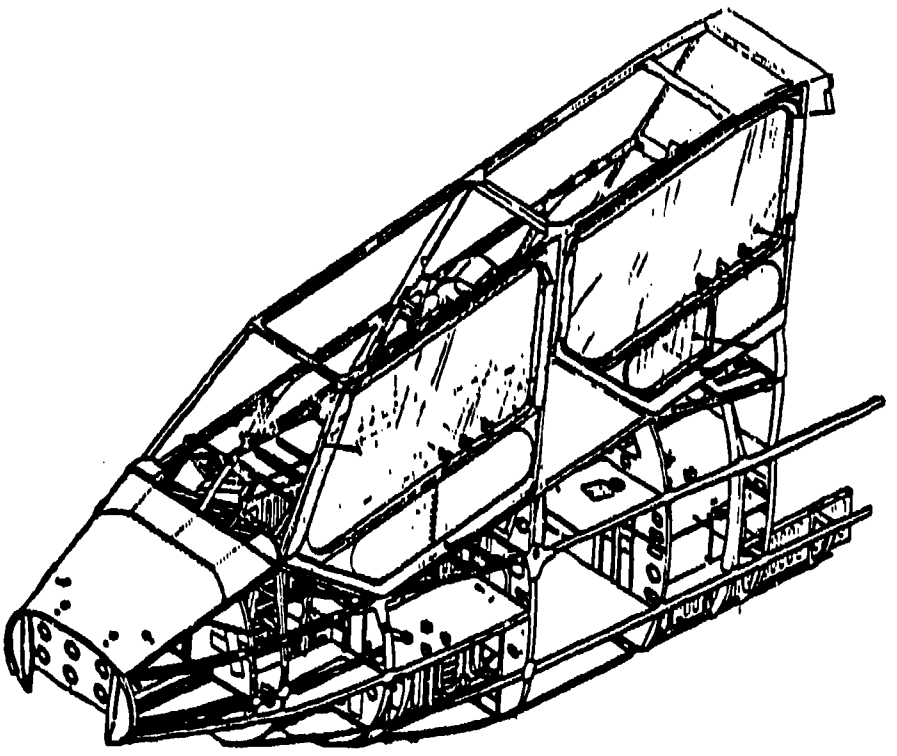

Figure A-2. YAH-63 forward fuselage structure.

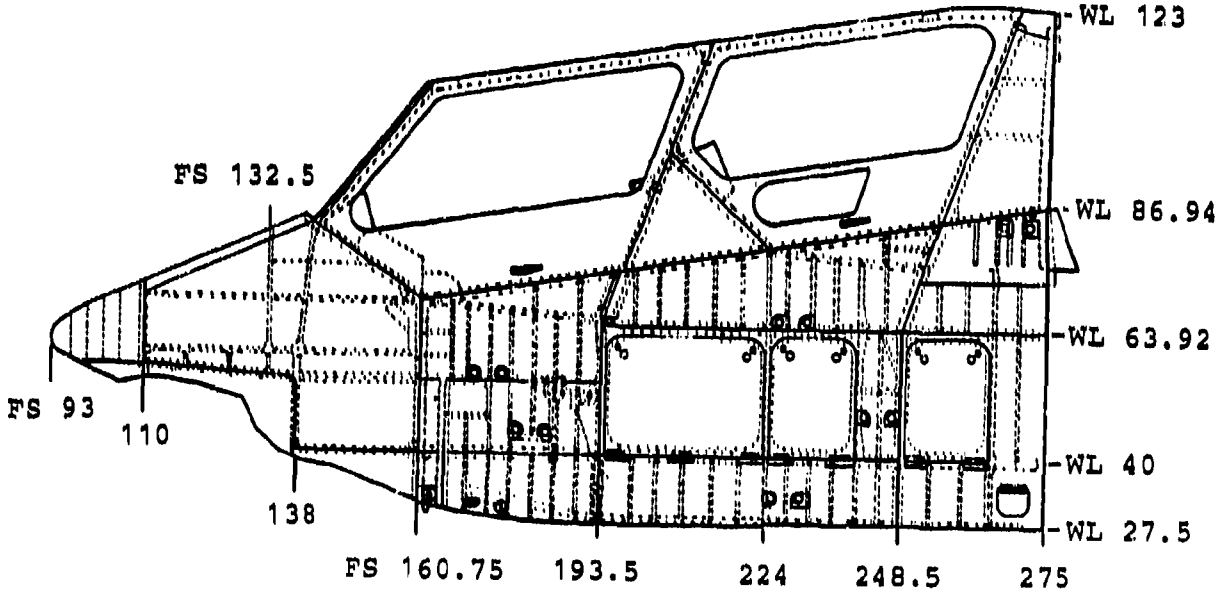

Figure A-3. YAH-63 forward fuselage structure line data.

bulkhead closed out the aft crew compartment, supported the aft crew seat, supported the electronics bay floors, and above WL 64 formed part of the rollover protection structure.

In addition to supporting the 360-lb gun/turret assembly and the 240-lb lower sight unit, the nose structure between FS 93 and FS 160.75 provided crashworthiness capability to protect the crew from injury for a 20-ft/sec longitudinal impact into a rigid barrier. The nose structure was designed to crush at a load less than that required to cause occupant injury or to exceed the retention strength of the seats, main rotor transmission, and engines. As a result, the occupant acceleration environment was within human tolerance levels and the potentially hazardous large mass items were prevented from displacing into the occupied area. Structure crushing past the FS 160.75 bulkhead was expected for the 20-ft/sec longitudinal impact condition; however, the reduction in occupied volume was not greater than the allowed 15% and protective structure around the tail rotor yaw control pedals prevented foot entrapment.

Aft of the FS 193.50 bulkhead, crushable fuselage structure was provided between WL 27.50 and WL 40 to meet the 42-ft/sec vertical crash impact condition. The structure consisting of the BL 24 longitudinal beams, side frames, and skin was designed to decelerate the aircraft to rest together with the high-energy landing gear system. The crushable structure controlled the crash impact loads to the large mass items, thereby preventing retention failures. In addition, the coordinated fuselage and seat design assured a noninjurious occupant acceleration environment, i.e., seat stroke capability was not exceeded.

To meet the 30-ft/sec lateral crash impact condition, the fuselage sidewall structure was designed to crush. The crushing load developed was less than that required to cause retention failure of the seats, main rotor pylon, and engines. Also, the occupant acceleration environment was reduced to tolerable levels while the occupied volume was maintained to at least 85% of original.

The rollover protection structure for the crew was incorporated to meet the military crashworthiness requirements. The aft rollover structure was formed by the FS 248.5 and FS 275 bulkheads, the WL 63.92 floor, the top canopy fitting, and skins. The forward rollover structure was provided by the FS 193.5 bulkhead. The structure introduced the rollover loads (see Table 1) into the lower airframe structure where a redundant reaction system was available.

The cockpit enclosure was a "greenhouse" arrangement with stretched acrylic transparencies and aluminum frames. The structure extended from FS 141 to FS 256. The left side panels were the cockpit doors which pivoted at the top.

As shown in Figure A-4, the YAH-63 prototype incorporated unconventional design approaches for crew seating and gun/sight arrangements in the forward fuselage. The pilot was located at the forward crew station to improve visibility for nap-of-the-earth flight operations. The 30mm weapon was installed forward and above the stabilized sight to reduce muzzle blast damage on the airframe, to meet weapon area coverage requirements, and to improve gunner visibility through the sight. For the T-41 test, the crew positions were reversed and the copilot/gunner was forward and the pilot aft.

Figure A-4 also illustrates the location of the jettisonable 30mm ammo container and the ammo chute routing. The container was installed in the belly structure below WL 40 between FS 224 and FS 306.5. The forward fuel cell was protected from container penetration by 3 inches of energy-absorbing, fire-suppressant foam and a 3/16-inch-thick aluminum plate.

A.1.2 Mid Fuselage and Inboard Wing

As shown in Figure A-5, the mid fuselage structure extended from FS 275 to the tailboom junction at FS 409 and supported the 3545-lb main rotor pylon, 925-lb engines, fuel cells, and wings. The structure was semi-monocoque construction with longerons, side skins, floors, and work decks providing the load paths.

The mid fuselage had six longerons (three per side) made from extruded and formed aluminum. Aft of the rear fuel cell canted bulkhead, four stringers per side and one along the bottom centerline were incorporated in addition to the longerons. The side skins around the fuel cells between FS 275 and FS 347 were sandwich construction with aluminum face sheets and honeycomb core. The face sheets were chem-etched as required. All other side skins were chem-etched aluminum sheets stiffened with aluminum stringers and frames. The fuel cell floors and decks above the fuel cells were sandwich panels with aluminum honeycomb core and face sheets. The engine deck utilized either titanium or aluminum sheet, depending on temperature environment.

The mid fuselage bulkheads were of built-up sheet metal construction having aluminum webs with extruded or bent aluminum caps; however, some of the bulkheads were sandwich

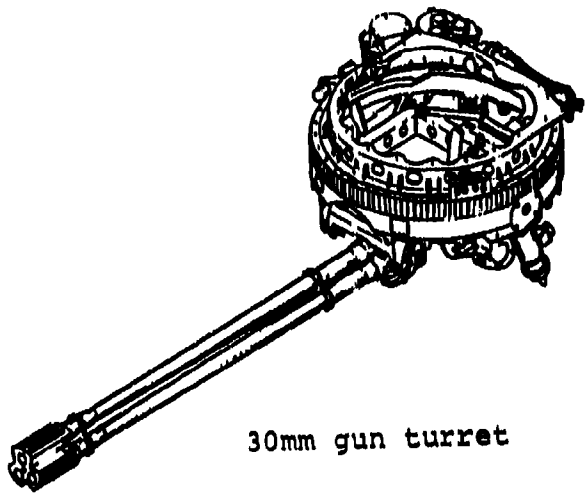

30mm gun turret

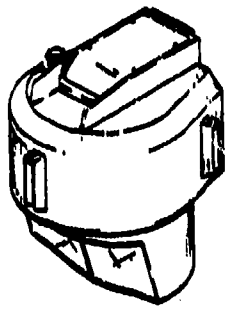

Lower sight unit

* Note: For T-41 crash test, pilot and copilot/gunner seating was reversed.

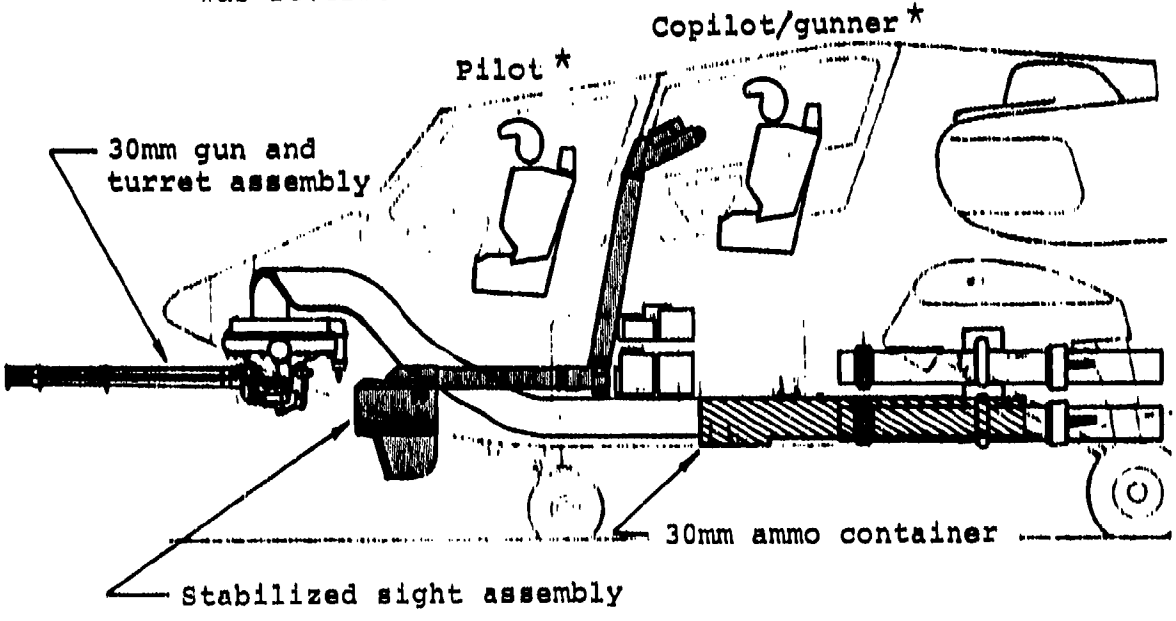

Figure A-4. YAH-63 30mm weapon and sight installation.

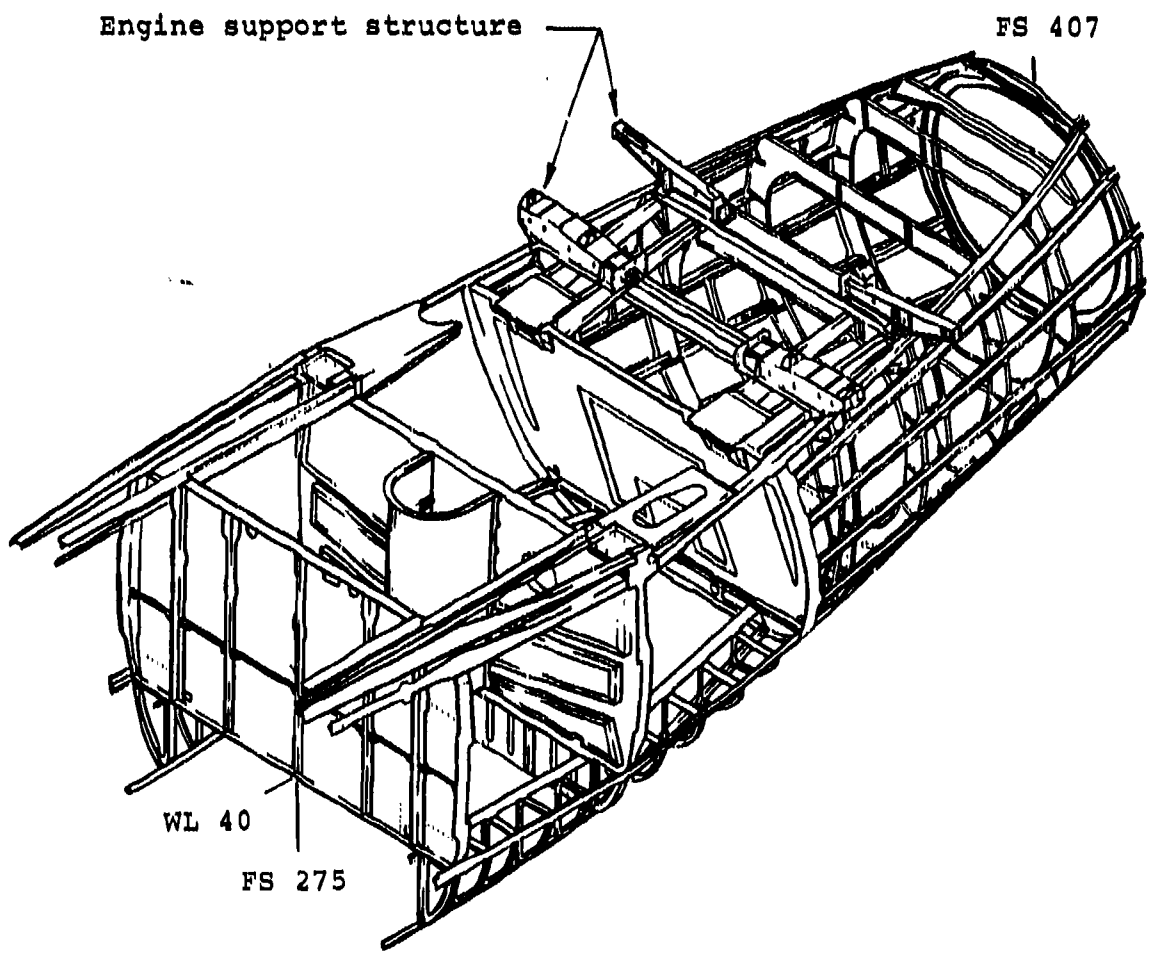

Figure A-5. YAH-63 mid fuselage structure.

reinforced. The major structural bulkhead at FS 275 was constructed of a chem-etched aluminum web with aluminum extruded caps and stiffeners. This bulkhead was located at the forward end of the forward fuel cell. The bulkhead provided support attachments for the front wing spar and the forward nodal pylon fittings. The FS 306.5 bulkhead was a sandwich panel with aluminum face sheets and honeycomb core. The bulkhead separated the forward and aft fuel cells. The rear wing spar and nodal pylon lateral crash stops were attached to this bulkhead. The canted bulkhead at FS 347 was a sandwich panel with aluminum face sheets and honeycomb core. The bulkhead closed the rear fuel cell and supported the aft nodal pylon fittings and aft jacking pad. The tailboom junction bulkhead at FS 409 was aluminum sheet and reacted the inplane kick loads introduced by the machined aluminum fittings splicing the tailboom stringers to the mid fuselage structure.

The fuselage structure below WL 40 from the FS 275 bulkhead to the FS 347 canted bulkhead was crushable structure similar to that described previously. Together with the landing gear, the crushable fuselage structure decelerated the aircraft to rest for the 42-ft/sec vertical impact condition. Crash loads were controlled to prevent retention strength failures of the main rotor pylon and engines. In addition, the fuel cell loads were attenuated to tolerable levels, preventing rupture and fuel spillage. The structure around the fuel cells maintained a protective shell to prevent rupture from large structural deformations or large mass item impingement.

The inboard wing (see Figure A-6) was a semi-monocoque single-cell box structure. The forward spar, the three outboard ribs, and the rear spar inboard of contour were built-up aluminum sheet and stringer construction. The wing leading and trailing edges were nonstructural fairings. The aft wing spar outboard of contour was a monolithic fitting providing main landing gear and outboard wing attachments. The rib at BL 32 was an aluminum honeycomb sandwich web with extruded caps. The two front spar caps were attached to the aft side of the FS 275 bulkhead and the two aft spar caps were attached to the front side of the FS 306.5 bulkhead. The spar caps reacted wing bending moments. Similarly, the wing spar webs were attached to the bulkheads and transferred shears. The upper and lower wing surfaces were attached to the mid fuselage side panels at the wing root rib using external skate angles.

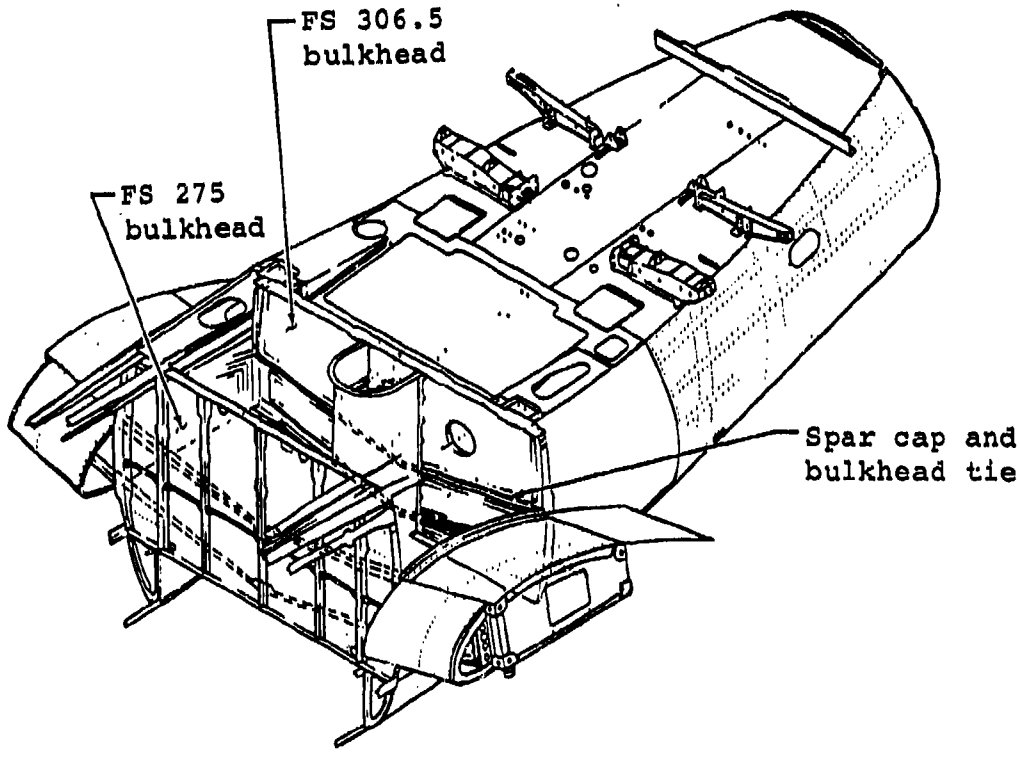

Figure A-6. YAH-63 mid fuselage and inboard wing structure.

The outboard wing structure shown in Figure A-7 was constructed the same as the inboard wing. The two sections were joined at the WS 21.19 splice using four bolts and tension-type fittings. The outboard wing provided support for the external stores.

The YAH-63 wing structure contributed to the overall aircraft crashworthiness capability in two ways. First, the high-strength wing acted to prevent the occurrence of rollover. The wings spanned to BL 96 such that a "righting" tendency was present for rollover accidents. Secondly, the wing structure crushing characteristics absorbed significant kinetic energy for the 30-ft/sec lateral crash impact condition. Wing crushing controlled the impact loads to the large mass items, preventing retention failure. Together with the forward fuselage sidewall, the wing attenuated the lateral crash impact energy and reduced to tolerable levels the occupant accelerations.

A.1.3 Tailboom

The tailboom and empennage structure extended aft of FS 409 and is shown in Figures A-8 and A-9. The tailboom was an aluminum sheet/stringer type structure with fifteen hat section stringers and frames spaced at 18-inch intervals. The tail rotor gearbox was attached between BS 340 and BS 353.

The empennage or "I-tail" consisted of a vertical fin with upper and lower horizontal tails. The empennage attached to the right side of the tailboom through two lugs at each of the BS 340, BS 353, and BS 364 bulkheads. The vertical fin was a two-cell box structure. The spars and ribs were sheet aluminum with machined attachment fittings to the tailboom and horizontal tails. The lower horizontal tail had two spars. The airfoil contour skin was an aluminum sheet with full-depth aluminum honeycomb between the front spar and trailing edge. The lower tail attached to the vertical fin at two points on each of the front and rear spars. The upper horizontal tail construction utilized three spars, each attached to the vertical fin at two points.

A.2 SUBSYSTEM COMPONENTS

A.2.1 Landing Gear

The YAH-63 prototype helicopter featured a high-energy fixed wheeled landing gear system to meet the Army crashworthiness requirements. The tricycle configuration consisted of a

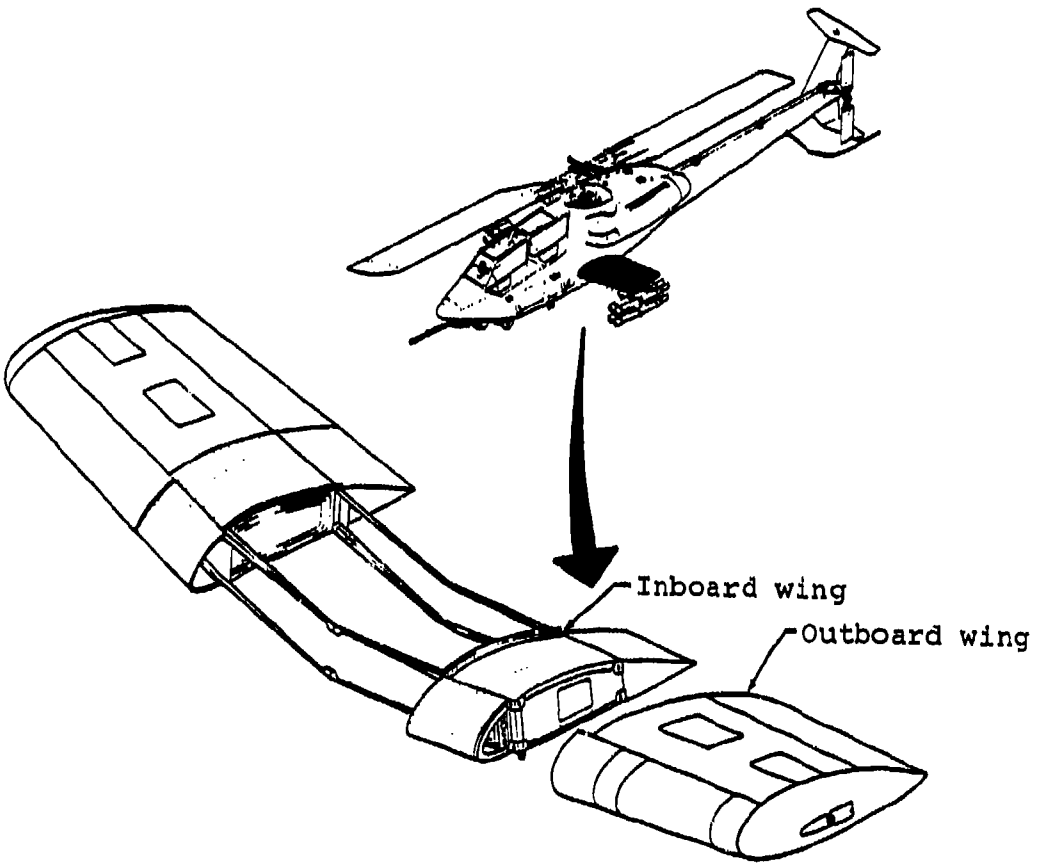

Figure A-7. YAH-63 wing structure.

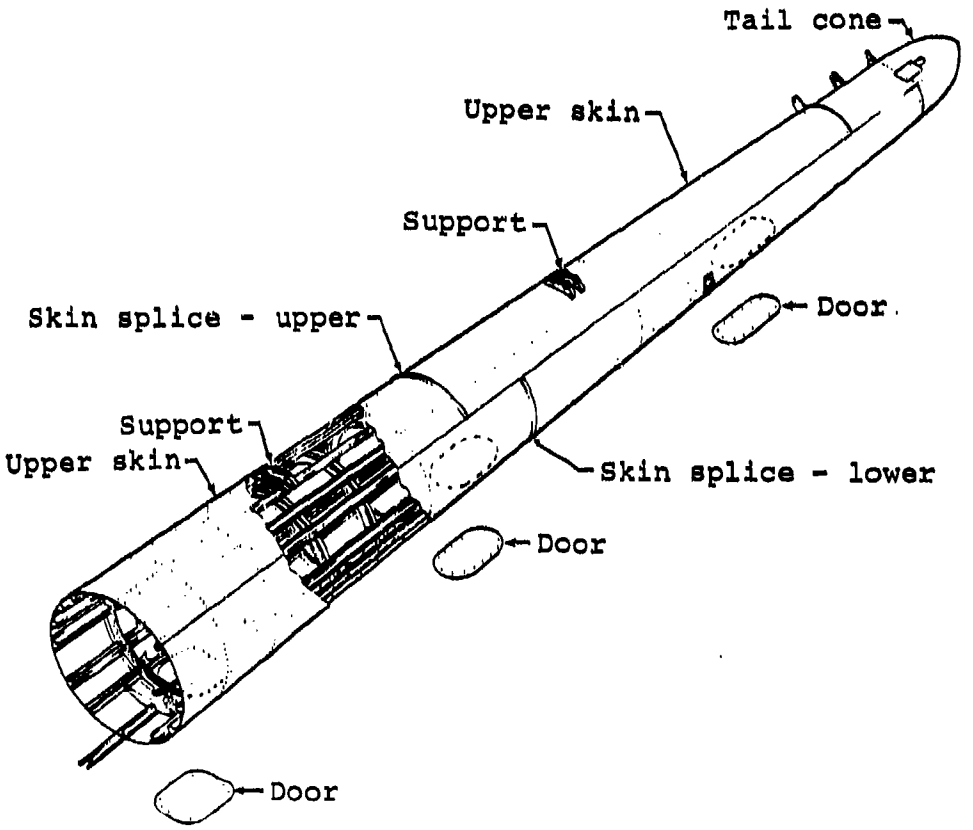

Figure A-8. YAH-63 tailboom structure.

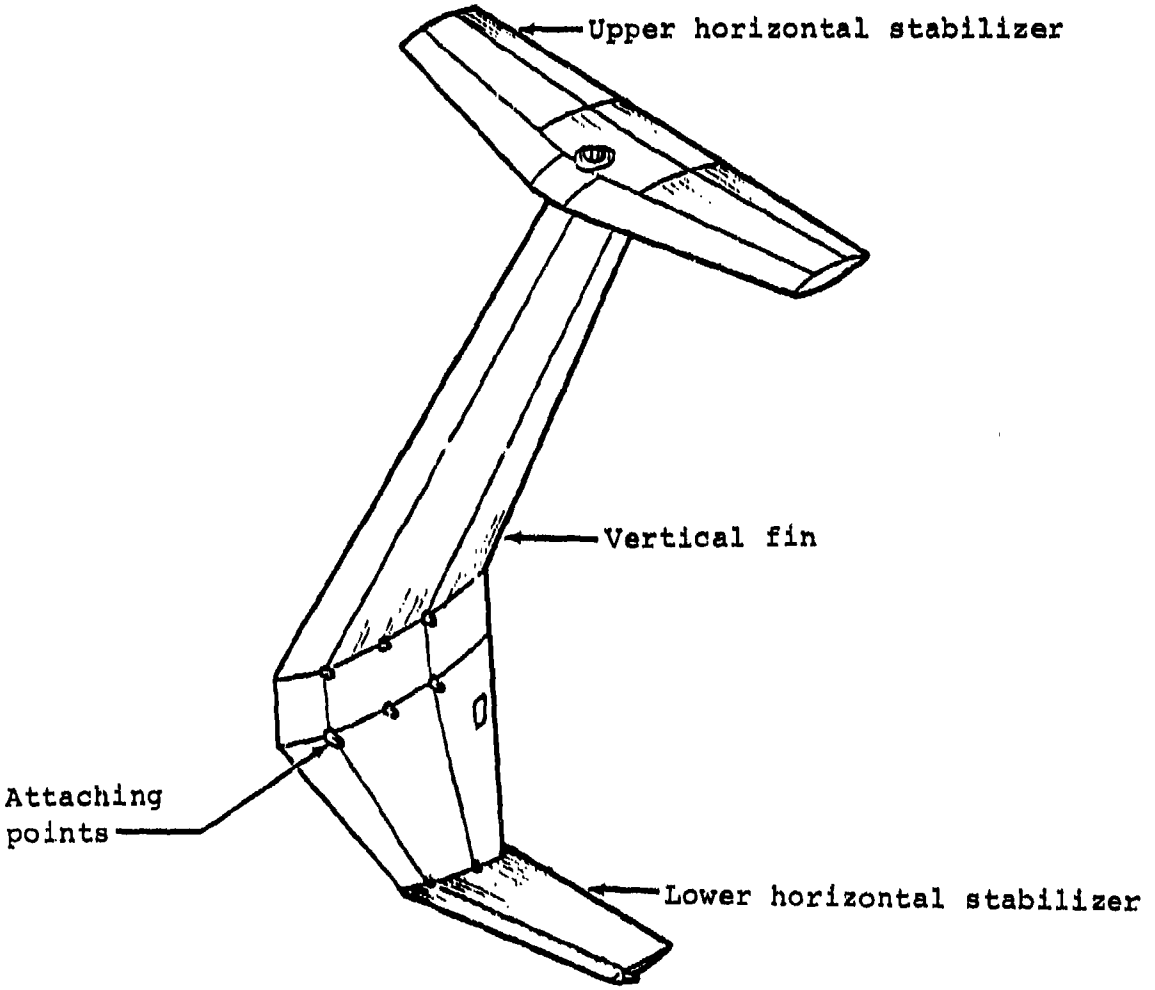

Figure A-9. YAH-63 I-tail structure.

forward fuselage-mounted nose gear and two inboard wing-mounted main gears. Menasco designed and manufactured the landing gear components as subcontractor to BHTI.

The prototype nose landing gear shown in Figure A-10 had dual 6.00-6 tires and wheels with full caster attachment to a support strut which incorporated a shimmy damper, self-centering device, and swivel lock. A two-bar linkage attached the swivel housing of the wheel support strut to the fuselage. The purpose of the parallel bar mechanism was to maintain the vertical orientation of the support strut throughout the spectrum of gear motions. A single stage air/oil shock strut equipped with a pressure relief valve was attached between the lower bar and the fuselage to attenuate both normal landing and crash impact loads. Kneeling capability for air transportability requirements was accomplished by removing hydraulic fluid from the shock strut.

As shown in Figure A-11, the left and right prototype main landing gears each had a single 8.50-10 wheel and tire assembly cantilevered from a support strut. Each strut incorporated an integral single-stage air/oil shock strut equipped with a pressure relief valve at the top end. The shock strut attenuated the vertical loads for both normal landing and crash impact conditions. The upper end of the strut was mounted to the aft spar of the inboard wing structure using lug attachment fittings. A pinned-end drag strut between the lower end of the shock strut and the forward spar of the inboard wing structure reacted the longitudinal landing gear drag loads. The main gears had crew-operated brakes, parking brakes, and parking locks. Kneeling of the gears for air transportability required replacement of the drag struts with extendable actuators.

The energy absorbing components in the YAH-63 prototype landing gear system were conventional single-stage air/oil shock struts equipped with pressure relief valves. For normal landing conditions involving low sink speeds (less than 12 ft/sec), the shock strut alone attenuated the vertical loads without actuating the relief valve mechanism. However, for higher velocity crash impact conditions, the piston compressed the hydraulic fluid in the cylinder at a high closure velocity which generated sufficient internal pressure to blow off the relief valve cap. Structural failure of the cap allowed the release of the pressurized hydraulic fluid through a specially designed orifice, thereby absorbing the crash impact energy. The blow-off valve concept limited the peak load developed in the shock strut

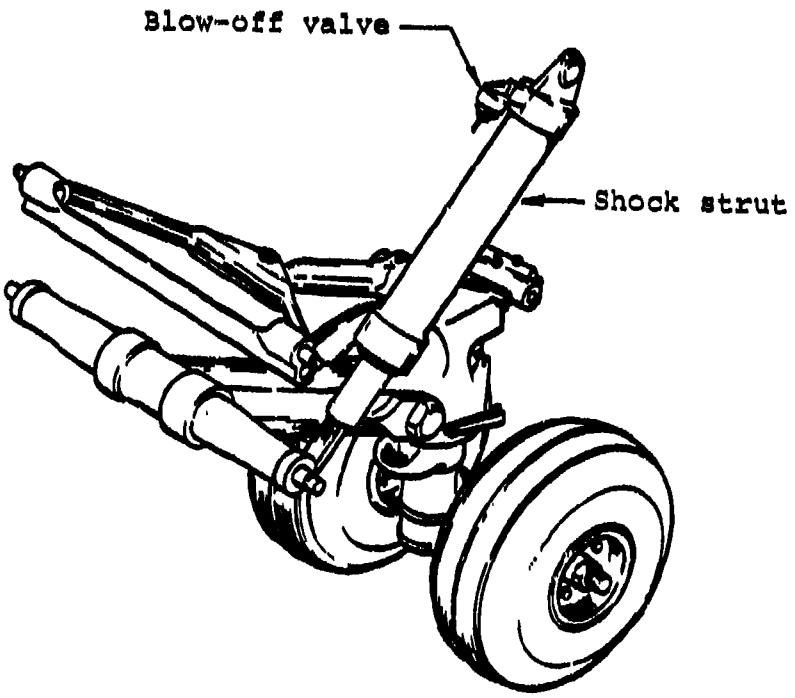

Figure A-10. YAH-63 nose landing gear.

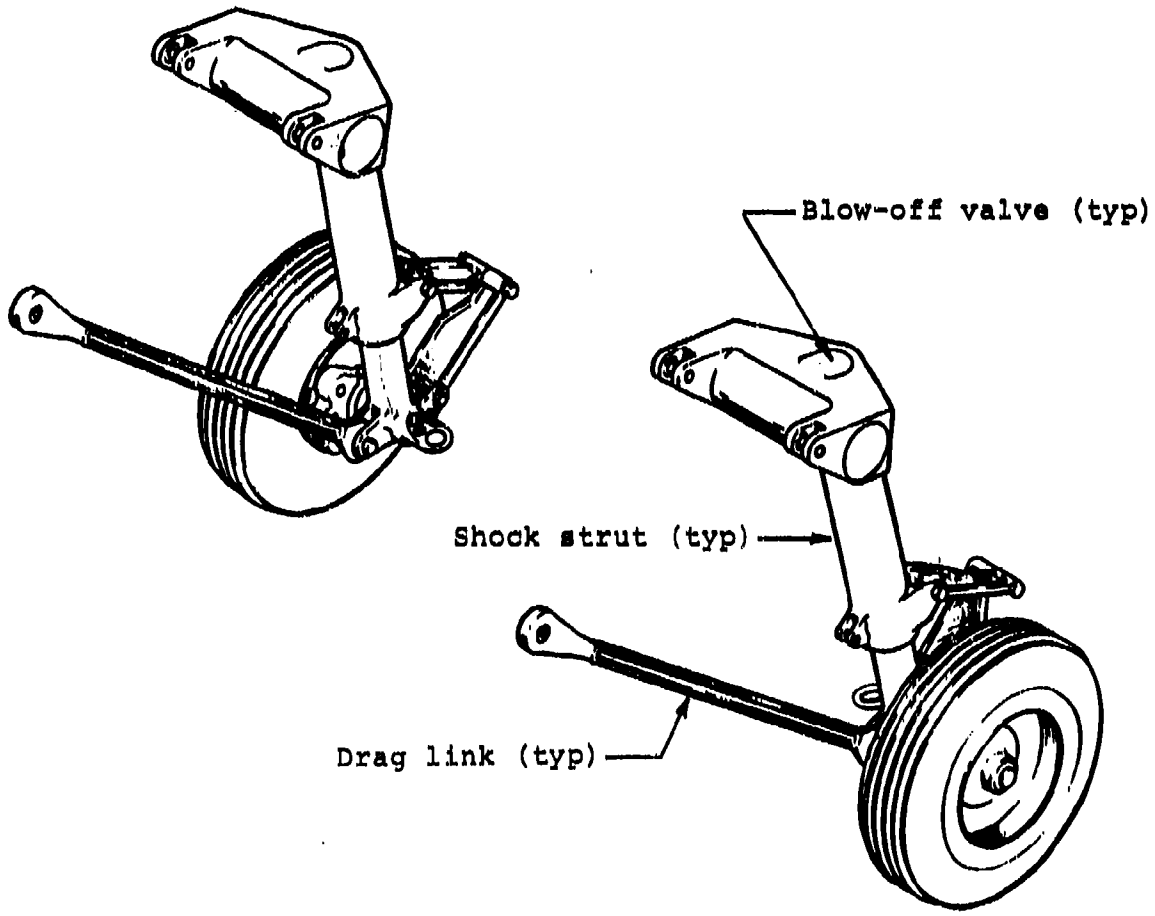

Figure A-11. YAH-63 main landing gears.

sc that the support structure did not fail prematurely. As a result, the landing gear system absorbed the maximum crash impact energy possible.

As shown in Figure A-12, a typical air/oil shock strut such as that used on the YAH-63 prototype characteristically does not provide an ideal rectangular-shaped load-deflection curve for maximum crash impact energy absorption capability. Instead, the attenuated load is dependent on the closure velocity of the piston in the cylinder. As the shock strut landing gear decelerates the helicopter, the closure velocity correspondingly decreases, which causes a reduction in the attenuated load. The rate sensitive behavior is not desirable, making the air/oil shock strut a less than efficient energy absorber. Mechanical load limiting devices are available for landing gear design applications that exhibit near ideal load-deflection characteristics.

Two promising concepts are the crushable honeycomb and tube cutter energy absorbers. Figure A-13 illustrates the proposed YAH-63 production nose gear design which employs the tube cutter.

A.2.2 Seats

The crashworthy, armored crew seats used in the YAH-63A were manufactured by Norton/Simula. The seats were bulkhead mounted at FS 193.5 and FS 248.5. Vertical energy-attenuation capability was achieved using compression-loaded invert tubes which attached the seat back to the fuselage. As shown in Figure A-14, each seat had a five-point restraint system to keep the occupant in place. The vertical seat height adjustment capability influenced the available stroke distance which was a minimum 12 inches.

A.2.3 Main Rotor Pylon and Engines

The YAH-63A main rotor pylon installation shown in Figure A-15 consisted of the blades, hub, mast, transmission, and nodal beam/focal mount isolation system. The two-bladed, semi-rigid main rotor system was 50 feet in diameter and the blade weighed 1099 lb. The 45-inch chord blades had dual stainless steel box beam construction. The fore body had steel skins wrapped around an aluminum honeycomb core while the after body had fiberglass skins around a Nomex core. The main rotor hub weighing 767 lb, was an all-elastomeric design and incorporated flapping springs for zero 'g' controllability. The steel mast was retractable for transportability. The "flat-pack" transmission had dual inputs and reduction stages and was rated at 2712 shp for maximum continuous power.

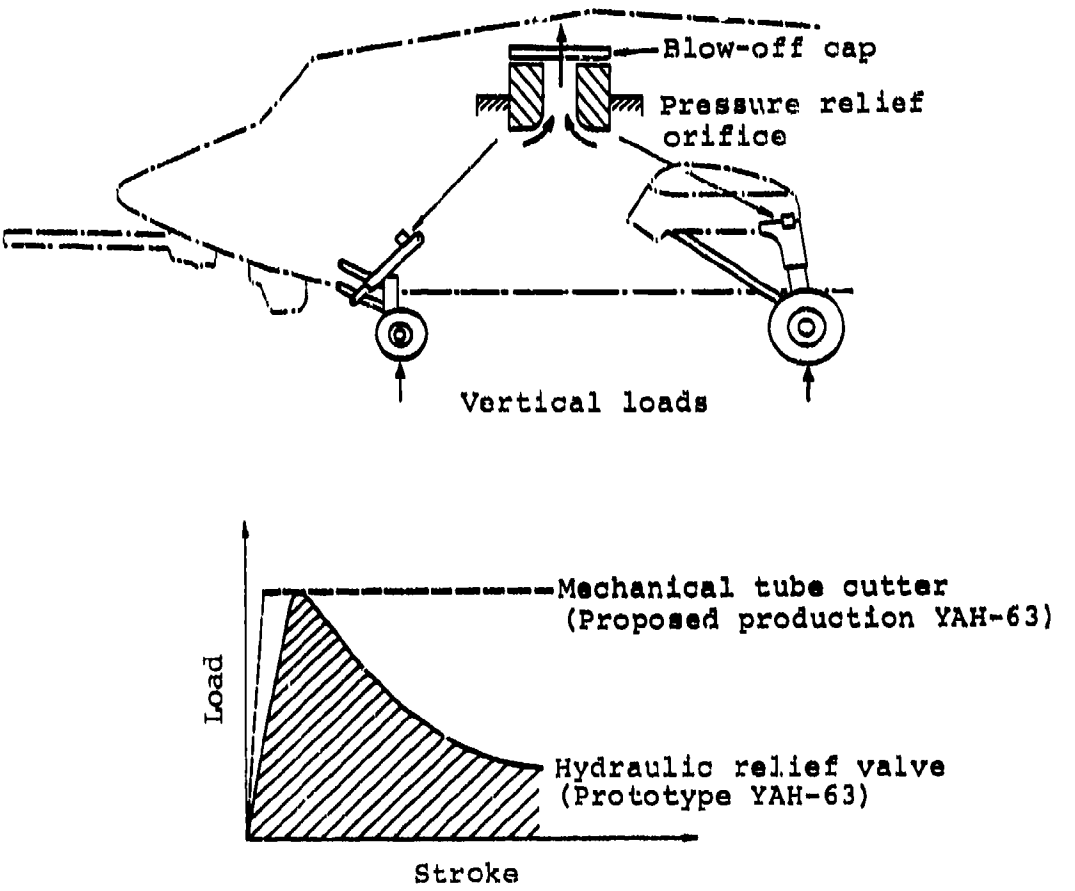

Figure A-12. YAH-63 prototype landing gear.

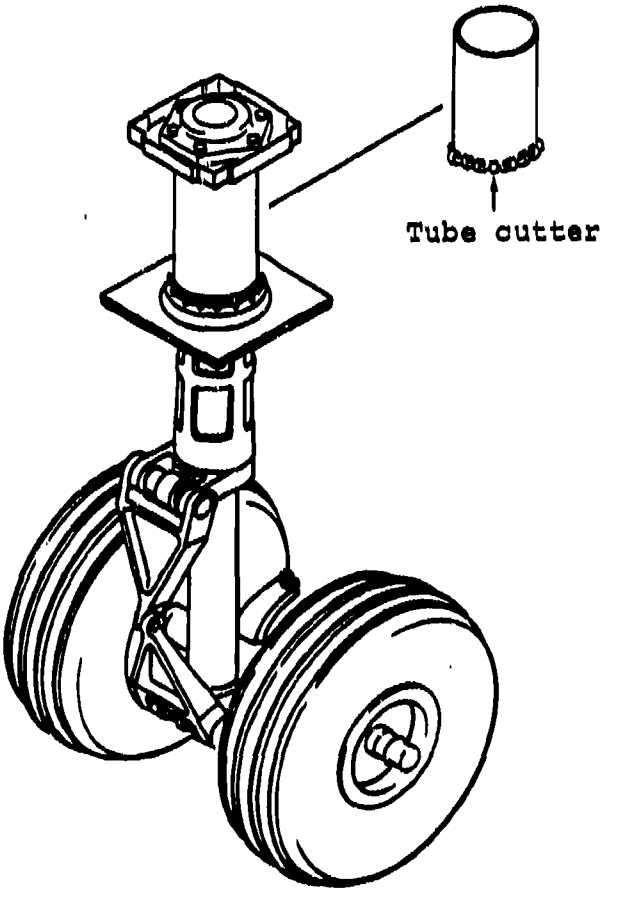

Figure A-13. Proposed production YAH-63 tube cutter nose landing gear.

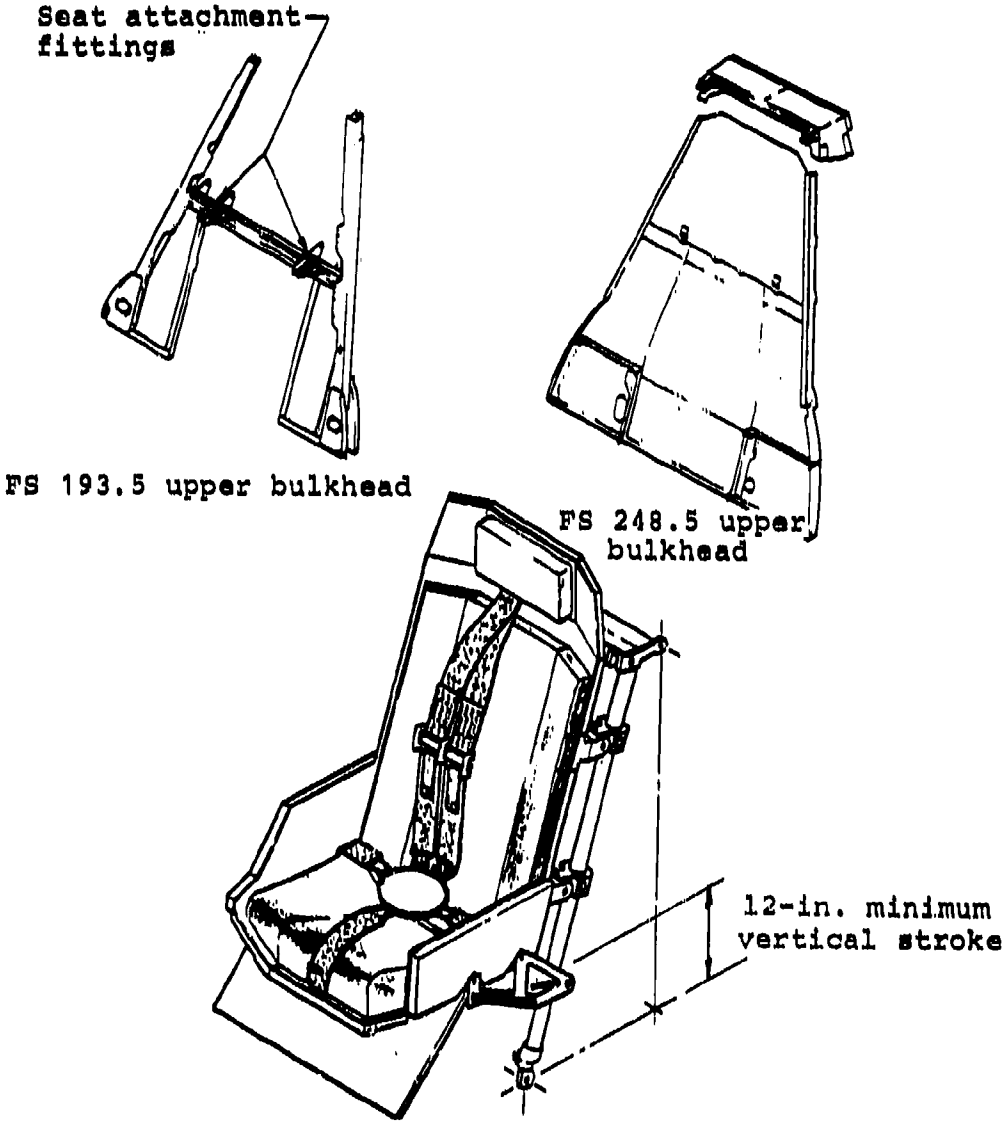

Figure A-14. YAH-63 prototype crew seat.

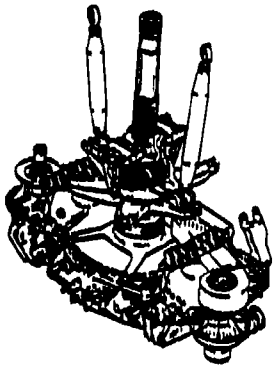

Main rotor mast
and transmission

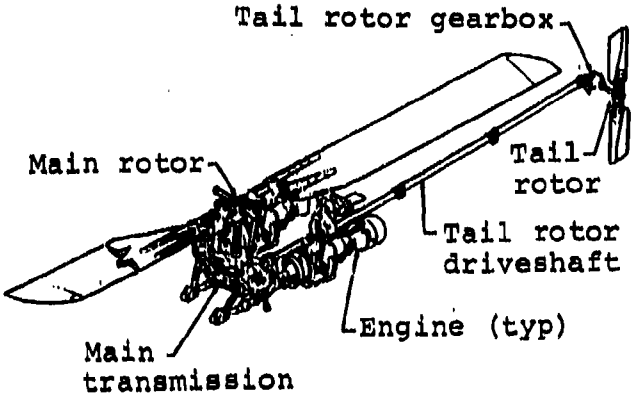

Drive system installation

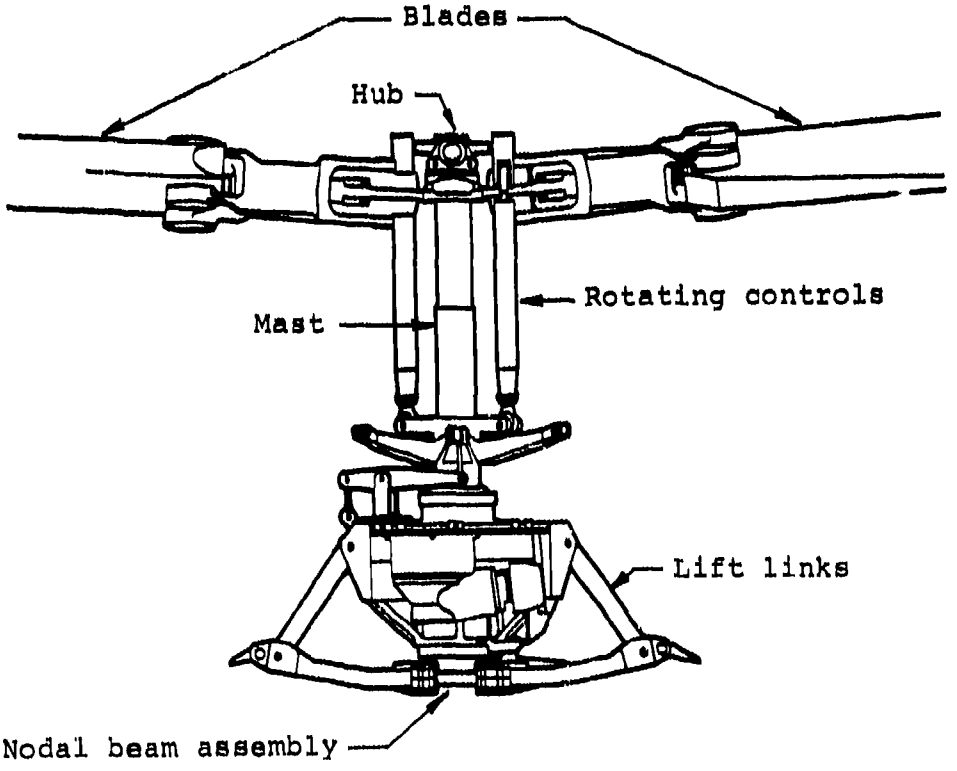

Figure A-15. YAH-63 main rotor pylon.

The nodal beam/focal mount main rotor pylon isolation system shown in detail in Figure A-16 substantially reduced fuselage vibration from the predominant main rotor two-per-rev excitation frequency. The transmission case was attached to the isolation system with four focused lift links and to the fuselage with longitudinal and lateral restraint springs. The focused pylon isolated fuselage vibration from the main rotor inplane shears and flapping moments, while the nodal beam flexures and tuning weights were sized to provide vertical vibration isolation.

To meet crashworthiness requirements, lateral crash links attached the transmission to the fuselage. The slotted links were not loaded during normal flight operations; however, in a crash impact, the crash links, together with the focal links, acted to retain the main rotor pylon system. The total system, including rotor, transmission, and mounting, weighed approximately 3545 lb.

The YAH-63 prototype powerplant installation included two General Electric T-700 advanced technology engines, each driving directly into the main transmission. Figure A-17 illustrates the mounting system used for each engine. For crashworthiness, the engines were widely separated and located outboard of the fuselage contour. Also, in the event of engine mount failure, the firewalls were capable of supporting and retaining the engines. Each installed engine weighed 463 lb.

A.2.4 Fuel System

Designed to meet MIL-F-38363 requirements, the suction feed fuel system in the YAH-63 prototype helicopter supplied fuel to the auxiliary power unit (APU) and T700 engines. The system met crashworthiness and combat survivability requirements. Compatible with JP-4 and JP-5 fuels, the system consisted of fuel storage, fuel feed, and fuel quantity gauging components. Also, the fuel system included provisions for priming, tank-to-engine crossfeed, tank-to-tank transfer, and refueling ports. The fuel system installation is illustrated in Figure A-18.

Two crashworthy fuel cells were located below the transmission deck, one forward and one aft of the FS 306.5 bulkhead. The tanks were self-sealing for .50 caliber ballistic threats with lower portions protected for 14.5 mm threats. The fuel cell interiors were filled with reticulated foam to minimize potential explosive or ram effects. The forward, aft, and bottom exterior sides were protected by 3 inches of fiberglass reinforced rigid foam. The two fuel tanks were

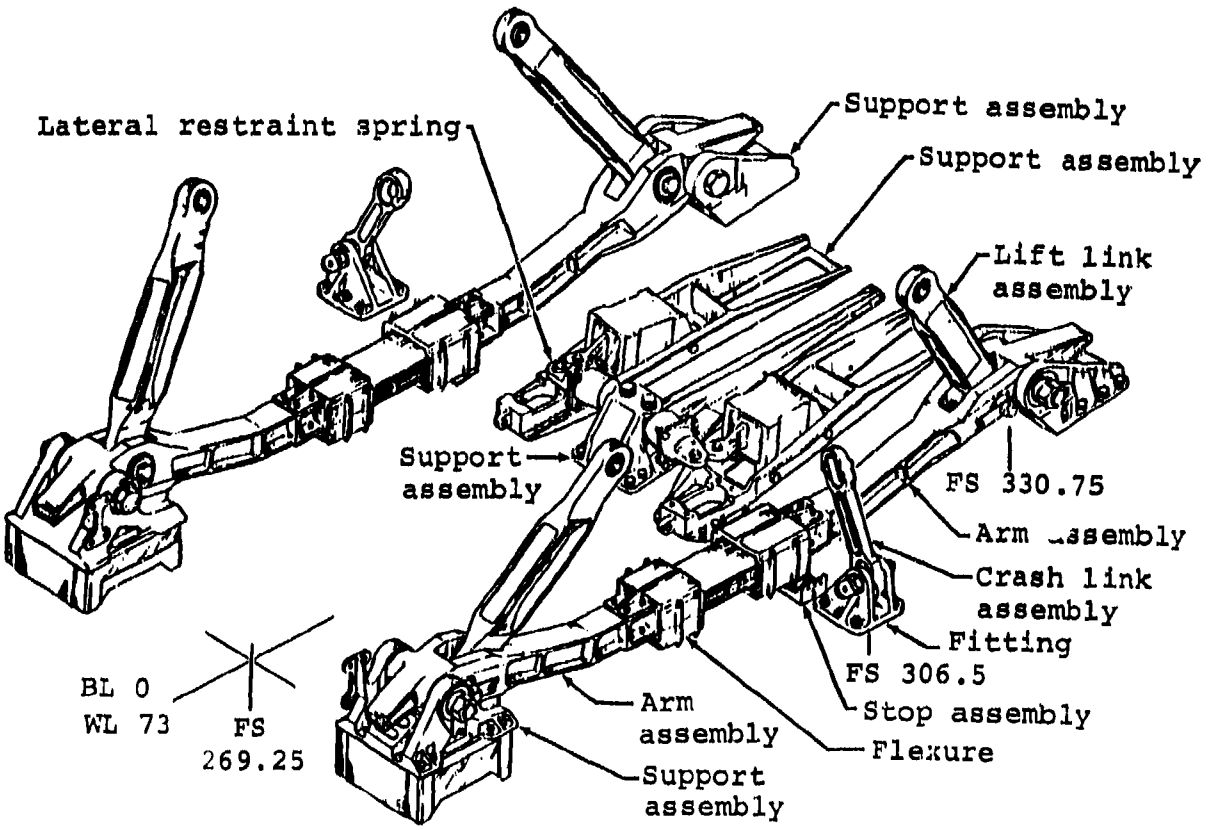

Figure A-16. YAH-63 main rotor pylon vibration isolation mounting system.

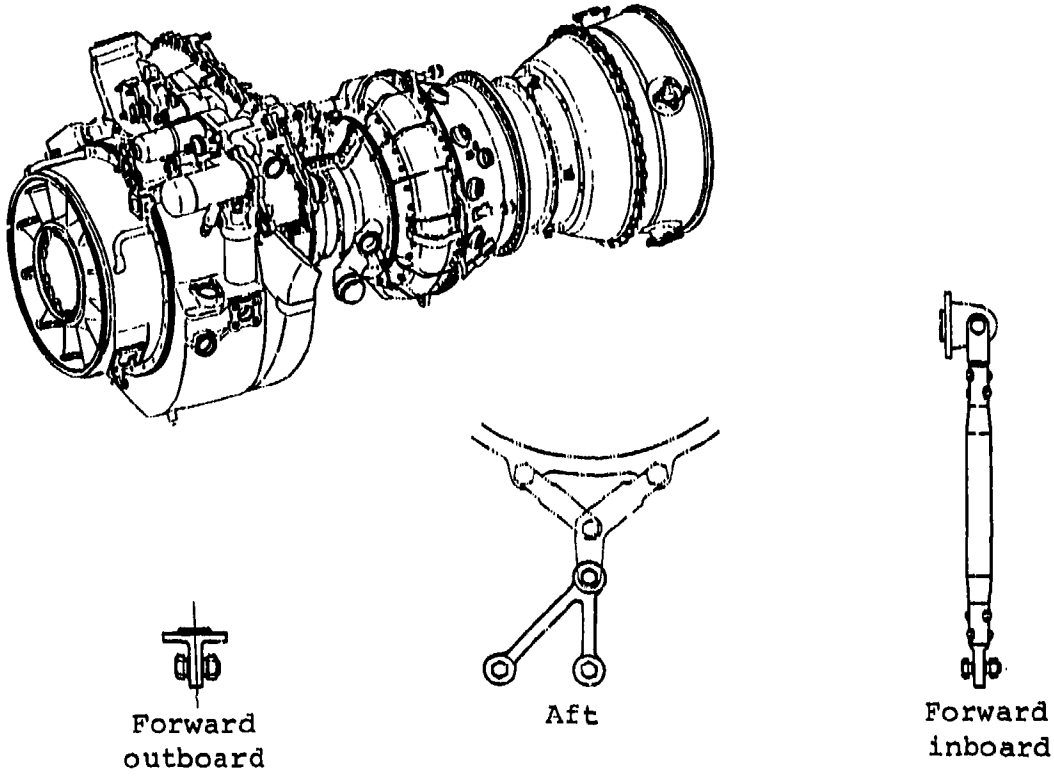

Figure A-17. YAH-63 T-700 engine and mounts.

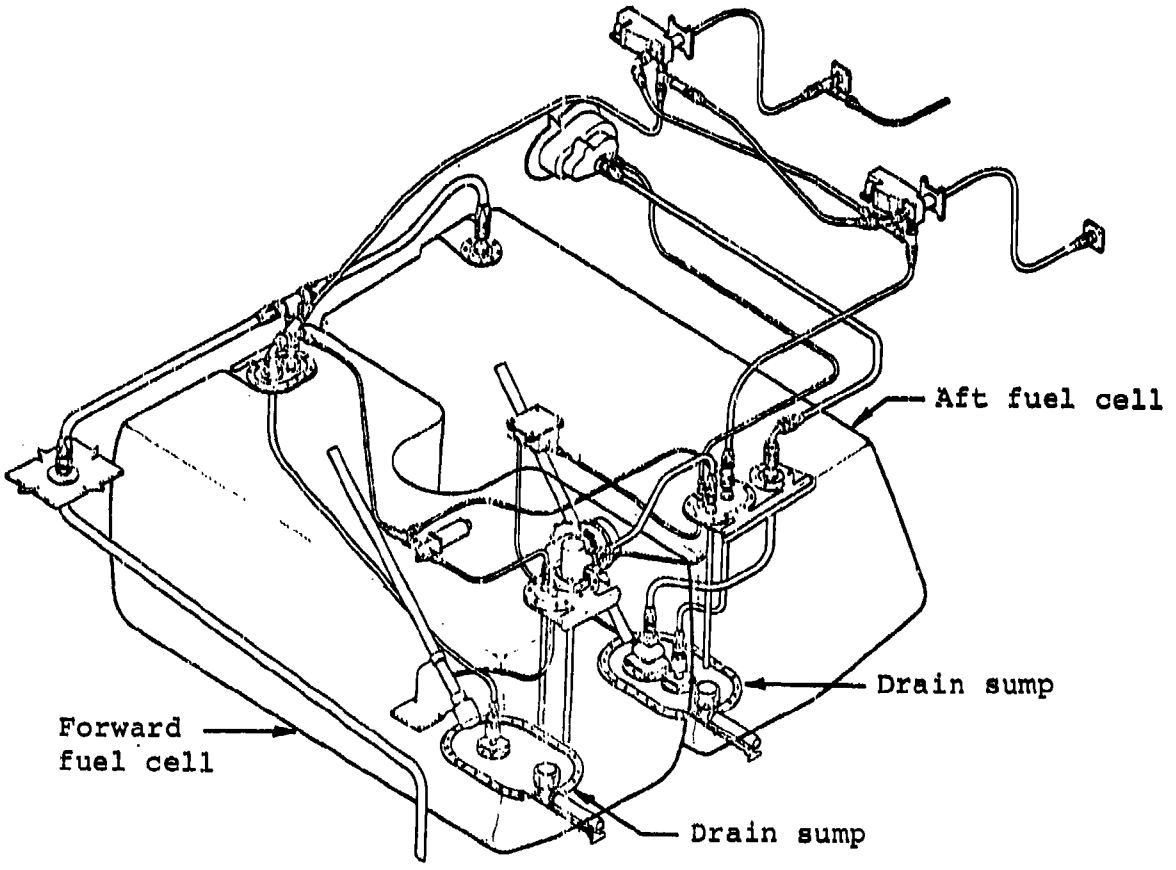

Figure A-18. YAH-63 fuel system installation.

joined by a self-sealing breakaway interconnect valve. Sump drains were located at the bottom of each tank having spring-loaded poppet-type valves which opened upward into the tank. Self-sealing breakaway valves were located externally at the tank ends of all fuel and vent lines and at the engine firewall of all feed lines to provide post-crash fire protection from fuel spillage.

To verify the crashworthiness capability of the fuel cells, drop tests were conducted in 1974. Both the forward and aft fuel cell passed the 65-ft drop with no tank rupture or fuel spillage.

APPENDIX B

STRUCTURAL ANALYSIS

The structural analysis conducted during the course of this program had as its purpose the derivation of input parameters for the KRASH computer code. The input parameters developed by structural analysis can be grouped into two general categories:

a. Those that define the linear and nonlinear load-deflection characteristics of the fuselage substructure,

b. Those that define the failure characteristics of the elements of fuselage structure, which may become frangible during impact inertia loadings and thus affect the airframe crash impact response.

LOAD-DEFLECTION CHARACTERISTICS

The load-deflection characteristics of two structural elements were analyzed to determine the behavior of the fuselage substructure during a crash impact. These two elements, the FS 193.50 bulkhead and the side frames from FS 193.50 to FS 306.50, are representative of the structure which is participating in the energy management system during a ground impact. Only that portion of these structures that is located below WL 40 is assumed to be crushing, while the structure above this waterline served as a backup for the crush zone. The reader is referred to the line drawing in Figure 3 and the fuselage section drawings in Figures A-1 and A-4 in Appendix A to gain a perspective for the location of the crush zone.

Bulkhead (FS 193.50)

Failure Load-Deflection

The FS 193.50 bulkhead shown in Figure B-1 is a sheet metal web which is vertically stiffened by angles and beads. These stiffening elements below WL 40 play an active part in the energy absorbing capability of the bulkhead. A section cut through the bulkhead below WL 40 illustrates the structure involved in the crush zone. The section above WL 40 is assumed to act as a back-up structure which reacts the crush zone impact forces and distributes them into the airframe.

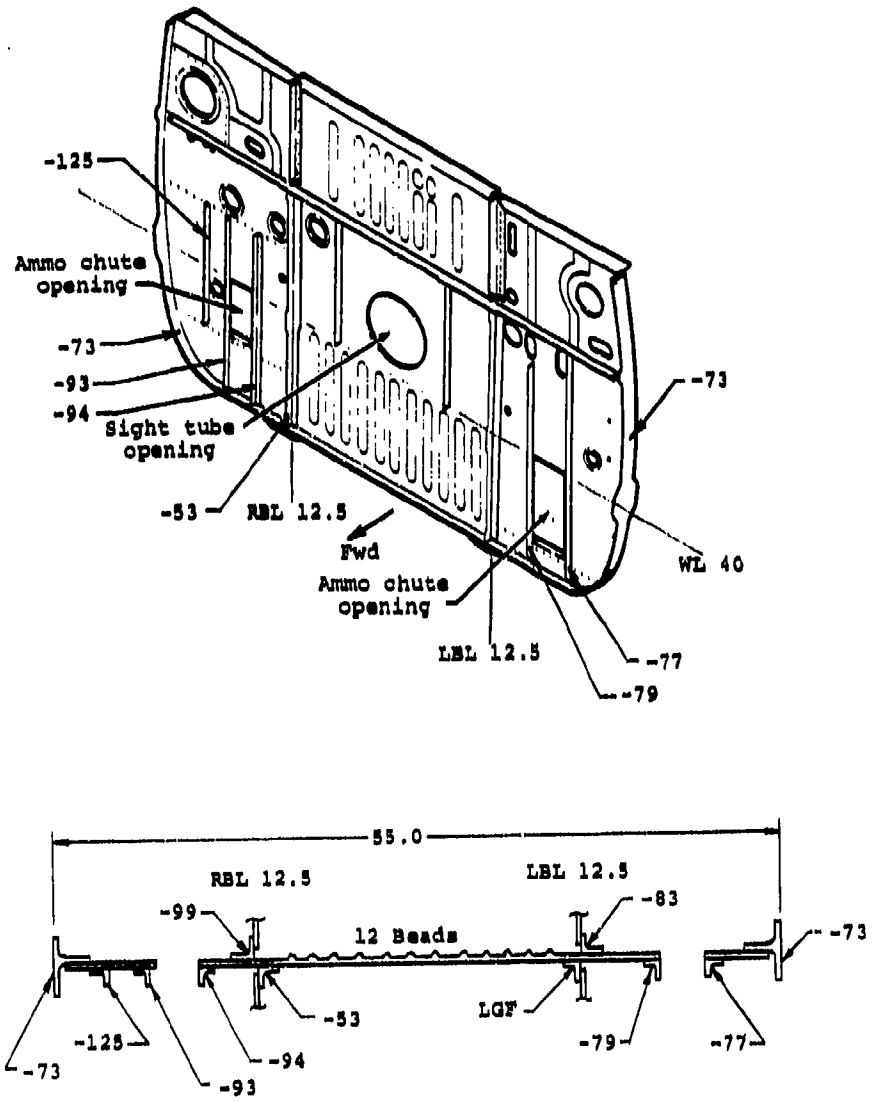

Figure B-1. FS 193.50 bulkhead.

This analysis assumes that the strains on the cross-section below WL 40 are uniform; as such the impact forces will distribute the loads to each element relative to its stiffness until a failure of an element occurs, at which time the load redistributes to the remaining unfailed elements. This redistribution will continue until the lower portion of the bulkhead totally collapses. This assumption enables the analyst to use strength-of-material approaches to define the failure modes and loads of the elements within the bulkhead. By combining the capabilities of each element involved in the load path, the analyst can derive the predicted failure load by summing the individual capabilities. For this analysis, the bulkhead has been divided into these structural elements:

1. The beaded web (±BL 10.92)
2. The RBL 12.5 intersection
3. The LBL 12.5 intersection
4. The -77 and -79 stiffeners
5. The -93 and -94 stiffeners
6. The -73 cap

1. <u>Beaded Web (±BL 10.92)</u>

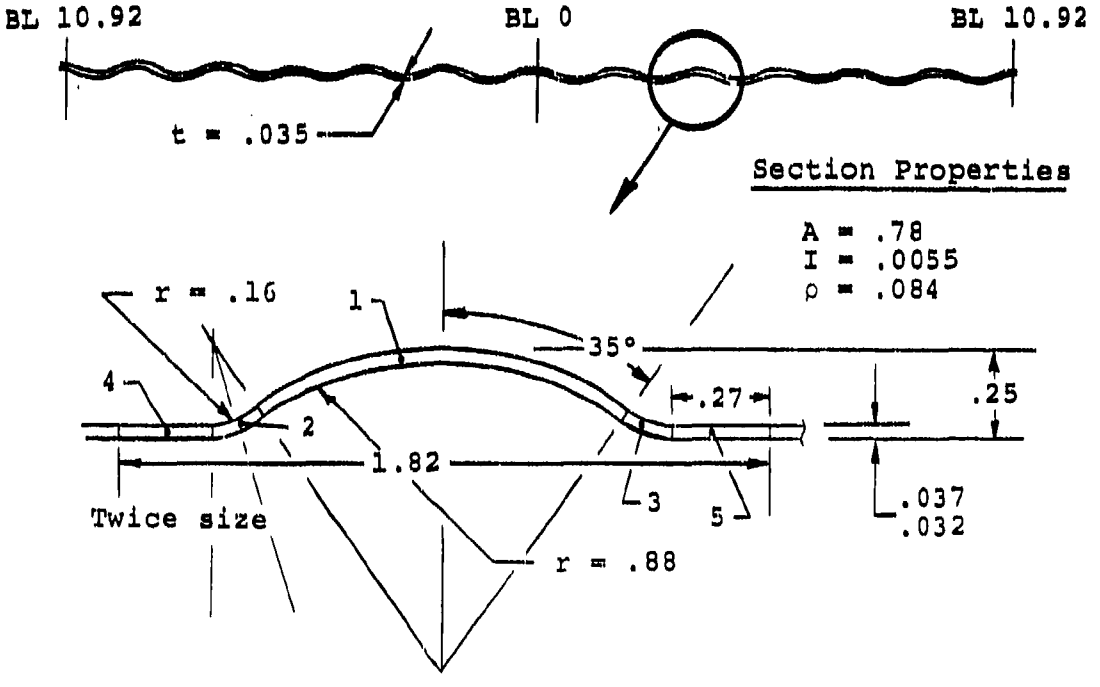

The critical mode of failure of the beaded web is that of an Euler column.

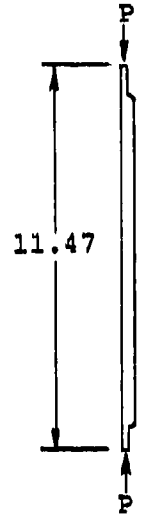

Failure Load

$$P_{cr} = \frac{\pi^2 EA}{(L'/\rho)^2}$$

$$P_{cr} = \frac{\pi^2(10.3)(10^6)(.78)}{\frac{11.47}{.084}^2} = \underline{4250 \text{ lb}}$$

Deflection at Failure

$$\Delta = \frac{P\ell}{AE}$$

$$\Delta = \frac{(4250)(11.47)}{(.78)(10.3)(10^6)} = \underline{.006 \text{ in.}}$$

2. RBL 12.5 Intersection

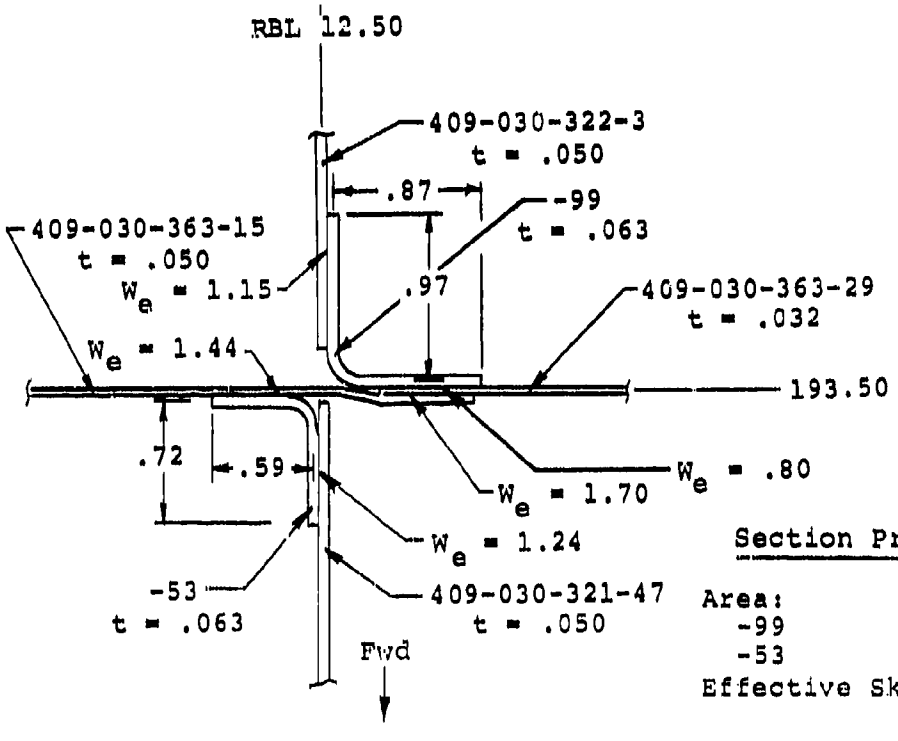

Section Properties

Area:	
-99	.116
-53	.082
Effective Skin:	.351
	.549

The RBL 12.5 intersection fails as a result of local crippling.

Failure Load

$$P_{cc} = \sum_{i}^{n} F_{cc_i}\, b_i t_i + F_{cc} \sum_{i}^{n} W_{e_i}\, t_{e_i}$$

where

F_{cc_i} = the crippling stress of element "i"

b_i = the length of element "i"

t_i = the thickness of element "i"

W_{e_i}, t_{e_i} = the effective width and thickness of the attached skin

$$F_{cc} = \frac{\sum_{i}^{n} F_{cc_i}\, b_i t_i}{\sum_{i}^{n} b_i t_i}$$

$$\sum_{i}^{n} F_{cc_i}\, b_i t_i = (47{,}450)(.59)(.063) + (39{,}125)(.72)(.063)$$

$$+ (30{,}800)(.97)(.063) + (34{,}130)(.87)(.063)$$

$$= 7290 \text{ lb}$$

$$F_{cc} = \frac{7290}{(.59+.72+.97+.87)(.063)} = 36{,}735 \text{ psi}$$

$$\sum_{i}^{n} W_{e_i}\, t_{e_i}\, F_{cc} = (36{,}735)\,[(1.44 + 1.24 + 1.15 + 1.70)(.050)$$

$$(.80)(.032)] = 11{,}100 \text{ lb}$$

$$P_{cc} = 7290 + 11{,}100 = \underline{18{,}390 \text{ lb}}$$

Deflection at Failure

$$\Delta = \frac{P\ell}{AE} = \frac{(18{,}390)(11.5)}{(.501)(10.3)(10^6)} = \underline{\underline{.041 \text{ in.}}}$$

3. LBL 12.5 Intersection

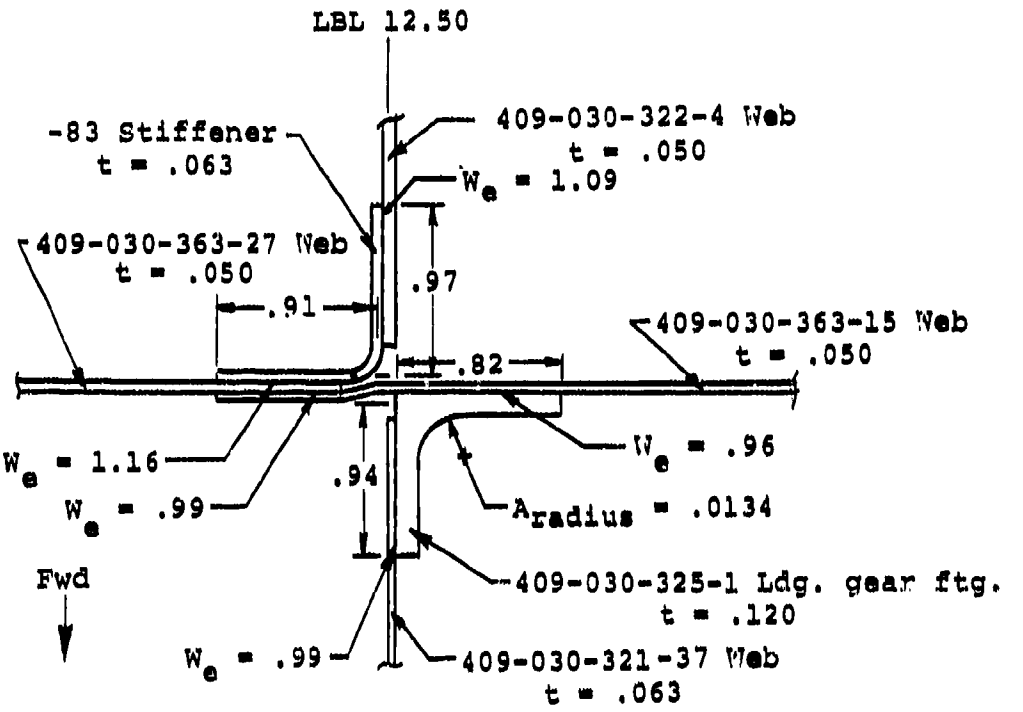

The LBL 12.5 intersection fails as a result of local crippling.

Failure Load

$$P_{cc} = \sum_i^n F_{cc_i}\, b_i t_i + F_{cc} \sum_i^n W_{e_i}\, t_{e_i}$$

where:

F_{cc_i} = the crippling stress of element "i"

b_i = the length of element "i"

t_i = the thickness of element "i"

W_{e_i}, t_{e_i} = the effective width and thickness of the attached skin

$$F_{cc} = \frac{\sum_{i}^{n} F_{cc_i}\, b_i t_i}{\sum_{i}^{n} b_i t_i}$$

$$\sum_{i}^{n} F_{cc_i}\, b_i t_i = (30,800)(.97)(.063) + (32,470)(.91)(.063)$$

$$+ (63,000)(.94)(.12) + (63,000)(.83)(.12)$$

$$+ (63,000)(.0134) = 17,910 \text{ lb}$$

$$F_{cc} = \frac{17,910}{(.97+.91)(.063)+(.94+.82)(.12)+(.0134)} = 52,210 \text{ psi}$$

$$F_{cc} \sum_{i}^{n} W_{e_i}\, t_{e_i} = (52,210)\,[(1.16 + 1.09 + .99 + .99)(.050)$$

$$+ (.96)(.063)] = 14,200 \text{ lb}$$

$$P_{cc} = 17,910 + 14,200 = \underline{32,110 \text{ lb}}$$

Deflection at Failure

$$\Delta = \frac{P\ell}{AE} = \frac{(32,110)(11.5)}{(.615)(10.3)(10^6)} = \underline{.058 \text{ in.}}$$

4. Stiffeners (-77, -79)

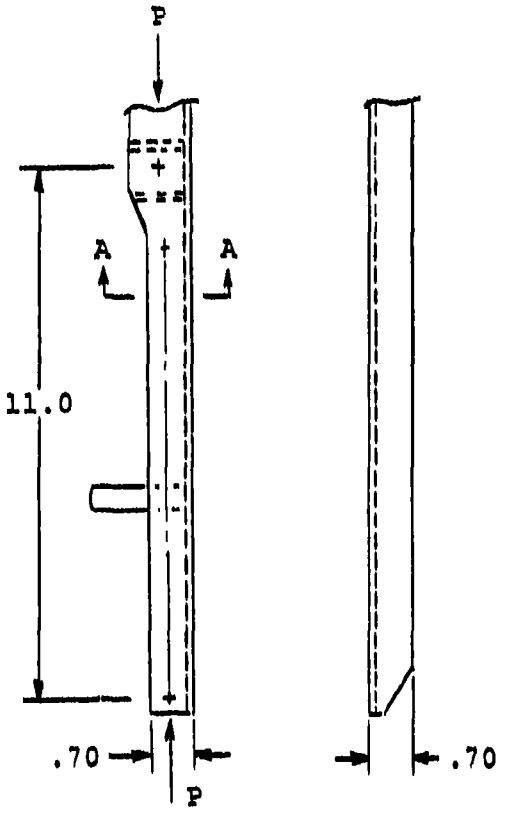

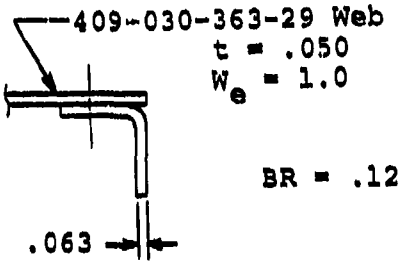

Section A-A

Section Properties

I = .0039
ρ = .216

These stiffeners fail as a result of column buckling loads. It is assumed that the initial failure is determined by the stiffness of the angle and that the adjoining web will act at the same stress level.

Failure Load

$$F_{cr} = \frac{\pi^2 E}{(\ell'/\rho)^2} = \frac{\pi^2 (10.5)(10^6)}{(11/.216)^2} = 39{,}960 \text{ psi}$$

$$\text{Area} = (2)(.67)(.063) + (1.0)(.050) = .134 \text{ in}^2$$

$$P_{cr} = (39{,}960)(.134) = 5350 \text{ lb/stiffener}$$

$$P_{cr} = (2)(5350) = \underline{10{,}700 \text{ lb}}$$

Deflection at Failure Load

$$\Delta = \frac{P\ell}{AE} = \frac{(10{,}700)(11)}{(.268)(10.5)(10^6)} = \underline{.042 \text{ in.}}$$

5. Stiffeners (-93, -94)

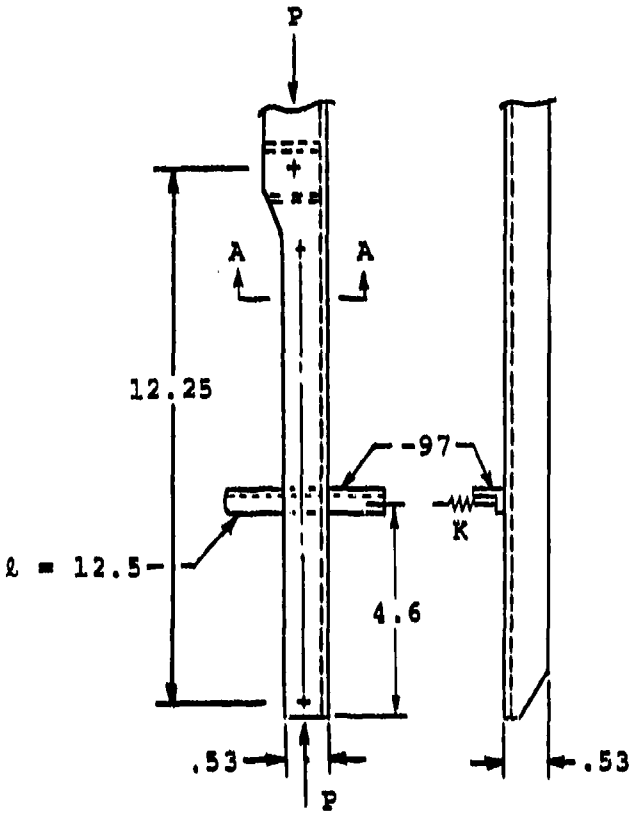

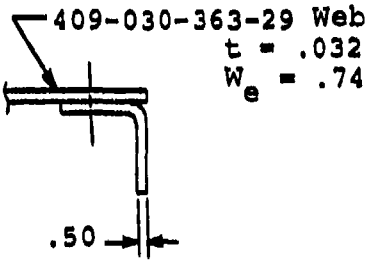

Section A-A

Section Properties

$I = .0014 \text{ in}^4$
$\rho = .164$ in

These stiffeners fail as a result of column buckling loads. It is assumed that the initial failure is determined by the stiffness of the angle and that the adjoining web will act at the same stress level. An elastic support is provided by the -97 angle.

Failure Load

$$\text{Stiffness (K) of elastic support} = \frac{48\,EI}{\ell^3}$$

$$= \frac{48(10.5)(10^6)(.0014)}{12.5^3}$$

$$= 361 \text{ lb/in.}$$

For stiffener: $\dfrac{K\ell^3}{EI} = \dfrac{(361)(12.25)^3}{(10.5)(10^6)(.0014)} = 45$

See figure below: $\frac{a}{\ell} = \frac{4.6}{12.25} = .376$

$c = 1.75$

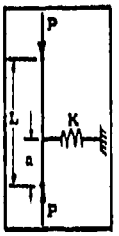

K is the spring constant with units of $\frac{lb}{in}$

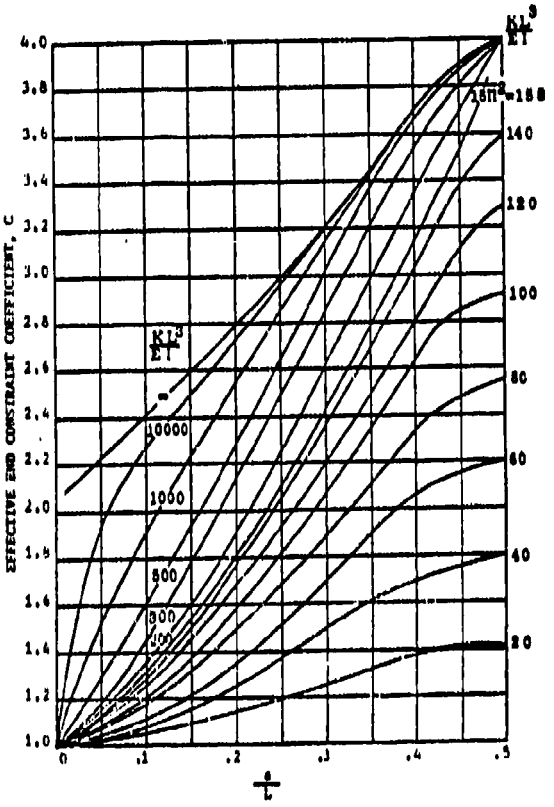

$$\ell' = \frac{\ell}{\sqrt{c}} \quad \frac{12.25}{\sqrt{1.75}}$$

$$\ell' = 9.26 \text{ in.}$$

$$F_{cr} = \frac{\pi^2 E}{(\ell'/\rho)^2} = \frac{\pi^2 (10.5)(10^6)}{(9.26/.164)^2} = 32{,}500 \text{ psi}$$

$$\text{Area} = (.74)(.032) + (2)(.505)(.05) = .074 \text{ in}^2$$

$$P_{cr} = (32{,}500)(.074) = 2410 \text{ lb/stiffener}$$

$$P_{cr} = (2)(2410) = \underline{4820 \text{ lb}}$$

Deflection at Failure

$$\Delta = \frac{P\ell}{AE} = \frac{(4820)(12.25)}{(.148)(10.5)(10^6)} = \underline{.038 \text{ in.}}$$

6. Cap (-73)

The failure of the cap is precipitated by beam-column action due to the eccentric load paths. Total failure is caused when the cap allowable crippling stress is attained.

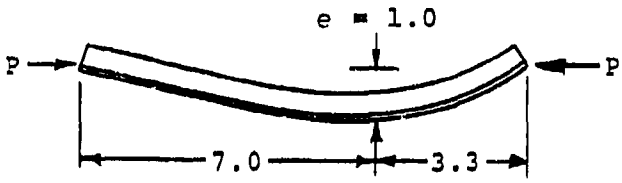

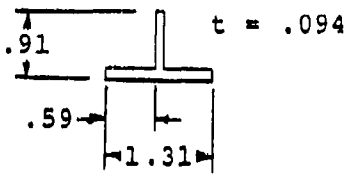

$I = .0141 \text{ in}^4$

$$F_{cc} = \frac{\sum_{i}^{n} F_{cc_i} b_i t_i}{\sum_{i}^{n} b_i t_i}$$

$$= \frac{(55,170)[(.65)(.094)+(.65)(.094)+(.863)(.099)]}{[(.65)(.094)+(.65)(.094)+(.863)(.094)]}$$

$F_{cc} = 55,170$ psi

Assuming linear strain distribution:

$$e_c = \frac{F_{cc}}{E} = \frac{55,170}{(10.7)(.06)} = .0052 \text{ in./in.}$$

$$e_t = \frac{.0052}{.688} (.91-.688) = .0017 \text{ in./in.}$$

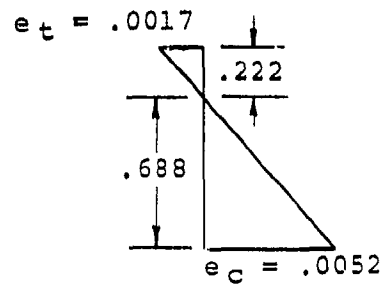

$$M_{all} = Pe = \frac{F_{cc} I}{c} = \frac{(55,170)(.0141)}{.688} = 1130 \text{ in.-lb}$$

Since $e = 1.0$ in.

Then $P = 1130$ lb/side

$P_{cr} = \underline{2260 \text{ lb/both sides}}$

Deflection at Failure

$$\Delta = \text{Deflection due to bending} + \frac{P\ell}{AE}$$

$$dv = \frac{1}{EI} \int_0^{3.3} \frac{PQ\ x^2}{3.32}\, dx \int_0^{7.0} P-\frac{Px}{7}\quad Q-\frac{Qx}{7}\, dx$$

$$V_{int} = \frac{3.43\ PQ}{EI}$$

$$V_{ext} = Q\ \Delta$$

$$\Delta = \frac{3.43\ P}{EI} = \frac{3.43\ (1130)}{(10.7)(10^6)(.0141)} = .026 \text{ in./bending}$$

$$\Delta = \frac{P\ell}{AE} = \frac{1130\ (10.3)}{(.203)(10.7)(10^6)} = .0054 \text{ in.}$$

$$\Delta_{total} = .026 + .0054 = \underline{.0314 \text{ in.}}$$

Post-Failure Nonlinear Load-Deflection

The determination of the post-failure nonlinear portion of the load-deflection curve is obtained by using the logic proposed by Wittlin and Park in Reference 9. The deflection curve is represented by the equation

$$P = \frac{1}{\left|\frac{\mu}{2}\left(\ell-\frac{\mu}{2}\right)\right|^{1/2}} \left|M_{min} + (M_{max} - M_{min})e^{-K\theta}\right|$$

where

μ = deflection

P = load

M_{max} = moment for the undeformed cross section

M_{min} = plastic hinge moment

K = constant = $\alpha \left(\frac{\gamma_o}{\gamma}\right)^2 \left(\frac{t_o}{t_w}\right)$

For angle-type stiffeners where

$$\gamma = \ell'/\rho = 12/(3)^{1/2}(.356) = 19.5,\ t_o = .032$$

$$\gamma_o = 20,\ \alpha = 5,\ t_w = .050$$

$$K = 3.38$$

θ = plastic hinge rotation

$$= \tan^{-1}\left\{\frac{\left[\frac{\mu}{2}\left(\ell-\frac{\mu}{2}\right)\right]}{\frac{\ell-\mu}{2}}\right\}^{1/2}$$

M_{max} is determined by the geometry of the undeformed cross-section shown below where

$$M_{max} = 1.15\ (M_{1,max} + M_{2,max})$$

where

$$M_{2,max} = \frac{1}{4}\,bt^2\,F_{cy} = \frac{1}{4}\,[(37.8)(.050)^2 + (11.5)(.032)^2]\,[66{,}000]$$

$$M_{2,max} = 1754 \text{ in.-lb}$$

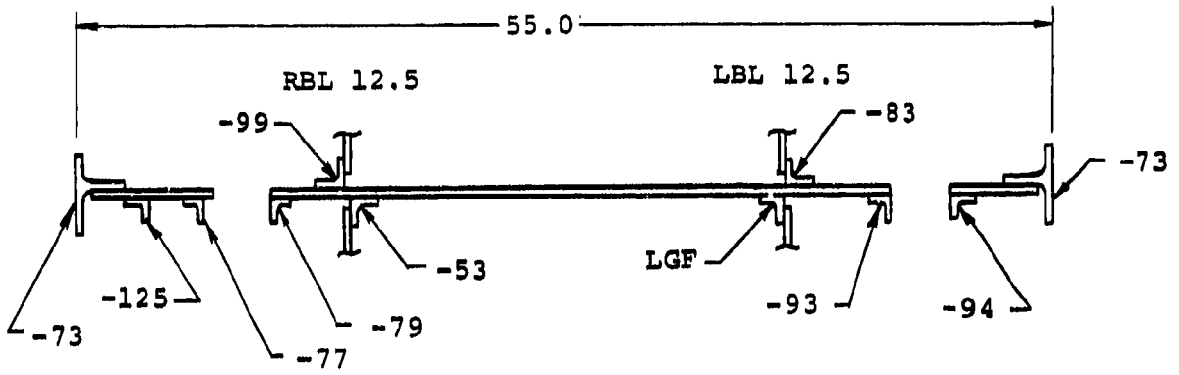

Element	Area	y	Ay	e	Σ Ae
-73	.203	.097	.0197	.095	.019
-125	.097	-.129	-.0125	-.131	.012
-77	.134	-.115	-.0154	-.117	.016
-79	.134	-.115	-.0154	-.117	.016
RBL int	.501	.016	.0080	.014	.007
Bead pnl	.780	.114	.0889	.112	.087
LBL int	.615	-.119	-.0732	-.121	.074
-93	.074	-.098	-.0073	-.10	.007
-94	.074	-.098	-.0073	-.10	.007
-73	.203	.097	.0197	.095	.019
	2.815		.0053		.266

$$\bar{y} = \frac{.0053}{2.815} = .002 \text{ in.}$$

$$M_{1,max} = \Sigma A_i e_i F_{cy} = (.266)(66,000) = 17,556 \text{ in.-lb}$$

$$M_{max} = 1.15\ (17,556 + 1754) = 22,205 \text{ in.-lb}$$

For the calculation of M_{min}, the upstanding legs of the stiffeners are assumed to be broken off because they are fabricated from a 7075 alloy.

$$M_{min} = 1.15\ (M_{1,min} + M_{2,min})$$

where

$$M_{2,min} = \frac{1}{4}\, bt^2\, F_{cy}$$

$$M_{2,min} = \frac{1}{4}\, [(37.8)(.050)^2 + (11.5)(.032)^2]\ [66,000]$$

$$M_{2,min} = 1754 \text{ in.-lb}$$

and

$$M_{1,min} = F_{cy} \Sigma |A_i e_i|$$

Area = 2.82 in²

$\bar{y}$ = .018 in. $M_{1,min}$ = 66,000 (.0538) = 3550 in.-lb

$\Sigma |A_i e_i|$ = .0538 in³

M_{min} = 1.15 (3550 + 1754) = 6100 in.-lb

Therefore, the nonlinear load-deflection curve is represented by

$$D = \frac{6100 + 16{,}105\ e^{-K\theta}}{\left| \frac{\mu}{2} \left(\ell - \frac{\mu}{2} \right) \right|^{1/2}}$$

Assuming that this deflection shape represents the post-failure behavior of the elements in the bulkhead, the curves in Figure B-2 are derived by matching the curve shapes to the failure loads. The bulkhead load-deflection curve shown in Figure B-3 is obtained by combining the element curves.

Side Frames (FS 193.50 to 306.50)

Failure Load-Deflection

The side frames, shown in Figure B-4, are stiffened beams and skins which form closed boxes similar to those tested and reported on in Reference 9. Because of this structural similarity, it has been assumed that the post-failure behavior of the YAH-63 structure will be like that of the tested specimens. The pre-failure behavior of the YAH-63 structure can be predicted using strength-of-material analysis. As in the analysis of the bulkhead, it will be assumed that the strains on the cross section below WL 40 are uniform and that the impact forces are distributed uniformly. It is also assumed that the loads are distributed within each element in the cross section relative to its stiffness. The pre-failure analysis will assume that the crushing capability of the side frames can be calculated by a summation of the individual components in the structure.

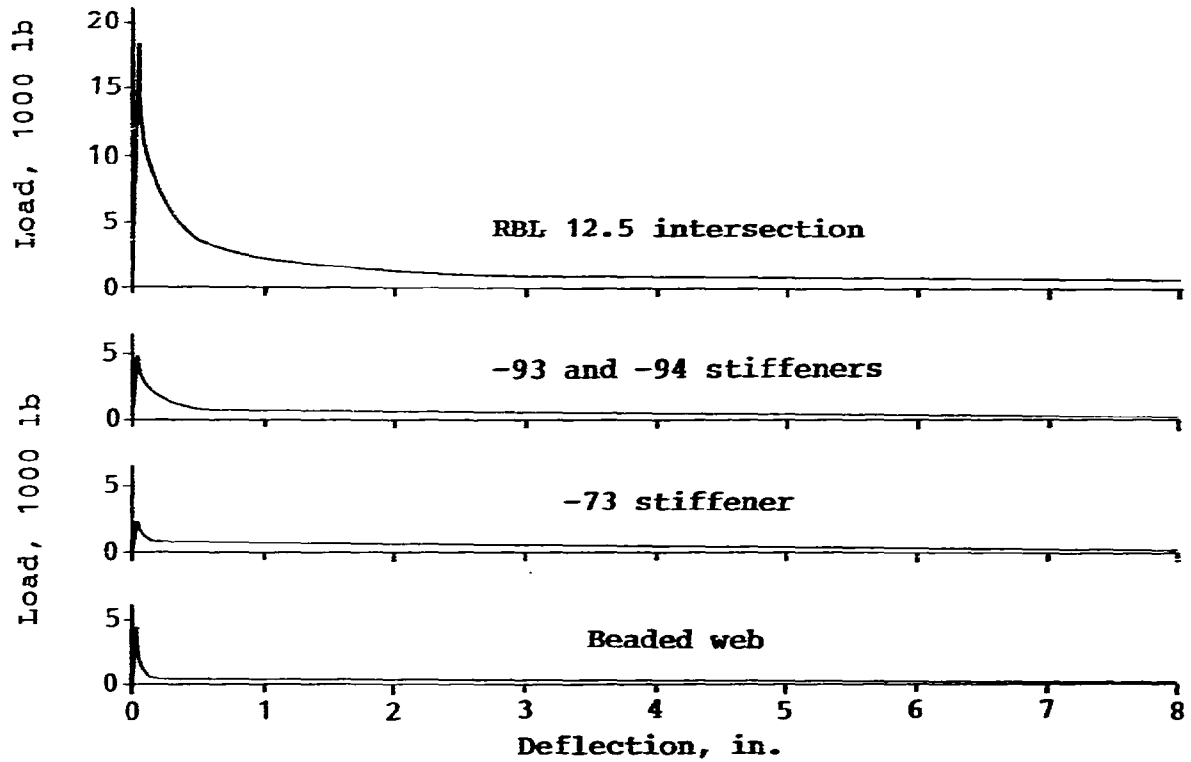

Figure B-2. Element load-deflection curves.

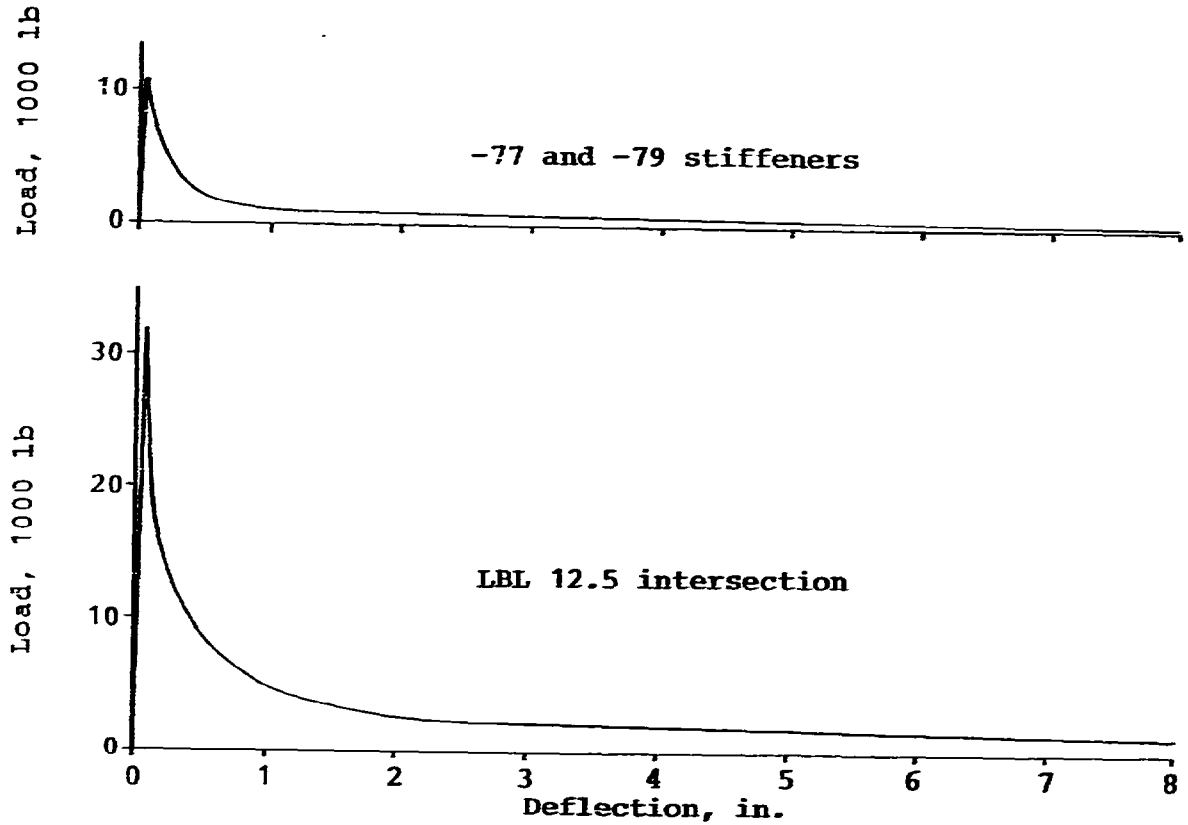

Figure B-2 (cont'd). Element load-deflection curves.

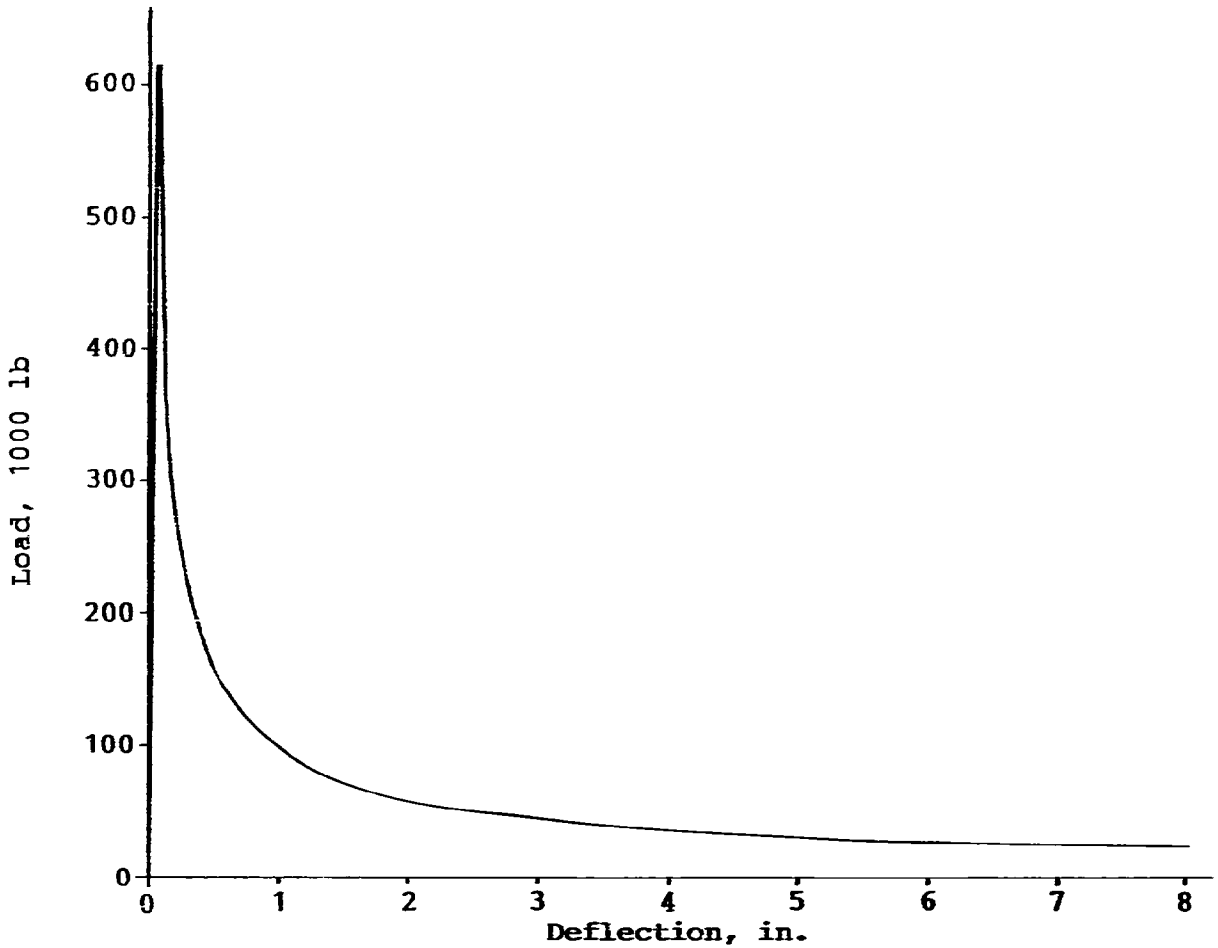

Figure B-3. Load-deflection curve for FS 193.50 bulkhead.

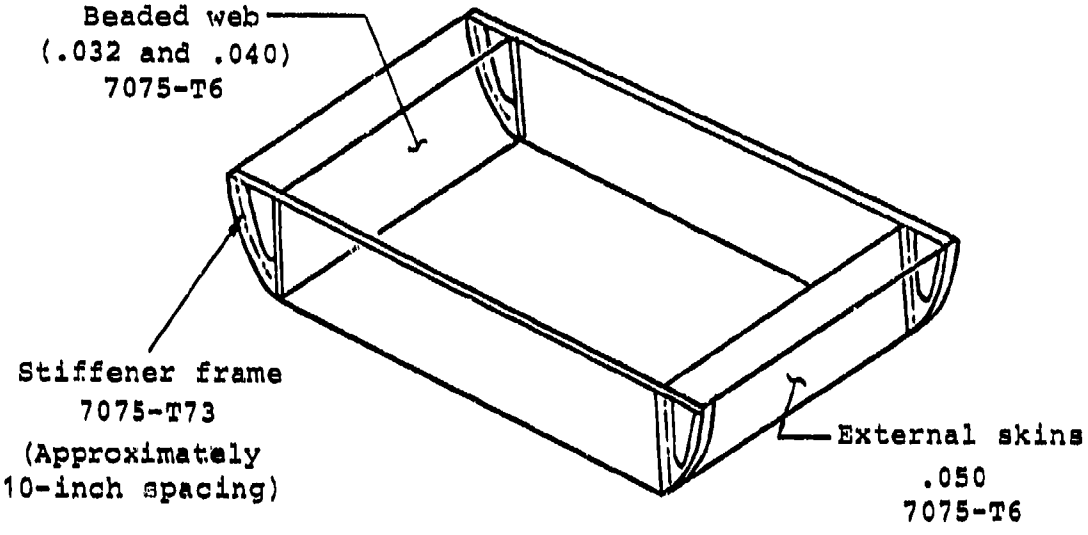

Typical box structure

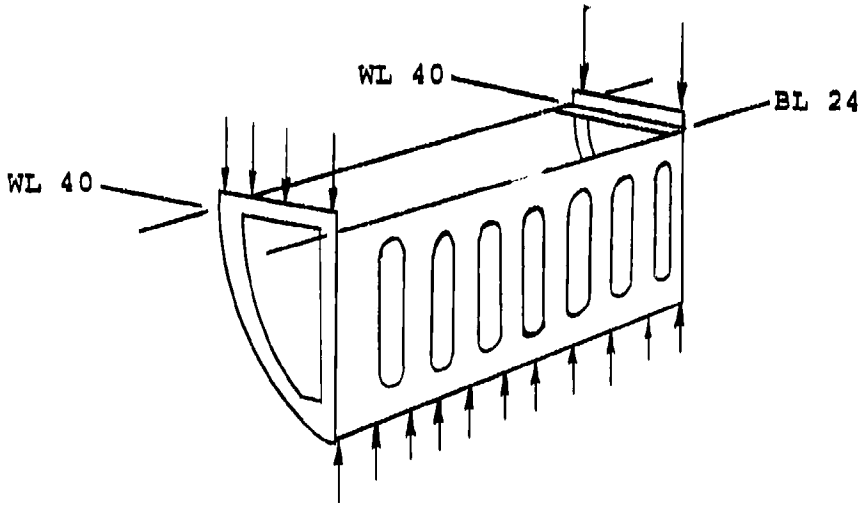

Typical crush load path

Figure B-4. Side frames.

The side frame consists of these structural elements:

1. Stiffener fittings
2. Beaded webs (BL 24 beams)
3. Skin

1. Stiffener Fittings

The stiffeners are spaced approximately 10 inches apart.

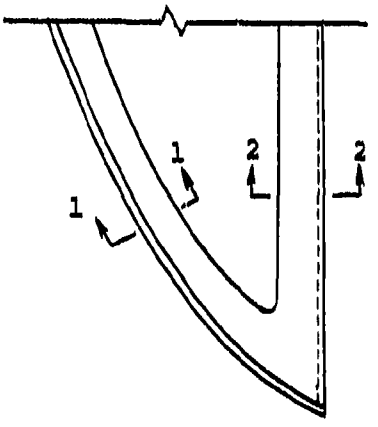

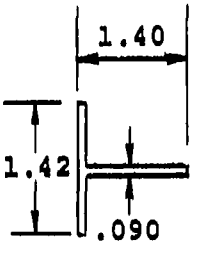

1-1

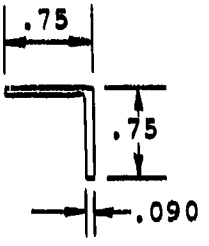

2-2

Material: 7075-T73
F_{tu} = 71,000 psi, F_{cy} = 63,000 psi
E_c = 10.4 (10^6) psi

This element will fail by crippling.

Failure Load

$$P_{cc} = \sum_{i}^{n} F_{cc_i} b_i t_i$$

$$P_{cc} = (63,000)(2)(.71)(.090) + (37,230)(1.355)(.090)$$
$$+ (63,000)(2)(.705)(.090) = \underline{20,600 \text{ lb}}/\text{stiffener}$$

2. Beaded Web (BL 24 Beam)

The failure mode of these beaded webs is similar to that of the bulkhead webs.

Failure Load

$$P_{cr} = \frac{\pi^2 EA}{(\ell'/\rho)^2}$$

where

$E = 10.3\ (10^6)$ psi

$A = .0696$ in^2

$\ell' = 11.5$ in.

$\rho = .084$ in.

$$P_{cr} = \frac{\pi^2\ (10.3)(10^6)(.0696)}{\left(\frac{11.5}{.084}\right)^2} = 378 \text{ lb/bead}$$

There are six beads in the 10-inch spacing.

$$P_{cr} = (6)(378) = \underline{2270 \text{ lb}} \text{ per side}$$

3. Skin

The side skins will fail as plate elements during the compression load.

Failure Load

Plate dimensions: a = 10 in., b = 10 in., t = .050 in.

Assume clamped edges:

$$P_{cr} = K\ E \left(\frac{t}{b}\right)^2 A$$

for

$a/b = 1.0$; $K = 9.4$

$A = 10\ (.050) = .50$ in^2

$E = 10.5\ (10^6)$ psi

$$P_{cr} = (9.4)(10.5)(10^6)\left(\frac{.05}{10}\right)^2 (.50) = \underline{1230 \text{ lb}} \text{ per side}$$

4. Total

Stiffener fittings: (20,600) (11) (2) = 453,200 lb

Beaded web: $(2270)\left(\frac{306.5 - 193.5}{10}\right)(2) = 51,300$ lb

Skin: $(1245)\left(\frac{306.5 - 193.5}{10}\right)(2) = 28,140$ lb

$$P_{cr} = \underline{532,640 \text{ lb}}$$

Post-Failure Nonlinear Load-Deflection

The shapes of the load-deflection curves shown in Figures 86 through 89 of Reference 9 are considered to be representative of the box-like structure of the YAH-63. The shapes of these curves are reproduced in nondimensionalized form in Figure B-5 along with the mean curve shape. This mean curve shape was chosen to represent the load-deflection behavior of the side frames. The load-deflection curve for the side frames was derived from the mean shape curve.

Vertical Fin Load-Deflection

The vertical fin load-deflection curve is shown in Figure B-6 and was determined by an analysis done during the prototype YAH-63 development. Rather than reanalyze the fin crushing characteristics, the existing data were used in the KRASH model and would be reviewed following the T-41 drop test if there was evidence of it being considerably difficult.

FAILURE CHARACTERISTICS

The failure characteristics of two structural components were analyzed during this study because it was felt that their failures would have a significant impact on the KRASH analysis. The two components, the nose and the tailboom, must resist large inertia forces during the impact because of the location of heavy mass items within the structure; additionally, there are local loads input from the nose landing gear and vertical fin.

Reference 9
Figures 86 - 89

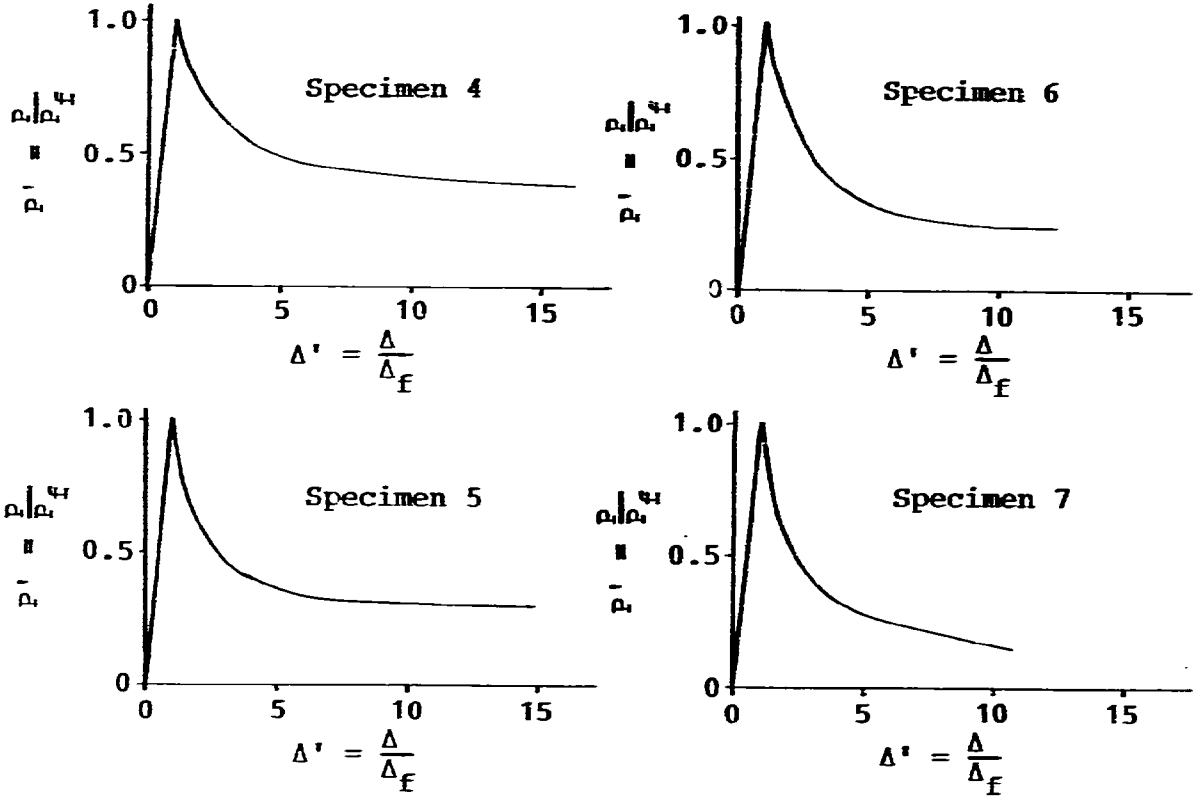

Figure B-5. Nondimensionalized curve shape.

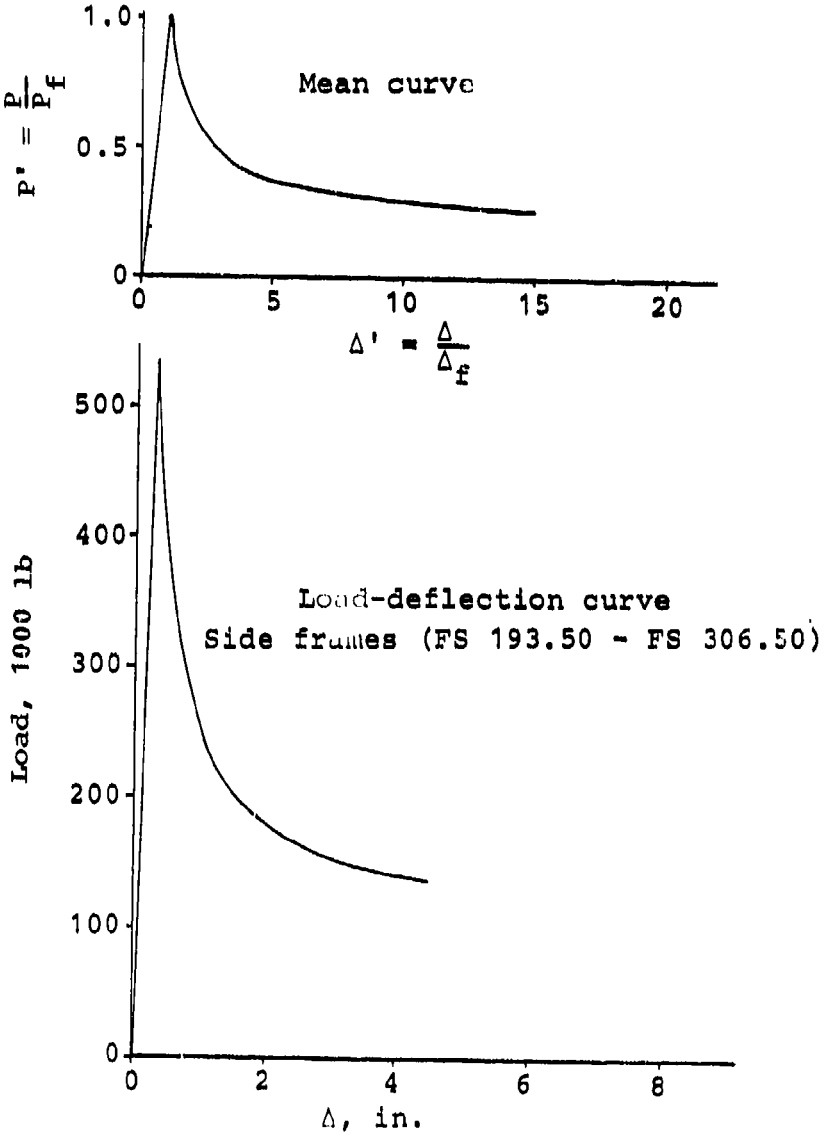

Figure B-5 (cont'd). Nondimensionalized curve shape.

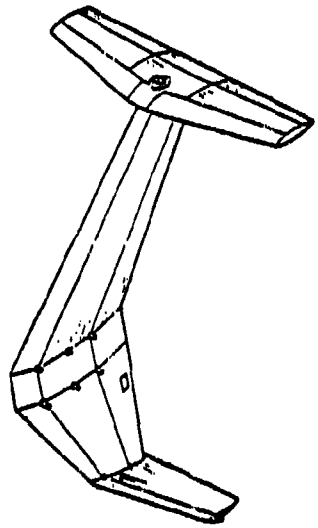

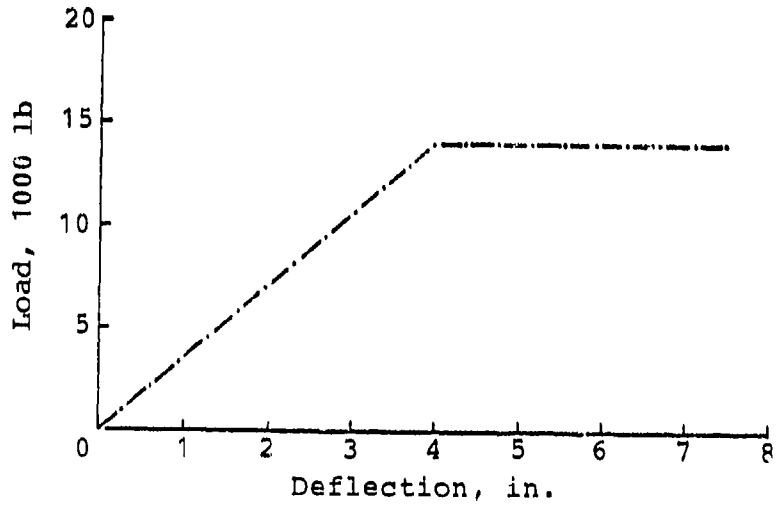

Figure B-6. Vertical fin load-deflection.

The analysis for each of these components uses the strength-of-materials approach. Failure is assumed to occur when the bending moment which acts on the cross section exceeds the allowable plastic bending moment. The failure modes on the compression side of the structure dictate the capability of the section. Failures of compression elements, because of crippling or overall stability, cause a shift of the neutral axis which in turn overloads the tension members, creating a catastrophic condition.

The sections analyzed and their computed failure moments are shown in Figures B-7 and B-8.

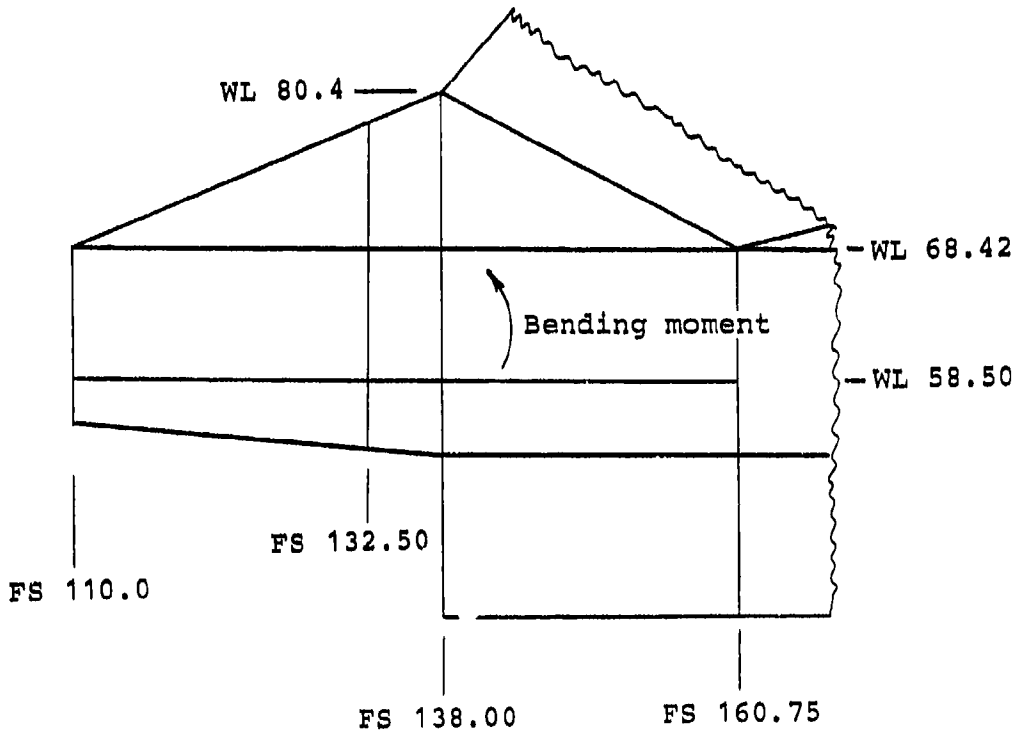

Maximum bending moment at FS 138.00 = ±801,400 in-lb

Figure B-7. Nose section failure.

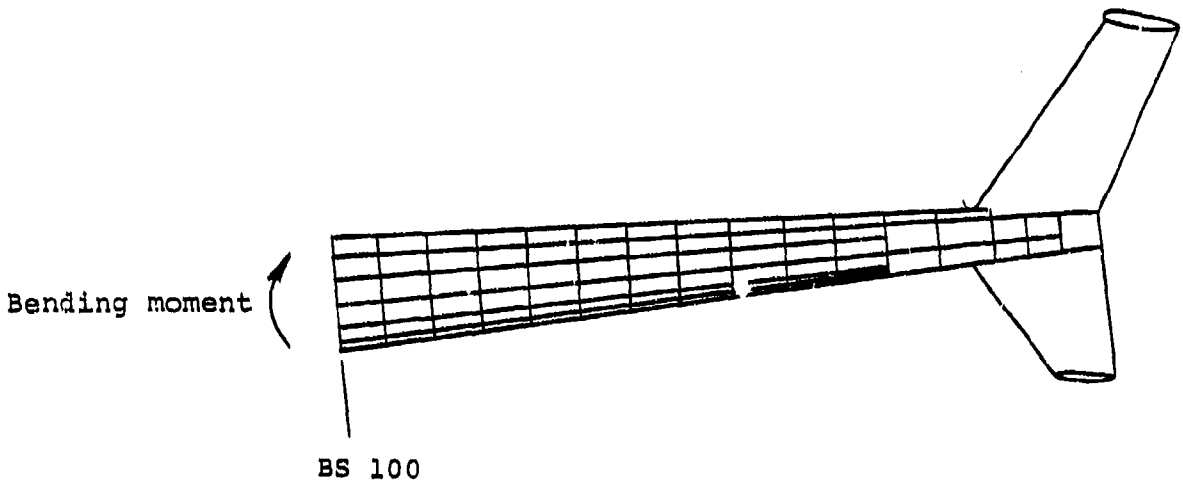

Maximum bending moment at BS 100 = ±3,585,000 in-lb

Figure B-8. Tailboom failure.

APPENDIX C

UNFILTERED TEST DATA TIME HISTORIES

Description	Location	Direction	Page
NASA instrumentation			
Accelerometers			
Nose gun turret	FS 120	Vertical	171
Copilot/gunner bulkhead	FS 193	Vertical	171
Pilot bulkhead	FS 251	Vertical	172
Pilot bulkhead	FS 251	Lateral	172
Pilot bulkhead	FS 251	Longitudinal	173
Right outboard wing tip	FS 280	Vertical	174
Right outboard wing tip	FS 280	Longitudinal	175
Left outboard wing tip	FS 280	Vertical	176
Left outboard wing tip	FS 280	Longitudinal	177
Aircraft cg	FS 290	Vertical	178
Aircraft cg	FS 290	Lateral	179
Aircraft cg	FS 290	Longitudinal	179
Transmission cg	FS 300	Vertical	179
Transmission cg	FS 300	Lateral	180
Transmission cg	FS 300	Longitudinal	180
Main rotor hub	FS 300	Lateral	180
Main rotor hub	FS 300	Longitudinal	180
Tailboom junction bulkhead	FS 411	Vertical	181
Tail rotor gearbox	FS 665	Vertical	182
Tail rotor gearbox	FS 665	Lateral	182
Pilot seat pan	FS 244	Vertical	183
Pilot seat pan	FS 244	Longitudinal	183
Pilot pelvis	FS 244	Vertical	183
Pilot pelvis	FS 244	Longitudinal	183
Pilot chest	FS 244	Vertical	184
Pilot chest	FS 244	Longitudinal	184
Pilot head	FS 244	Vertical	184
Pilot head	FS 244	Lateral	184
Pilot head	FS 244	Longitudinal	184
Pressure transducers			
Forward fuel cell	FS 292	----	185
Aft fuel cell	FS 322	----	185
Nose gear shock strut	FS 160	----	186
Right main gear shock strut	FS 314	----	186
Left main gear shock strut	FS 314	----	187

Description	Location	Direction	Page
Displacement potentiometers			
Copilot/gunner seat	FS 183	Vertical	188
Pilot seat	FS 244	Vertical	188
Nose gear shock strut	FS 185	Pitch	189
Right main gear shock strut	FS 314	Pitch	189
Left main gear shock strut	FS 314	Pitch	189
Strain gages			
Right main gear drag link	FS 308	Axial	190
Left main gear drag link	FS 308	Axial	190
ATL instrumentation			
Accelerometers			
Pilot bulkhead	FS 251	Vertical	191
Pilot seat pan	FS 244	Vertical	191
Transmission cg	FS 300	Vertical	192
Transmission cg	FS 300	Longitudinal	192
Strain gages			
Right pilot seat attenuator	FS 244	Axial	193
Left pilot seat attenuator	FS 244	Axial	193
Right forward transmission lift link	FS 265	Axial	194
Left forward transmission lift link	FS 265	Axial	194
Right aft transmission lift link	FS 330	Axial	195
Left aft transmission lift link	FS 330	Axial	195
Right transmission crash link	FS 300	Axial	196
Left transmission crash link	FS 300	Axial	196
NADC instrumentation			
Accelerometers			
Copilot/gunner bulkhead	FS 212	Vertical	197
Copilot/gunner bulkhead	FS 212	Lateral	197
Copilot/gunner bulkhead	FS 212	Longitudinal	197
Copilot/gunner seat pan	FS 183	Vertical	198

Description	Location	Direction	Page
Copilot/gunner seat pan	FS 183	Lateral	198
Copilot/gunner seat pan	FS 183	Longitudinal	198
Copilot/gunner pelvis	FS 183	Vertical	199
Copilot/gunner pelvis	FS 183	Lateral	199
Copilot/gunner pelvis	FS 183	Longitudinal	199
Copilot/gunner chest	FS 183	Vertical	200
Copilot/gunner chest	FS 183	Lateral	200
Copilot/gunner chest	FS 183	Longitudinal	200
Copilot/gunner head	FS 183	Vertical	201
Copilot/gunner head	FS 183	Lateral	201
Copilot/gunner head	FS 183	Longitudinal	201
AIRS crash sensor	FS 212	Vertical	N/A
AIRS crash sensor	FS 212	Lateral	N/A
Pressure transducers			
Right IBAHRS	FS 183	----	202
Left IBAHRS	FS 183	----	N/A
Displacement potentiometers			
Copilot/gunner seat	FS 183	Vertical	202
Strain gages			
Right copilot/gunner lap belt	FS 183	Axial	N/A
Left copilot/gunner lap belt	FS 183	Axial	N/A
Copilot/gunner shoulder belt	FS 183	Axial	N/A
Copilot/gunner negative-g strap	FS 183	Axial	N/A
Right copilot/gunner seat attenuator	FS 183	Axial	N/A
Left copilot/gunner seat attenuator	FS 183	Axial	N/A
Miscellaneous			
Crash sensor pulse switch	FS 183	On/off	N/A

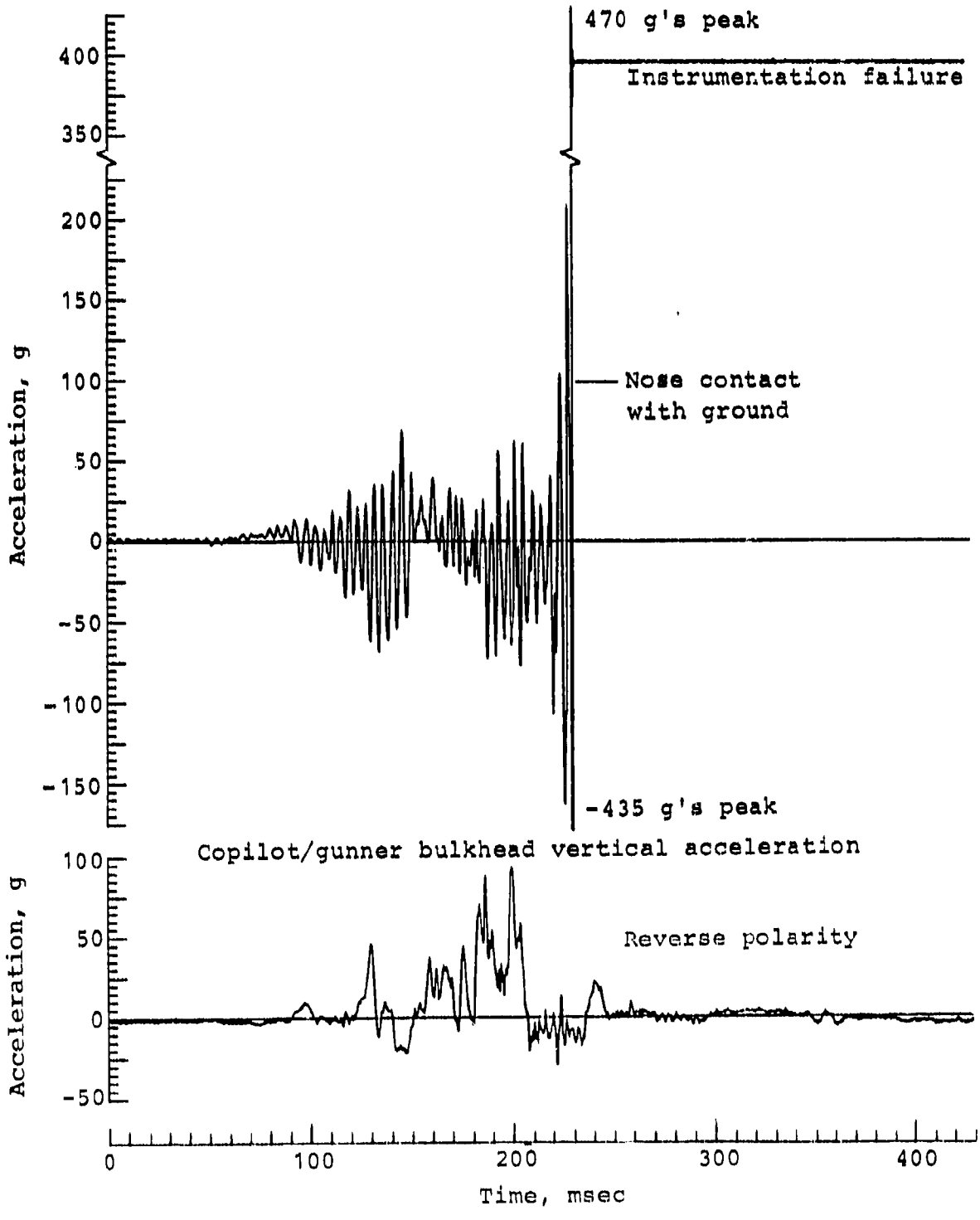
Nose gun turret vertical acceleration
470 g's peak
Instrumentation failure
Nose contact with ground
-435 g's peak
Acceleration, g
400
350
200
150
100
50
0
-50
-100
-150
Copilot/gunner bulkhead vertical acceleration
Reverse polarity
100
50
0
-50
0
100
200
300
400
Time, msec

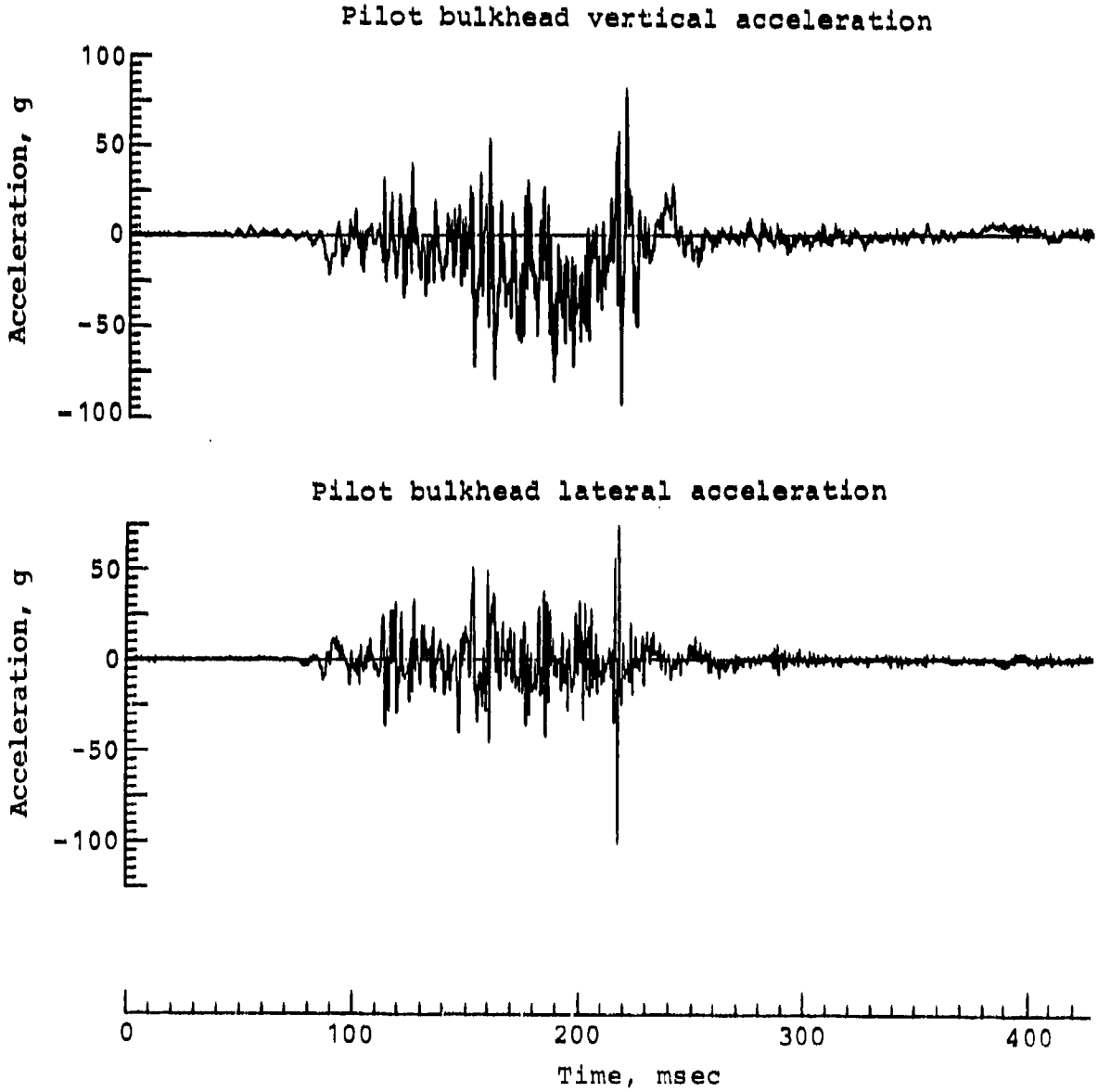
Pilot bulkhead vertical acceleration
Acceleration, g
100
50
0
-50
-100
Pilot bulkhead lateral acceleration
Acceleration, g
50
0
-50
-100
0
100
200
300
400
Time, msec

Pilot bulkhead longitudinal acceleration

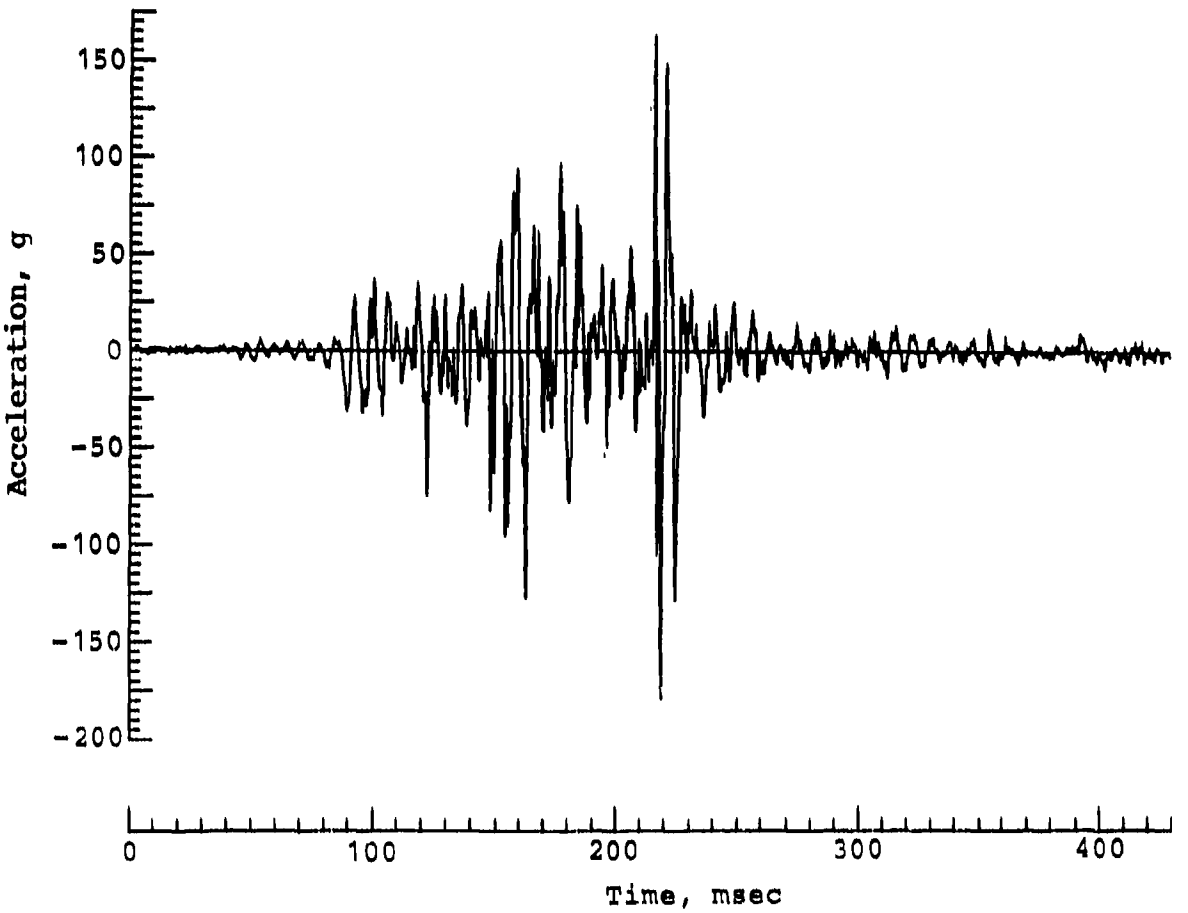

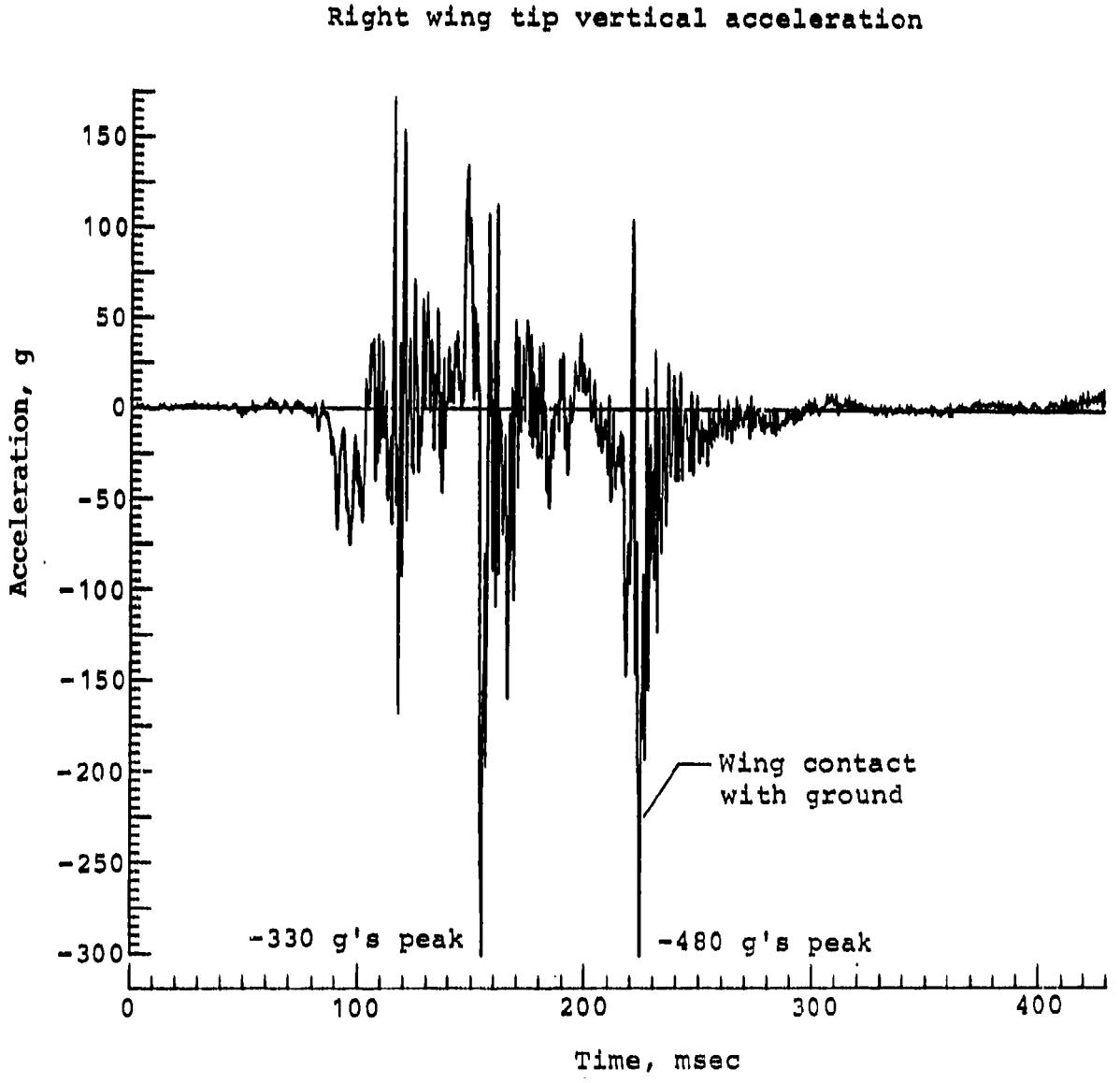
Right wing tip vertical acceleration
Acceleration, g
150
100
50
0
-50
-100
-150
-200
-250
-300
0
100
200
300
400
Time, msec
Wing contact
with ground
-330 g's peak
-480 g's peak

Right wing tip longitudinal acceleration

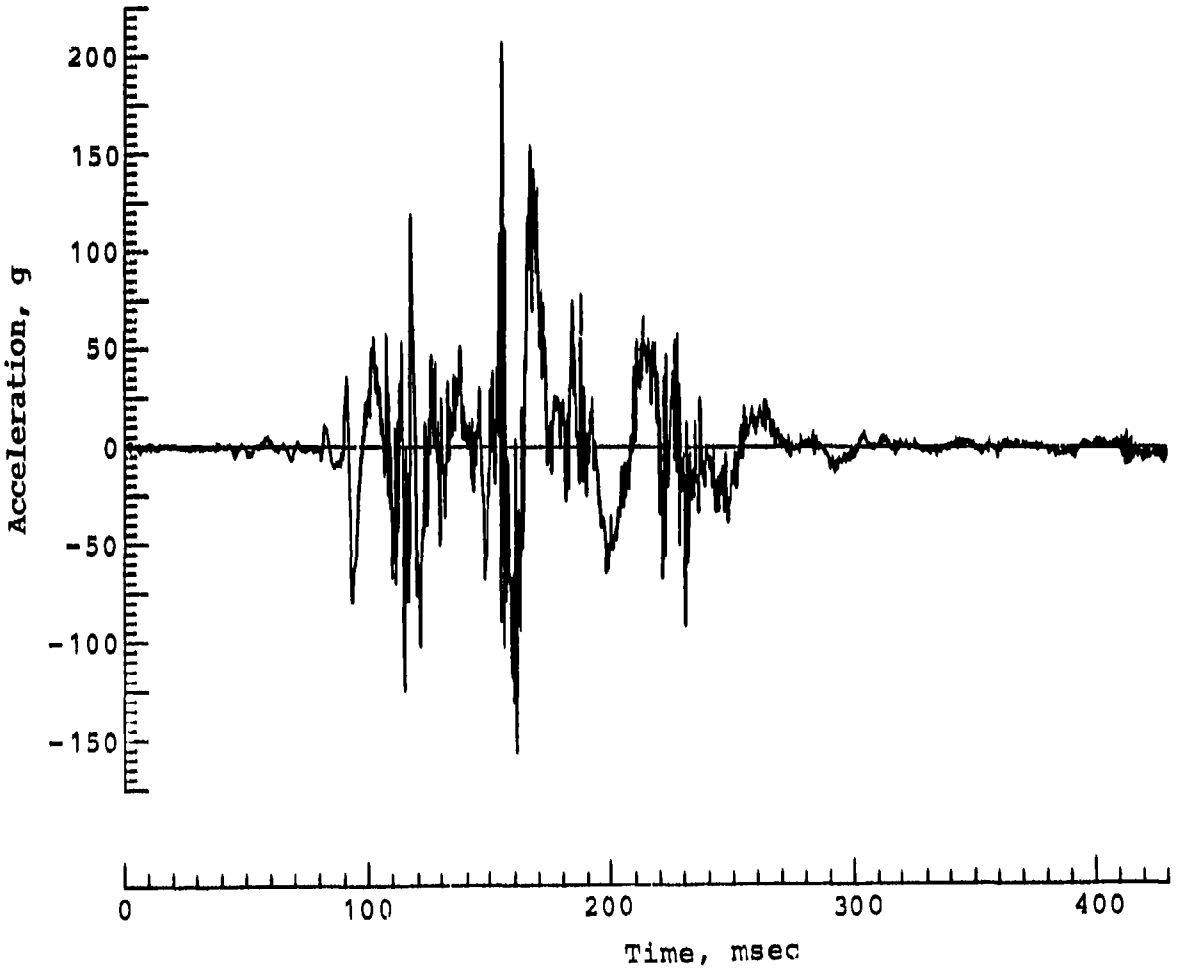

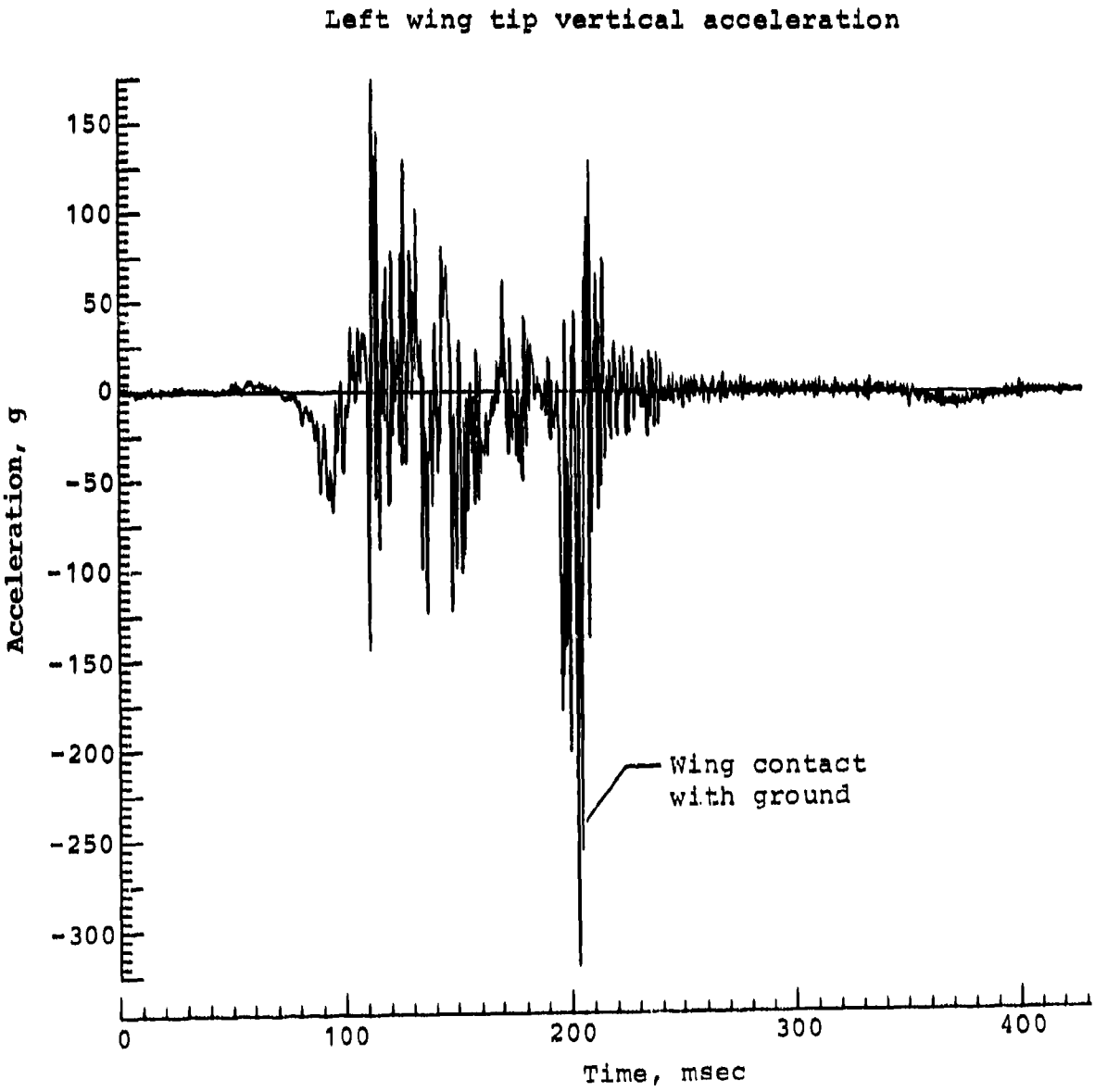
Left wing tip vertical acceleration
150
100
50
0
-50
-100
-150
-200
-250
-300
Acceleration, g
0
100
200
300
400
Time, msec
Wing contact
with ground

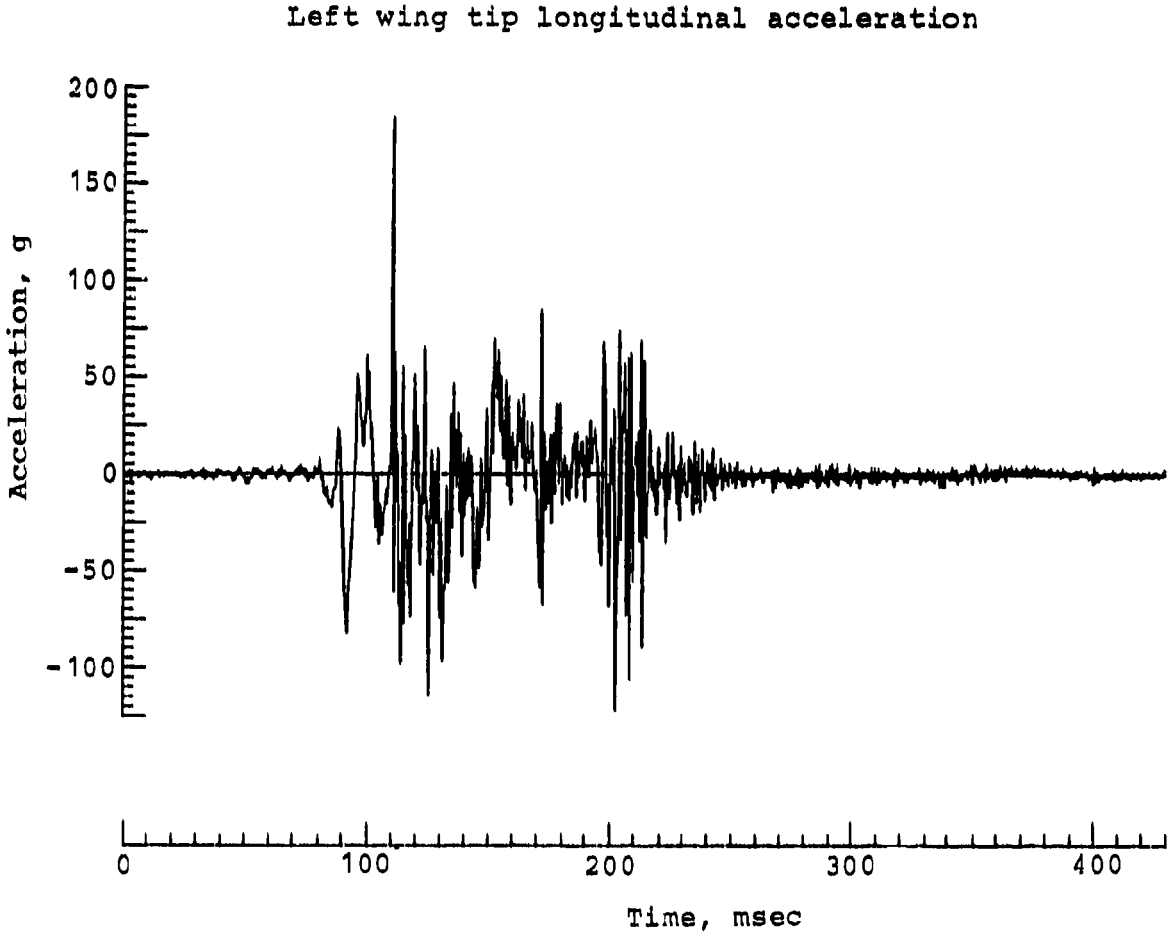
Left wing tip longitudinal acceleration
200
150
100
50
0
-50
-100
Acceleration, g
0
100
200
300
400
Time, msec

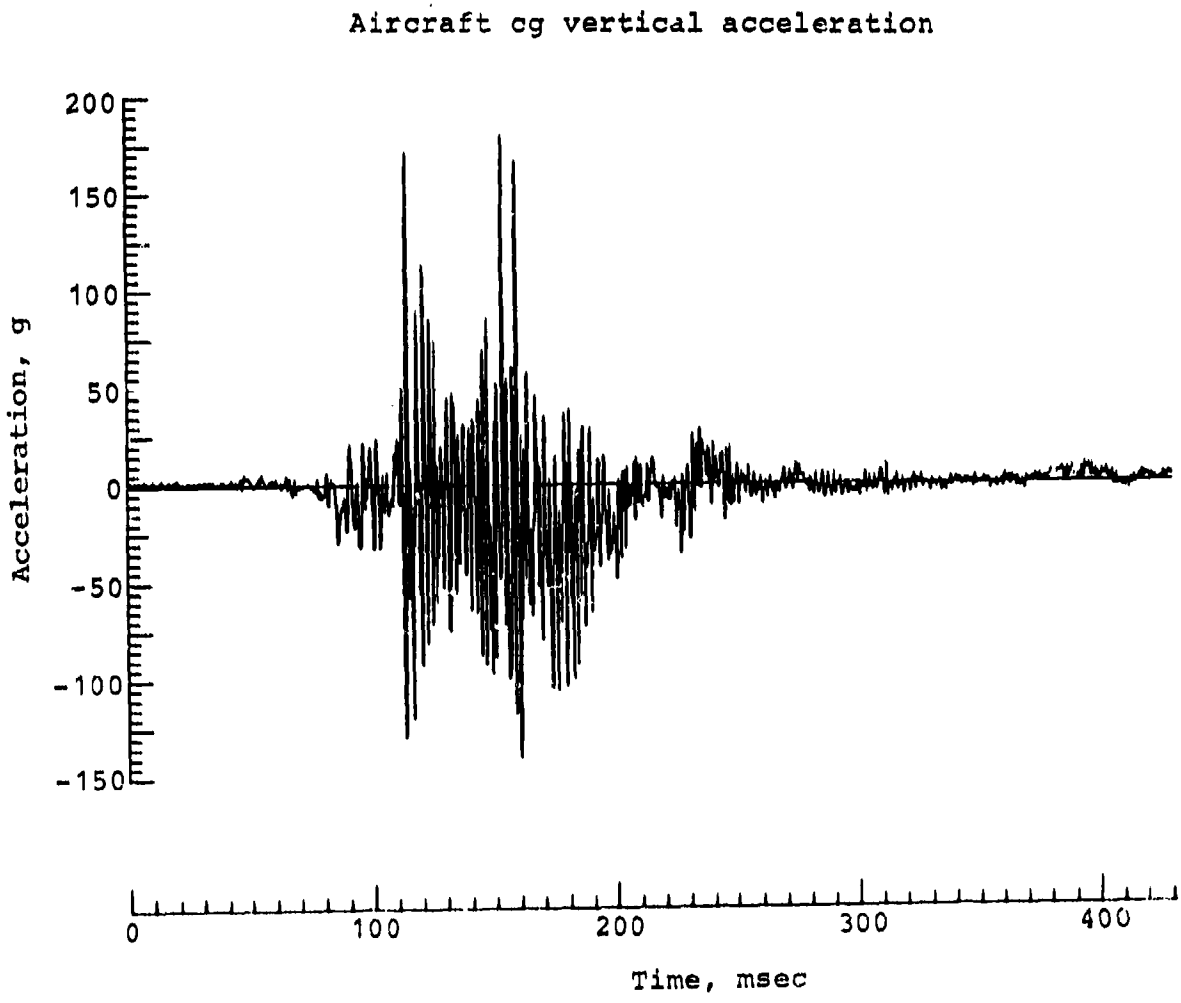
Aircraft cg vertical acceleration
200
150
100
50
0
-50
-100
-150
Acceleration, g
0
100
200
300
400
Time, msec

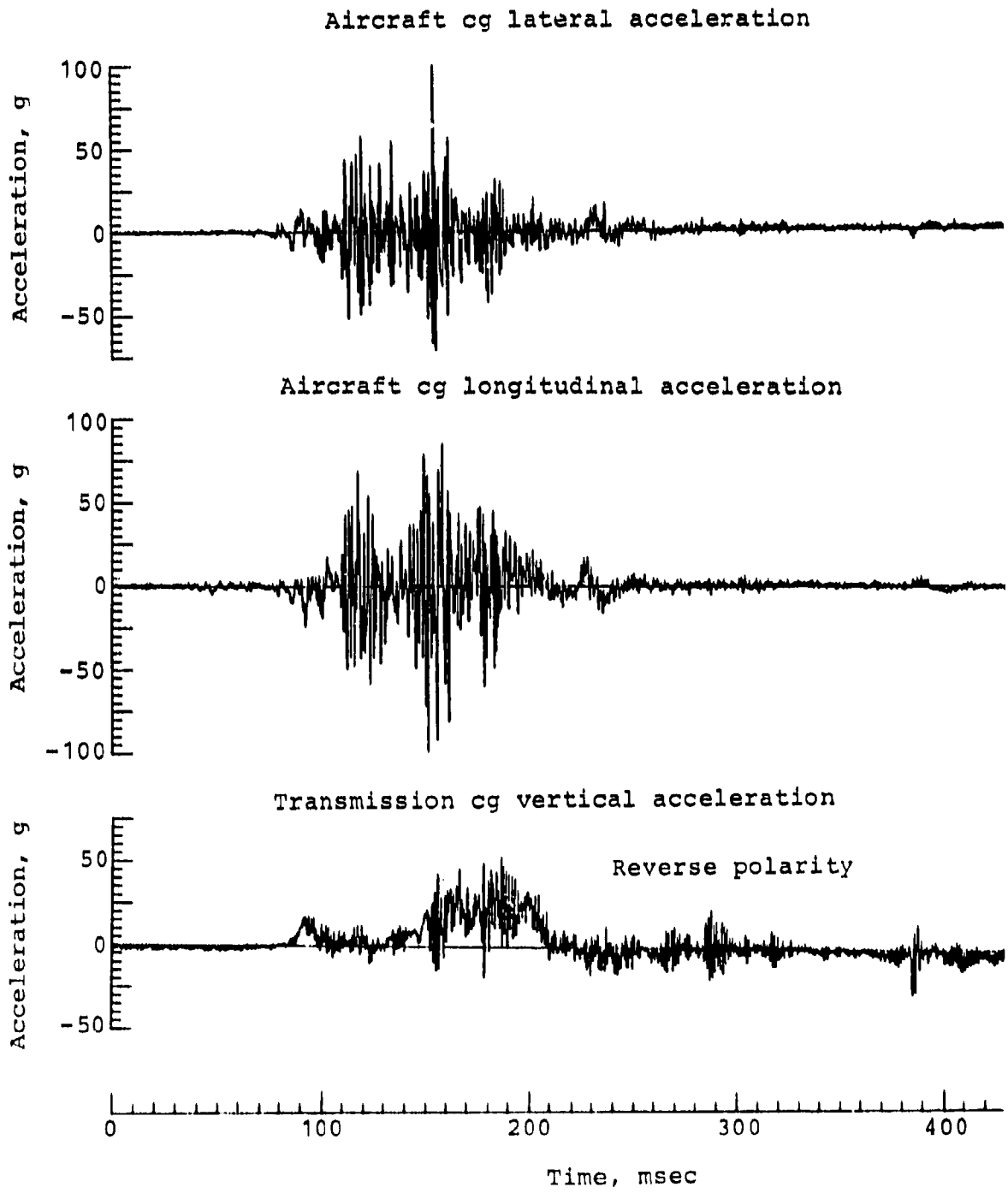
Aircraft cg lateral acceleration
Acceleration, g
100
50
0
-50
Aircraft cg longitudinal acceleration
Acceleration, g
100
50
0
-50
-100
Transmission cg vertical acceleration
Acceleration, g
50
0
-50
Reverse polarity
0
100
200
300
400
Time, msec

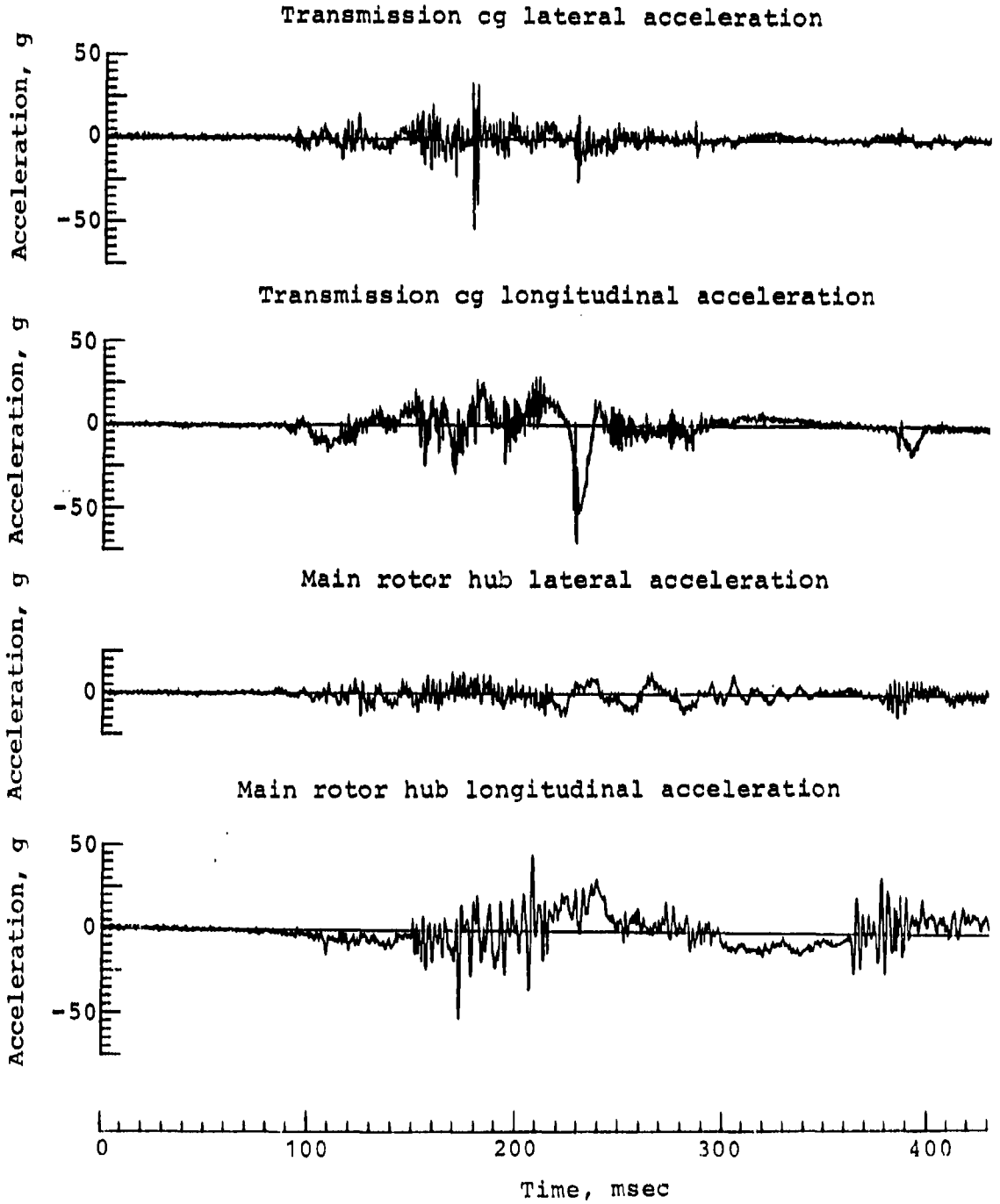
Transmission cg lateral acceleration
Acceleration, g
50
0
-50
Transmission cg longitudinal acceleration
Acceleration, g
50
0
-50
Main rotor hub lateral acceleration
Acceleration, g
0
Main rotor hub longitudinal acceleration
Acceleration, g
50
0
-50
0
100
200
300
400
Time, msec

Tailboom junction vertical acceleration

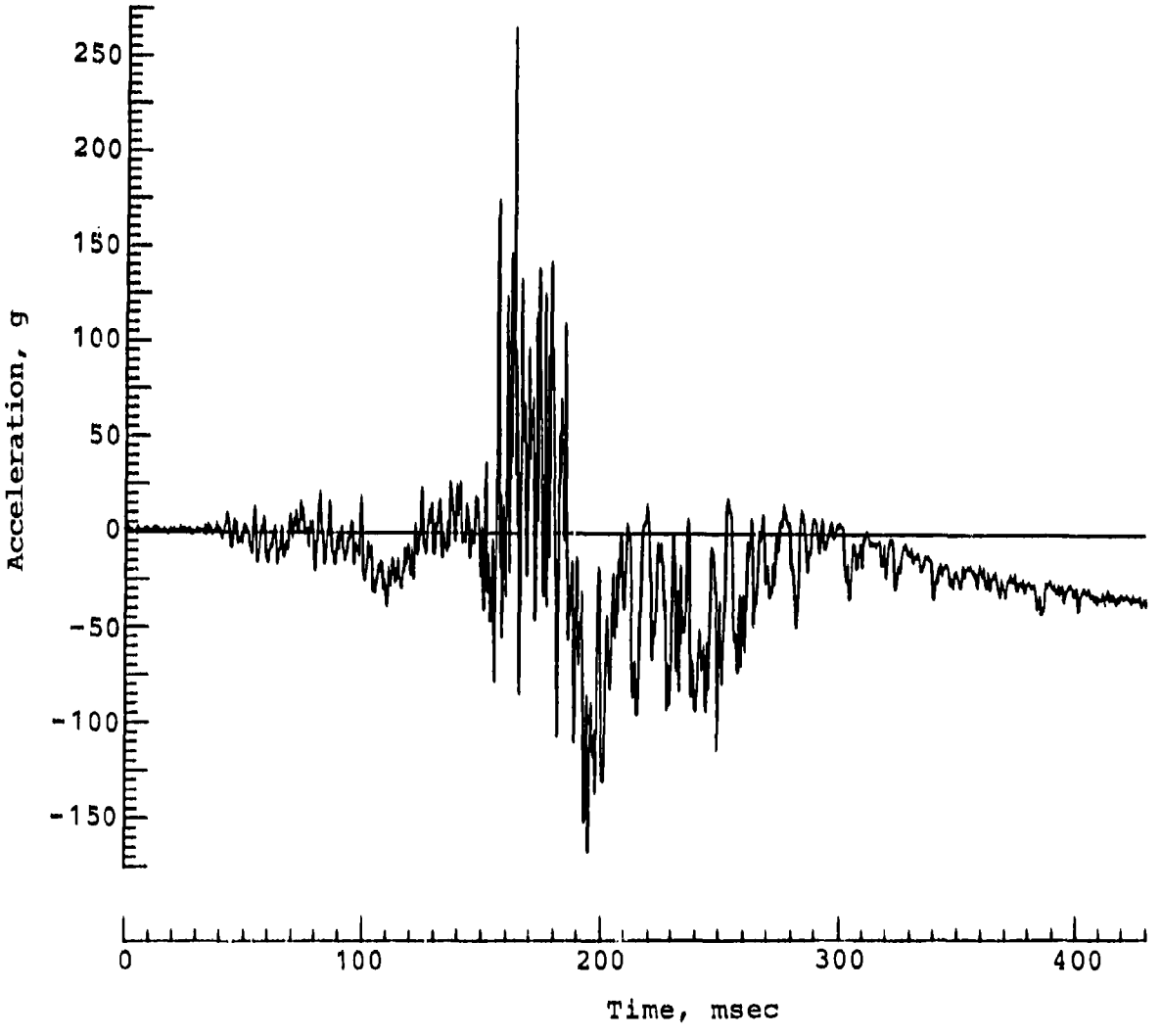

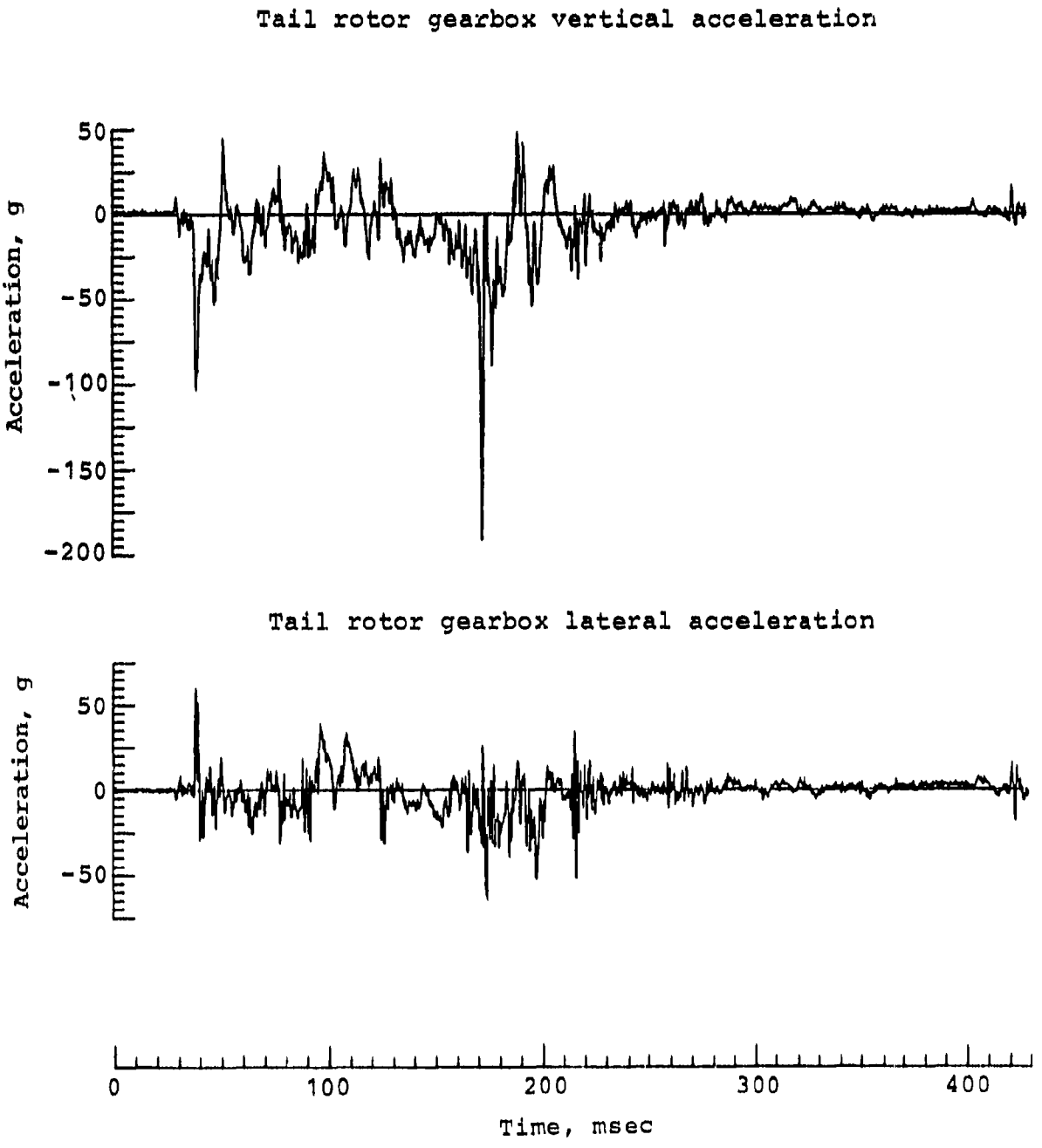
Tail rotor gearbox vertical acceleration
Acceleration, g
50
0
-50
-100
-150
-200
Tail rotor gearbox lateral acceleration
Acceleration, g
50
0
-50
0
100
200
300
400
Time, msec

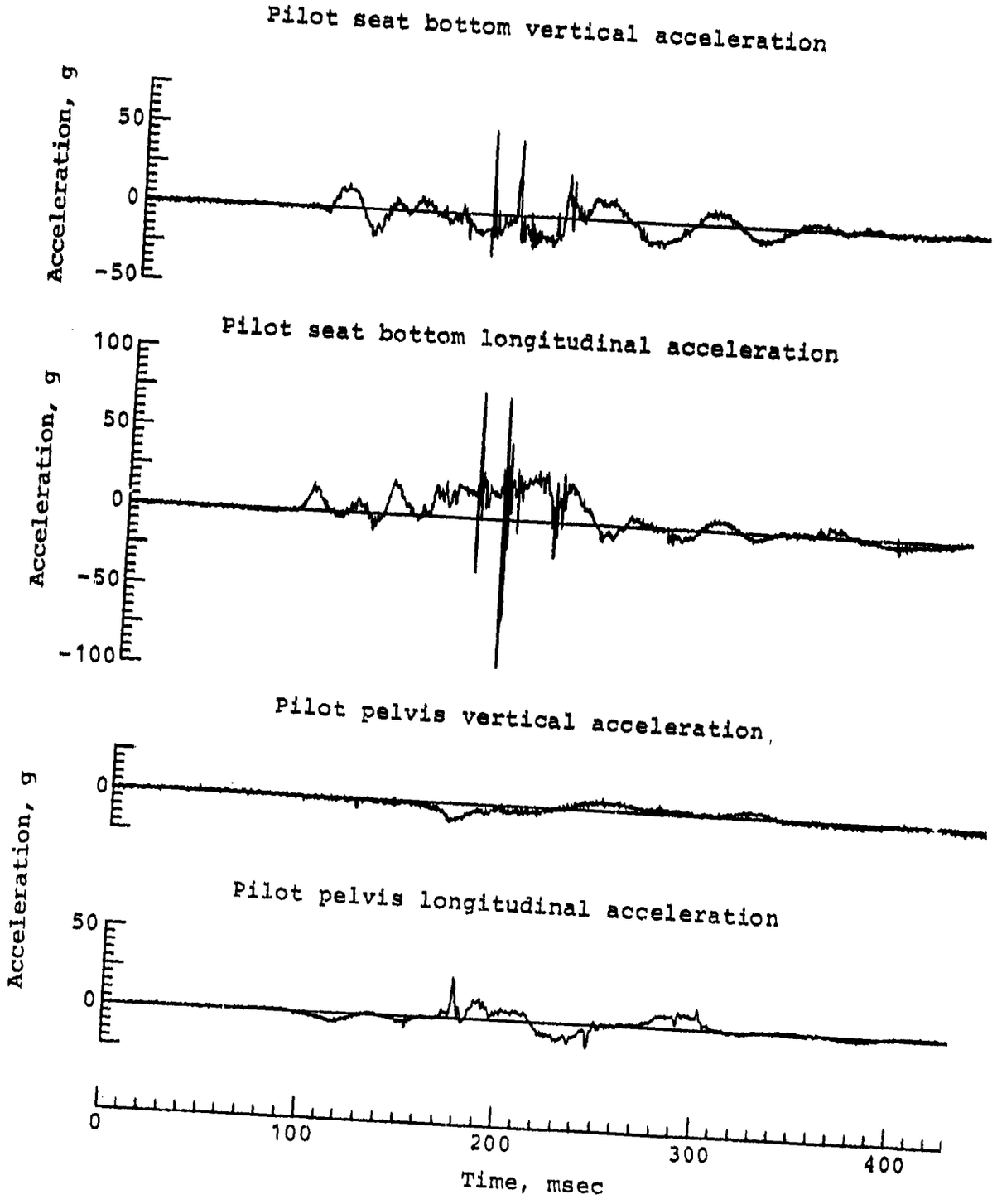
Pilot seat bottom vertical acceleration
Acceleration, g
50
0
-50
Pilot seat bottom longitudinal acceleration
Acceleration, g
100
50
0
-50
-100
Pilot pelvis vertical acceleration
Acceleration, g
0
Pilot pelvis longitudinal acceleration
Acceleration, g
50
0
0
100
200
300
400
Time, msec

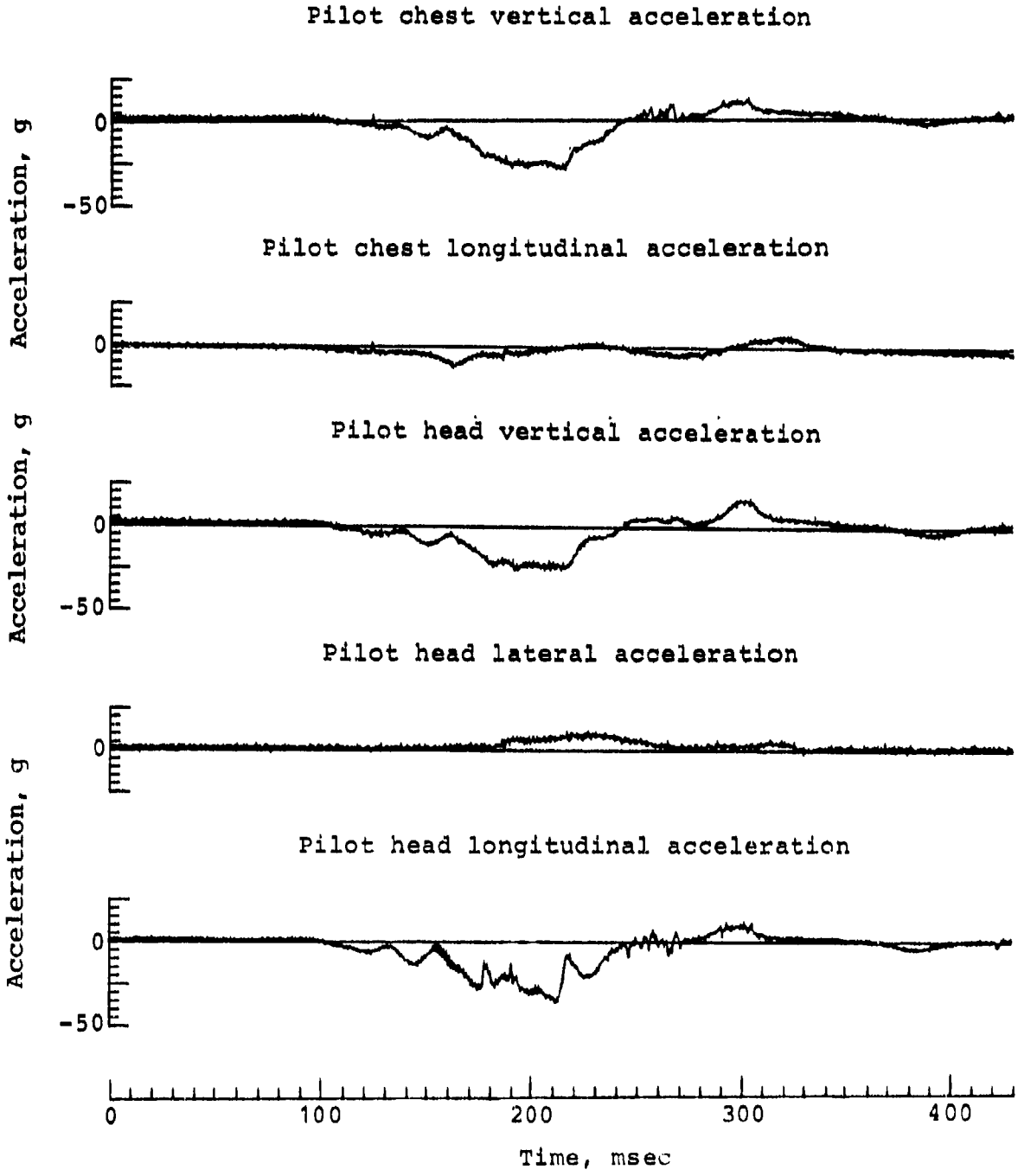
Pilot chest vertical acceleration
Acceleration, g
0
-50
Pilot chest longitudinal acceleration
Acceleration, g
0
Pilot head vertical acceleration
Acceleration, g
0
-50
Pilot head lateral acceleration
Acceleration, g
0
Pilot head longitudinal acceleration
Acceleration, g
0
-50
0
100
200
300
400
Time, msec

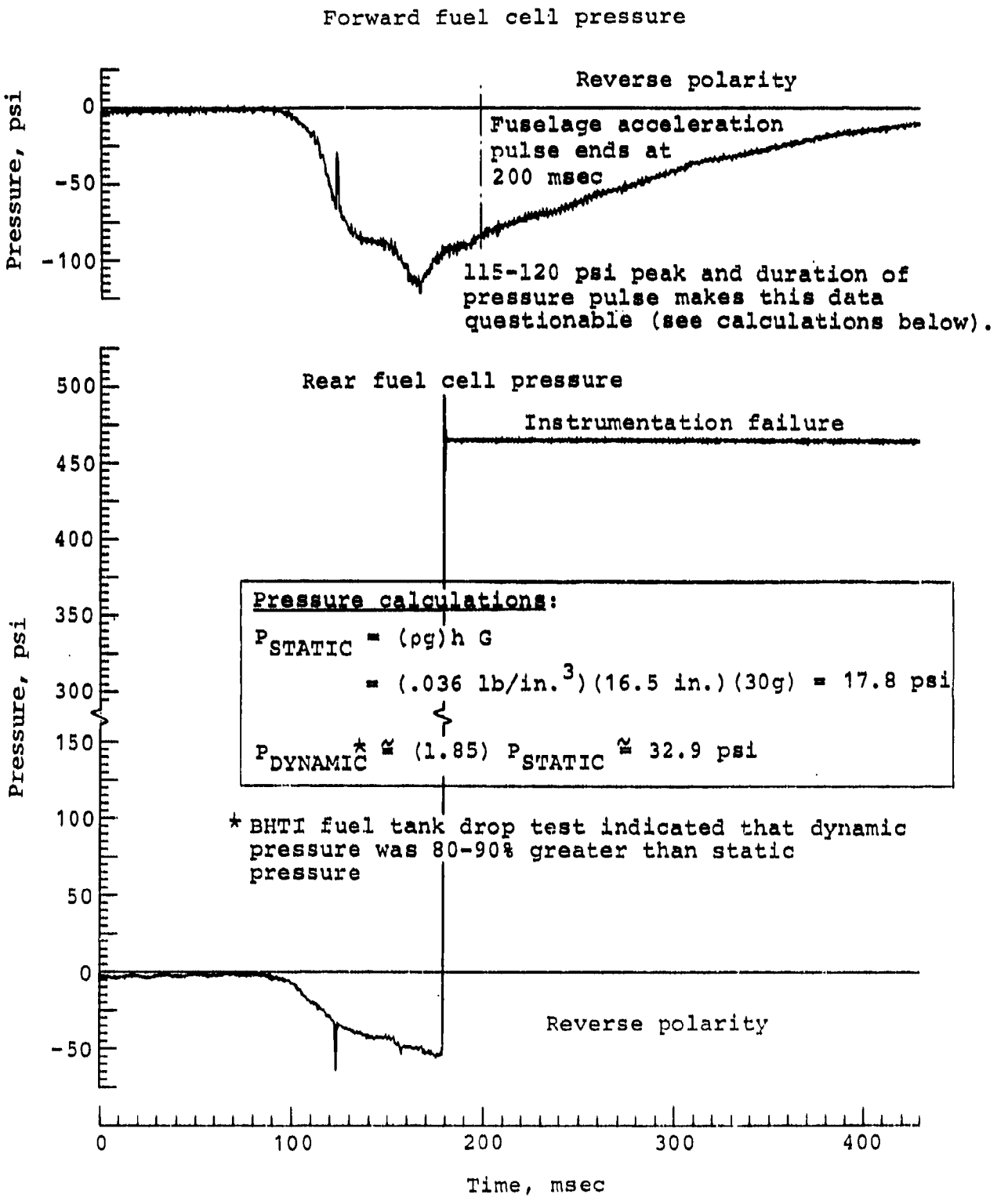
Forward fuel cell pressure
Reverse polarity
Fuselage acceleration pulse ends at 200 msec
115-120 psi peak and duration of pressure pulse makes this data questionable (see calculations below).
Pressure, psi
0
-50
-100
Rear fuel cell pressure
Instrumentation failure
Pressure calculations:
P_{STATIC} = (ρg)h G
= (.036 lb/in.^{3})(16.5 in.)(30g) = 17.8 psi
$P_{DYNAMIC}^{*} \cong (1.85)\ P_{STATIC} \cong 32.9$ psi
* BHTI fuel tank drop test indicated that dynamic pressure was 80-90% greater than static pressure
500
450
400
350
300
150
100
50
0
-50
Reverse polarity
0
100
200
300
400
Time, msec

* Long time constant exponential decay in pressure time history indicates transducer or charge amplifier malfunction due to open circuit possibly caused by overload (overpressure, thermal shock, etc.) to piezoelectric pressure transducer.

Nose gear shock strut pressure

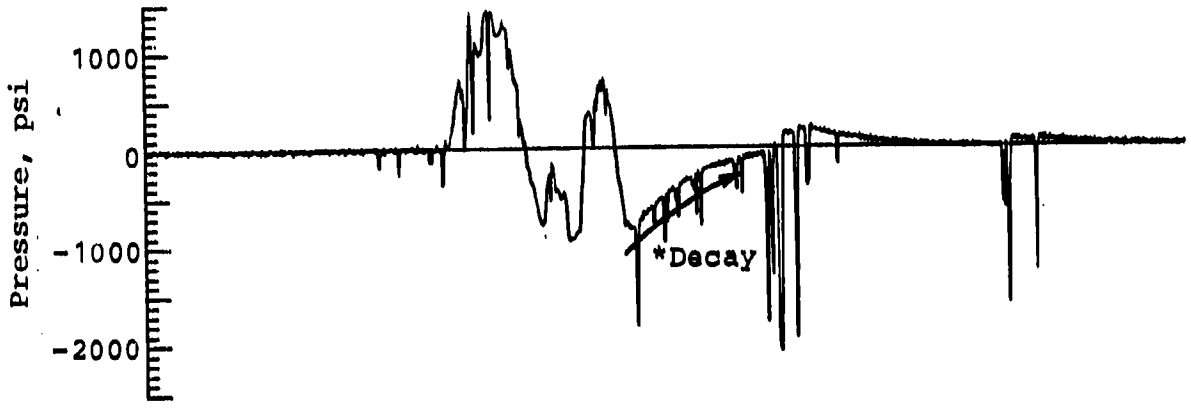

Right main gear shock strut pressure
Reverse polarity

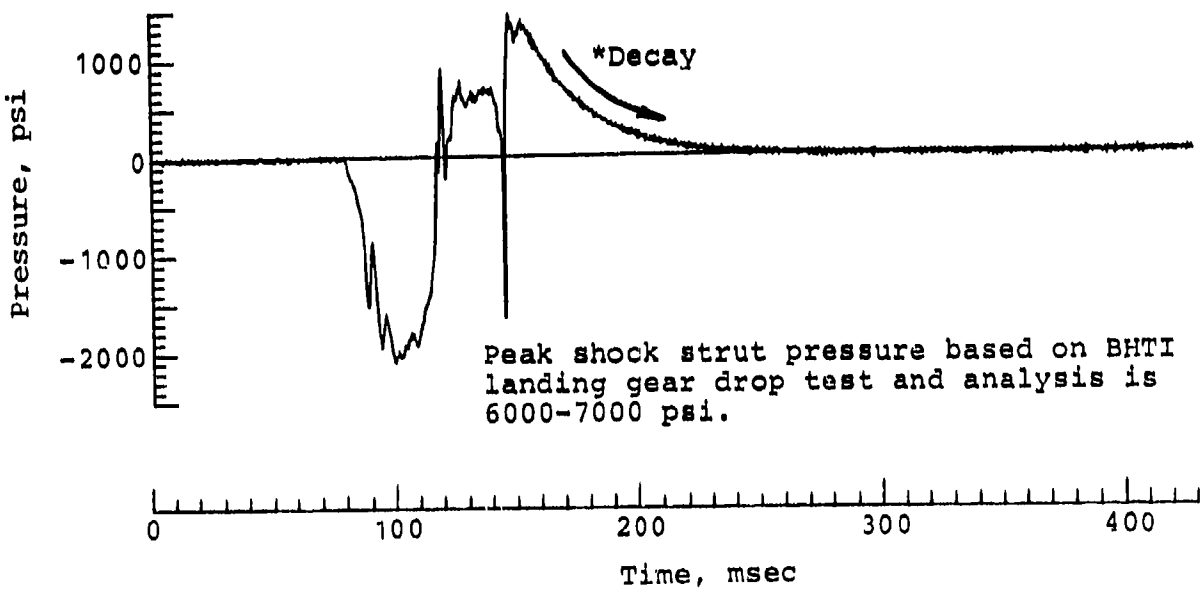

Peak shock strut pressure based on BHTI landing gear drop test and analysis is 6000-7000 psi.

Left main gear shock strut pressure

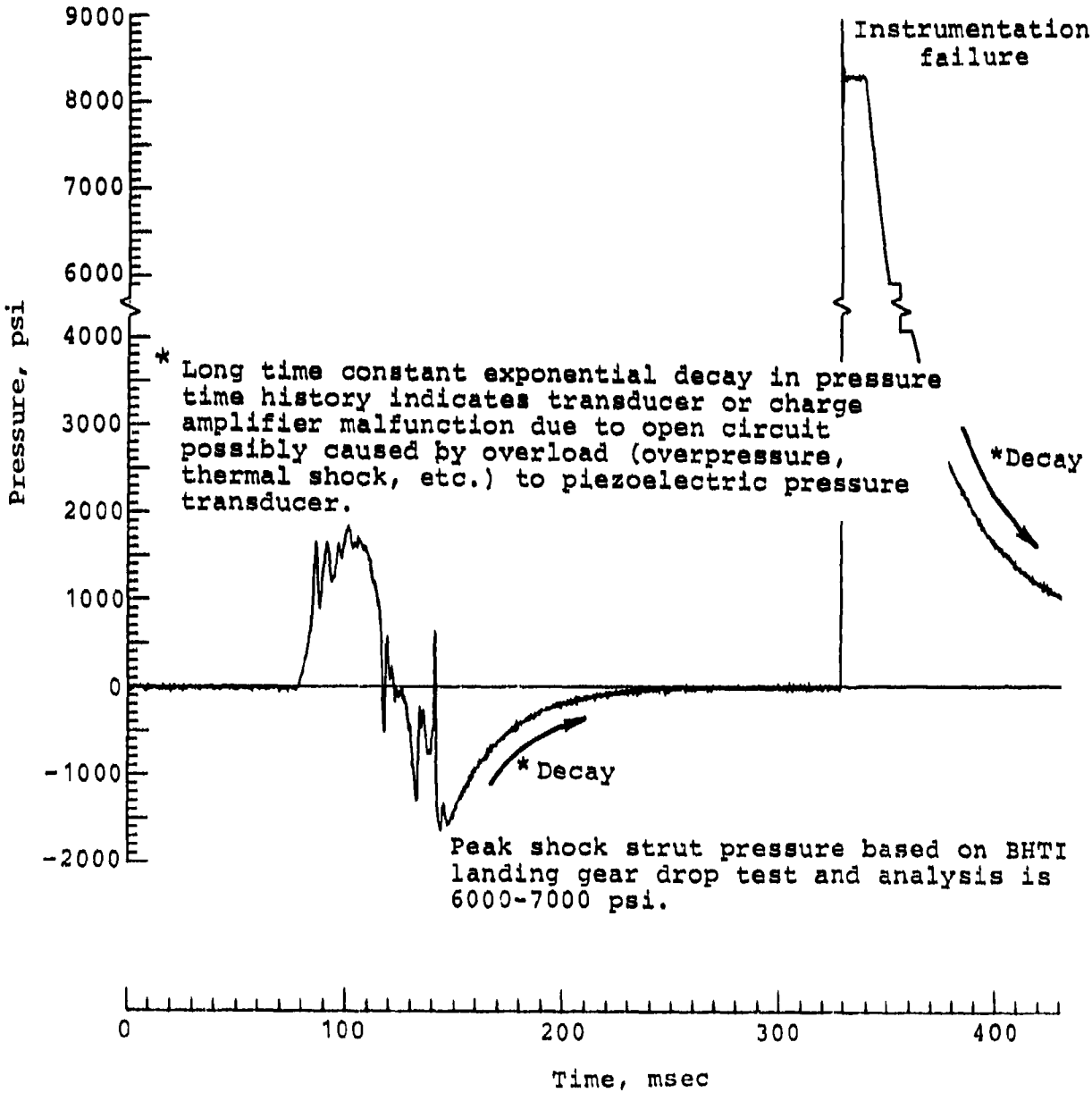

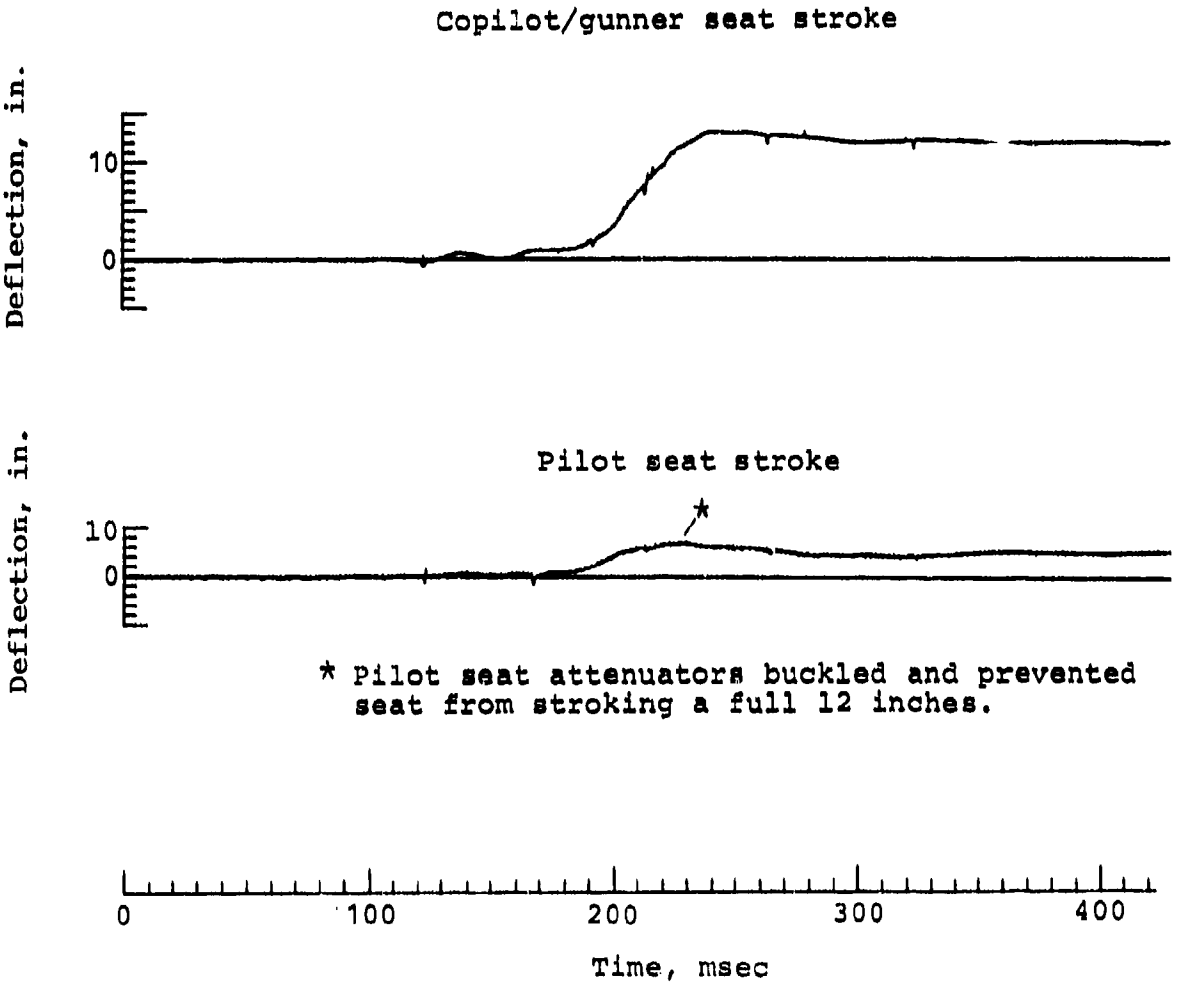
Copilot/gunner seat stroke
Deflection, in.
10
0
Pilot seat stroke
Deflection, in.
10
0
* Pilot seat attenuators buckled and prevented seat from stroking a full 12 inches.
0
100
200
300
400
Time, msec

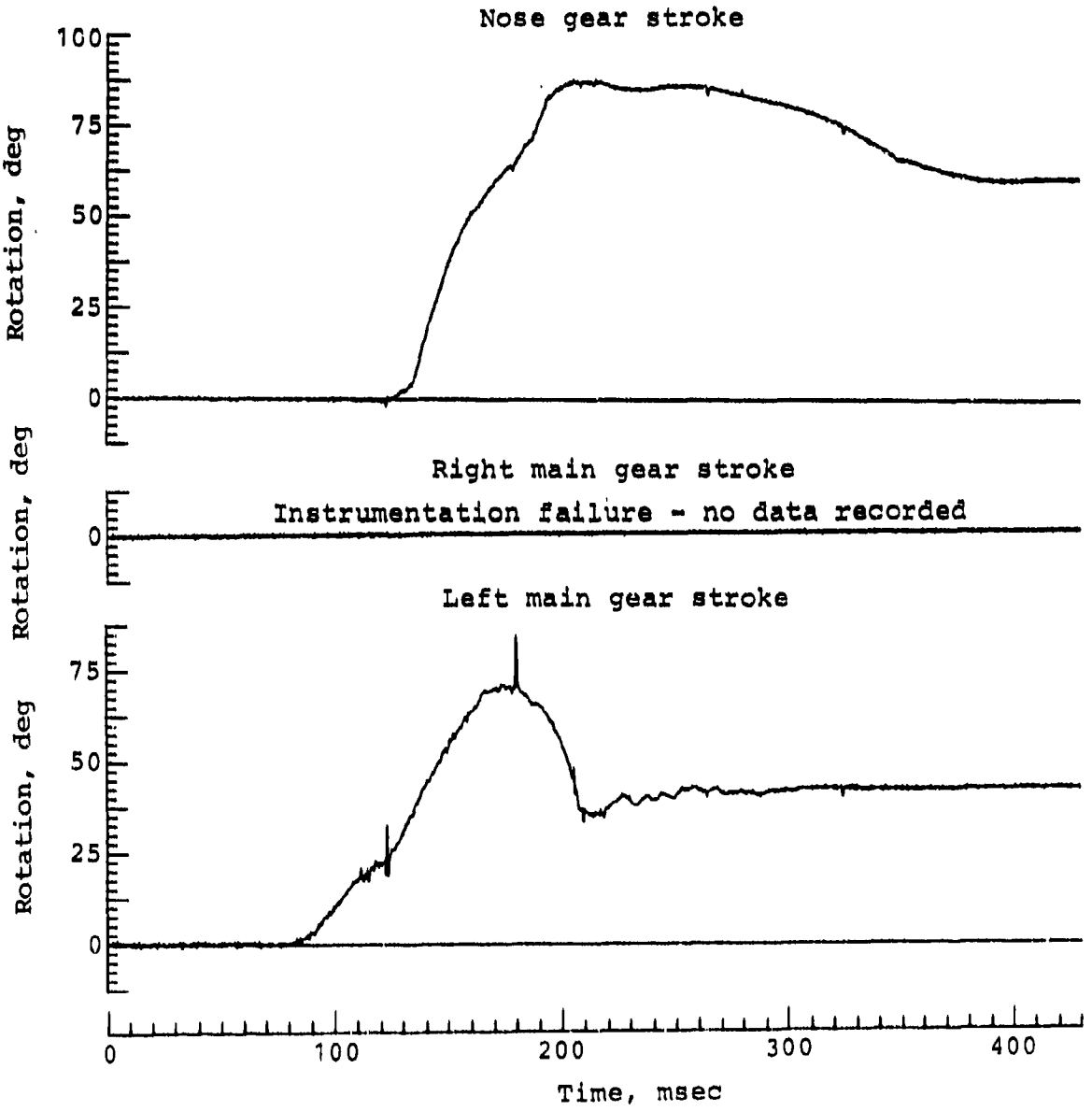
Nose gear stroke
Rotation, deg
100
75
50
25
0
Right main gear stroke
Instrumentation failure - no data recorded
Rotation, deg
0
Left main gear stroke
Rotation, deg
75
50
25
0
0
100
200
300
400
Time, msec

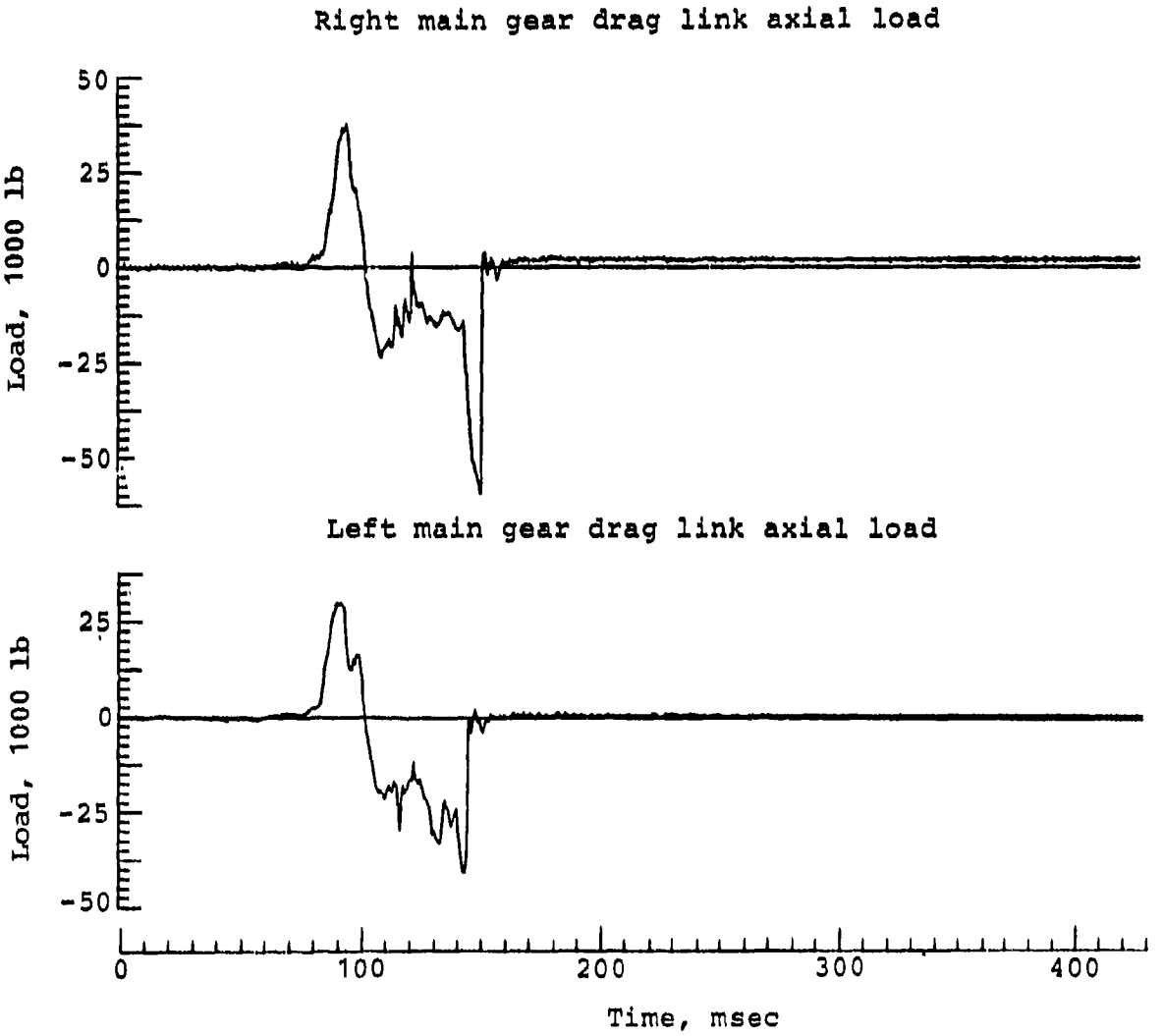
Right main gear drag link axial load
Load, 1000 lb
50
25
0
-25
-50
Left main gear drag link axial load
Load, 1000 lb
25
0
-25
-50
0
100
200
300
400
Time, msec

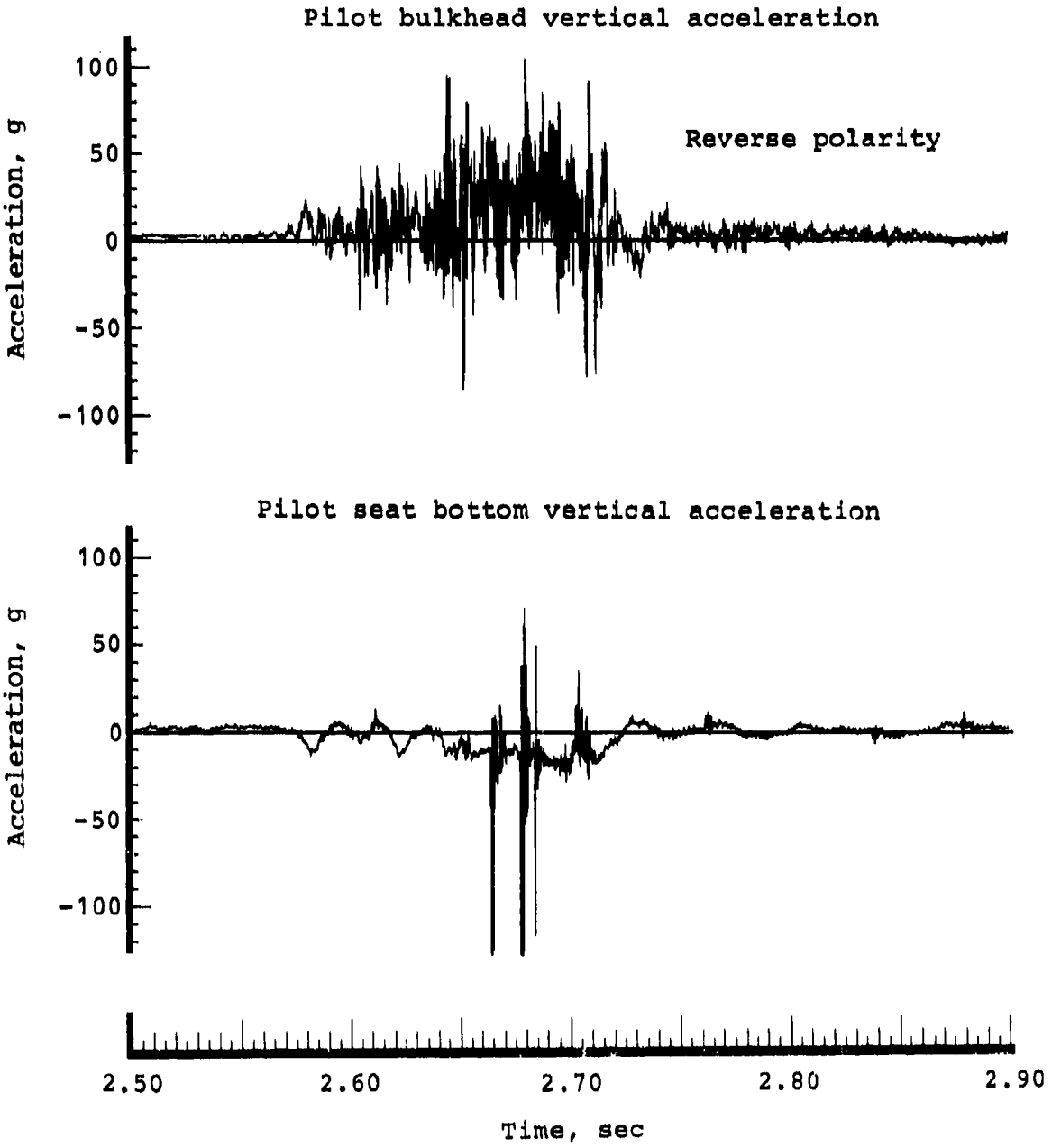
Pilot bulkhead vertical acceleration
Reverse polarity
Acceleration, g
100
50
0
-50
-100
Pilot seat bottom vertical acceleration
Acceleration, g
100
50
0
-50
-100
2.50
2.60
2.70
2.80
2.90
Time, sec

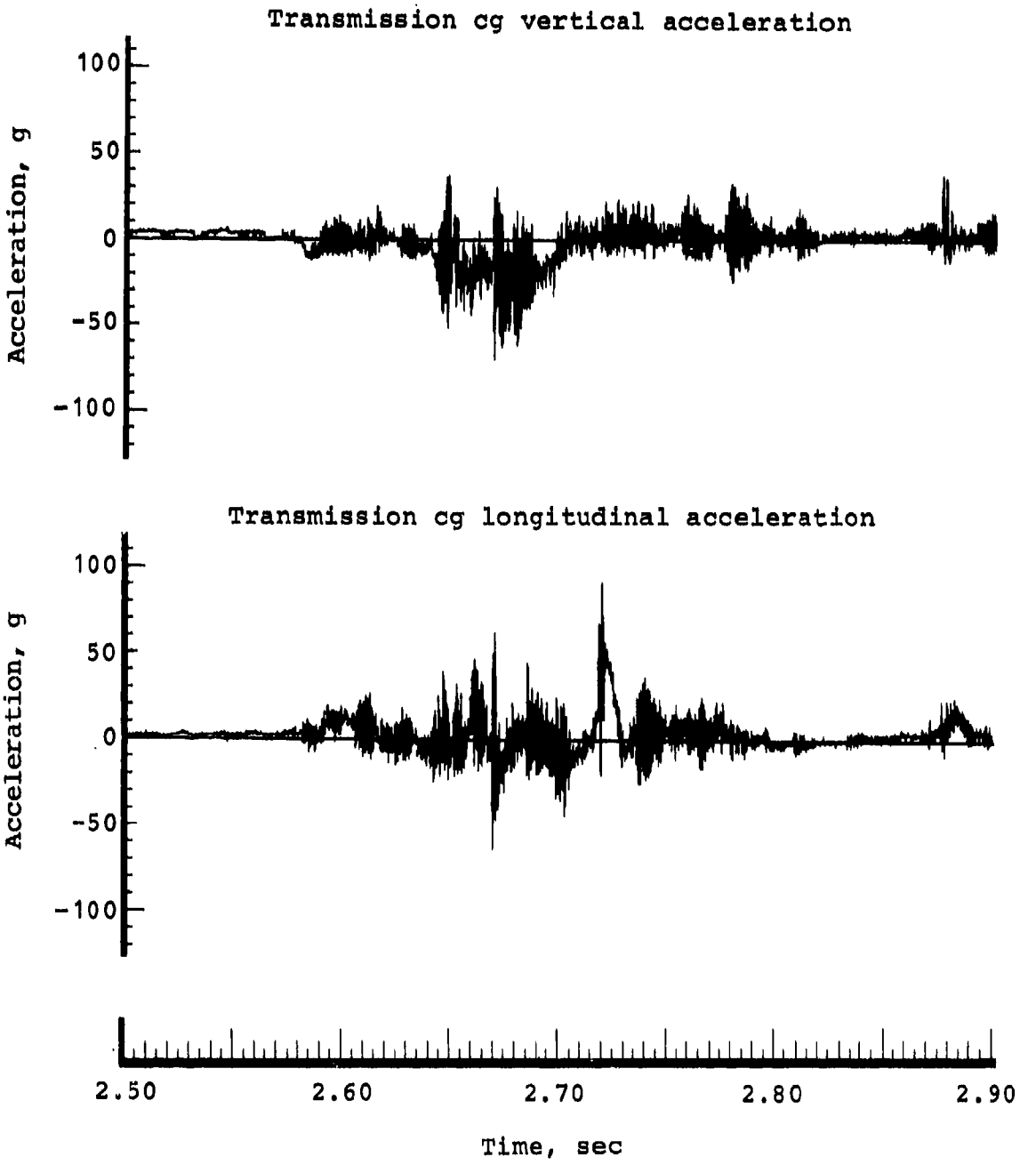
Transmission cg vertical acceleration
Acceleration, g
100
50
0
-50
-100
Transmission cg longitudinal acceleration
Acceleration, g
100
50
0
-50
-100
2.50
2.60
2.70
2.80
2.90
Time, sec

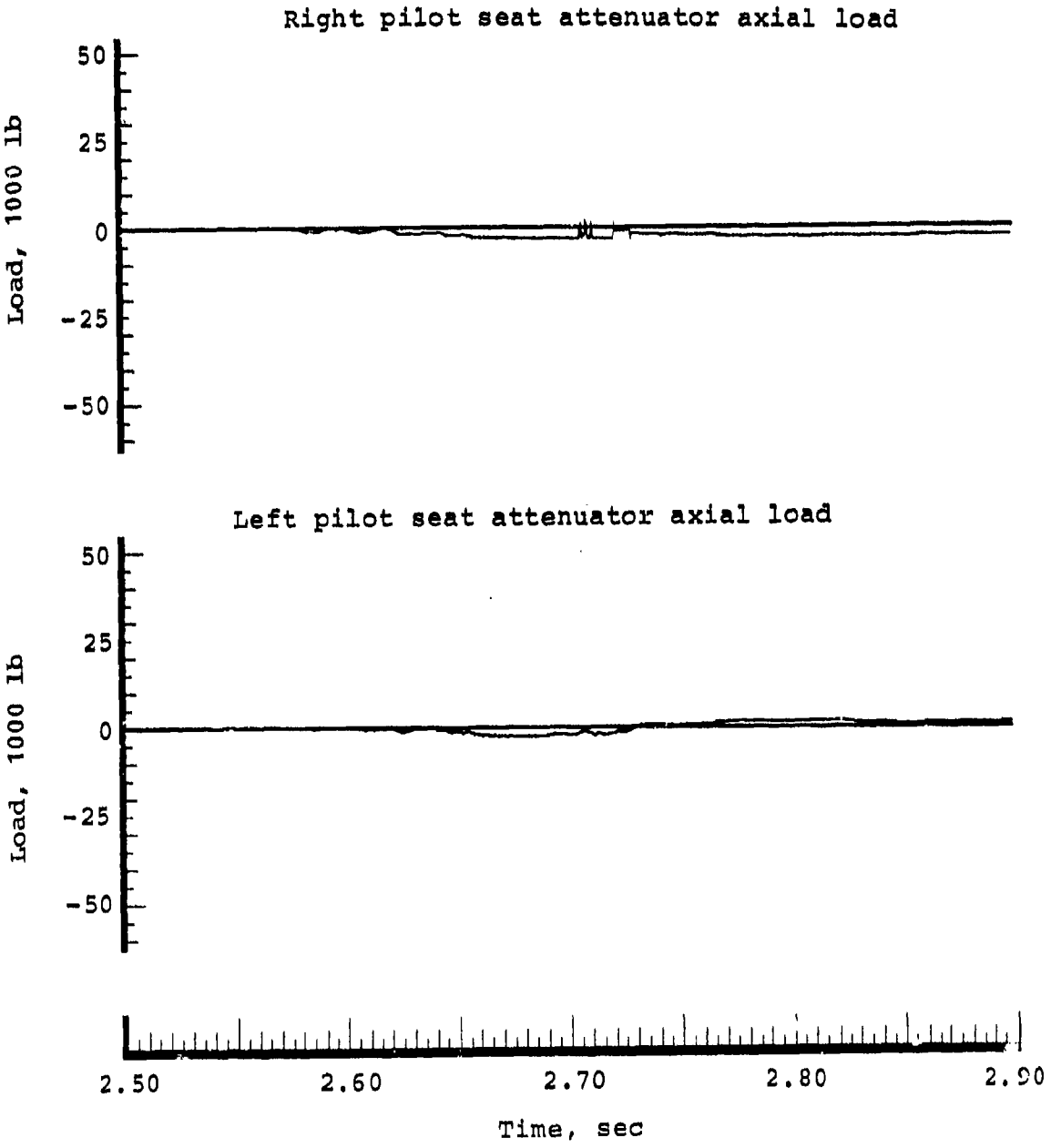
Right pilot seat attenuator axial load
Load, 1000 lb
50
25
0
-25
-50
Left pilot seat attenuator axial load
Load, 1000 lb
50
25
0
-25
-50
2.50
2.60
2.70
2.80
2.90
Time, sec

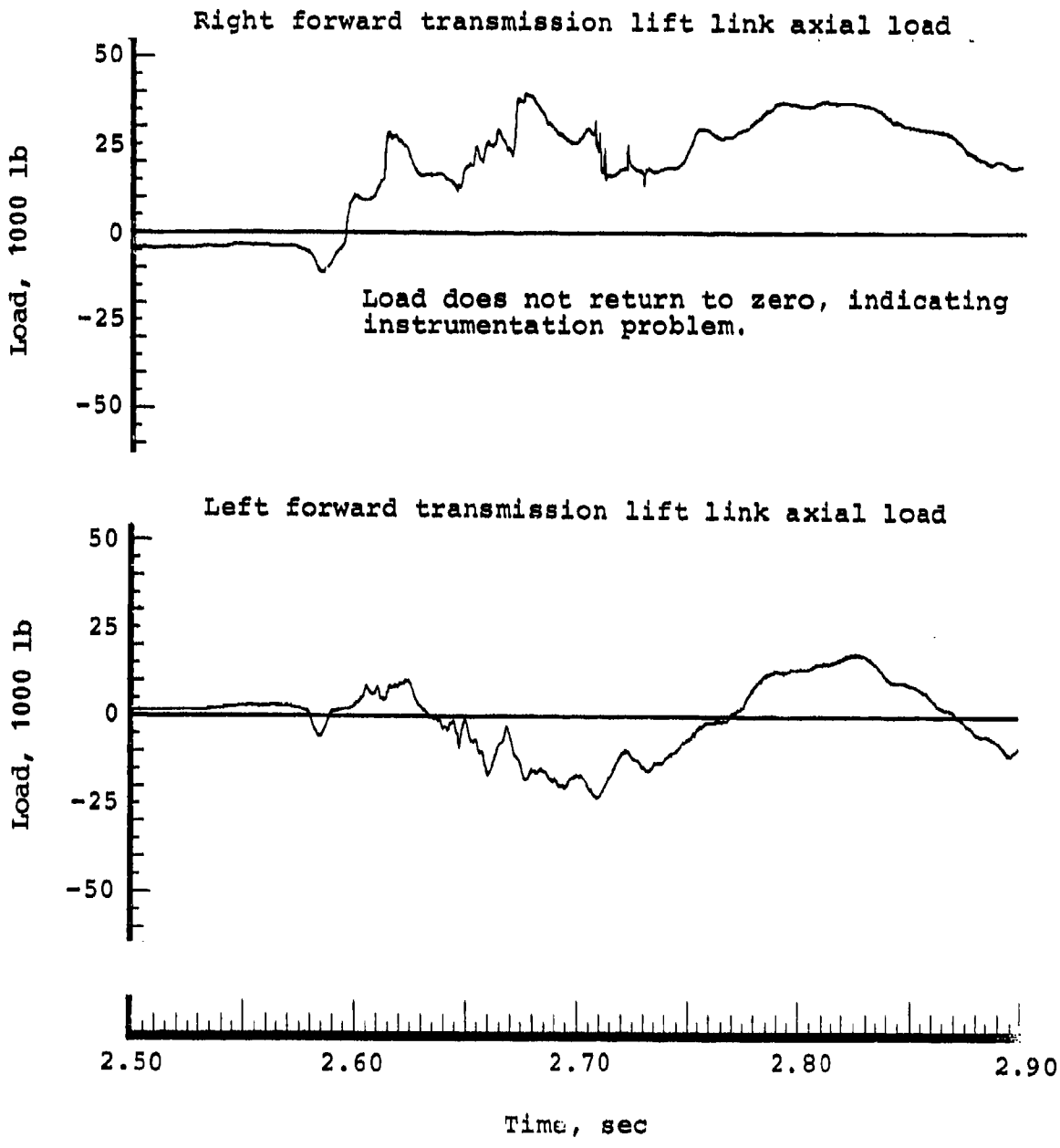
Right forward transmission lift link axial load
50
25
0
-25
-50
Load, 1000 lb
Load does not return to zero, indicating instrumentation problem.
Left forward transmission lift link axial load
50
25
0
-25
-50
Load, 1000 lb
2.50
2.60
2.70
2.80
2.90
Time, sec

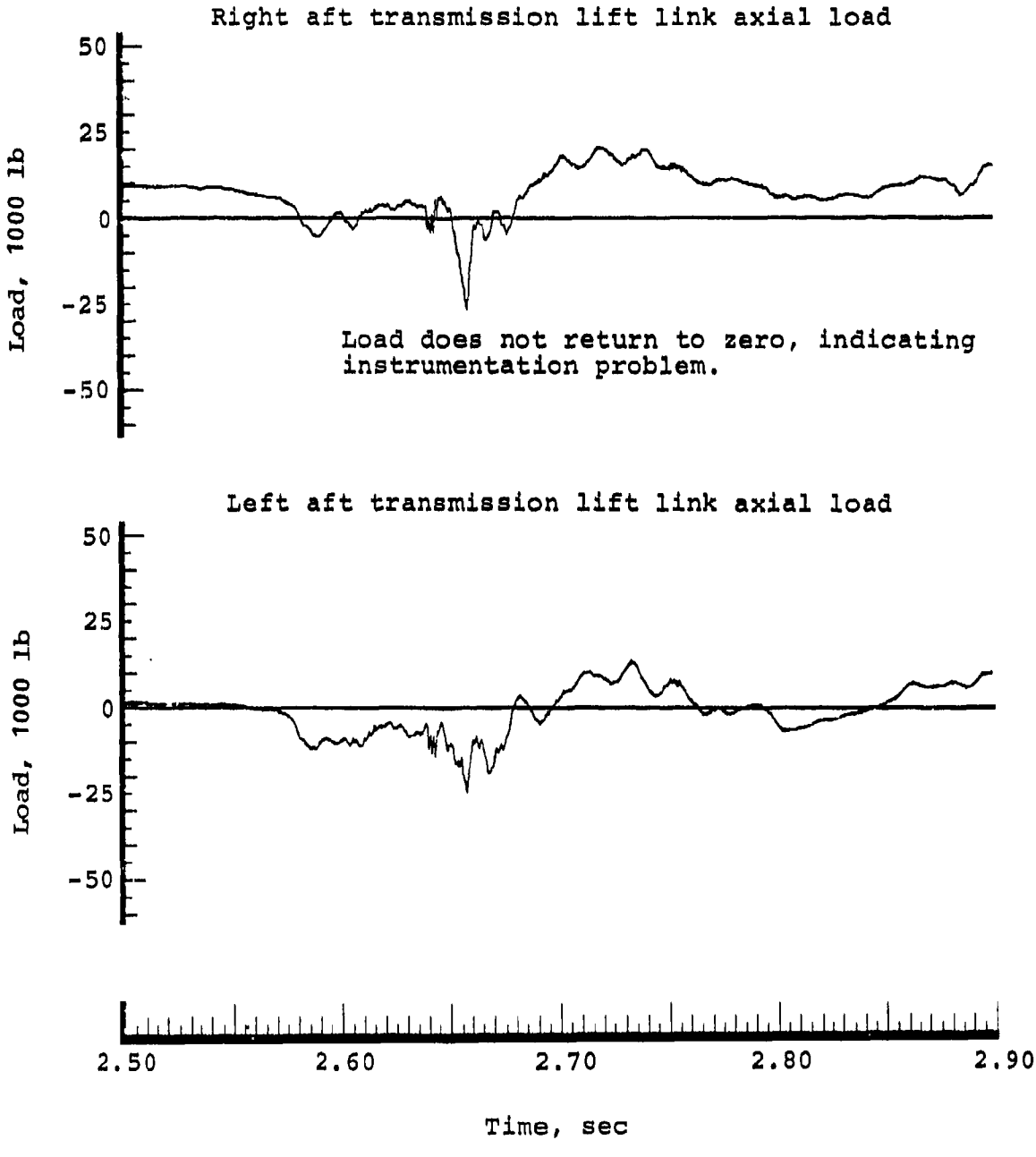
Right aft transmission lift link axial load
Load, 1000 lb
50
25
0
-25
-50
Load does not return to zero, indicating instrumentation problem.
Left aft transmission lift link axial load
Load, 1000 lb
50
25
0
-25
-50
2.50
2.60
2.70
2.80
2.90
Time, sec

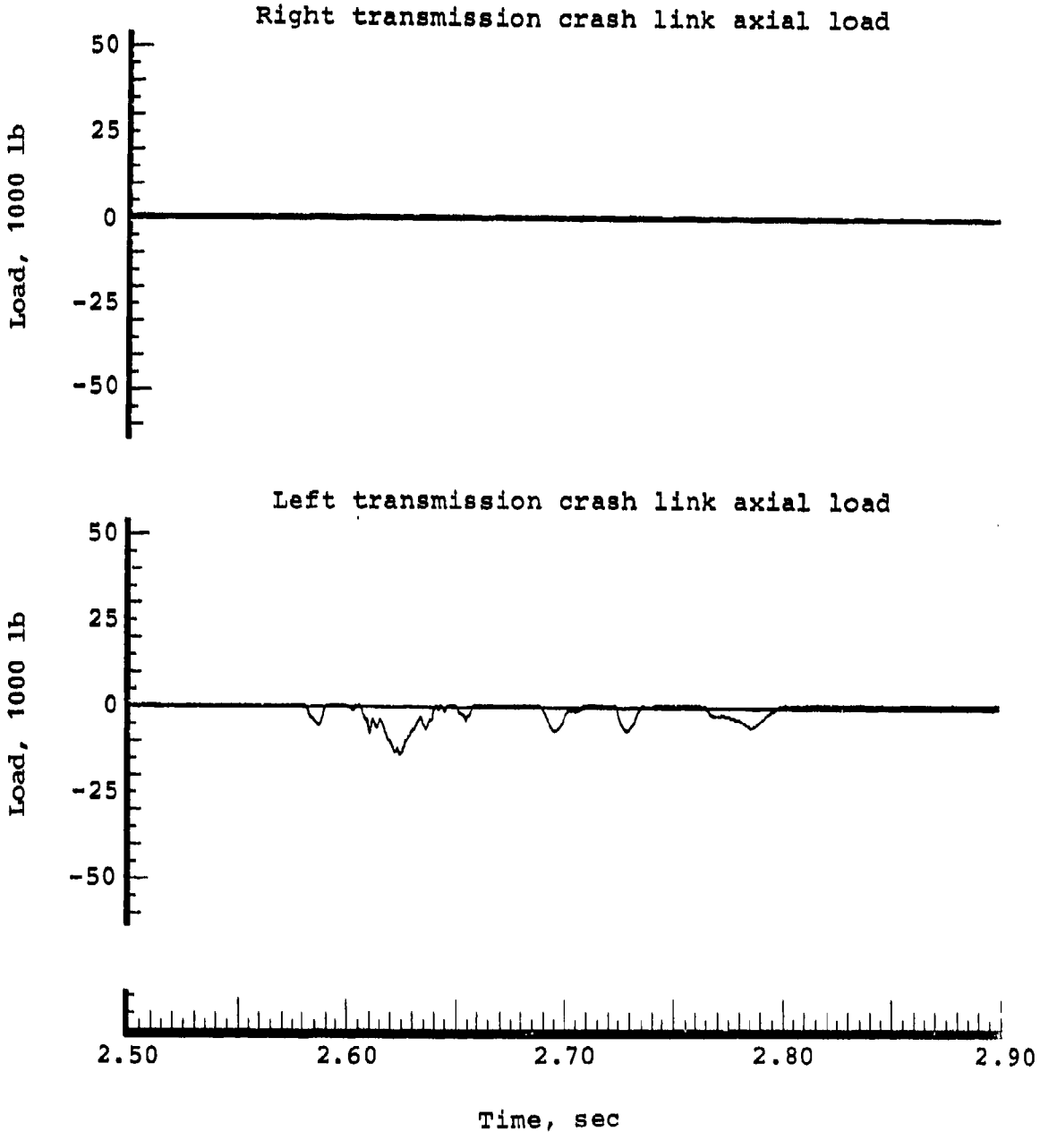
Right transmission crash link axial load
Load, 1000 lb
50
25
0
-25
-50
Left transmission crash link axial load
Load, 1000 lb
50
25
0
-25
-50
2.50
2.60
2.70
2.80
2.90
Time, sec

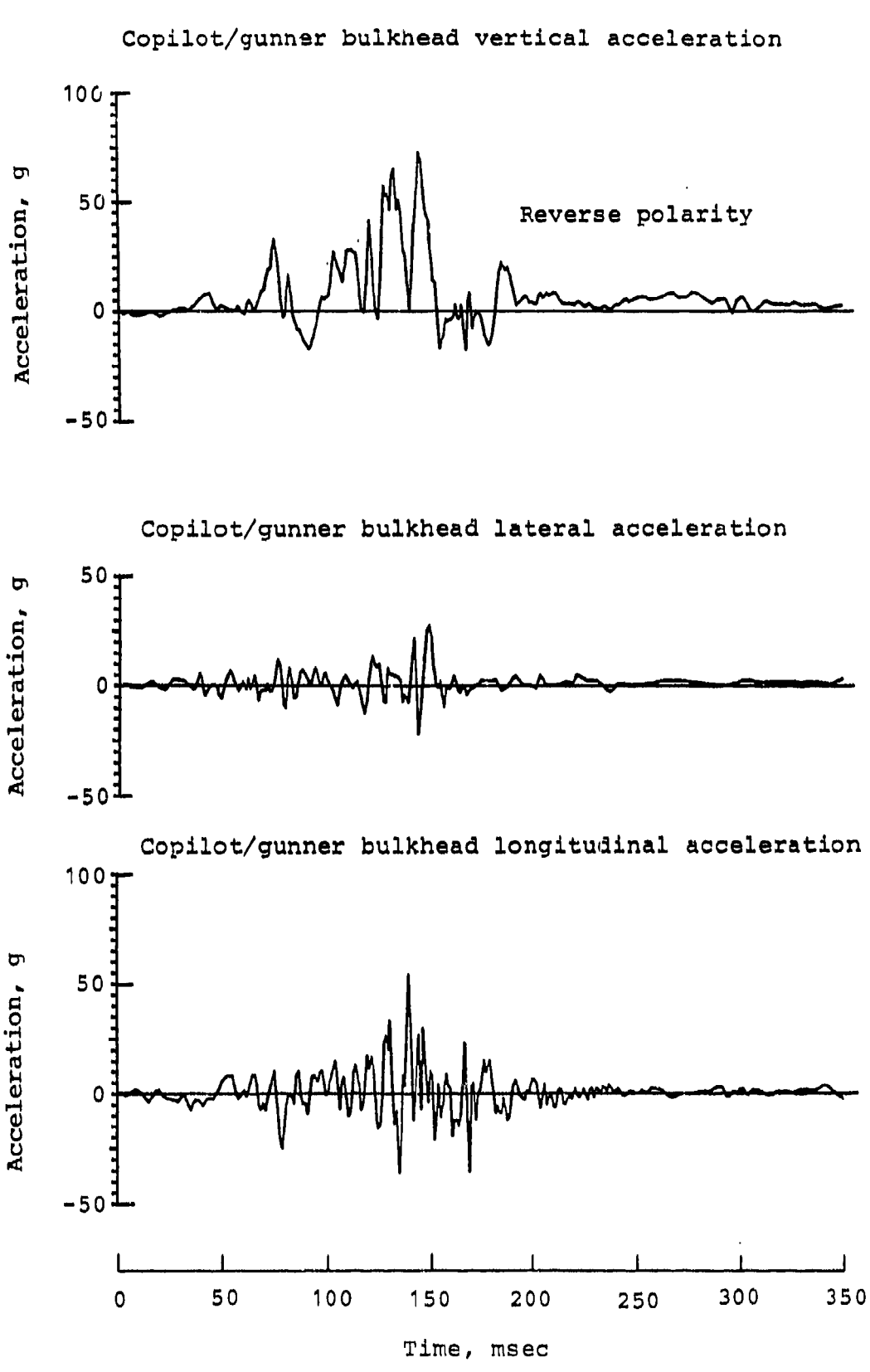
Copilot/gunner bulkhead vertical acceleration
Acceleration, g
100
50
0
-50
Reverse polarity
Copilot/gunner bulkhead lateral acceleration
Acceleration, g
50
0
-50
Copilot/gunner bulkhead longitudinal acceleration
Acceleration, g
100
50
0
-50
0
50
100
150
200
250
300
350
Time, msec

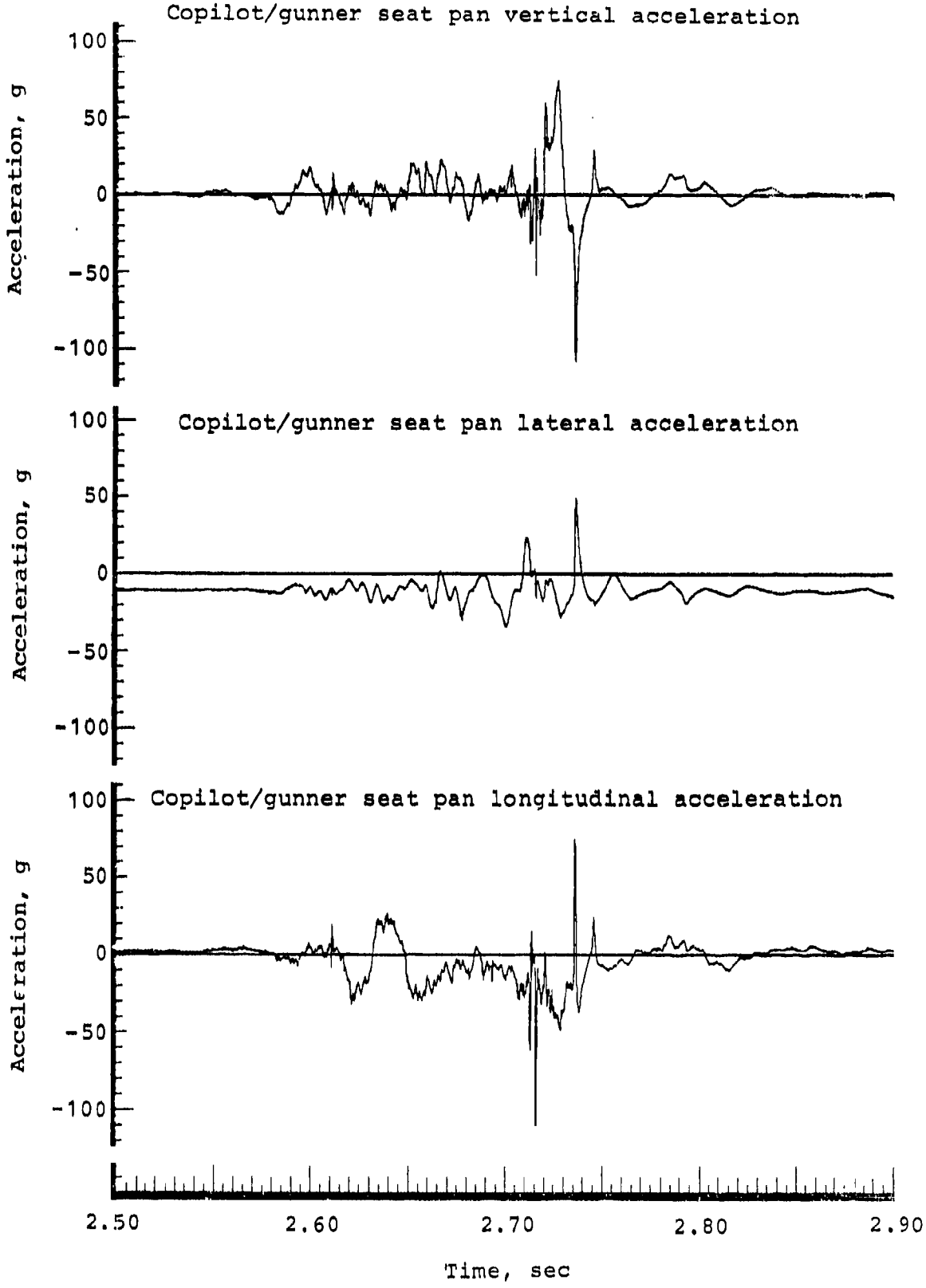
Copilot/gunner seat pan vertical acceleration
Acceleration, g
100
50
0
-50
-100
Copilot/gunner seat pan lateral acceleration
Acceleration, g
100
50
0
-50
-100
Copilot/gunner seat pan longitudinal acceleration
Acceleration, g
100
50
0
-50
-100
2.50
2.60
2.70
2.80
2.90
Time, sec

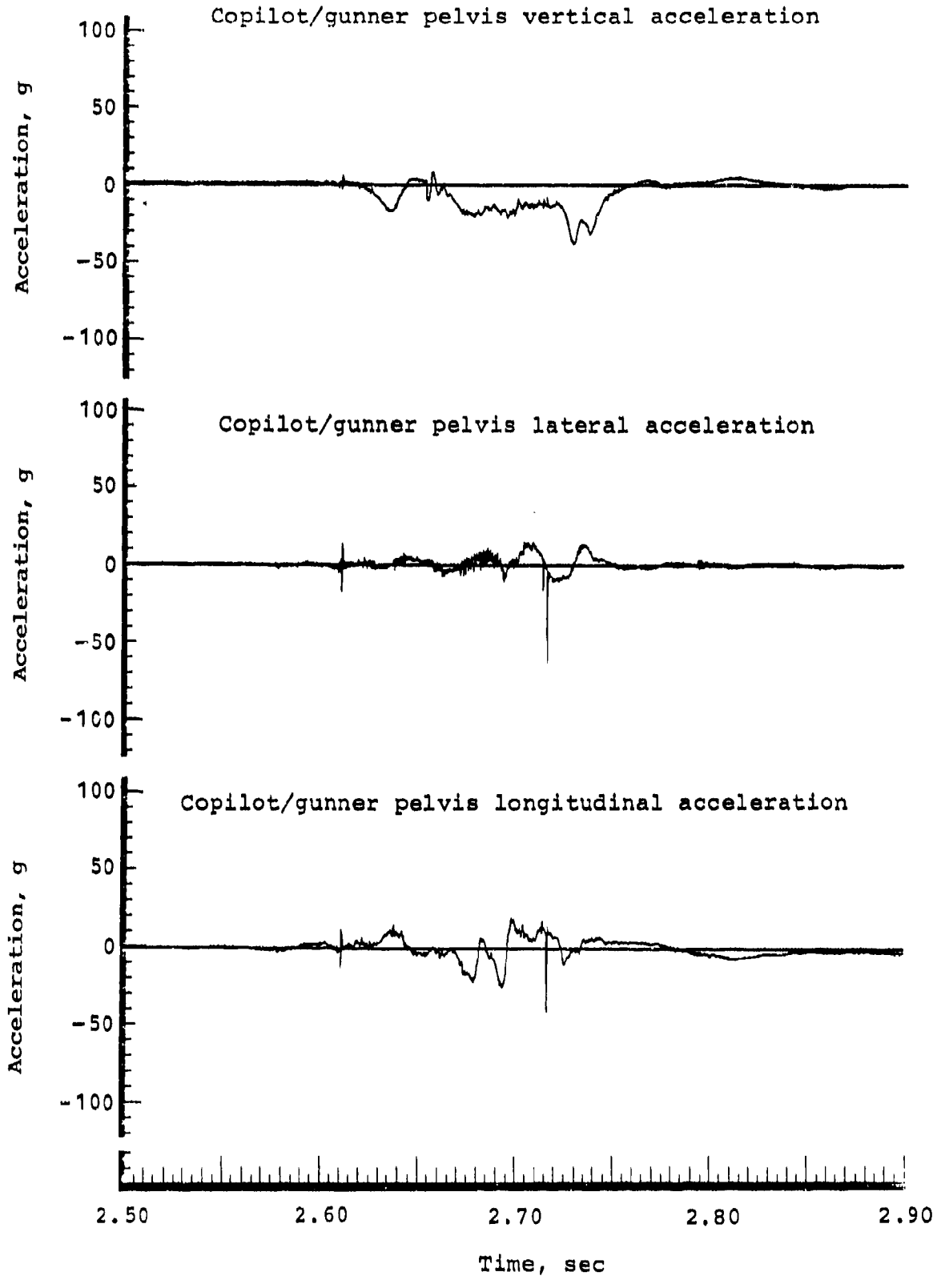
Copilot/gunner pelvis vertical acceleration
Acceleration, g
100
50
0
-50
-100
Copilot/gunner pelvis lateral acceleration
Acceleration, g
100
50
0
-50
-100
Copilot/gunner pelvis longitudinal acceleration
Acceleration, g
100
50
0
-50
-100
2.50
2.60
2.70
2.80
2.90
Time, sec

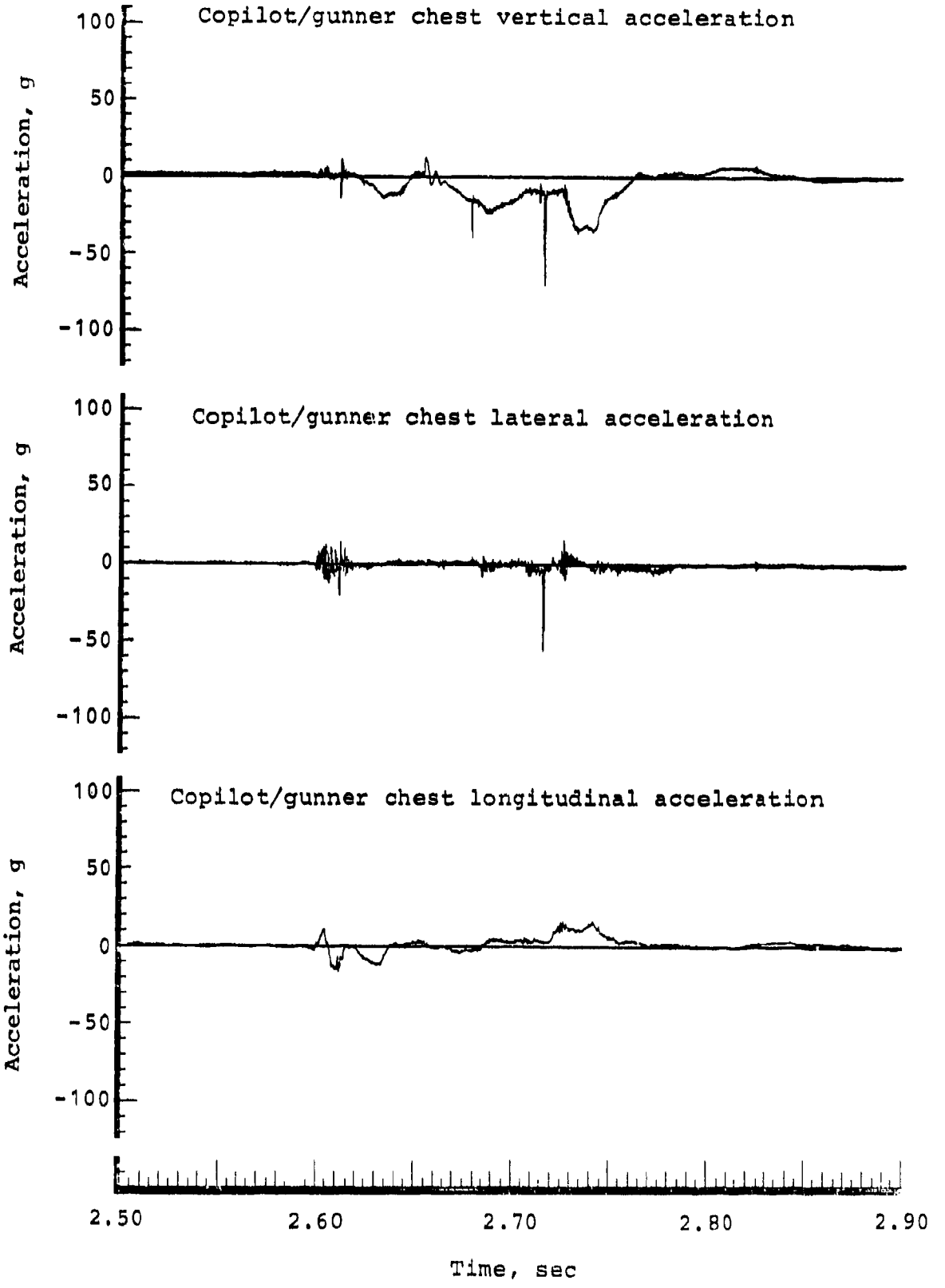
Copilot/gunner chest vertical acceleration
Acceleration, g
100
50
0
-50
-100
Copilot/gunner chest lateral acceleration
Acceleration, g
100
50
0
-50
-100
Copilot/gunner chest longitudinal acceleration
Acceleration, g
100
50
0
-50
-100
2.50
2.60
2.70
2.80
2.90
Time, sec

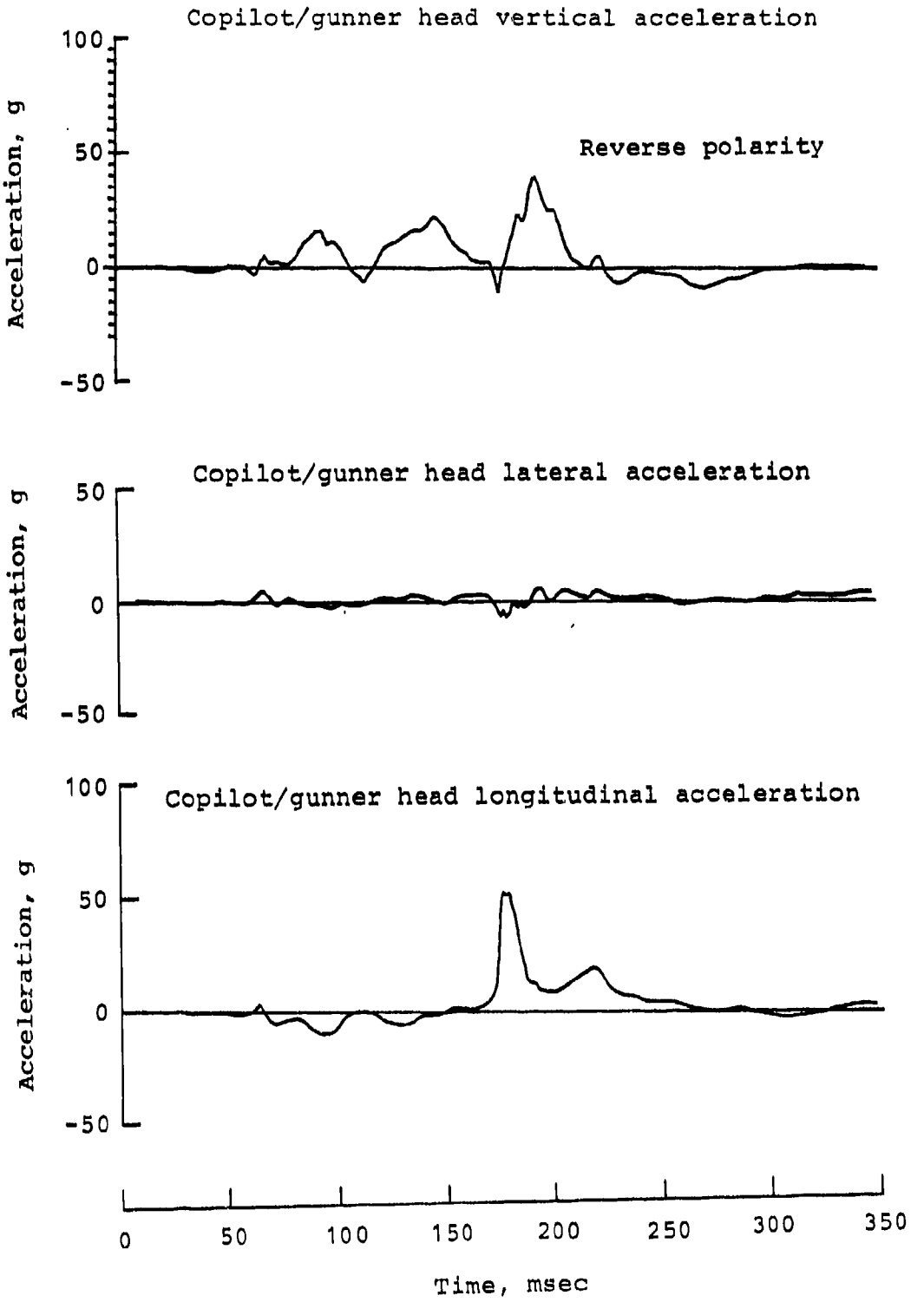
Copilot/gunner head vertical acceleration
Acceleration, g
100
50
0
-50
Reverse polarity
Copilot/gunner head lateral acceleration
Acceleration, g
50
0
-50
Copilot/gunner head longitudinal acceleration
Acceleration, g
100
50
0
-50
0
50
100
150
200
250
300
350
Time, msec

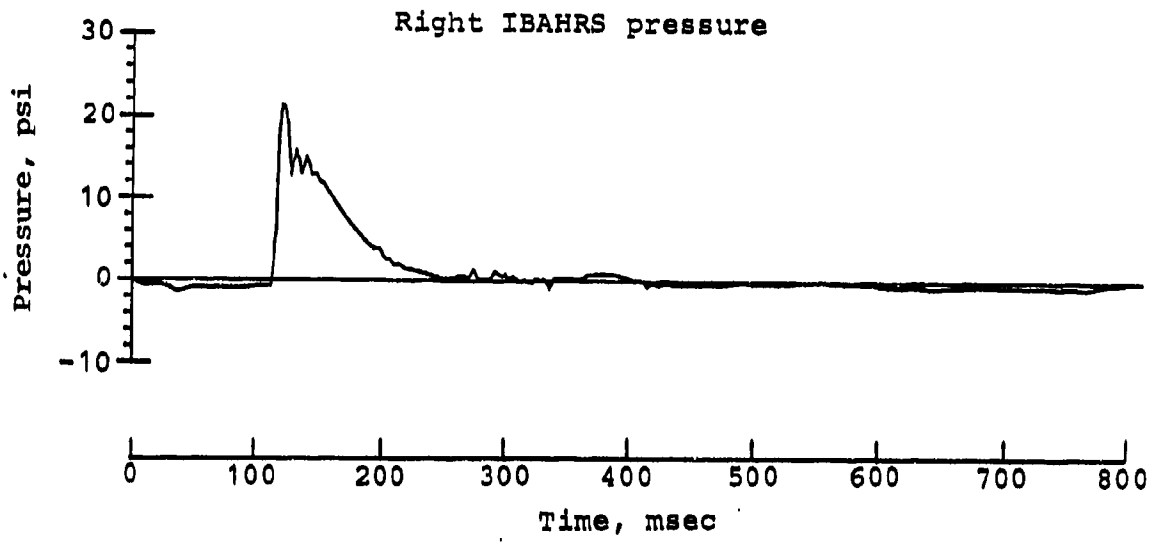
Right IBAHRS pressure
Pressure, psi
30
20
10
0
-10
0
100
200
300
400
500
600
700
800
Time, msec

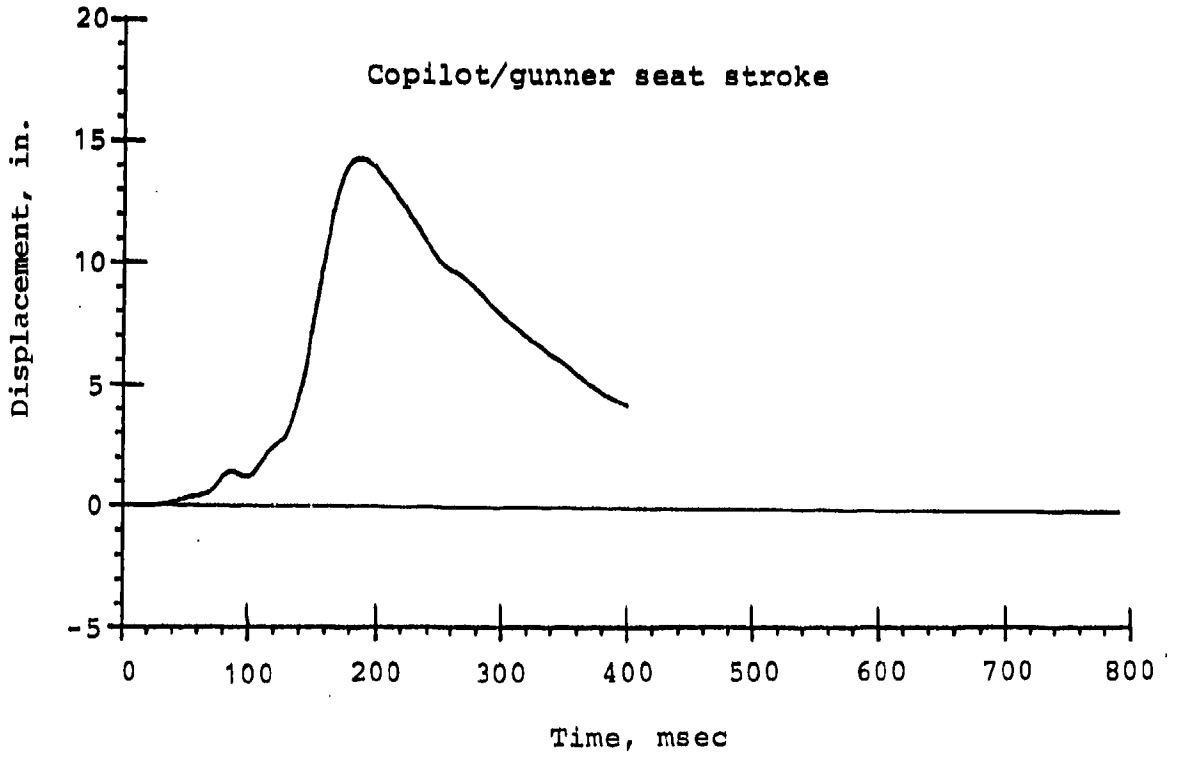
Copilot/gunner seat stroke
Displacement, in.
20
15
10
5
0
-5
0
100
200
300
400
500
600
700
800
Time, msec

APPENDIX D

KRASH MATH MODEL LISTING

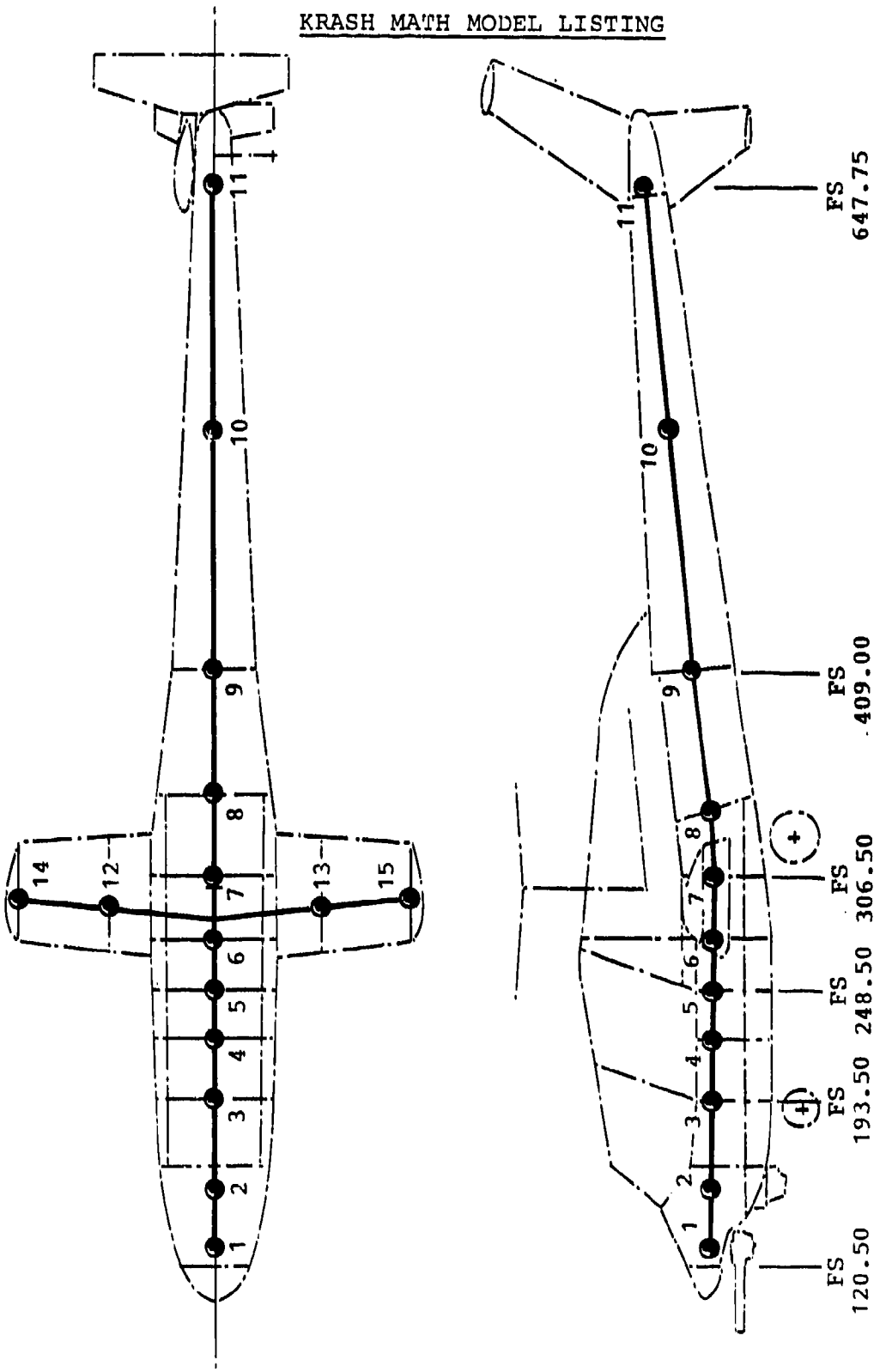

Figure D-1. KRASH math model of fuselage and wings.

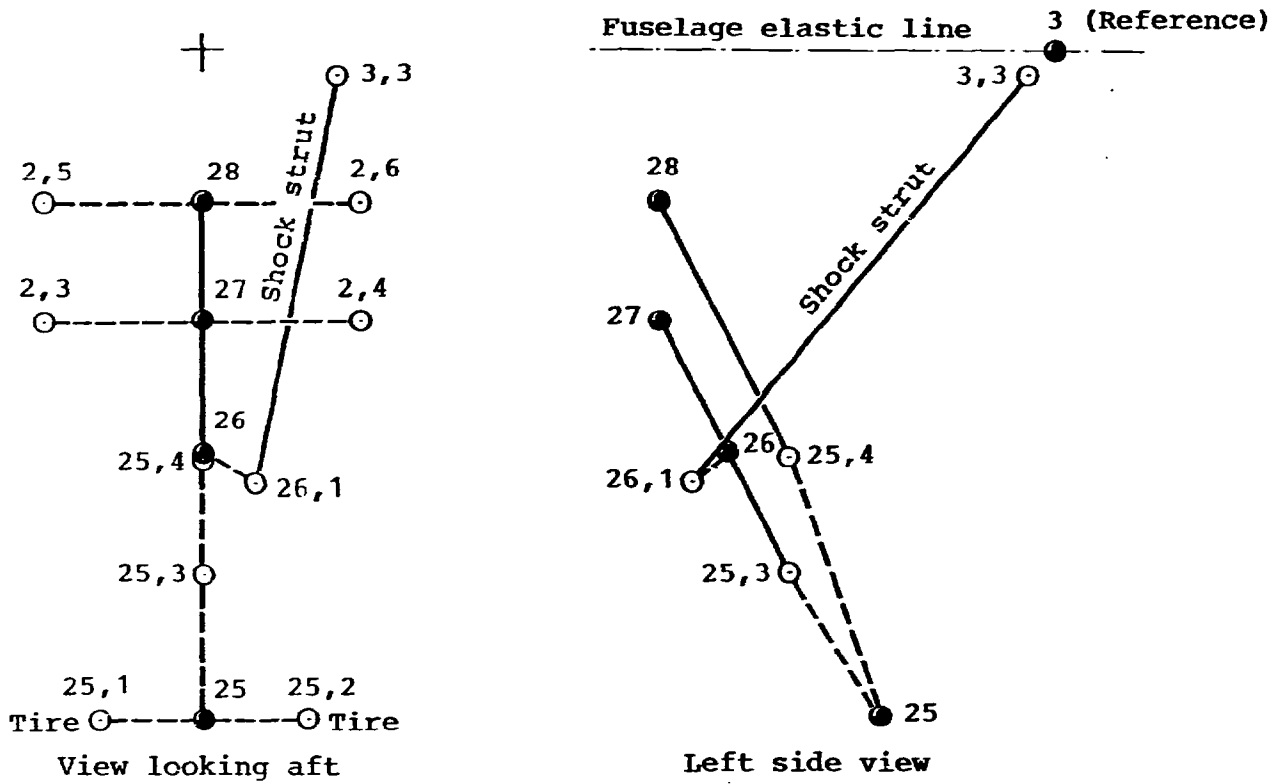

Figure D-2. KRASH math model of nose landing gear.

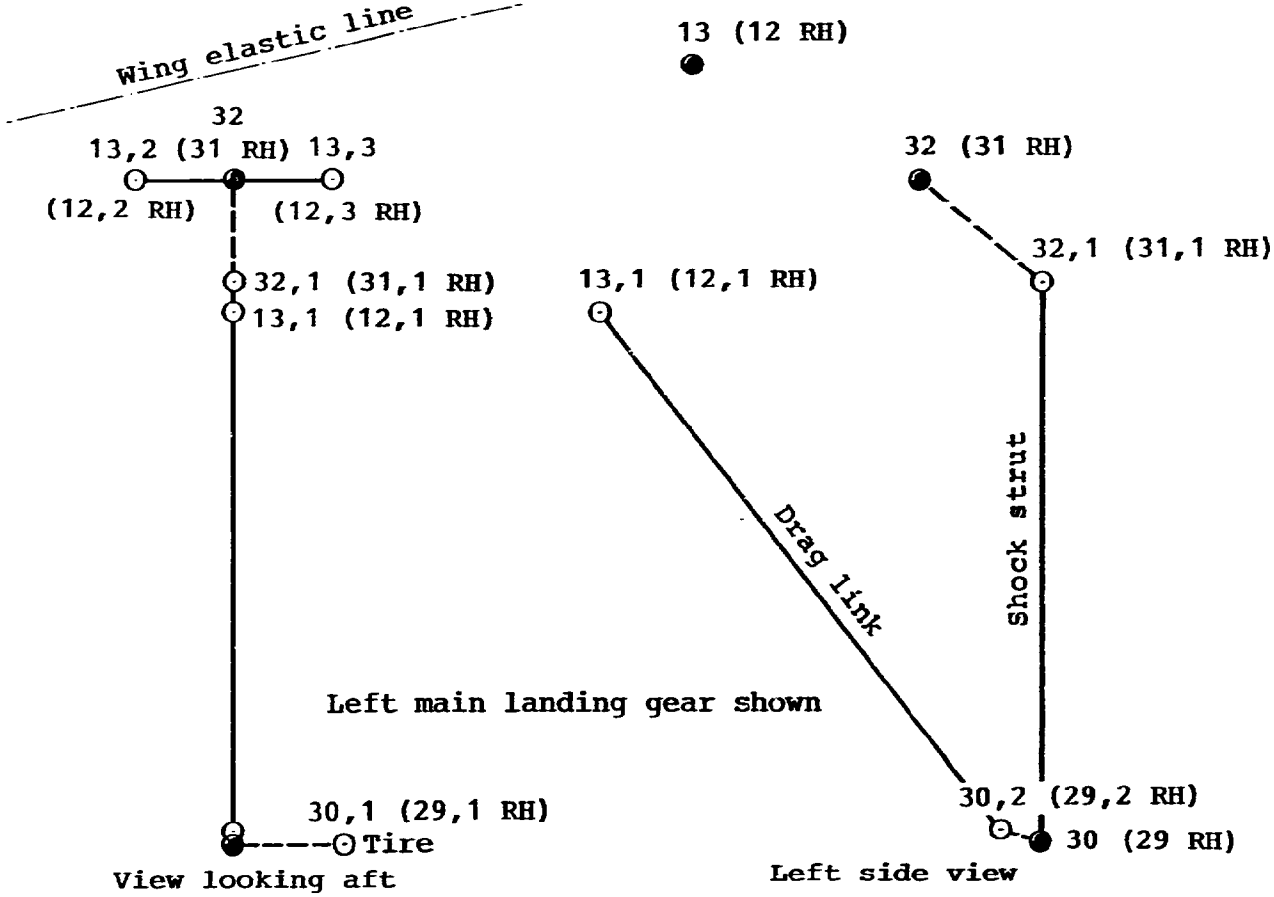

Figure D-3. KRASH math model of main landing gear.

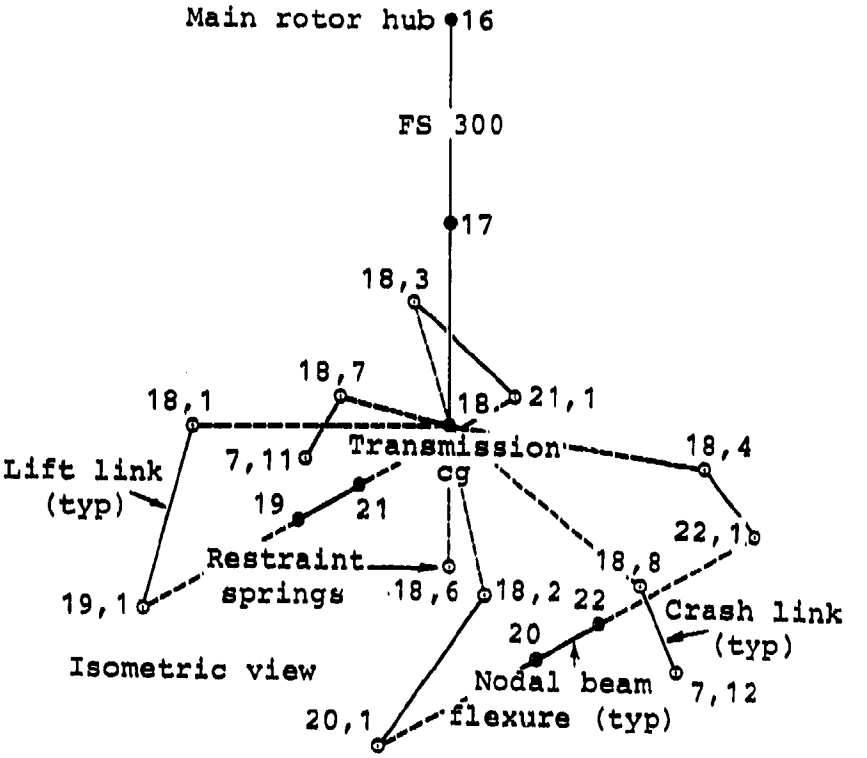

Figure D-4. KRASH math model of main rotor pylon.

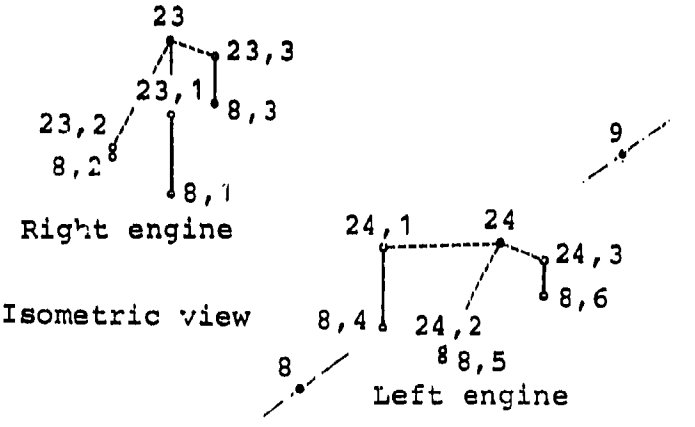

Figure D-5. KRASH math model of engines.

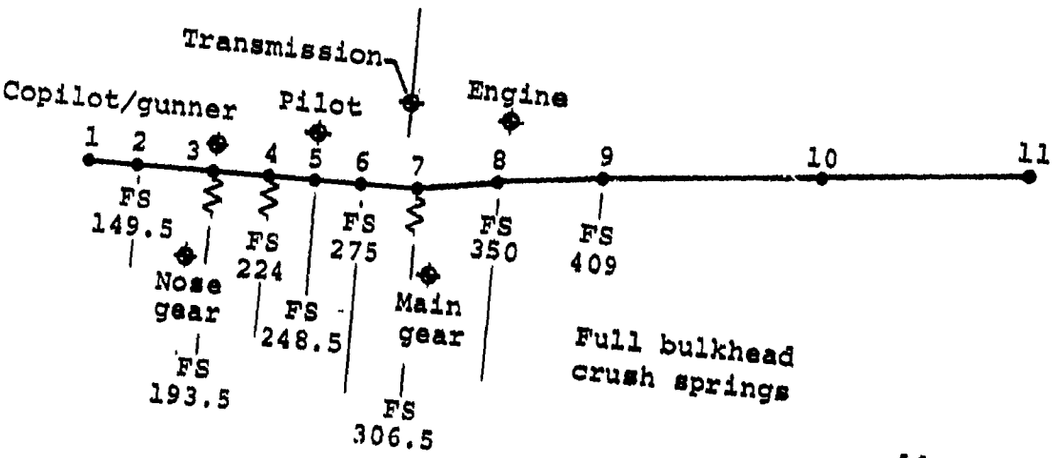

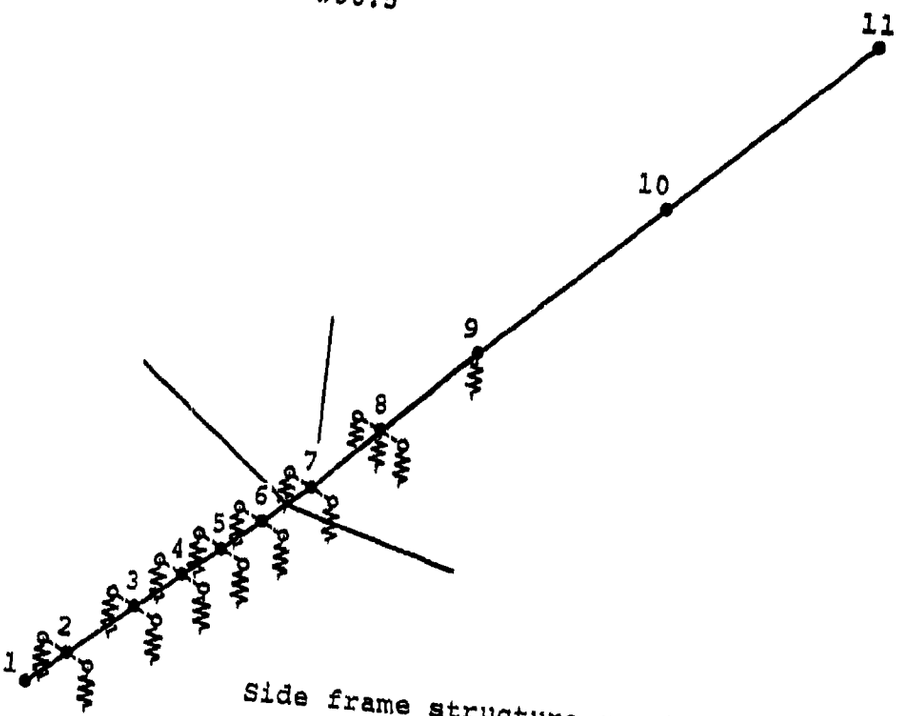

Figure D-6. KRASH math model of lower fuselage crushable structure.

```
YAH-63A ACTUAL   LANGLEY TEST-FUSE CRUSH BEAMS-0.1 FRICTION-20 JULY 82        0001
MOD FAIL OF L/G, NOSE, & T/B-ADD FUSE/BKHD CRUSH-TMAX=200MSEC-DT=5USEC       0002
12345678901234567890123456789012345678901234567890123456789012345678901234  0003
   54   28   76   21   73    9    4    2    0    0    0    0    2    0       0004
    0    4    0    4    0    0    0327503275032750    0    0                 0005
                                                                            0006
                                                                            0007
      1000  0.000005     0.250       0.0       0.0       0.0                0008
                                                                            0009
    1    1    1    1    1    0    1    0    1                              0010
    0    0    0    0    0    0    0    0    0    0                         0011
   433.20       0.0     576.00                                              0012
      0.0       0.0        0.0                                              0013
-.0087266   1614429        0.0       0.0       0.0       0.0               0014
   726.99     120.50       0.00     53.00    126.17    153.26     55.29     0101
   564.36     149.50       0.00     53.00    696.20    587.80    276.87     0102
   537.58     193.50       0.00     53.00    809.49    650.18    393.27     0103
   436.57     224.00       0.00     53.00    891.27    714.49    345.20     0104
   563.83     248.50       0.00     53.00    857.25    632.23    307.55     0105
   707.09     275.00       0.00     53.00   1195.04    903.05    494.53     0106
  2387.54     306.50       0.00     53.00   1466.20   2667.22   2355.16     0107
   964.54     350.00       0.00     60.00   1902.73   1531.64   1419.89     0108
   755.11     409.00       0.00     67.00    913.15    900.48   1056.69     0109
   144.47     530.75       0.00     78.70     92.67    337.83    320.75     0110
   454.87     647.75       0.00     89.94   1533.16   1691.72    766.44     0111
    99.31     290.95     -43.00     64.72     24.34     41.00     47.07     0112
    99.85     290.95      43.00     64.72     23.78     37.91     44.54     0113
    52.59     293.41     -90.00     75.57     13.53     23.29     33.67     0114
    51.89     293.41      90.00     75.57     13.51     23.36     33.80     0115
   963.00     300.00       1.90    154.00      1.00      1.00      1.00     0116
   258.02     300.00       1.09    126.86      1.00      1.00      1.00     0117
  1741.20     300.00       0.29     99.71   1808.55   1358.03   1430.05     0118
     5.98     295.50     -18.00     80.50      1.00      1.00      1.00     0119
```

5.98	295.50	18.00	80.50	1.00	1.00	1.00	0120
5.98	304.50	-18.00	80.50	1.00	1.00	1.00	0121
5.98	304.50	18.00	80.50	1.00	1.00	1.00	0122
480.00	356.30	-30.00	96.60	6.57	222.56	222.56	0123
480.00	356.30	30.00	94.82	6.57	222.56	222.56	0124
117.90	180.06	0.00	2.15	13.92	13.92	7.48	0125
36.50	168.32	0.00	22.20	6.88	12.99	6.88	0126
27.30	163.00	0.00	32.40	1.86	3.14	1.86	0127
12.60	163.00	0.00	41.40	0.71	1.35	0.71	0128
64.10	317.77	-41.50	5.35	6.79	12.97	6.79	0129
64.10	317.77	41.50	5.35	6.79	12.97	6.79	0130
150.80	308.50	-41.50	56.00	68.36	68.36	4.88	0131
150.80	308.50	41.50	56.00	68.36	68.36	4.88	0132
219.50	193.50	0.00	68.34	100.00	100.00	100.00	0133
74.50	193.50	0.00	78.34	40.00	40.00	40.00	0134
74.50	193.50	0.00	78.34	40.00	40.00	40.00	0135
219.50	248.50	0.00	78.99	100.00	100.00	100.00	0136
74.50	248.50	0.00	88.99	40.00	40.00	40.00	0137
74.50	248.50	0.00	88.99	40.00	40.00	40.00	0138
10.00	149.50	-12.50	34.75	2.84	2.84	20.00	0139
10.00	149.50	12.50	34.75	2.84	2.84	20.00	0140
10.00	193.50	-12.50	28.50	5.12	5.13	20.00	0141
10.00	193.50	12.50	28.50	5.12	5.13	20.00	0142
10.00	224.00	-12.50	28.50	5.10	5.11	20.00	0143
10.00	224.00	12.50	28.50	5.10	5.11	20.00	0144
10.00	248.50	-12.50	28.50	5.13	5.14	20.00	0145
10.00	248.50	12.50	28.50	5.13	5.14	20.00	0146
10.00	275.00	-12.50	28.50	5.14	5.14	20.00	0147
10.00	275.00	12.50	28.50	5.14	5.14	20.00	0148
10.00	306.50	-12.50	31.00	4.17	4.18	20.00	0149
10.00	306.50	12.50	31.00	4.17	4.18	20.00	0150
10.00	350.00	-12.50	37.47	4.75	4.75	20.00	0151
10.00	350.00	0.00	37.47	4.75	4.75	20.00	0152

10.00		350.00	12.50	37.47	4.15	4.75	20.00	0153
10.00		409.00	0.00	46.08	4.11	4.11	20.00	0154
1	2	149.50	-12.50	53.00				0201
2	2	149.50	12.50	53.00				0202
3	2	163.00	-12.15	32.40				0203
4	2	163.00	12.15	32.40				0204
5	2	163.00	-12.15	41.40				0205
6	2	163.00	12.15	41.40				0206
1	3	193.50	-12.50	53.00				0207
2	3	193.50	12.50	53.00				0208
3	3	191.50	10.25	51.00				0209
1	4	224.00	-12.50	53.00				0210
2	4	224.00	12.50	53.00				0211
1	5	248.50	-12.50	53.00				0212
2	5	248.50	12.50	53.00				0213
1	6	275.00	-12.50	53.00				0214
2	6	275.00	12.50	53.00				0215
1	7	269.25	-18.00	80.50				0216
2	7	269.25	18.00	80.50				0217
3	7	330.75	-18.00	80.50				0218
4	7	330.75	18.00	80.50				0219
5	7	306.50	0.00	77.35				0220
6	7	307.50	1.00	77.35				0221
7	7	300.00	0.26	80.29				0222
8	7	290.11	0.00	54.79				0223
9	7	306.50	-12.50	53.00				0224
10	7	306.50	12.50	53.00				0225
11	7	306.50	-28.00	78.25				0226
12	7	306.50	28.00	78.25				0227
1	8	346.54	-19.20	83.13				0228
2	8	346.49	-30.00	83.64				0229
3	8	364.38	-30.00	82.60				0230
4	8	346.54	19.20	81.35				0231

5	8	346.49	30.00	81.86	0232
6	8	364.21	30.00	82.58	0233
7	8	350.00	-12.50	60.00	0234
8	8	350.00	12.50	60.00	0235
1	11	647.75	-13.50	89.94	0236
1	12	284.00	-41.50	46.00	0237
2	12	308.50	-34.00	56.00	0238
3	12	308.50	-49.00	56.00	0239
1	13	284.00	41.50	46.00	0240
2	13	308.50	34.00	56.00	0241
3	13	308.50	49.00	56.00	0242
1	18	283.36	-22.06	97.07	0243
2	18	283.36	22.06	97.07	0244
3	18	316.63	-22.06	97.07	0245
4	18	316.63	22.06	97.07	0246
5	18	307.50	0.00	77.35	0247
6	18	300.00	0.26	81.29	0248
7	18	306.50	-23.03	88.90	0249
8	18	306.50	22.40	86.88	0250
9	18	306.50	-23.03	88.90	0251
10	18	306.50	22.40	86.88	0252
1	19	272.00	-18.00	80.50	0253
1	20	272.00	18.00	80.50	0254
1	21	328.00	-18.00	80.50	0255
1	22	328.00	18.00	80.50	0256
1	23	345.33	-19.20	95.64	0257
2	23	346.37	-30.00	84.86	0258
3	23	363.67	-30.00	89.95	0259
1	24	345.33	19.20	93.86	0260
2	24	346.37	30.00	83.05	0261
3	24	363.68	30.00	88.02	0262
1	25	180.06	-8.00	2.15	0263
2	25	180.06	8.00	2.15	0264

```
     3   25     173.03       0.00      13.18                                  0265
     4   25     173.03       0.00      22.06                                  0266
     1   26     165.67       4.00      20.15                                  0267
     1   29     317.77     -50.00       5.35                                  0268
     2   29     314.72     -41.50       6.47                                  0269
     1   30     317.77      50.00       5.35                                  0270
     2   30     314.72      41.50       6.47                                  0271
     1   31     317.77     -41.50      48.27                                  0272
     1   32     317.77      41.50      48.27                                  0273
0    1    3      17.00      0.100 1000000.0      0.0       0.0               0301
0   39    3       1.00      0.100 1169616.5      0.0       0.0               0302
0    2    3      22.50      0.100 1000000.0      0.0       0.0               0303
0   40    3       1.00      0.100 1169616.5      0.0       0.0               0304
0   41    3       1.00      0.100 1169616.5      0.0       0.0               0305
0    3    3      25.50      0.100 1000000.0      0.0       0.0               0306
0   42    3       1.00      0.100 1169616.5      0.0       0.0               0307
0   43    3       1.00      0.100 2109144.5      0.0       0.0               0308
0    4    3      25.50      0.100 1000000.0      0.0       0.0               0309
0   44    3       1.00      0.100 2109144.5      0.0       0.0               0310
0   45    3       1.00      0.100 1955752.2      0.0       0.0               0311
0    5    3      13.00      0.100 1000000.0      0.0       0.0               0312
0   46    3       1.00      0.100 1955752.2      0.0       0.0               0313
0   47    3       1.00      0.100 2224188.8      0.0       0.0               0314
0    6    3      13.00      0.100 1000000.0      0.0       0.0               0315
0   48    3       1.00      0.100 2224188.8      0.0       0.0               0316
0   49    3       1.00      0.100 2876106.2      0.0       0.0               0317
0    7    3      23.00      0.100 1000000.0      0.0       0.0               0318
0   50    3       1.00      0.100 2876106.2      0.0       0.0               0319
0   51    3       1.00      0.100 2620452.3      0.0       0.0               0320
0   52    3       1.00      0.100 2620452.3      0.0       0.0               0321
0   53    3       1.00      0.100 2620452.3      0.0       0.0               0322
0   54    3       1.00      0.100 4525073.7      0.0       0.0               0323
1   11    3      49.94      0.100   50000.0      0.0       0.0               0324
```

```
1 25    3      8.50      0.100 1000000.0       0.0        0.0                    0325
2 25    3      8.50      0.100 1000000.0       0.0        0.0                    0326
1 29    3     12.50      0.100 1000000.0       0.0        0.0                    0327
1 30    3     12.50      0.100 1000000.0       0.0        0.0                    0328
 0.010000  0.100000  0.750000  8.000000   10000.0     1000.0        0.0          0401
 0.100000  0.100001  1.000000  1.000001  116961.7  1169616.5        0.0          0402
 0.010000  0.100000  0.750000  8.000000   10000.0     1000.0        0.0          0403
 0.100000  0.100001  1.000000  1.000001  116961.7  1169616.5        0.0          0404
 0.100000  0.100001  1.000000  1.000001  116961.7  1169616.5        0.0          0405
 0.010000  0.100000  0.750000  8.000000   10000.0     1000.0        0.0          0406
 0.100000  0.100001  1.000000  1.000001  116961.7  1169616.5        0.0          0407
 0.100000  0.100001  1.000000  1.000001  210914.5  2109144.5        0.0          0408
 0.010000  0.100000  0.750000  8.000000   10000.0     1000.0        0.0          0409
 0.100000  0.100001  1.000000  1.000001  210914.5  2109144.5        0.0          0410
 0.100000  0.100001  1.000000  1.000001  195575.2  1955752.2        0.0          0411
 0.010000  0.100000  0.750000  8.000000   10000.0     1000.0        0.0          0412
 0.100000  0.100001  1.000000  1.000001  195575.2  1955752.2        0.0          0413
 0.100000  0.100001  1.000000  1.000001  222418.9  2224188.8        0.0          0414
 0.010000  0.100000  0.750000  8.000000   10000.0     1000.0        0.0          0415
 0.100000  0.100001  1.000000  1.000001  222418.9  2224188.8        0.0          0416
 0.100000  0.100001  1.000000  1.000001  287610.6  2876106.2        0.0          0417
 0.010000  0.100000  0.750000  8.000000   10000.0     1000.0        0.0          0418
 0.100000  0.100001  1.000000  1.000001  287610.6  2876106.2        0.0          0419
 0.100000  0.100001  1.000000  1.000001  262045.2  2620452.3        0.0          0420
 0.100000  0.100001  1.000000  1.000001  262045.2  2620452.3        0.0          0421
 0.100000  0.100001  1.000000  1.000001  262045.2  2620452.3        0.0          0422
 0.100000  0.100001  1.000000  1.000001  452507.4  4525073.7        0.0          0423
 4.000000  4.000001 24.000000 24.000001   14000.0    14000.0        0.0          0424
 2.000000  2.000001  4.100000  4.100001    3000.0     8502.0        0.0          0425
 2.000000  2.000001  4.100000  4.100001    3000.0     8502.0        0.0          0426
 2.000000  2.000001  5.900000  5.900001    5200.0    22750.0        0.0          0427
 2.000000  2.000001  5.900000  5.900001    5200.0    22750.0        0.0          0428
0  1 0  2     16.39    100.00    690.52   2841.03         0.0 1.00 1.00 4        0501
```

0	2	0	3	13.71	100.00	1254.66	4140.23	0.0	1.00	1.00	4	0502
0	3	0	4	9.42	100.00	2082.95	4372.46	0.0	1.00	1.00	4	0503
0	4	0	5	9.56	528.57	2555.10	4171.63	0.0	1.00	1.00	4	0504
0	5	0	6	10.50	1300.00	2650.00	4170.00	0.0	1.00	1.00	4	0505
0	6	0	7	10.16	1588.89	2268.89	4352.22	0.0	1.00	1.00	4	0506
0	7	0	8	8.61	1441.38	2166.44	3702.18	0.0	1.00	1.00	4	0507
0	8	0	9	6.39	1142.37	1526.61	1810.00	0.0	1.00	1.00	4	0508
0	10	0	9	6.54	1216.98	1099.87	1080.39	0.0	1.00	1.0011		0509
0	11	0	10	4.68	499.80	373.60	396.04	0.0	1.00	1.0011		0510
8	7	0	12	14.01	508.92	404.31	2694.23	0.0	1.00	1.00	4	0511
0	12	0	14	10.94	351.57	256.11	1672.15	0.0	1.00	1.00	4	0512
8	7	0	13	14.01	508.92	404.31	2694.23	0.0	1.00	1.00	4	0513
0	13	0	15	10.94	351.57	256.11	1672.15	0.0	1.00	1.00	4	0514
0	16	0	17	8.23	49.97	24.99	24.99	0.0	1.00	1.00	1	0515
0	17	0	18	10.00	64.43	32.21	32.21	0.0	1.00	1.00	1	0516
1	18	1	19	1.00	0.00	0.00	0.00	0.0	1.00	1.00	4	0517
2	18	1	20	1.00	0.00	0.00	0.00	0.0	1.00	1.00	4	0518
3	18	1	21	1.00	0.00	0.00	0.00	0.0	1.00	1.00	4	0519
4	18	1	22	1.00	0.00	0.00	0.00	0.0	1.00	1.00	4	0520
1	7	1	19	0.013924	2.465557	0.008775	0.008775	0.0	1.00	1.00	1	0521
2	7	1	20	0.013924	2.465557	0.008775	0.008775	0.0	1.00	1.00	1	0522
3	7	1	21	0.013924	2.465557	0.008775	0.008775	0.0	1 00	1.00	1	0523
4	7	1	22	0.013924	2.465557	0.008775	0.008775	0.0	1.00	1.00	1	0524
0	19	0	21	0.022935	4.037565	0.154813	0.154813	0.0	1.00	1.00	1	0525
0	20	0	22	0.022935	4.037565	0.154813	0.154813	0.0	1.00	1.00	1	0526
5	7	5	18	0.0002300	0.00	0.00	0.00	0.0	1.00	1.00	1	0527
6	7	5	18	0.0004333	0.00	0.00	0.00	0.0	1.00	1.00	1	0528
11	7	7	18	0.81175	0.00	0.00	0.00	0.0	0.69	0.50	4	0529
11	7	9	18	0.81175	0.00	0.00	0.00	0.0	0.69	0.50	4	0530
12	7	8	18	0.81175	0.00	0.00	0.00	0.0	0.69	0.50	4	0531
12	7	10	18	0.81175	0.00	0.00	0.00	0.0	0.69	0.50	4	0532
1	8	1	23	0.07280	0.00	0.00	0.00	0.0	0.35	0.35	1	0533
2	8	2	23	0.56560	0.1018	0.0942	0.0075	0.0	0.70	0.20	1	0534

3	8	3	23	1.00000	0.00	0.00	0.00	0.0	1.00	1.00	1	0535
4	8	1	24	0.07280	0.00	0.00	0.00	0.0	0.35	0.35	1	0536
5	8	2	24	0.56560	0.1018	0.0942	0.0075	0.0	0.70	0.20	1	0537
6	8	3	24	1.00000	0.00	0.00	0.00	0.0	1.00	1.00	1	0538
3	2	0	27	1.49	150.22	75.11	75.11	0.0	1.00	1.00	4	0539
4	2	0	27	1.49	150.22	75.11	75.11	0.0	1.00	1.00	4	0540
5	2	0	28	0.52	27.54	13.77	13.77	0.0	1.00	1.00	4	0541
6	2	0	28	0.52	27.54	13.77	13.77	0.0	1.00	1.00	4	0542
3	25	0	26	0.69	11.92	5.96	5.96	0.0	1.00	1.00	4	0543
0	26	0	27	0.69	11.92	5.96	5.96	0.0	1.00	1.00	4	0544
4	25	0	28	0.60	47.78	23.89	23.89	0.0	1.00	1.00	4	0545
3	3	1	26	.31983555	0.00	0.00	0.00	0.0	1.00	1.00	4	0546
1	12	2	29	4.36	0.00	0.00	0.00	0.0	1.00	1.00	4	0547
1	13	2	30	4.36	0.00	0.00	0.00	0.0	1.00	1.00	4	0548
2	12	0	31	0.71	0.00	3.34	3.34	0.0	1.00	1.0012		0549
3	12	0	31	0.71	0.00	3.34	3.34	0.0	1.00	1.0012		0550
0	29	1	31	.23556948	191.06	95.53	95.53	0.0	1.00	1.00	4	0551
2	13	0	32	0.71	0.00	3.34	3.34	0.0	1.00	1.0012		0552
3	13	0	32	0.71	0.00	3.34	3.34	0.0	1.00	1.0012		0553
0	30	1	32	.23556948	191.06	95.53	95.53	0.0	1.00	1.00	4	0554
0	3	0	33	.06228040	30.18	226.13	226.13	0.0	1.00	1.00	4	0555
0	33	0	34	1.00	1.00	1.00	1.00	0.0	1.00	1.00	9	0556
0	33	0	35	1.00	1.00	1.00	1.00	0.0	1.00	1.0010		0557
0	5	0	36	.10551940	48.39	1113.89	1113.89	0.0	1.00	1.00	4	0558
0	36	0	37	1.00	1.00	1.00	1.00	0.0	1.00	1.00	9	0559
0	36	0	38	1.00	1.00	1.00	1.00	0.0	1.00	1.0010		0560
1	2	0	39	0.2032905	8.3993	12.1272	12.1272	0.0	1.00	1.00	4	0561
2	2	0	40	0.2032905	8.3993	12.1272	12.1272	0.0	1.00	1.00	4	0562
1	3	0	41	0.2729105	11.5052	29.3170	29.3170	0.0	1.00	1.00	4	0563
2	3	0	42	0.2729105	11.5052	29.3170	29.3170	0.0	1.00	1.00	4	0564
1	4	0	43	0.4921337	11.4281	29.2032	29.2032	0.0	1.00	1.00	4	0565
2	4	0	44	0.4921337	11.4281	29.2032	29.2032	0.0	1.00	1.00	4	0566
1	5	0	45	0.4563422	11.3520	29.3403	29.3403	0.0	1.00	1.00	4	0567

```
 2  5 0 46 0.4563422    11.3520    29.3403    29.3403        0.0 1.00 1.00 4   0568
 1  6 0 47 0.5189774    11.6203    29.4380    29.4380        0.0 1.00 1.00 4   0569
 2  6 0 48 0.5189774    11.6203    29.4380    29.4380        0.0 1.00 1.00 4   0570
 9  7 0 49 0.6026127    10.7651    21.5184    21.5184        0.0 1.00 1.00 4   0571
10  7 0 50 0.6026127    10.7651    21.5184    21.5184        0.0 1.00 1.00 4   0572
 7  8 0 51 0.5872309    11.4503    26.1736    26.1736        0.0 1.00 1.00 4   0573
 0  8 0 52 0.5872309    11.4503    26.1736    26.1736        0.0 1.00 1.00 4   0574
 8  8 0 53 0.5872309    11.4503    26.1736    26.1736        0.0 1.00 1.00 4   0575
 0  9 0 54 0.9446630    10.6162    21.0972    21.0972        0.0 1.00 1.00 4   0576
   11       10.00E06    3.75E06    35000.0    34000.0    17000.0                0601
   12       10.50E06    0.00       35000.0    34000.0    17000.0                0602
 1  7 1 19    1    0    0    0        0.0        1.0        1.0        1.0      0701
 2  7 1 20    1    0    0    0        0.0        1.0        1.0        1.0      0702
 3  7 1 21    1    0    0    0        0.0        1.0        1.0        1.0      0703
 4  7 1 22    1    0    0    0        0.0        1.0        1.0        1.0      0704
 2  8 2 23    1    1    0    0        0.0        0.0        1.0        1.0      0705
 5  8 2 24    1    1    0    0        0.0        0.0        1.0        1.0      0706
 3 25 0 26    1    0    0    0        0.0        1.0        1.0        1.0      0707
 0 26 0 27    0    0    1    0        1.0        1.0        0.0        1.0      0708
 4 25 0 28    1    0    1    0        0.0        1.0        0.0        1.0      0709
11  7 7 18   -1    2.4425                                                      0801
11  7 9 18    1    2.4425                                                      0802
12  7 8 18   -1    2.4425                                                      0803
12  710 18    1    2.4425                                                      0804
      0.04                                                                    1100
 3  3 1 26    1   14      0.506      0.0                                       1201
 0 29 1 31    1   14      1.350      0.0                                       1202
 0 30 1 32    1   14      1.350      0.0                                       1203
 0  3 0 33    1   12      0.100      0.0                                       1204
 0  5 0 36    1   12      0.100      0.0                                       1205
 1  2 0 39    1   14      0.300      0.0                                       1206
 2  2 0 40    1   14      0.300      0.0                                       1207
 1  3 0 41    1   14      0.300      0.0                                       1208
```

```
 2  3 0 42     1    14      0.300        0.0                    1209
 1  4 0 43     1    14      0.300        0.0                    1210
 2  4 0 44     1    14      0.300        0.0                    1211
 1  5 0 45     1    14      0.300        0.0                    1212
 2  5 0 46     1    14      0.300        0.0                    1213
 1  6 0 47     1    14      0.300        0.0                    1214
 2  6 0 48     1    14      0.300        0.0                    1215
 9  7 0 49     1    14      0.300        0.0                    1216
10  7 0 50     1    14      0.300        0.0                    1217
 7  8 0 51     1    14      0.300        0.0                    1218
 0  8 0 52     1    14      0.300        0.0                    1219
 8  8 0 53     1    14      0.300        0.0                    1220
 0  9 0 54     1    14      0.300        0.0                    1221
   0.00000   1.00000                                          130101
   0.50600   1.00000                                          130102
   0.50601   0.20624                                          130103
   1.43300   0.20624                                          130104
   1.43301   0.06063                                          130105
   2.27800   0.06063                                          130106
   2.27801  -0.05646                                          130107
   8.85100  -0.05646                                          130108
   8.85101  -0.03258                                          130109
  14.53400  -0.03258                                          130110
  14.53401   1.00000                                          130111
  25.00000   1.00000                                          130112
  50.00000   1.00000                                          130113
 100.00000   1.00000                                          130114
   0.00000   1.00000                                          130201
   1.35000   1.00000                                          130202
   1.35001   0.21603                                          130203
   2.35000   0.21603                                          130204
   2.35001   0.02169                                          130205
   4.15000   0.02169                                          130206
```

```
  4.15001  -0.10227                                                  130207
  9.80000  -0.10227                                                  130208
  9.80001  -0.06339                                                  130209
 15.33000  -0.06339                                                  130210
 15.33001   1.00000                                                  130211
 25.00000   1.00000                                                  130212
 50.00000   1.00000                                                  130213
100.00000   1.00000                                                  130214
  0.00000   1.00000                                                  130301
  1.35000   1.00000                                                  130302
  1.35001   0.21603                                                  130303
  2.35000   0.21603                                                  130304
  2.35001   0.02169                                                  130305
  4.15000   0.02169                                                  130306
  4.15001  -0.10227                                                  130307
  9.80000  -0.10227                                                  130308
  9.80001  -0.06339                                                  130309
 15.33000  -0.06339                                                  130310
 15.33001   1.00000                                                  130311
 25.00000   1.00000                                                  130312
 50.00000   1.00000                                                  130313
100.00000   1.00000                                                  130314
  0.00000   1.00000                                                  130401
  0.10000   1.00000                                                  130402
  0.10001   0.00000                                                  130403
  2.00000   0.00000                                                  130404
  4.00000   0.00000                                                  130405
  6.00000   0.00000                                                  130406
  8.00000   0.00000                                                  130407
 10.00000   0.00000                                                  130408
 12.00000   0.00000                                                  130409
 12.00001  10.00000                                                  130410
 15.00000  10.00000                                                  130411
```

```
15.34000  10.00000
 0.00000   1.00000
 0.10000   1.00000
 0.10001   0.00000
 2.00000   0.00000
 4.00000   0.00000
 6.00000   0.00000
 8.00000   0.00000
10.00000   0.00000
12.00000   0.00000
12.00001  10.00000
20.00000  10.00000
25.99000  10.00000
 0.00000  1.000000
 0.30000  1.000000
 0.30001 -0.255495
 1.00000 -0.255495
 1.00001 -0.018132
 4.50000 -0.018132
 4.50001  0.000000
 6.50000  0.000000
 6.50001  0.018132
10.00000  0.018132
10.00001  0.255495
10.70000  0.255495
10.70001  1.000000
11.00000  1.000000
 0.00000  1.000000
 0.30000  1.000000
 0.30001 -0.255495
 1.00000 -0.255495
 1.00001 -0.018132
 4.50000 -0.018132
```

```
130412
130501
130502
130503
130504
130505
130506
130507
130508
130509
130510
130511
130512
130601
130602
130603
130604
130605
130606
130607
130608
130609
130610
130611
130612
130613
130614
130701
130702
130703
130704
130705
130706
```

```
 4.50001   0.000000                                                  130707
 6.50000   0.000000                                                  130708
 6.50001   0.018132                                                  130709
10.00000   0.018132                                                  130710
10.00001   0.255495                                                  130711
10.70000   0.255495                                                  130712
10.70001   1.000000                                                  130713
11.00000   1.000000                                                  130714
 0.00000   1.000000                                                  130801
 0.30000   1.000000                                                  130802
 0.30001  -0.255495                                                  130803
 1.00000  -0.255495                                                  130804
 1.00001  -0.018132                                                  130805
 4.50000  -0.018132                                                  130806
 4.50001   0.000000                                                  130807
 6.50000   0.000000                                                  130808
 6.50001   0.018132                                                  130809
10.00000   0.018132                                                  130810
10.00001   0.255495                                                  130811
10.70000   0.255495                                                  130812
10.70001   1.000000                                                  130813
11.00000   1.000000                                                  130814
 0.00000   1.000000                                                  130901
 0.30000   1.000000                                                  130902
 0.30001  -0.255495                                                  130903
 1.00000  -0.255495                                                  130904
 1.00001  -0.018132                                                  130905
 4.50000  -0.018132                                                  130906
 4.50001   0.000000                                                  130907
 6.50000   0.000000                                                  130908
 6.50001   0.018132                                                  130909
10.00000   0.018132                                                  130910
10.00001   0.255495                                                  130911
```

10.70000	0.255495	130912
10.70001	1.000000	130913
11.00000	1.000000	130914
0.00000	1.000000	131001
0.30000	1.000000	131002
0.30001	-0.255495	131003
1.00000	-0.255495	131004
1.00001	-0.018132	131005
4.50000	-0.018132	131006
4.50001	0.000000	131007
6.50000	0.000000	131008
6.50001	0.018132	131009
10.00000	0.018132	131010
10.00001	0.255495	131011
10.70000	0.255495	131012
10.70001	1.000000	131013
11.00000	1.000000	131014
0.00000	1.000000	131101
0.30000	1.000000	131102
0.30001	-0.255495	131103
1.00000	-0.255495	131104
1.00001	-0.018132	131105
4.50000	-0.018132	131106
4.50001	0.000000	131107
6.50000	0.000000	131108
6.50001	0.018132	131109
10.00000	0.018132	131110
10.00001	0.255495	131111
10.70000	0.255495	131112
10.70001	1.000000	131113
11.00000	1.000000	131114
0.00000	1.000000	131201
0.30000	1.000000	131202

```
 0.30001 -0.255495                                                131203
 1.00000 -0.255495                                                131204
 1.00001 -0.018132                                                131205
 4.50000 -0.018132                                                131206
 4.50001  0.000000                                                131207
 6.50000  0.000000                                                131208
 6.50001  0.018132                                                131209
10.00000  0.018132                                                131210
10.00001  0.255495                                                131211
10.70000  0.255495                                                131212
10.70001  1.000000                                                131213
11.00000  1.000000                                                131214
 0.00000  1.000000                                                131301
 0.30000  1.000000                                                131302
 0.30001 -0.255495                                                131303
 1.00000 -0.255495                                                131304
 1.00001 -0.018132                                                131305
 4.50000 -0.018132                                                131306
 4.50001  0.000000                                                131307
 6.50000  0.000000                                                131308
 6.50001  0.018132                                                131309
10.00000  0.018132                                                131310
10.00001  0.255495                                                131311
10.70000  0.255495                                                131312
10.70001  1.000000                                                131313
11 00000  1.000000                                                131314
 0.00000  1.000000                                                131401
 0.30000  1.000000                                                131402
 0.30001 -0.255495                                                131403
 1.00000 -0.255495                                                131404
 1.00001 -0.018132                                                131405
 4.50000 -0.018132                                                131406
 4.50001  0.000000                                                131407
```

```
 6.50000  0.000000                                                131408
 6.50001  0.018132                                                131409
10.00000  0.018132                                                131410
10.00001  0.255495                                                131411
10.70000  0.255495                                                131412
10.70001  1.000000                                                131413
11.00000  1.000000                                                131414
 0.00000  1.000000                                                131501
 0.30000  1.000000                                                131502
 0.30001 -0.255495                                                131503
 1.00000 -0.255495                                                131504
 1.00001 -0.018132                                                131505
 4.50000 -0.018132                                                131506
 4.50001  0.000000                                                131507
 6.50000  0.000000                                                131508
 6.50001  0.018132                                                131509
10.00000  0.018132                                                131510
10.00001  0.255495                                                131511
10.70000  0.255495                                                131512
10.70001  1.000000                                                131513
11.00000  1.000000                                                131514
 0.00000  1.000000                                                131601
 0.30000  1.000000                                                131602
 0.30001 -0.255495                                                131603
 1.00000 -0.255495                                                131604
 1.00001 -0.018132                                                131605
 4.50000 -0.018132                                                131606
 4 50001  0.000000                                                131607
 6.50000  0.000000                                                131608
 6.50001  0.018132                                                131609
10.00000  0.018132                                                131610
10.00001  0.255495                                                131611
10.70000  0.255495                                                131612
```

```
 10.70001   1.000000                                                131613
 11.00000   1.000000                                                131614
  0.00000   1.000000                                                131701
  0.30000   1.000000                                                131702
  0.30001  -0.255495                                                131703
  1.00000  -0.255495                                                131704
  1.00001  -0.018132                                                131705
  4.50000  -0.018132                                                131706
  4.50001   0.000000                                                131707
  6.50000   0.000000                                                131708
  6.50001   0.018132                                                131709
 10.00000   0.018132                                                131710
 10.00001   0.255495                                                131711
 10.70000   0.255495                                                131712
 10.70001   1.000000                                                131713
 11.00000   1.000000                                                131714
  0.00000   1.000000                                                131801
  0.30000   1.000000                                                131802
  0.30001  -0.255495                                                131803
  1.00000  -0.255495                                                131804
  1.00001  -0.018132                                                131805
  4.50000  -0.018132                                                131806
  4.50001   0.000000                                                131807
  6.50000   0.000000                                                131808
  6.50001   0.018132                                                131809
 10.00000   0.018132                                                131810
 10.00001   0.255495                                                131811
 10 70000   0.255495                                                131812
 10.70001   1.000000                                                131813
 11.00000   1.000000                                                131814
  0.00000   1.000000                                                131901
  0.30000   1.000000                                                131902
  0.30001  -0.255495                                                131903
```

```
 1.00000 -0.255495
 1.00001 -0.018132
 4.50000 -0.018132
 4.50001  0.000000
 6.50000  0.000000
 6.50001  0.018132
10.00000  0.018132
10.00001  0.255495
10.70000  0.255495
10.70001  1.000000
11.00000  1.000000
 0.00000  1.000000
 0.30000  1.000000
 0.30001 -0.255495
 1.00000 -0.255495
 1.00001 -0.018132
 4.50000 -0.018132
 4.50001  0.000000
 6.50000  0.000000
 6.50001  0.018132
10.00000  0.018132
10.00001  0.255495
10.70000  0.255495
10.70001  1.000000
11.00000  1.000000
 0.00000  1.000000
 0.30000  1.000000
 0.30001 -0.255495
 1.00000 -0.255495
 1.00001 -0.018132
 4.50000 -0.018132
 4.50001  0.000000
 6.50000  0.000000
```

```
131904
131905
131906
131907
131908
131909
131910
131911
131912
131913
131914
132001
132002
132003
132004
132005
132006
132007
132008
132009
132010
132011
132012
132013
132014
132101
132102
132103
132104
132105
132106
132107
132108
```

```
  6.50001  0.018132                                                                  132109
 10.00000  0.018132                                                                  132110
 10.00001  0.255495                                                                  132111
 10.70000  0.255495                                                                  132112
 10.70001  1.000000                                                                  132113
 11.00000  1.000000                                                                  132114
   33   35   36   38                                                                   1700
0  1 0  2   10.0E10   10.0E10   10.0E10   10.0E10 1001875.0   10.0E10                 1801
3  3 1 26   92586.0   10.0E10   10.0E10   10.0E10   10.0E10   10.0E10                 1803
0 29 1 31  138750.0   10.0E10   10.0E10   10.0E10   10.0E10   10.0E10                 1805
0 30 1 32  138750.0   10.0E10   10.0E10   10.0E10   10.0E10   10.0E10                 1807
0  1 0  2   10.0E10   10.0E10   10.0E10   10.0E10 1001875.0   10.0E10                 1901
3  3 1 26   92586.0   10.0E10   10.0E10   10.0E10   10.0E10   10.0E10                 1903
0 29 1 31  138750.0   10.0E10   10.0E10   10.0E10   10.0E10   10.0E10                 1905
0 30 1 32  138750.0   10.0E10   10.0E10   10.0E10   10.0E10   10.0E10                 1907
END
```

APPENDIX E

UNFILTERED AND 20 HZ FILTERED KRASH ANALYSIS TIME HISTORIES

Mass Point/ Beam Element	Description	Location	Direction	Page
Mass point accelerations				
1	Nose gun turret	FS 120.50	Vertical	229
3	Copilot/gunner bulkhead	FS 193.50	Vertical	230
5	Pilot bulkhead	FS 248.50	Vertical	231
7	Aircraft cg	FS 306.50	Vertical	232
7	Aircraft cg	FS 306.50	Longitudinal	233
9	Tailboom junction bulkhead	FS 409.00	Vertical	234
11	Tail rotor gearbox	FS 647.75	Vertical	235
14	Right outboard wing tip	FS 293.41	Vertical	236
15	Left outboard wing tip	FS 293.41	Vertical	237
16	Main rotor hub	FS 300.00	Longitudinal	238
18	Transmission cg	FS 300.00	Vertical	239
18	Transmission cg	FS 300.00	Longitudinal	240
33	Copilot/gunner seat pan and pelvis	FS 193.50	Vertical	241
34	Copilot/gunner chest	FS 193.50	Vertical	242
36	Pilot seat pan and pelvis	FS 248.50	Vertical	243
37	Pilot chest	FS 248.50	Vertical	244
Beam element deflections				
46 (3, 3-26, 1)	Nose gear shock strut	FS 178.59	Axial	245
46 (3, 3-26, 1)	Nose gear shock strut	FS 178.59	Pitch	246
51 (29, 0-31, 1)	Right main gear shock strut	FS 317.77	Axial	247
54 (30, 0-32, 1)	Left main gear shock strut	FS 317.77	Axial	248
55 (3, 0-33, 0)	Copilot/gunner seat	FS 193.50	Axial	249
58 (5, 0-36, 0)	Pilot seat	FS 248.50	Axial	250
Beam element loads				
17 (18, 1-19, 1)	Right forward transmission lift link	FS 277.68	Axial	251
18 (18, 2-20, 1)	Left forward transmission lift link	FS 277.68	Axial	252
19 (18, 3-21, 1)	Right aft transmission lift link	FS 322.32	Axial	253
20 (18, 4-22, 1)	Left aft transmission lift link	FS 322.32	Axial	254

Mass Point/ Beam Element	Description	Location	Direction	Page
31 (7,12-18, 8)	Left transmission crash link (compression)	FS 306.50	Axial	255
47 (12, 1-29, 2)	Right main gear drag link	FS 299.36	Axial	256
48 (13, 1-30, 2)	Left main gear drag link	FS 299.36	Axial	257

Nose gun turret vertical acceleration (mass point 1)

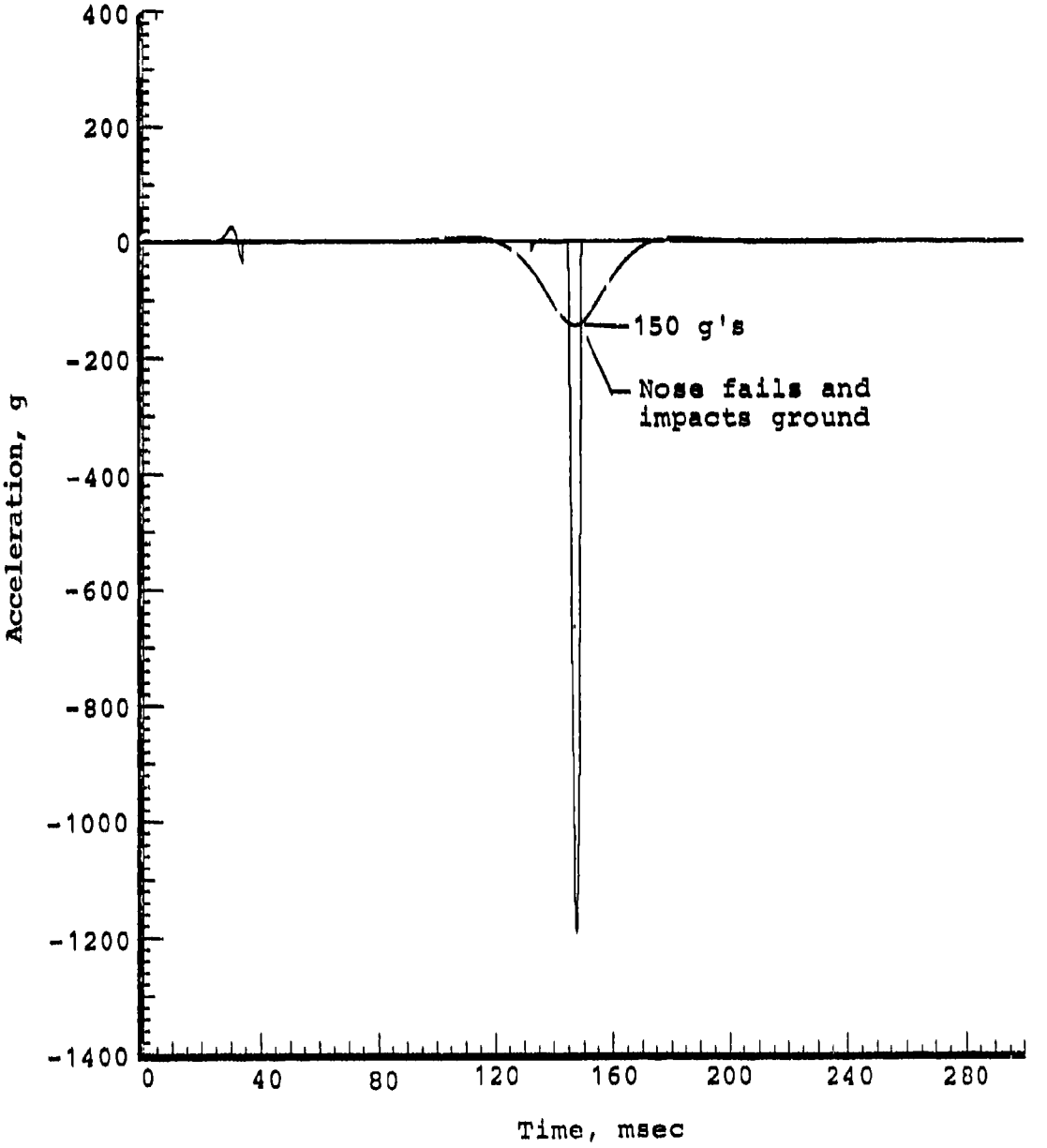

Copilot/gunner bulkhead vertical acceleration

(mass point 3)

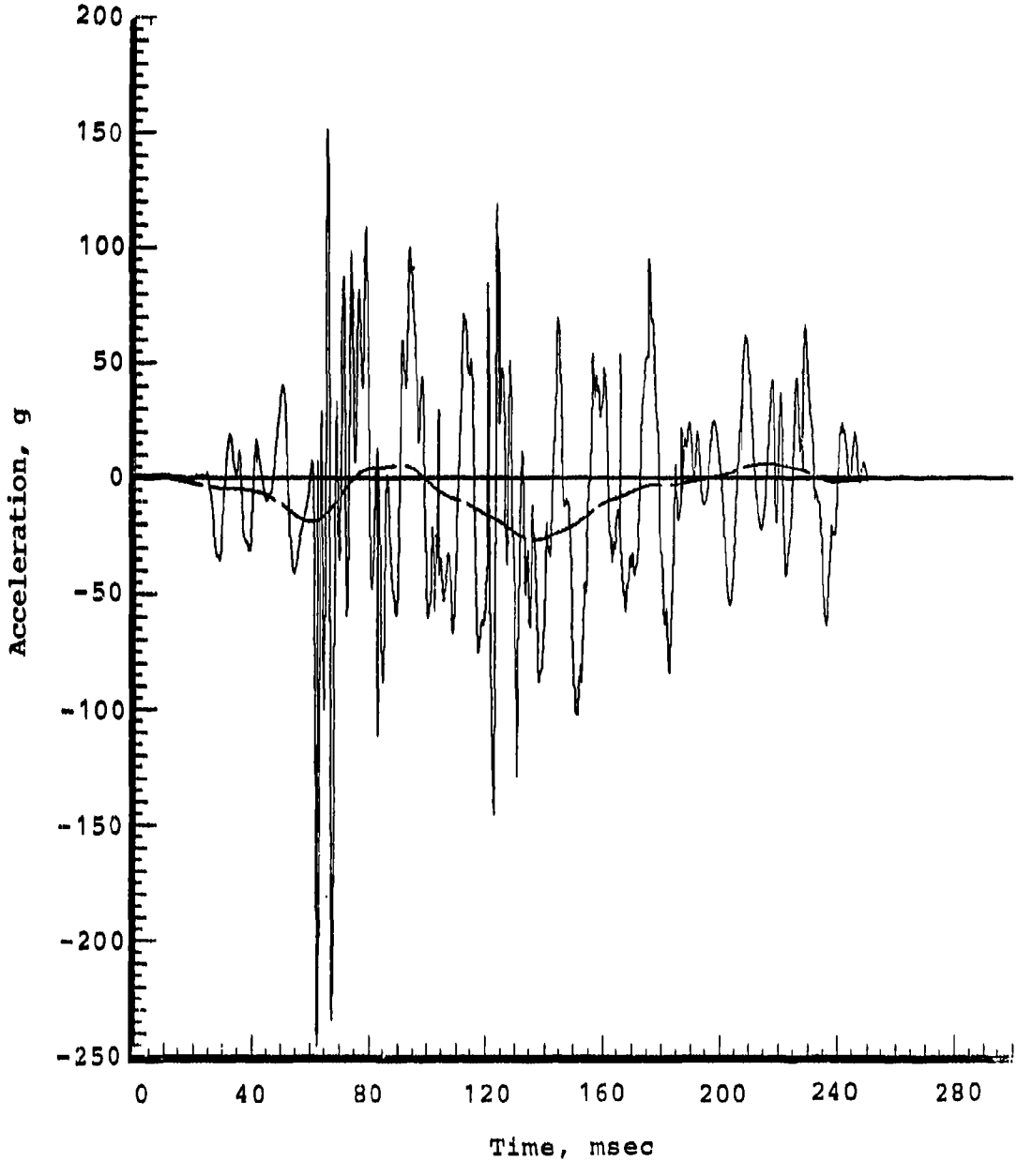

Pilot bulkhead vertical acceleration (mass point 5)

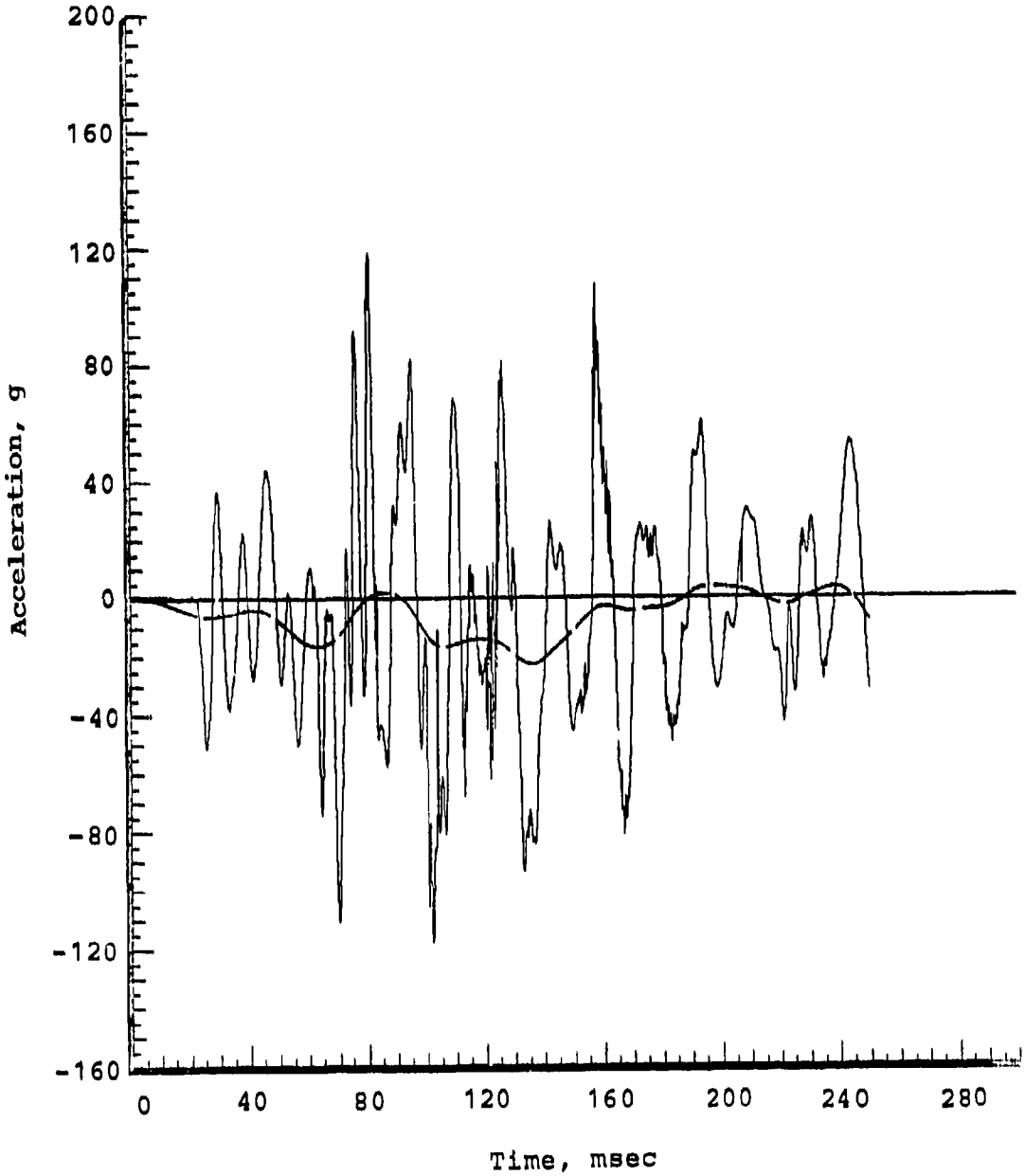

Aircraft cg vertical acceleration (mass point 7)

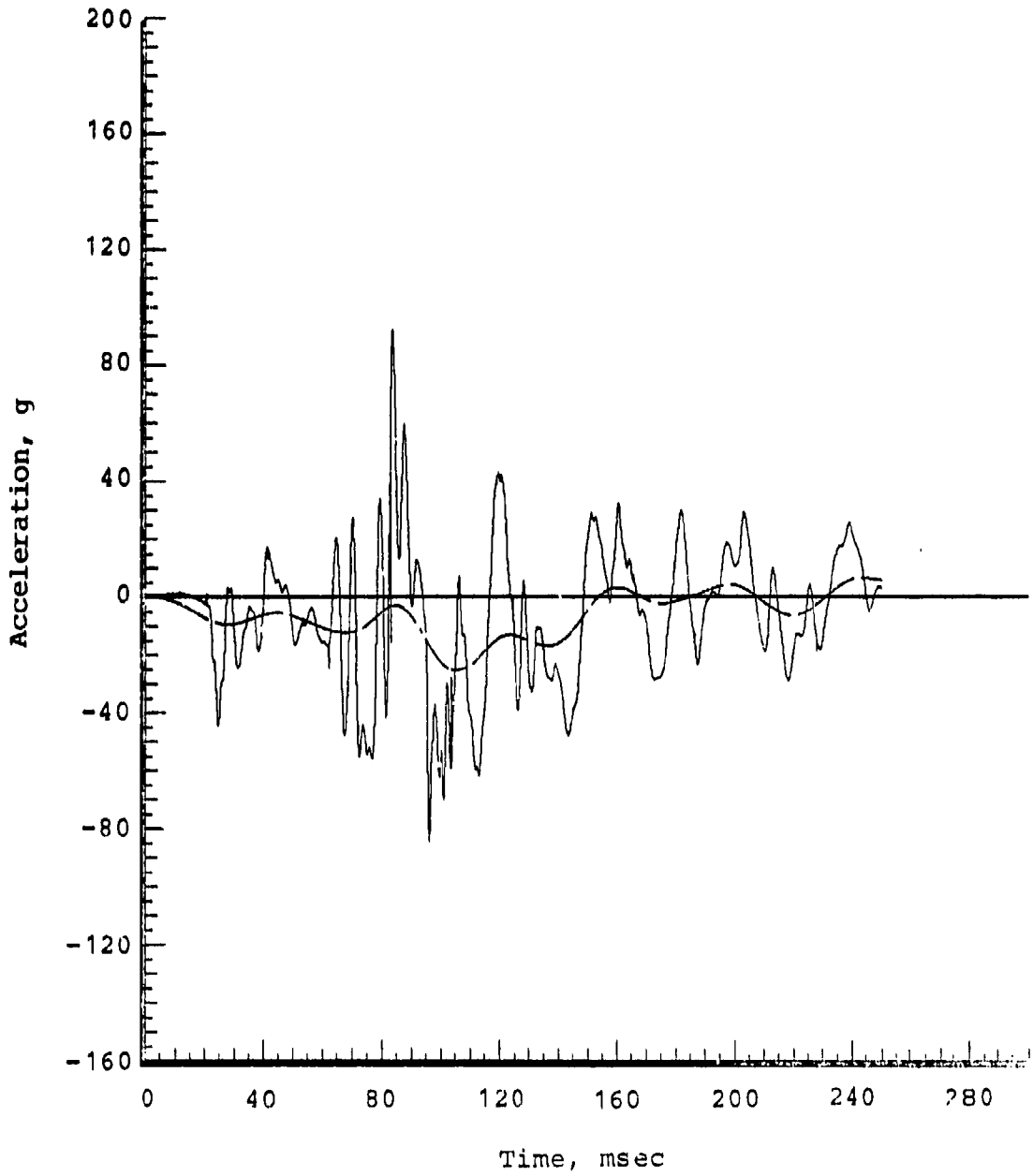

Aircraft cg longitudinal acceleration (mass point 7)

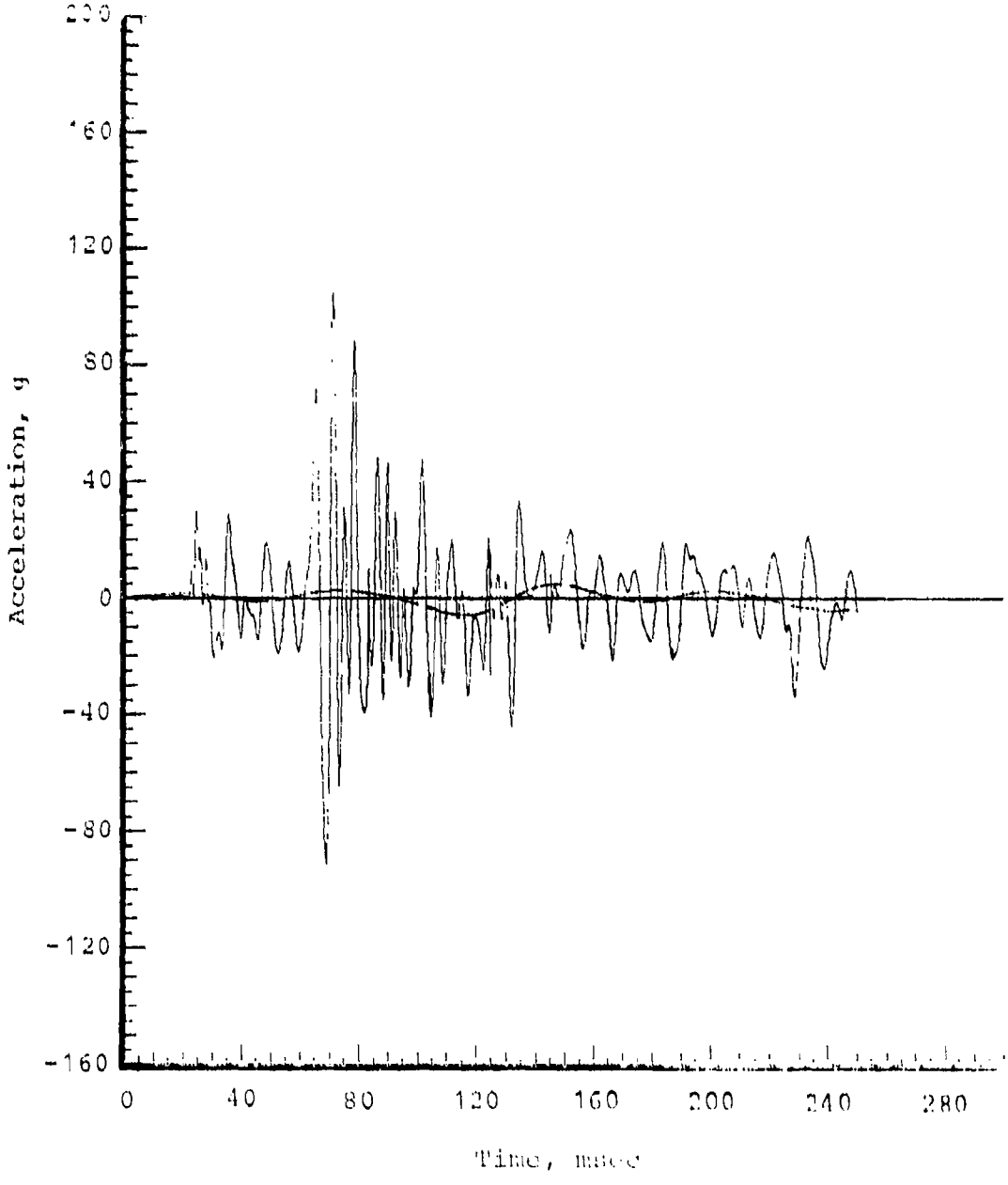

Tailboom junction bulkhead vertical acceleration

(mass point 9)

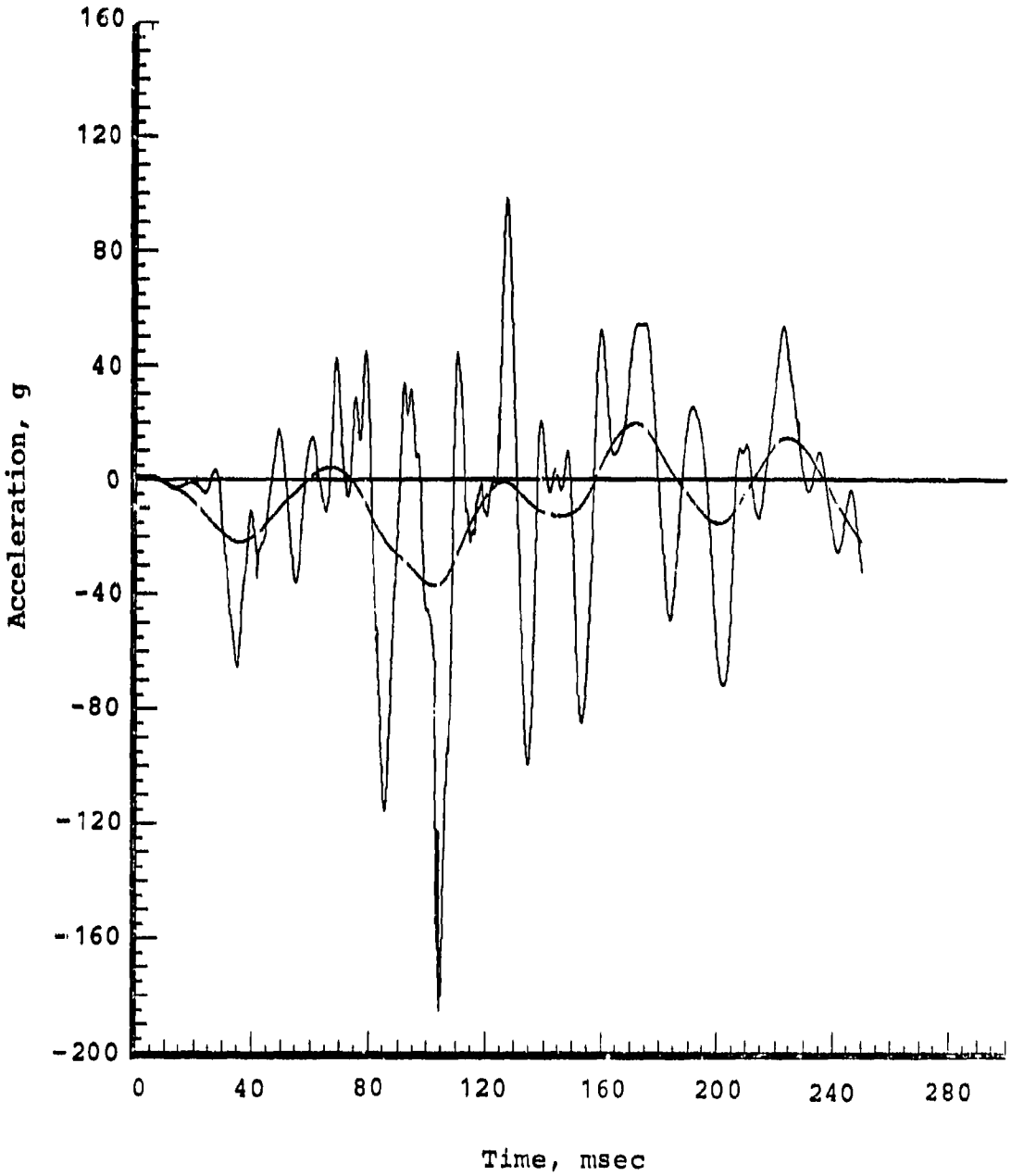

Tail rotor gearbox vertical acceleration (mass point 11)

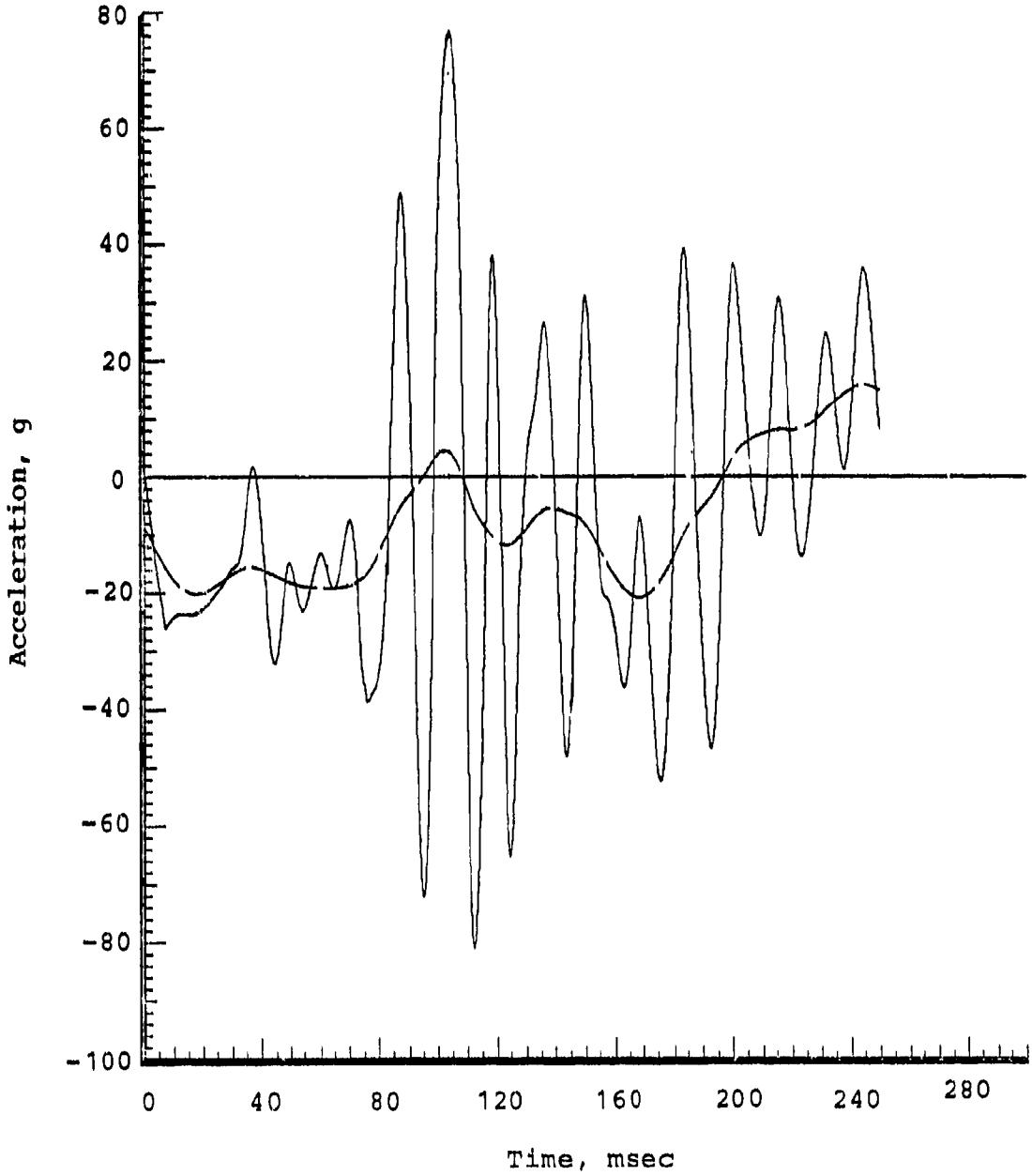

Right wing tip vertical acceleration (mass point 14)

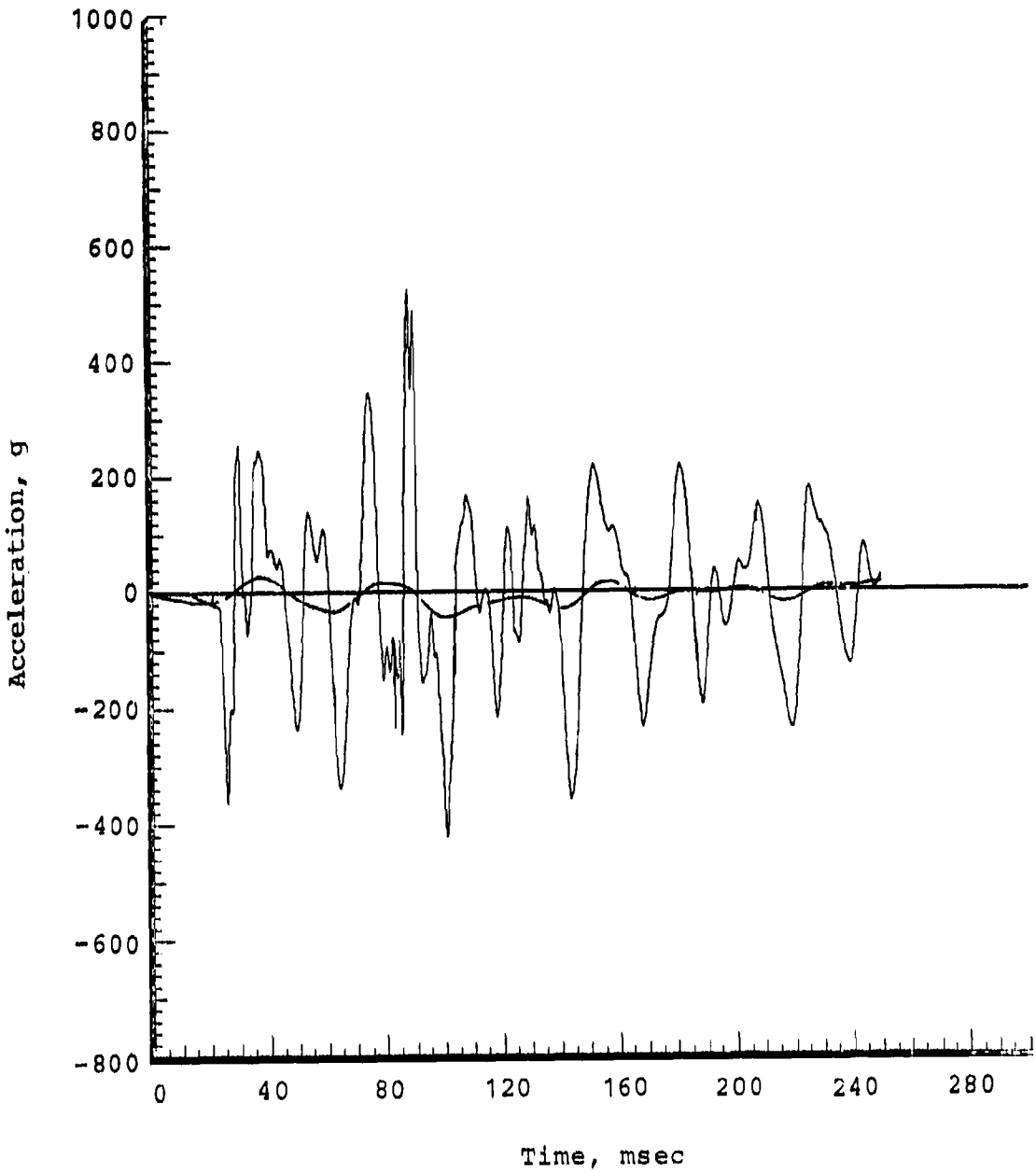

Left wing tip vertical acceleration (mass point 15)

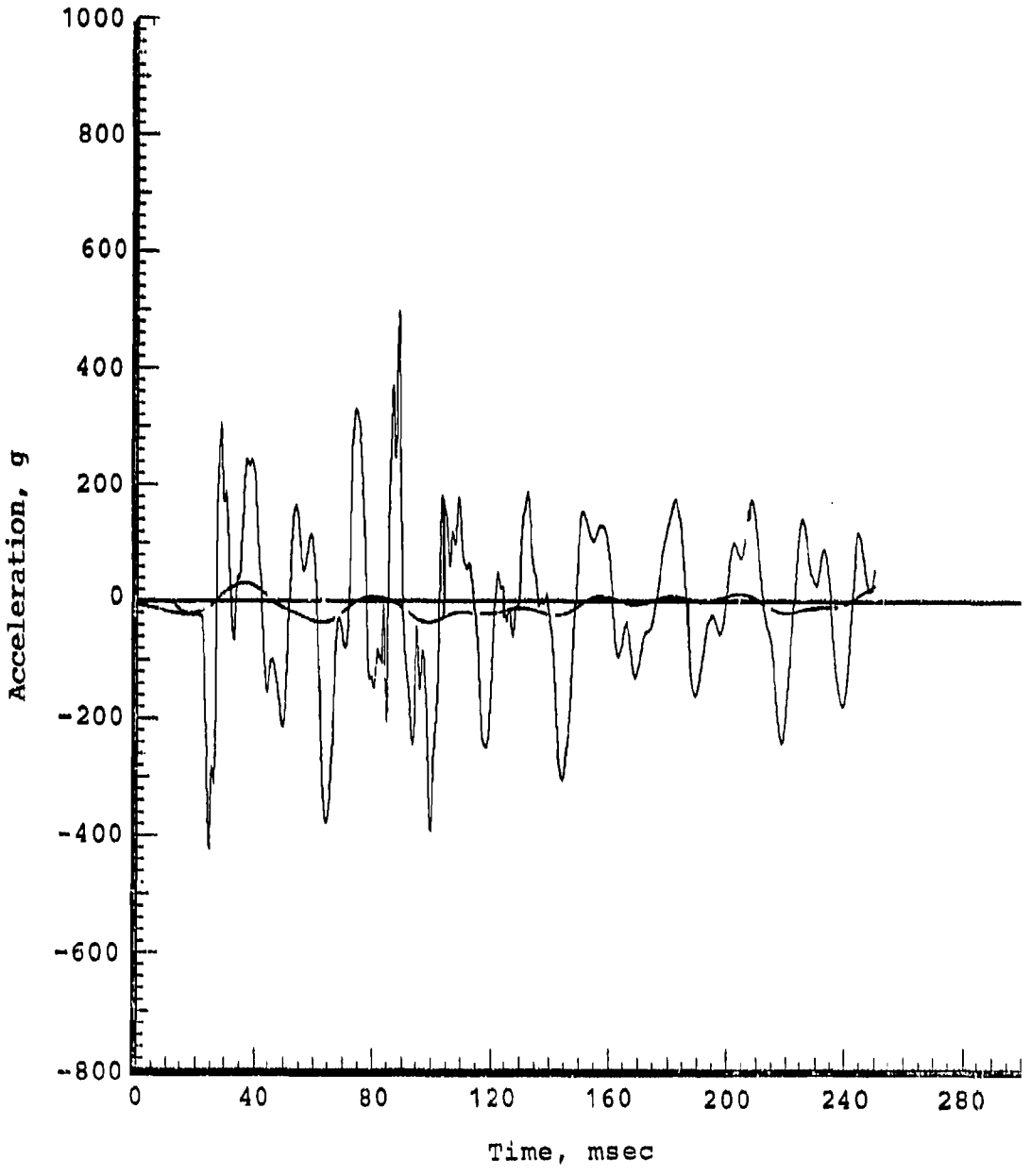

Main rotor hub longitudinal acceleration (mass point 16)

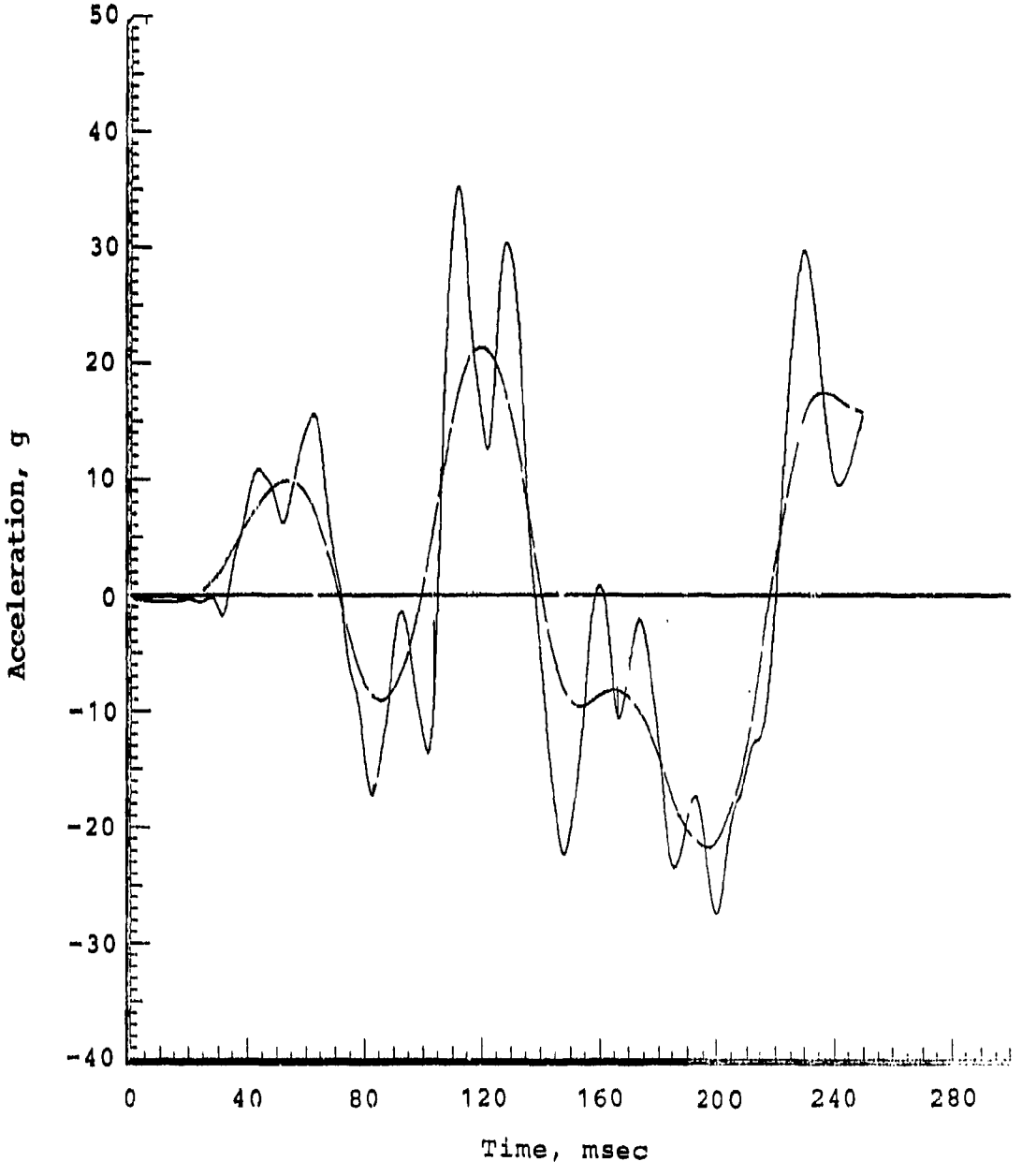

Transmission cg vertical acceleration (mass point 18)

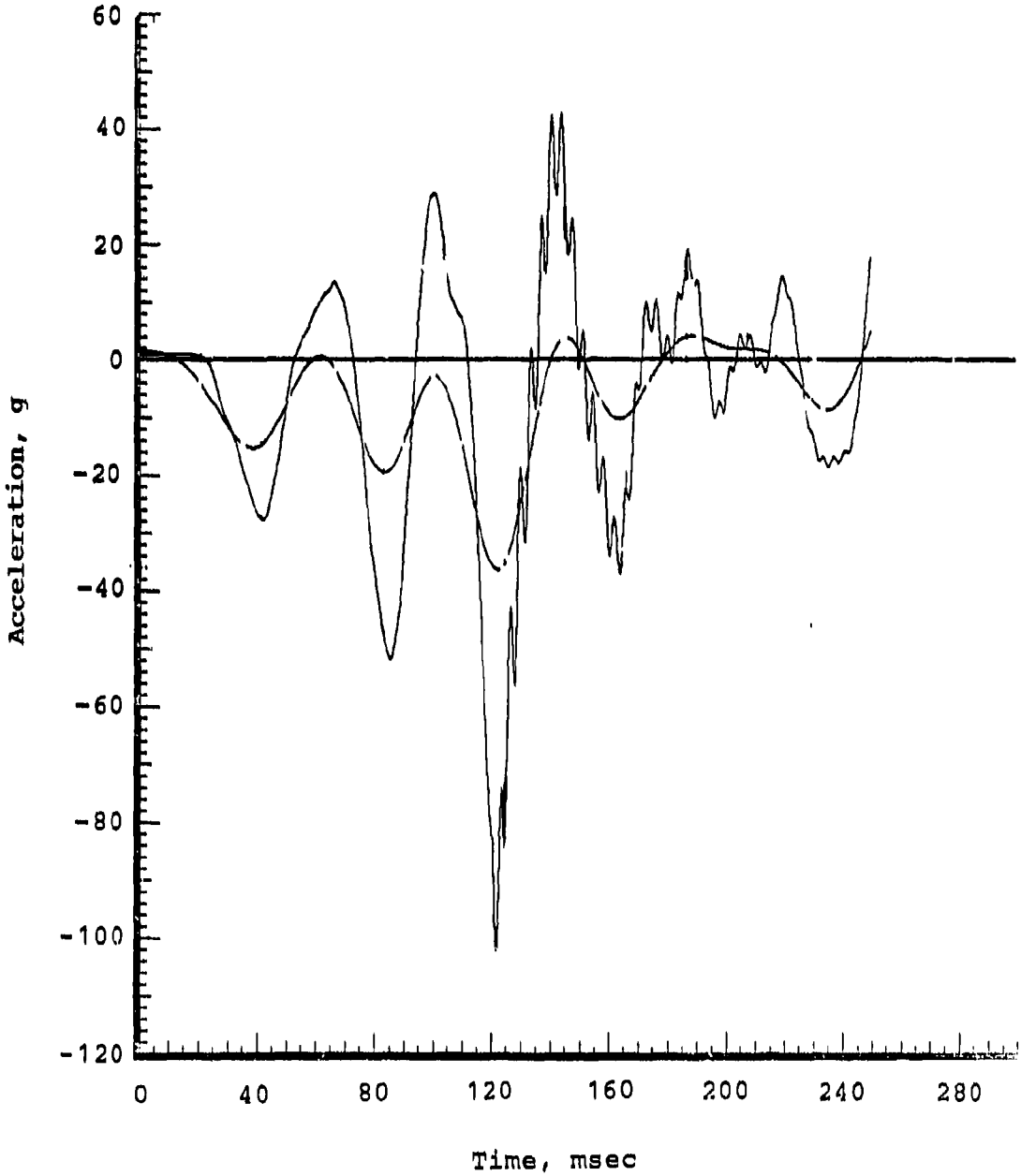

Transmission cg longitudinal acceleration (mass point 18)

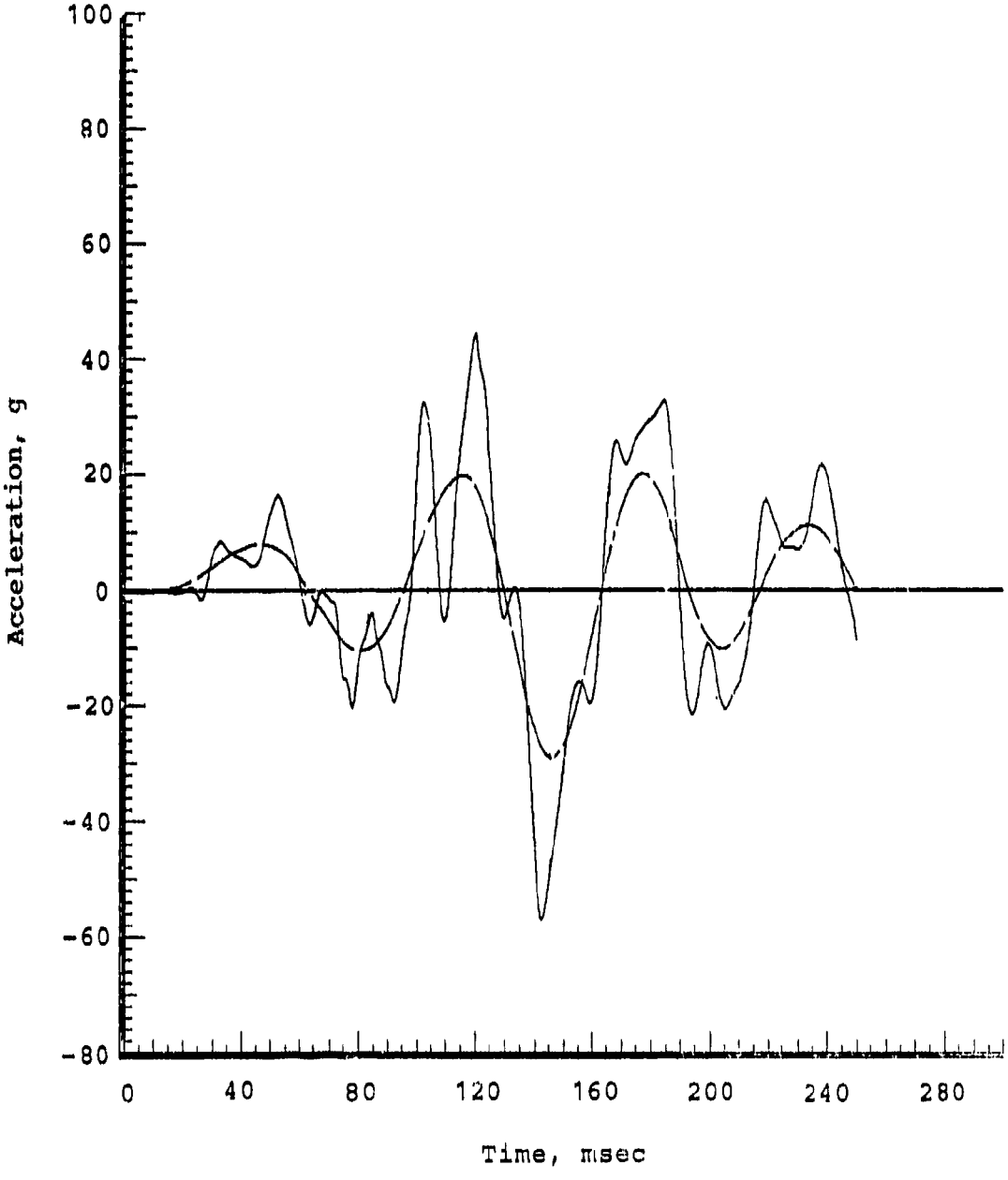

Copilot/gunner seat pan and pelvis vertical acceleration

(mass point 33)

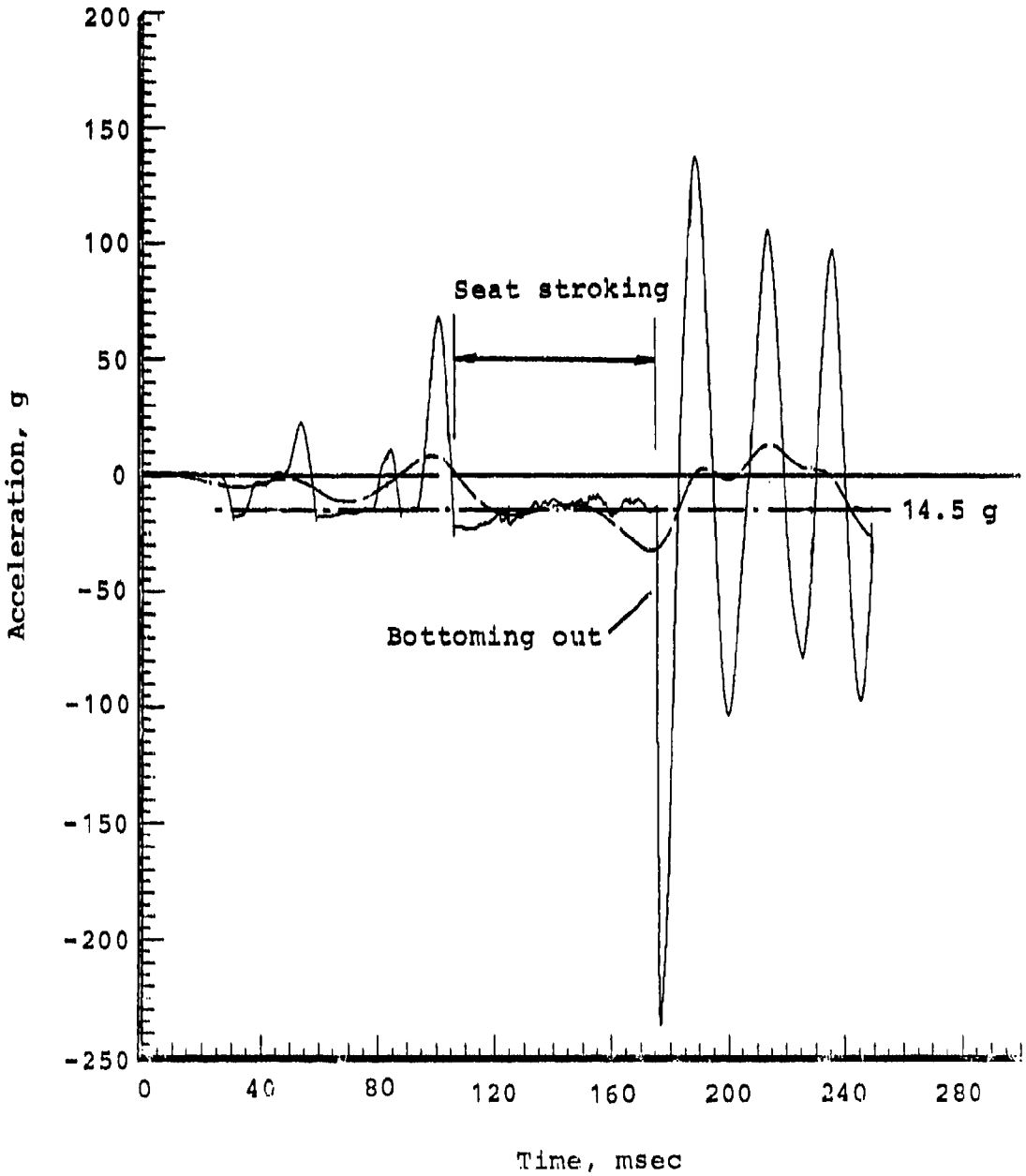

Copilot/gunner chest vertical acceleration (mass point 34)

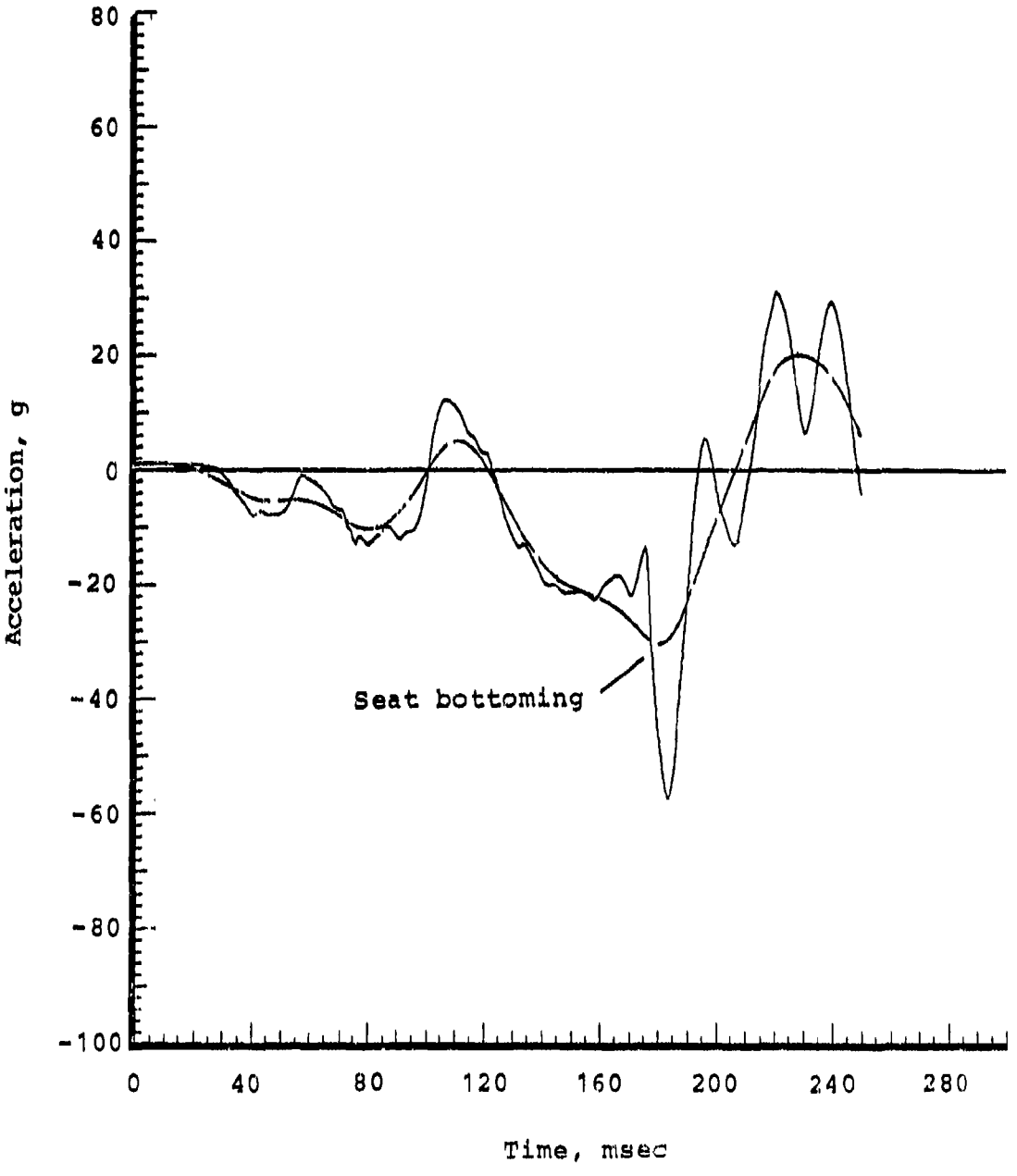

Pilot seat pan and pelvis vertical acceleration

(mass point 36)

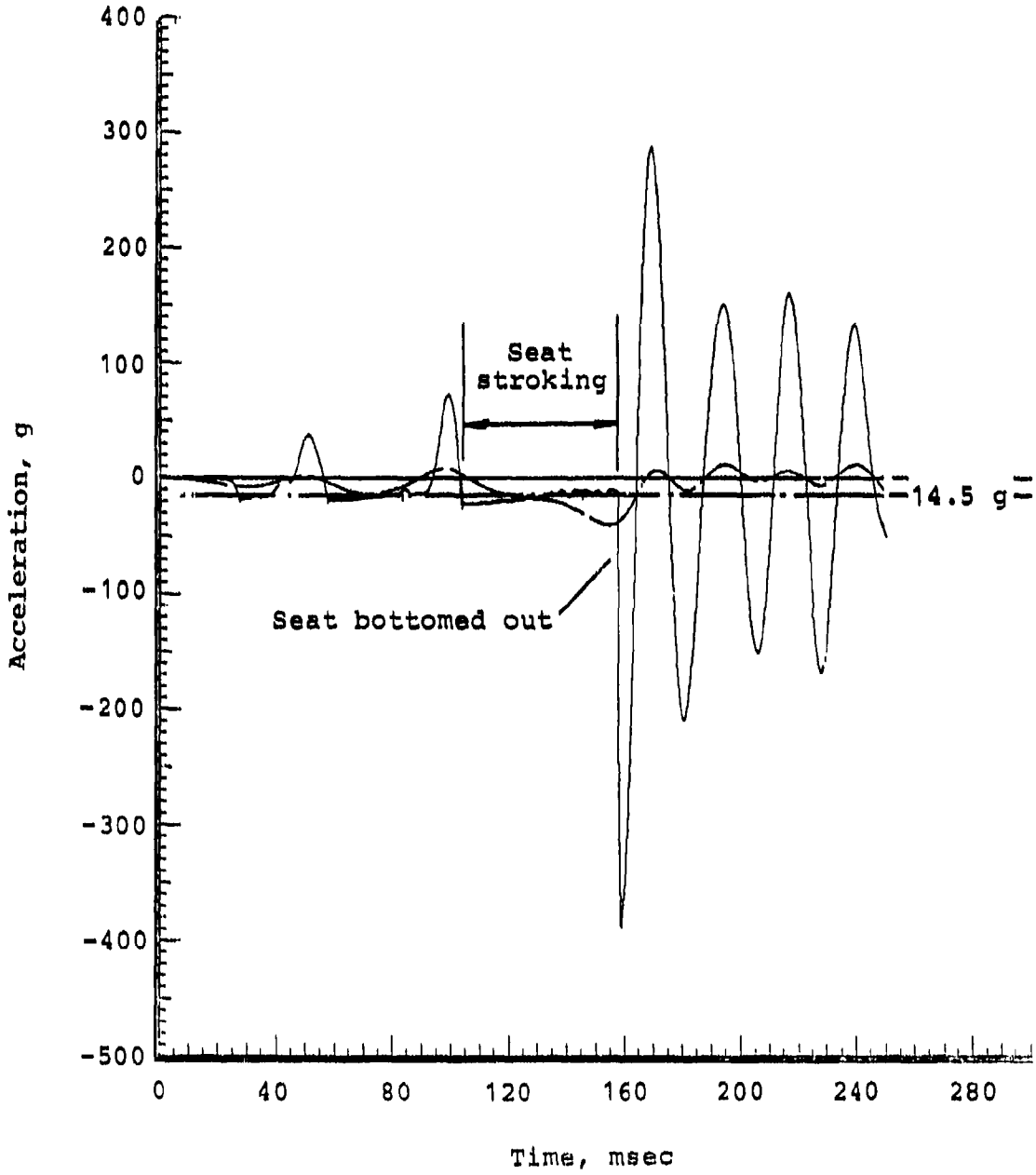

Pilot chest vertical acceleration (mass point 37)

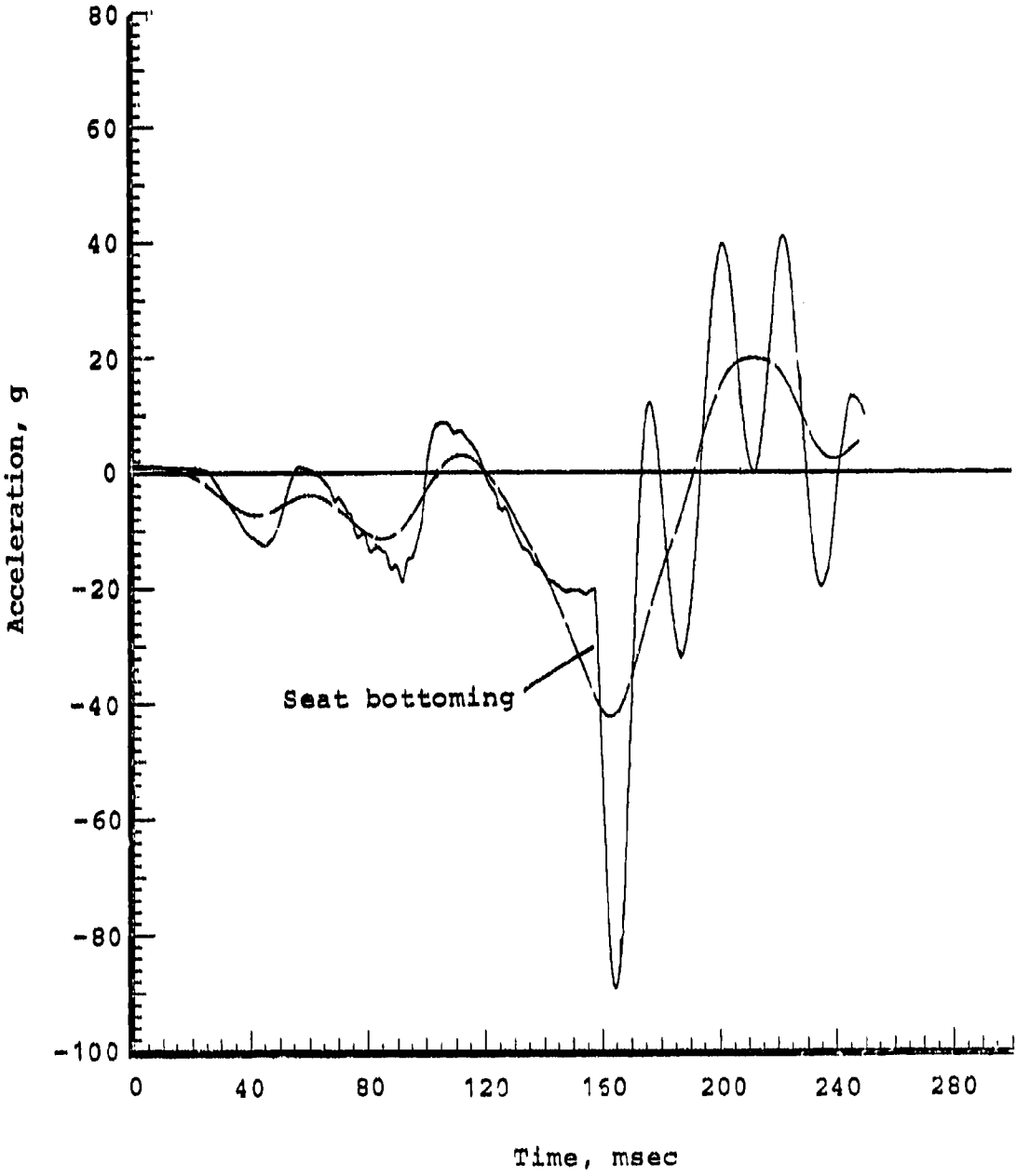

Nose landing gear shock strut axial deflection (beam 46)

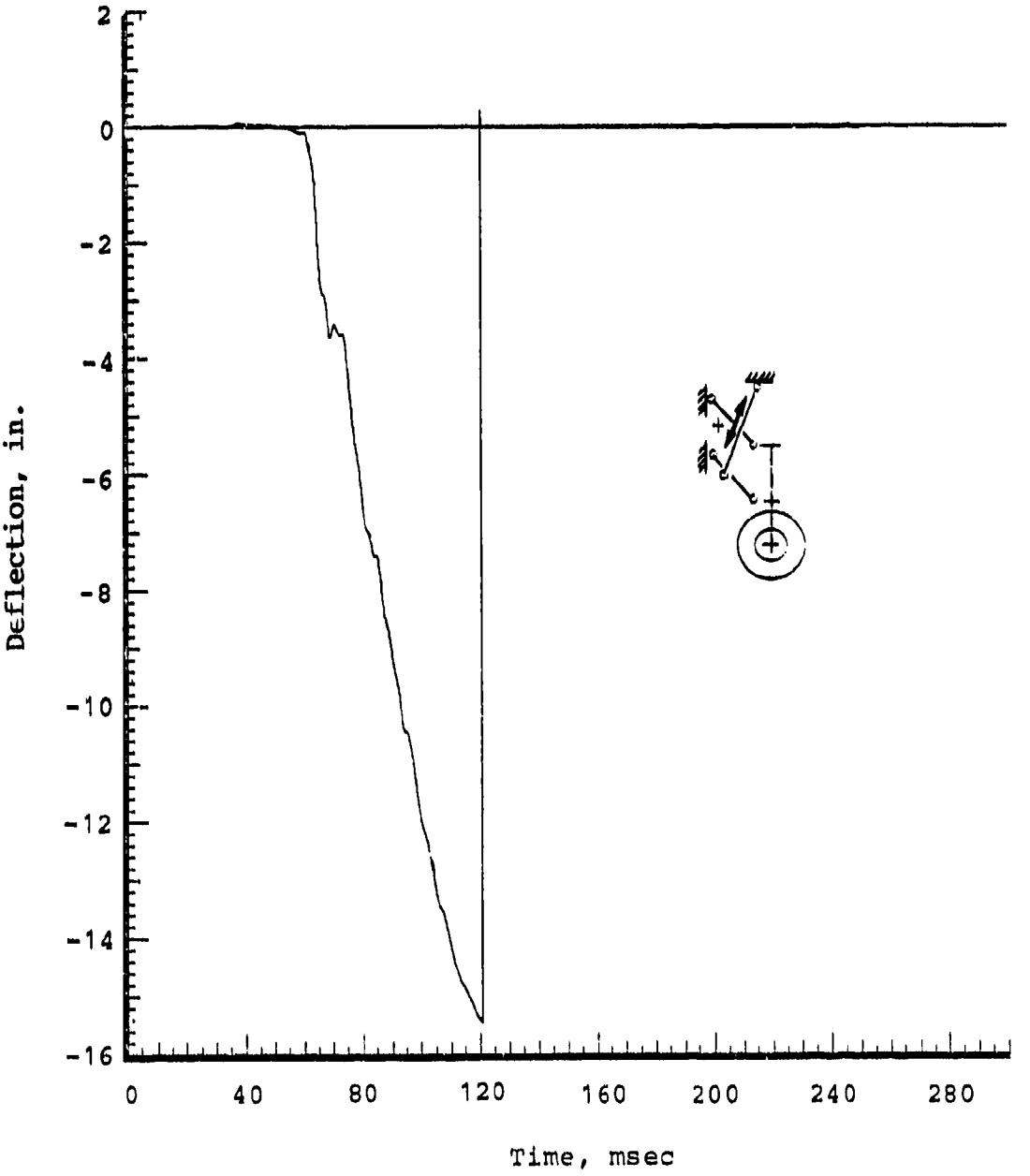

Nose landing gear shock strut pitch rotation (beam 46)

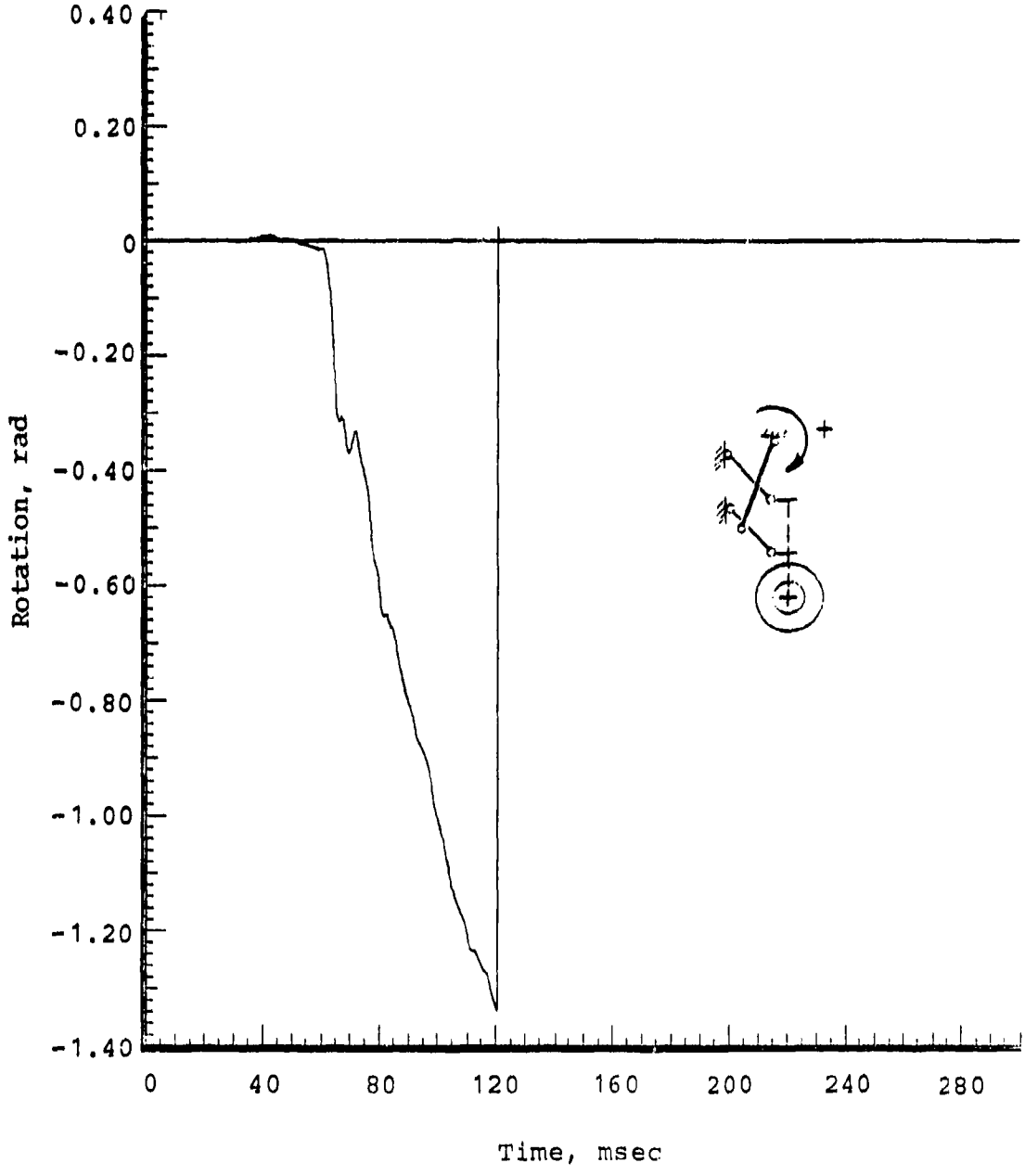

Right main landing gear shock strut axial deflection

(beam 51)

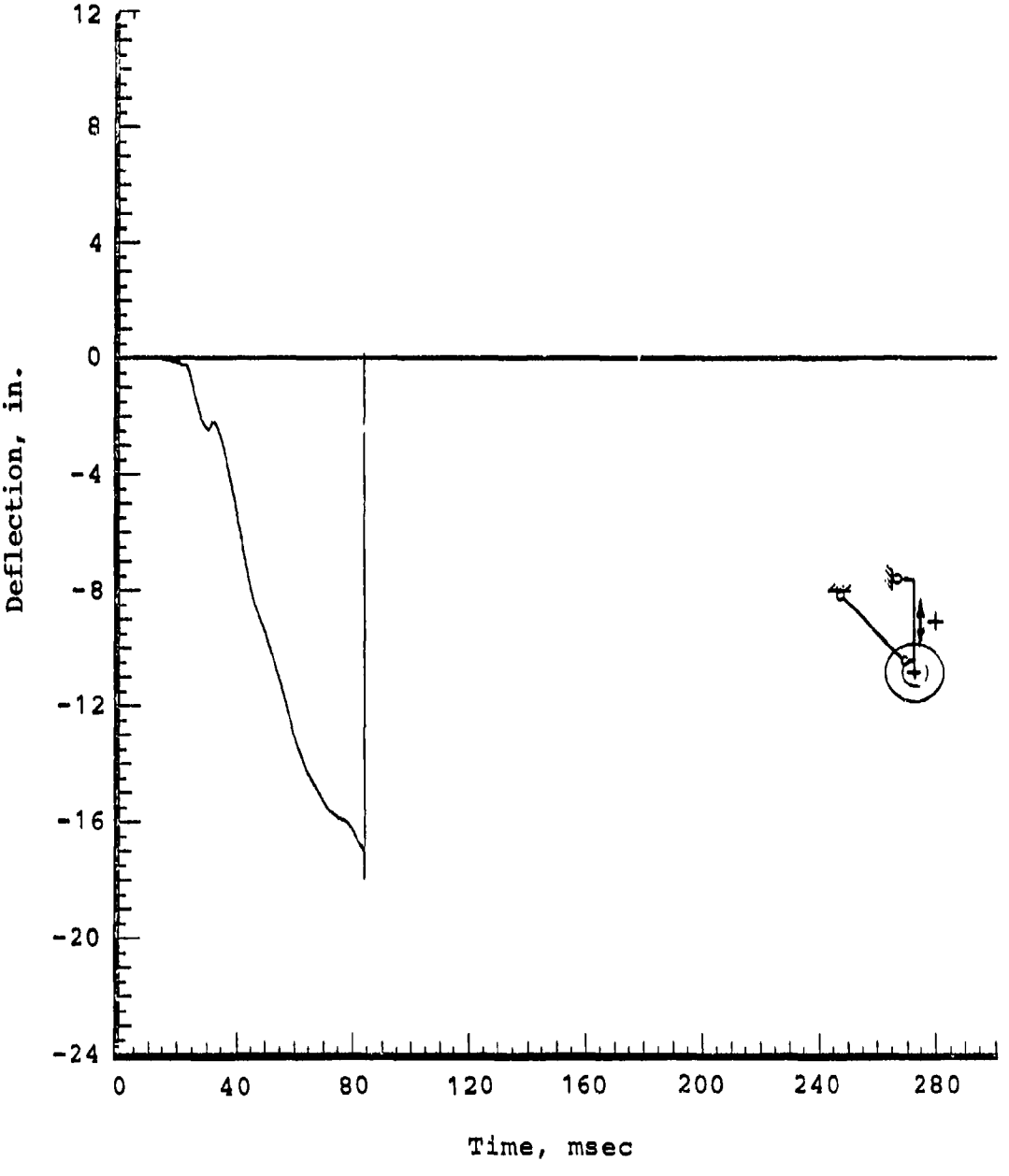

Left main landing gear shock strut axial deflection

(beam 54)

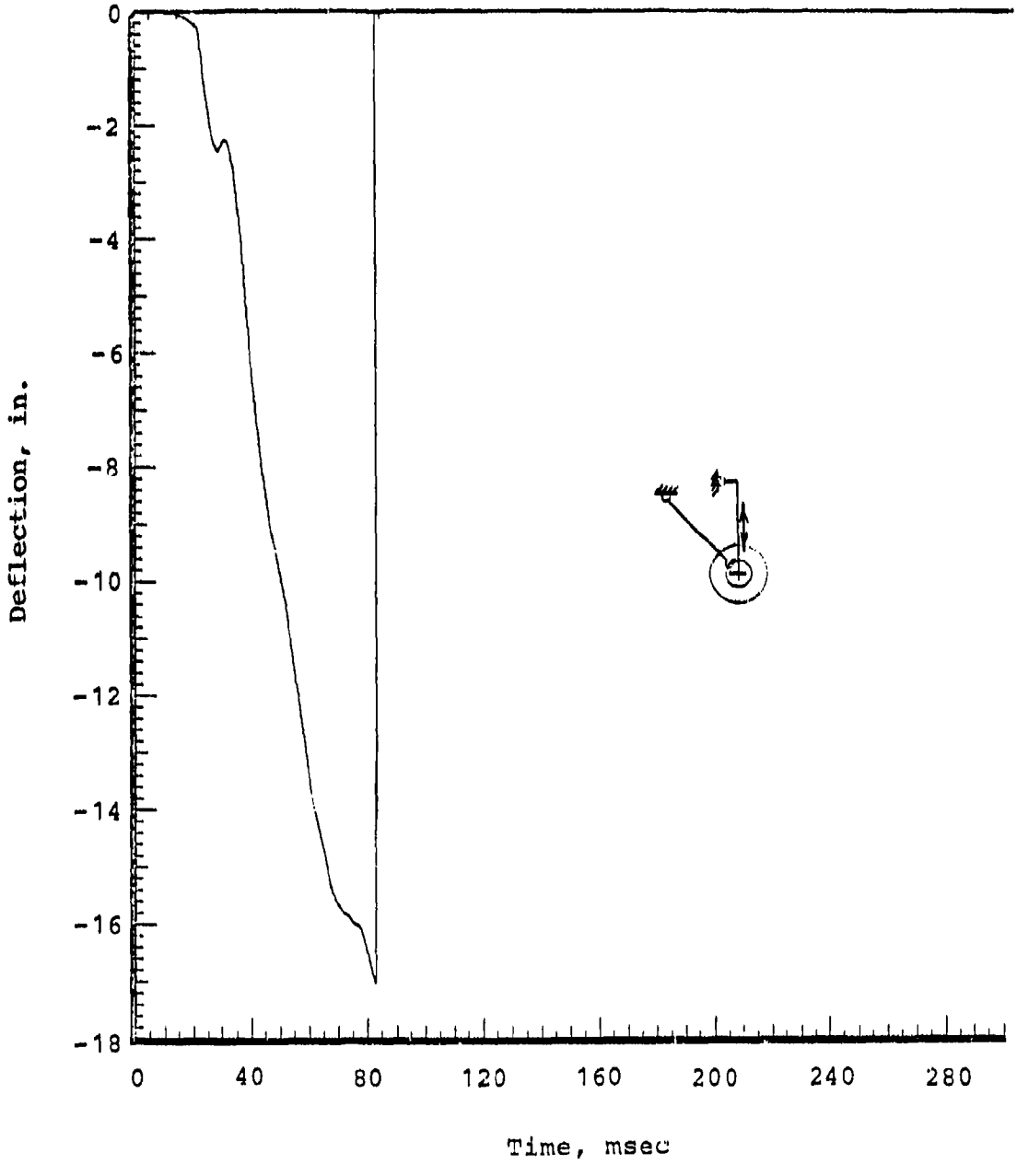

Copilot/gunner seat attenuator stroke (beam 55)

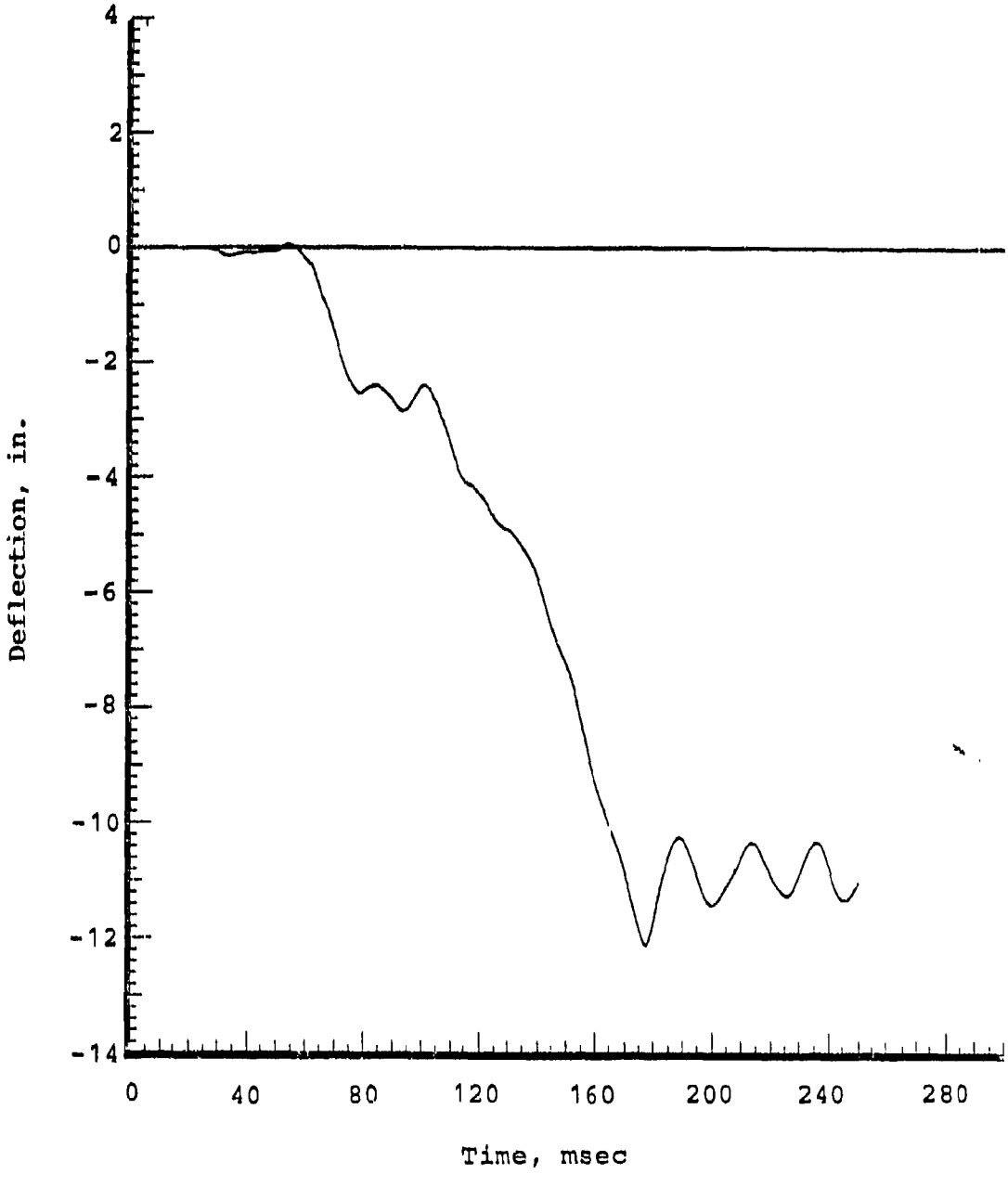

Pilot seat attenuator stroke (beam 58)

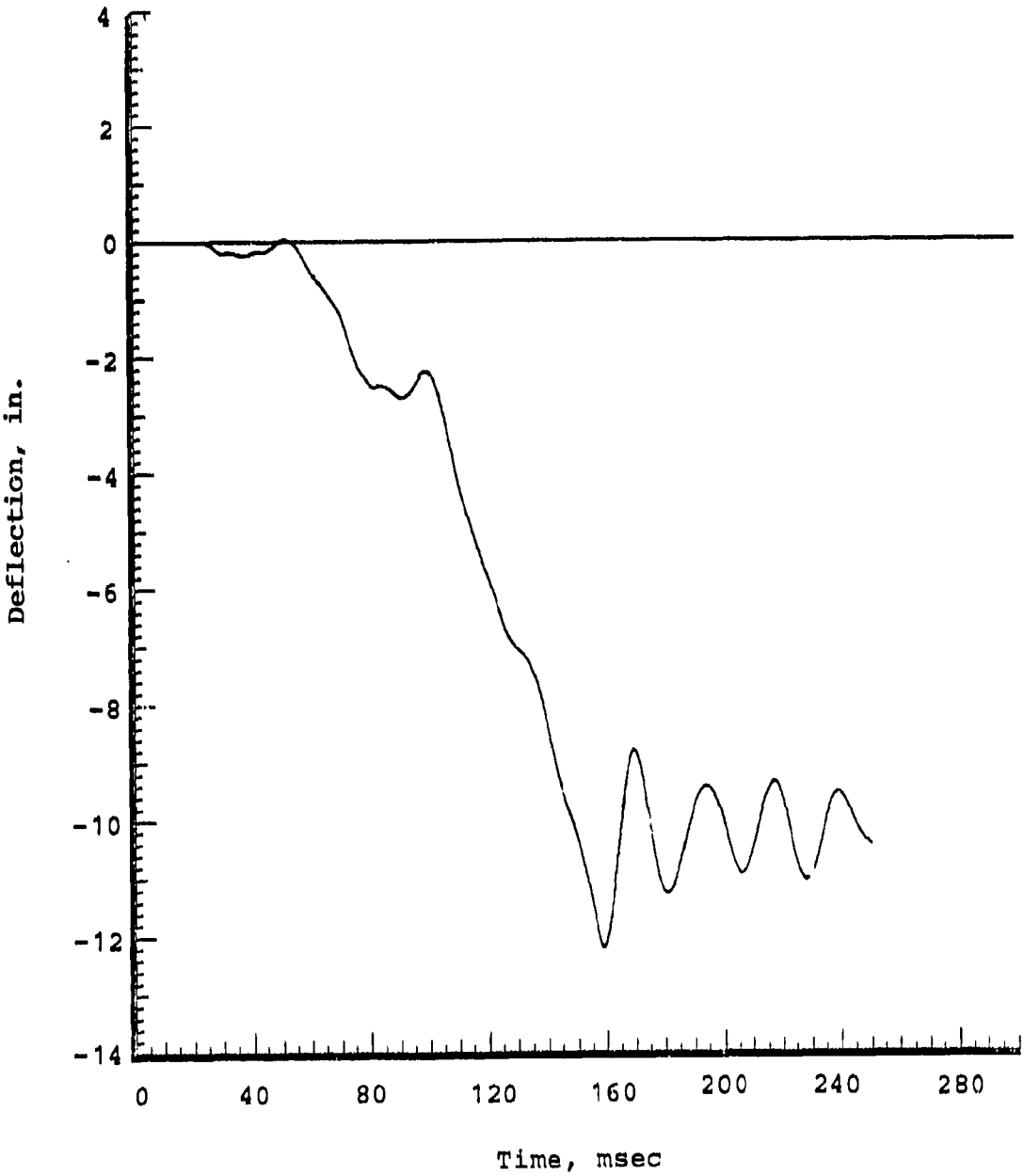

Right forward transmission lift link axial load (beam 17)

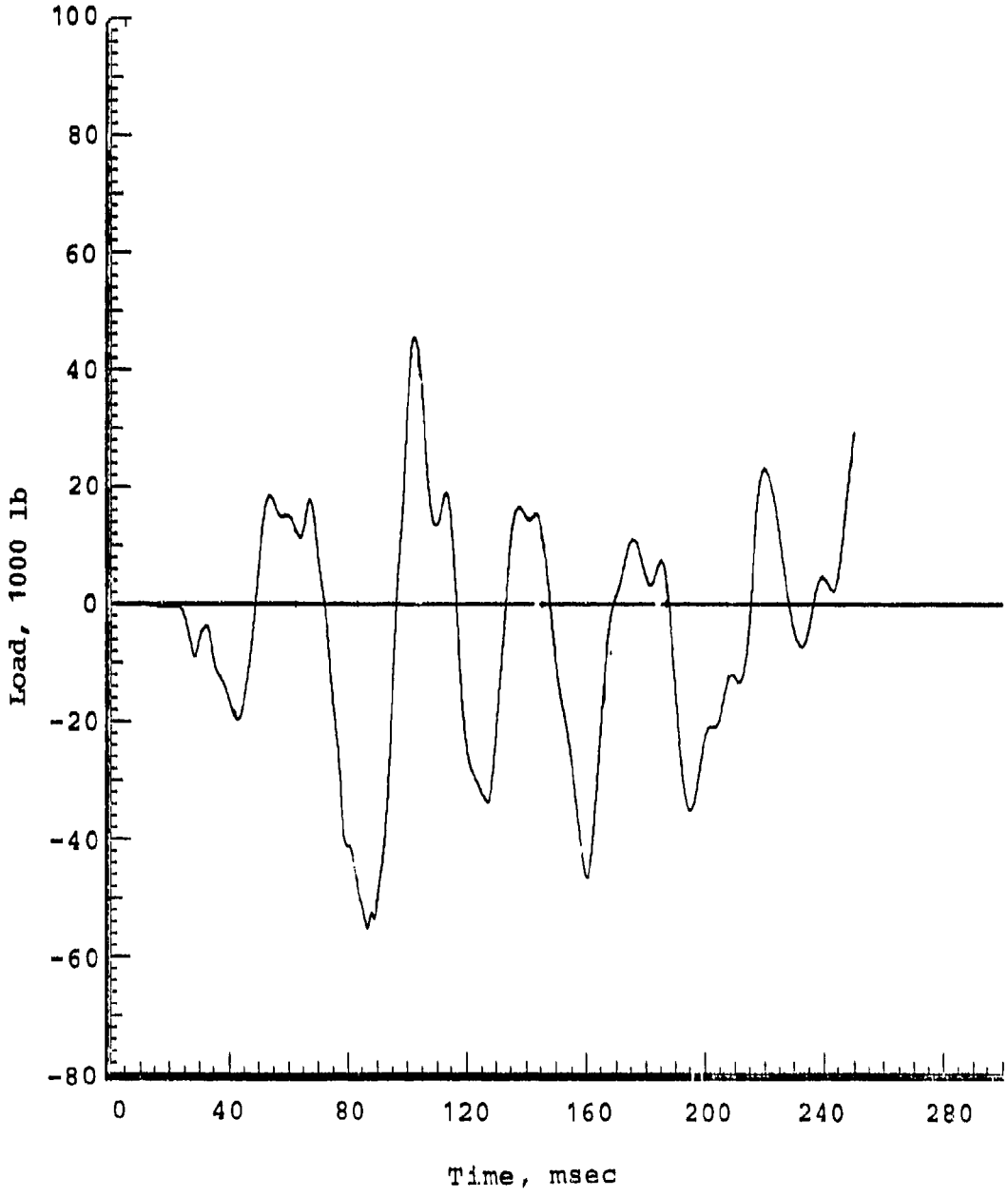

Left forward transmission lift link axial load (beam 18)

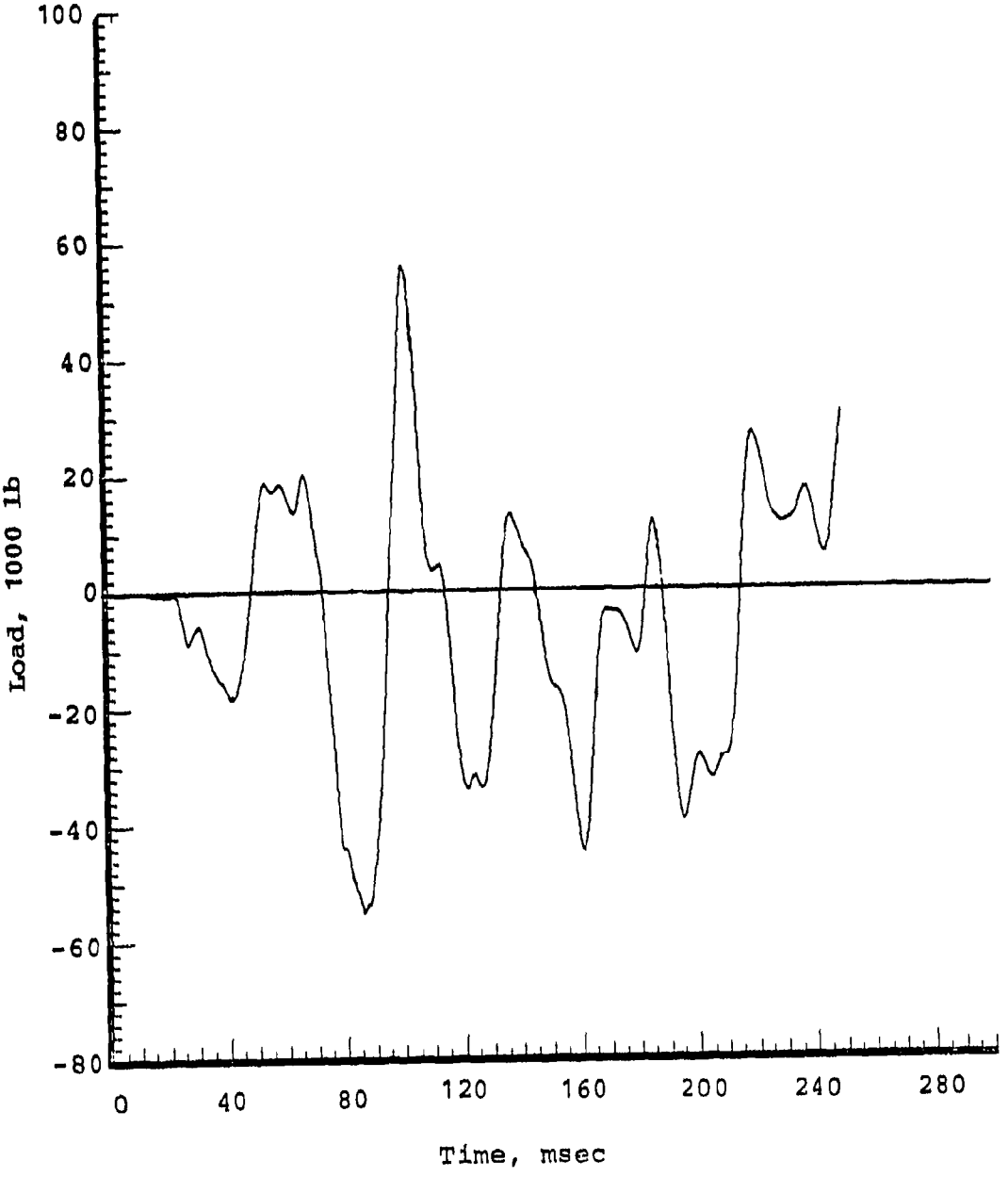

Right aft transmission lift link axial load (beam 19)

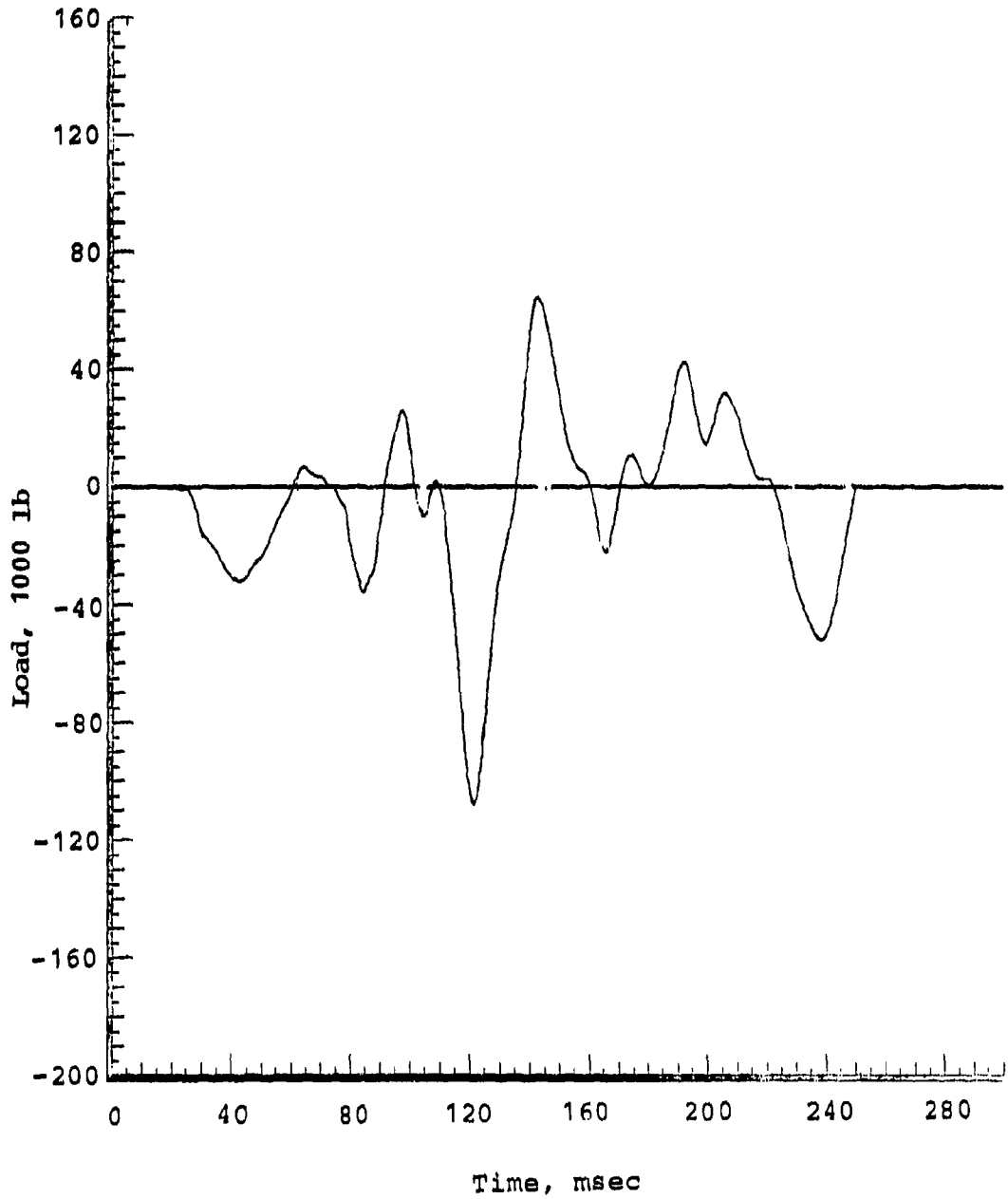

Left aft transmission lift link axial load (beam 20)

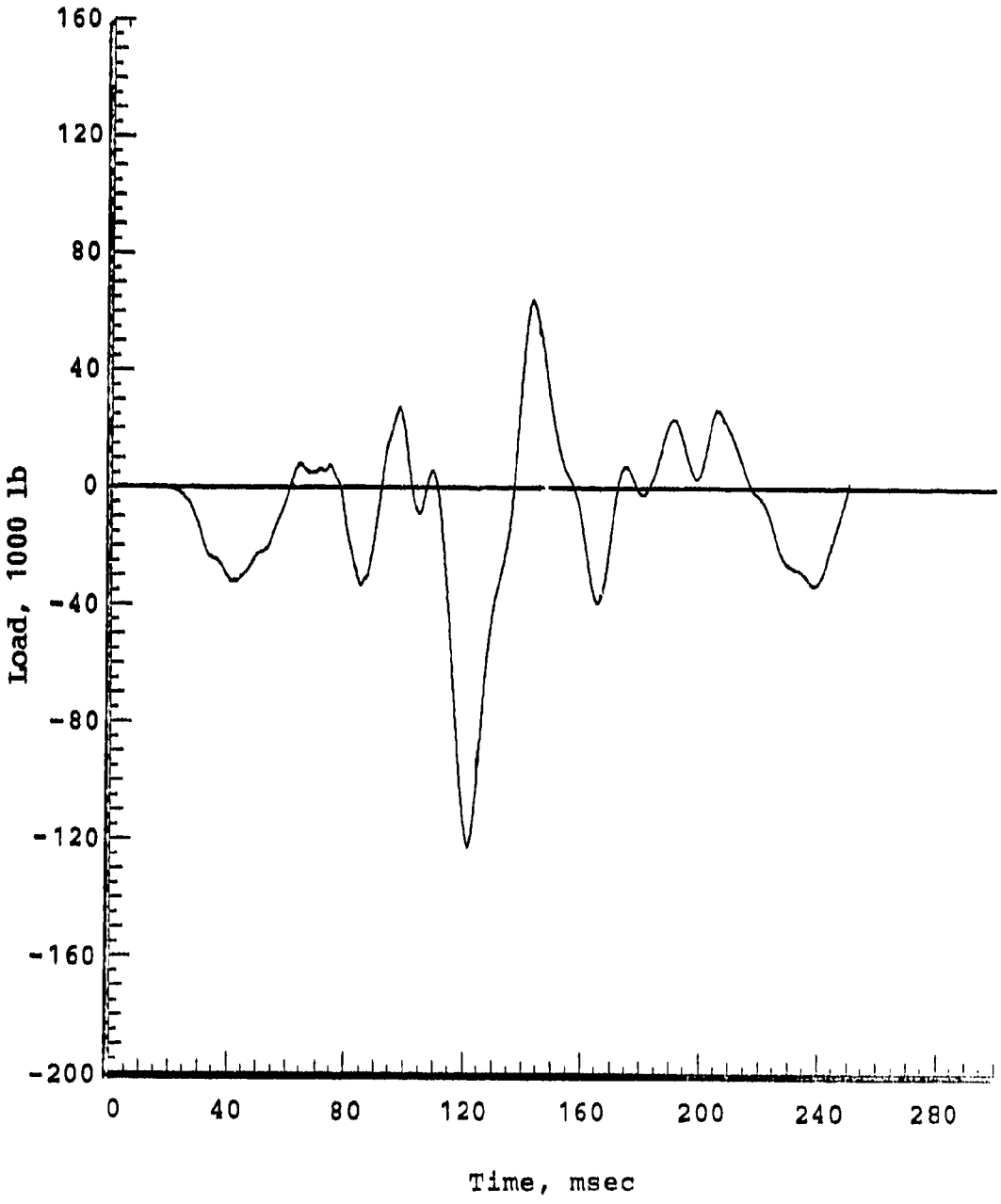

Left transmission crash link - compression (beam 31)

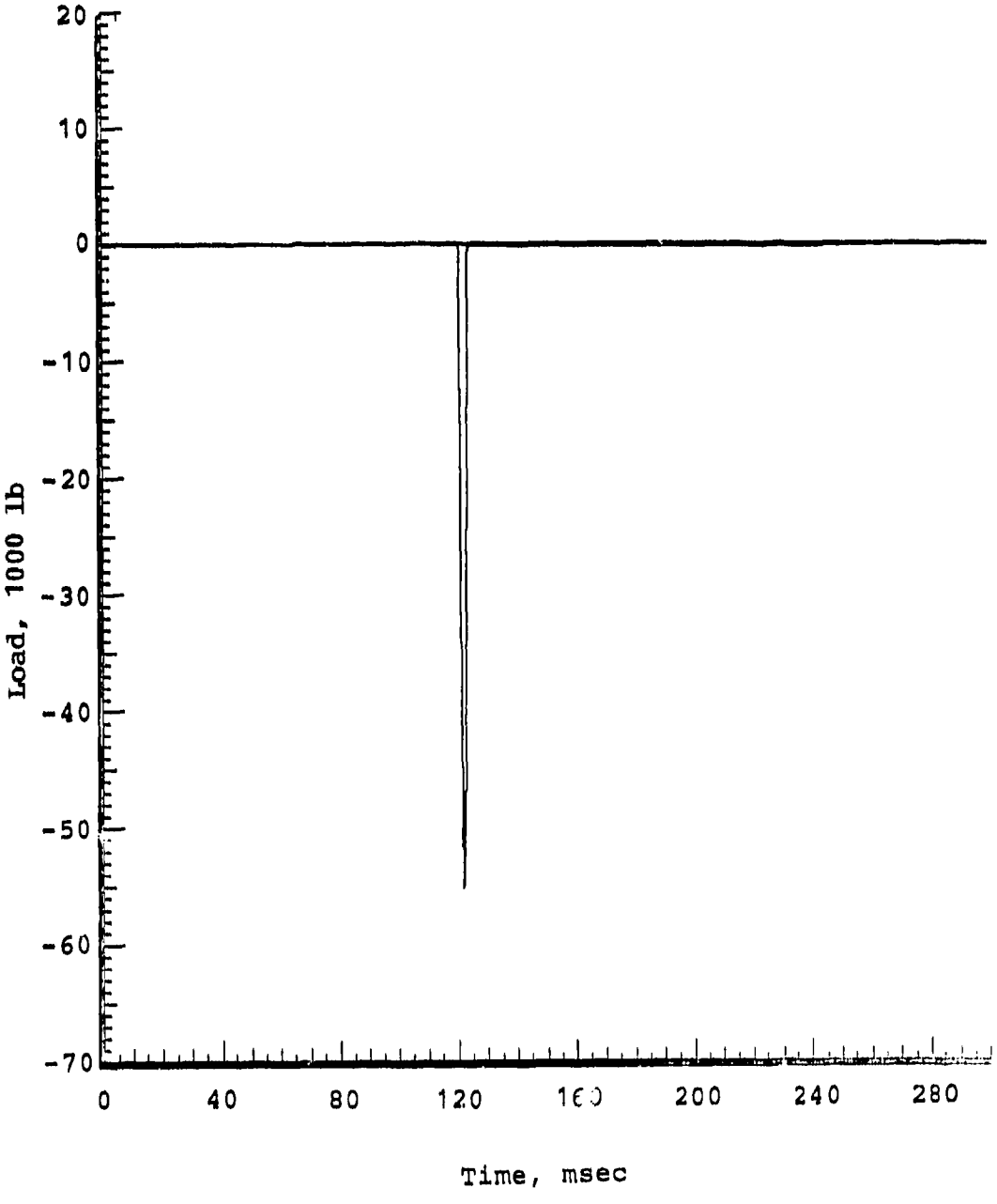

Right main landing gear drag link axial load (beam 47)

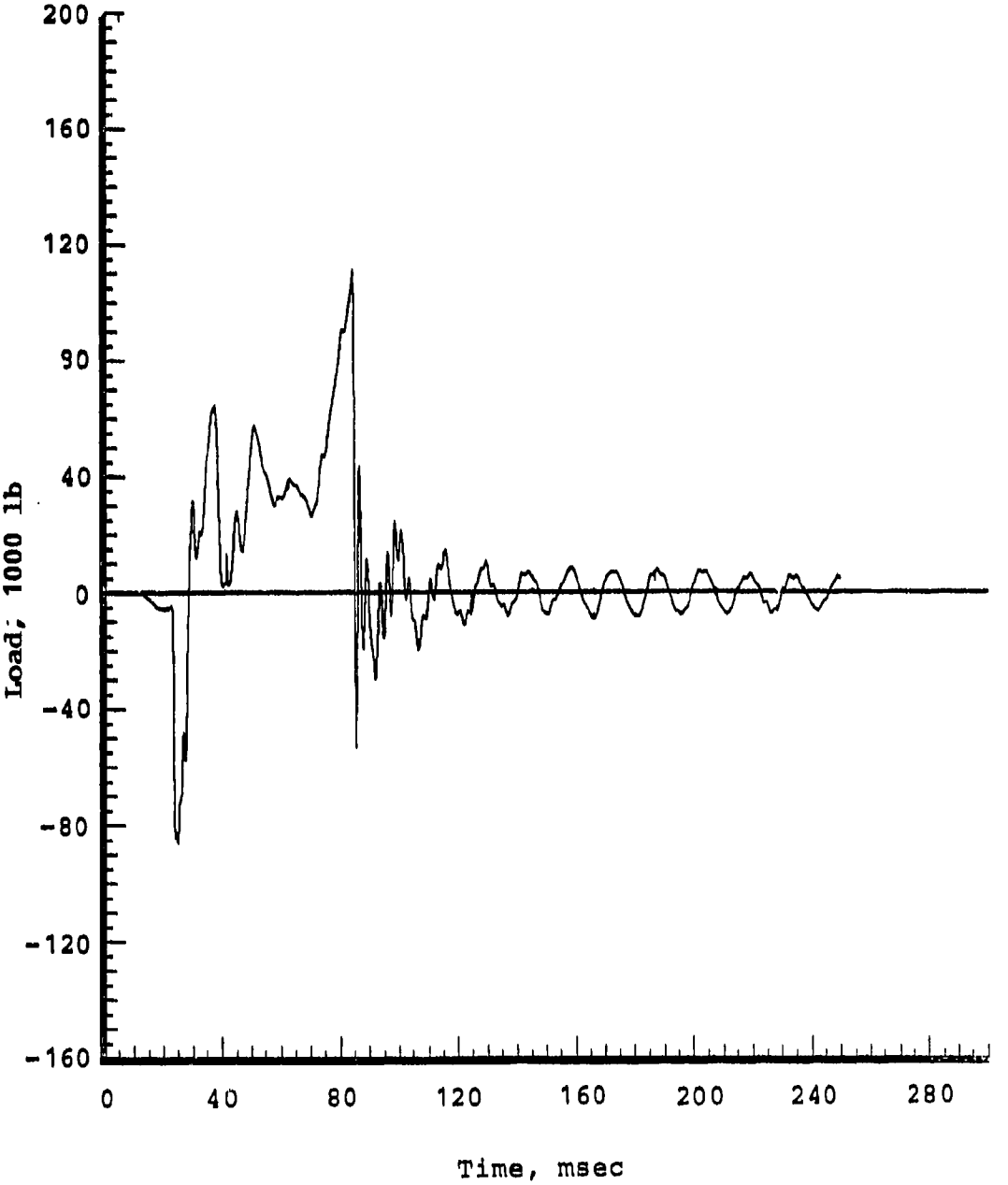

Left main landing gear drag link axial load (beam 48)

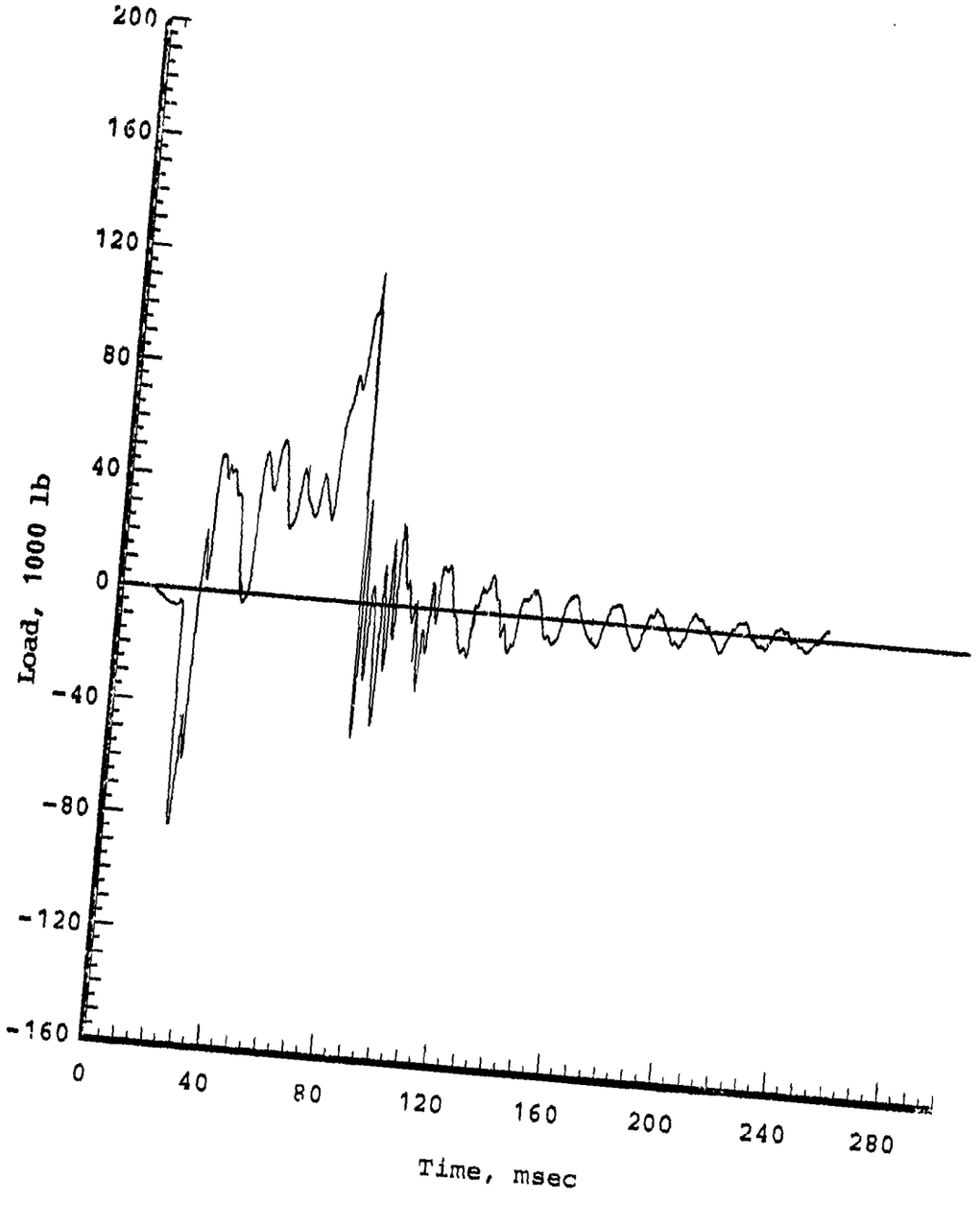

646-83